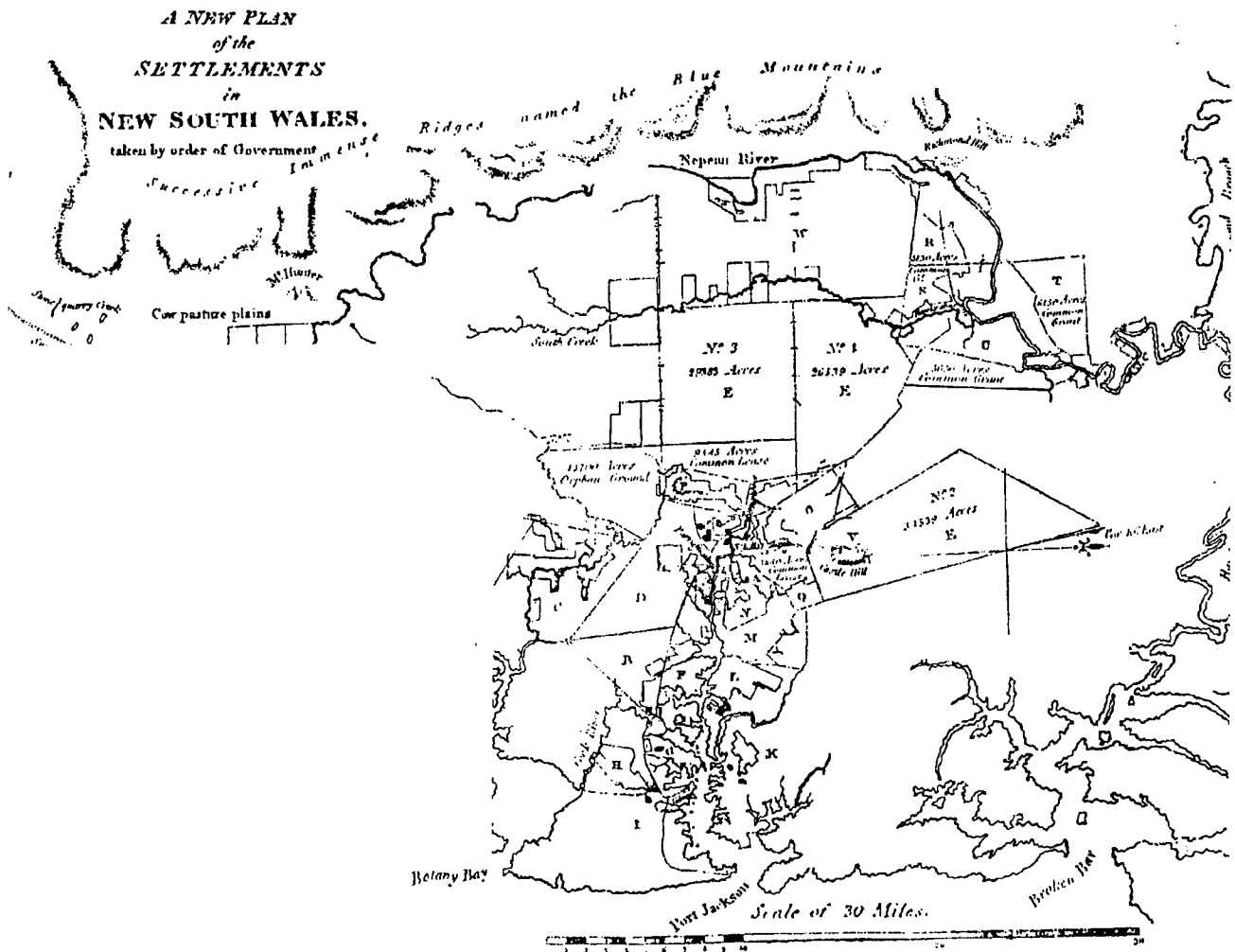


REAL-TIME ESTIMATION OF IONOSPHERIC DELAY USING GPS MEASUREMENTS

LAO-SHENG LIN



UNISURV S-51, 1998

Reports from

SCHOOL OF GEOMATIC ENGINEERING

THE UNIVERSITY OF NEW SOUTH WALES SYDNEY NSW 2052 AUSTRALIA



UNISURV REPORT S-51, 1998

**REAL-TIME ESTIMATION OF
IONOSPHERIC DELAY USING
GPS MEASUREMENTS**

LAO-SHENG LIN

Received: June, 1997
Accepted: November, 1997

SCHOOL OF GEOMATIC ENGINEERING
UNIVERSITY OF NEW SOUTH WALES
SYDNEY NSW 2052
AUSTRALIA

COPYRIGHT ©

No part may be reproduced without written permission

National Library of Australia

Card No. and ISBN 0 7334 1664 0

ABSTRACT

When radio waves such as the GPS signals propagate through the ionosphere, they experience an extra time delay. The ionospheric delay can be eliminated (to the first order) through a linear combination of L1 and L2 observations from dual-frequency GPS receivers. Taking advantage of this dispersive principle, one or more dual-frequency GPS receivers can be used to determine a model of the ionospheric delay across a region of interest and, if implemented in real-time, can support single-frequency GPS positioning and navigation applications.

There are, however, several factors which affect the accuracy of real-time ionospheric delay estimation. The research objectives of this thesis were: (1) to develop algorithms to obtain accurate absolute Total Electron Content (TEC) estimates from dual-frequency GPS observables, and (2) to develop an algorithm to improve the accuracy of real-time ionosphere modelling. In order to fulfil these objectives, four algorithms have been proposed in this thesis.

A “*multi-day multipath template technique*” is proposed to mitigate the pseudo-range multipath effects at static GPS reference stations. This technique is based on the assumption that the multipath disturbance at a static station will be constant if the physical environment remains unchanged from day to day. The multipath template, either single-day or multi-day, can be generated from the previous days’ GPS data. Experiments have shown that: (1) the performance of the multi-day multipath template generated from the data of the previous 5 days is better than that of other multi-day multipath templates, and (2) the performance of the multi-day multipath template is superior to that of the single-day multipath template.

A “*real-time failure detection and repair algorithm*” is proposed to detect and repair the GPS carrier phase “failures”, such as the occurrence of cycle slips. The proposed algorithm uses two procedures: (1) application of a statistical test on the state difference estimated from robust and conventional Kalman filters in order to detect and identify the

carrier phase failure, and (2) application of a Kalman filter algorithm to repair the “identified carrier phase failure”. From the test results, it has been demonstrated that the TEC “failure” caused by carrier phase cycle slips can be detected and repaired promptly and correctly in real-time.

A “*L1/L2 differential delay estimation algorithm*” is proposed to estimate GPS satellite transmitter and receiver L1/L2 differential delays. This algorithm, based on the single-site modelling technique, is able to estimate the sum of the satellite and receiver L1/L2 differential delay for each tracked GPS satellite. Based on the experimental results, it can be concluded that: (1) the estimation precision of the SPR (Satellite-Plus-Receiver) differential delay is of the order of ± 0.43 ns, (2) the estimated satellite differential delay values using UNSW algorithm agreed with that estimated by PL, DLR and JPL to within 0.5 ns, and (3) the estimated satellite differential delay values using UNSW algorithm agreed with those estimated by NRCan, IAG and IfE to within 1.1 ns.

A “*UNSW grid-based algorithm*” is proposed to improve the accuracy of real-time ionosphere modelling. The proposed algorithm is similar to the conventional grid-based algorithm. However, two modifications were made to the algorithm: (1) an “*exponential function*” is adopted as the weighting function, and (2) the “*grid-based ionosphere model*” estimated from the previous day is used to predict the ionospheric delay ratios between the grid point and reference points. Comparing the test results of the proposed grid-based algorithm and the conventional grid-based algorithm, the standard deviations of the “TEC prediction residuals” (differences between the vertical TEC values derived from GPS observables at a user site and that derived from regional ionosphere modelling) can be reduced significantly, by approximately 29 to 31 percent in the case of the PGGGA data, 10 to 20 percent in the case of the GSI data, and 36 percent in the case of the ARGN data.

ACKNOWLEDGEMENTS

I would like to express my sincere thanks to Associate Professor Chris Rizos, my supervisor, for his valuable suggestions, patient guidance and encouragement throughout my study and this research.

A special thanks to the late Bernie Hirsch for his assistance on computer hardware and software refinement. I also wish to thank the Satellite Navigation and Positioning (SNAP) group in the school, past and present members, and also all the staff of the School of Geomatic Engineering (formerly the School of Surveying), The University of New South Wales, Sydney, Australia.

I would like to express my gratitude to Professor Børje Forssell (Norway), Professor Richard Langley and Mr. Attila Komjathy (UNB, Canada), Professor Stelios P. Mertikas (Technical University of Crete, Chania, Greece), Dr. Bruce Harvey (UNSW, Australia), Dr. Esther Sardon (DLR, Germany), Dr. Joachim Feltens (EDS, Germany), Dr. Lambert Wanninger (Technical University Dresden, Germany), Dr. Yue-Jin Wang (IPS, Australia) for providing me with valuable suggestions and (or) reference articles. I also wish to thank the Australian Survey and Land Information Group (AUSLIG), Geographic Survey Institute (GSI), and the Scripps Institution of Oceanography (SIO) for providing us with GPS data sets.

My employer, the Topographic Service, Combined Service Forces, and the Government of Taiwan, Republic of China, are acknowledged for the study leave and financial support they granted throughout this period. I would like to express my sincere thanks to General Fu-Sheng Sun, Director of Topographic Service, for his support and encouragement.

Last, but not least, my special thanks goes to my wife, Ming Chang, who substituted for my absence for my children, Kai-Wei, and Ying-Chen. Their sacrifices and understanding have indeed made this struggle a worthwhile one. Finally, I wish to thank my beloved mother, for the constant prayers and encouragement she offered us.

TABLE OF CONTENTS

ABSTRACT	i
ACKNOWLEDGEMENTS	iii
TABLE OF CONTENTS	v
LIST OF FIGURES	xi
LIST OF TABLES	xvi

1. INTRODUCTION

1.1 The Global Positioning System as a Tool for Ionosphere Modelling and Monitoring	1
1.2 Motivations for the Investigations	3
1.3 Research Objectives	4
1.4 Methodology and Scope of the Research	6
1.5 Outline of the Thesis	8
1.6 Contributions of this Research	10

2. IONOSPHERE AND GPS

2.1 Introduction to Ionosphere	11
2.2 The Global Positioning System	14
2.2.1 General Description of the GPS System	14
2.2.2 GPS Observables	17
2.2.3 Error Sources	19
2.2.3.1 Satellite Clock Errors	19
2.2.3.2 Orbital Errors	20
2.2.3.3 Ionospheric Delay	20
2.2.3.4 Tropospheric Delay	21
2.2.3.5 Receiver Clock Errors	21
2.2.3.6 Receiver Measurement Errors	21

2.2.3.7 Multipath.....	22
2.2.3.8 L1/L2 Differential Delay	22
2.2.3.9 Phase Centre Offsets and Imaging.....	23
2.3 Major Ionospheric Effects on GPS	24
2.4 Total Electron Content.....	27
2.4.1 Dependence of Total Electron Content on Solar Flux	28
2.4.2 Ionospheric Models.....	29
2.4.2.1 Empirical and Physical Models of the Ionosphere	29
2.4.2.2 Single-Frequency User Ionospheric Algorithm	31
2.5 Ionospheric Delay Estimation Using GPS Measurements.....	34
2.5.1 Observation Equations.....	34
2.5.2 Potential Limitations in Absolute TEC	
Estimation Using GPS	37
2.5.3 Potential Limitations in Real-Time	
TEC Estimation Using GPS.....	39
3. USING MULTIPATH TEMPLATE TECHNIQUE TO IMPROVE THE	
REAL-TIME IONOSPHERIC DELAY ESTIMATION ACCURACY	
3.1 Introduction.....	41
3.2 Methods to Mitigate GPS Multipath Effects.....	42
3.3 Multi-Day Multipath Template Generation Methodology.....	45
3.3.1 Pseudo-Range Multipath Detection Equations	45
3.3.2 Multipath Template Generation	50
3.4 Program “MULTIPAT”	56
3.5 Experimental Results and Discussion	57
3.5.1 Daily Repetition of Single-Day Multipath Templates.....	58
3.5.2 Performance of Single-Day Multipath Templates	60
3.5.2.1 Performance Characteristics of Single-Day	
Multipath Templates	60
3.5.2.2 Performance Comparisons as a Function of	
Satellite PRNs.....	62

3.5.2.3 Performance Comparisons as a Function of Satellite Elevation	65
3.5.2.4 Performance Comparisons as a Function of Satellite Azimuth.....	66
3.5.3 Performance of Multi-Day Multipath Templates	68
3.5.4 Comments on Multipath Template Technique.....	71
3.6 Application in Real-Time Ionospheric Delay Estimation	72
3.7 Concluding Remarks	73
4. REAL-TIME FAILURE DETECTION AND REPAIR IN TEC ESTIMATION USING GPS BY ROBUST AND CONVENTIONAL KALMAN FILTER STATE ESTIMATES	
4.1 Introduction	74
4.2 Conventional and Robust Kalman Filter.....	76
4.3 Real-Time Failure Detection and Repair in Ionospheric Delay Estimation.....	80
4.3.1 Concept.....	81
4.3.2 Detection and Identification Step	83
4.3.3 Repair Step	83
4.4 Program “REALTEC”	86
4.5 Experimental Results and Discussion.....	89
4.5.1 Data Description.....	89
4.5.2 Test I – Cycle Slip Detection and Repair.....	90
4.5.2.1 UNSW Case – Post-Processing Mode.....	90
4.5.2.2 UNSW Case – Real-Time Mode	91
4.5.3 Test II – Effectiveness of the Multipath Template.....	93
4.5.3.1 UNSW Case	93
4.5.3.2 PGGGA Case.....	94
4.6 Concluding Remarks	96

5. AN ALGORITHM TO ESTIMATE GPS SATELLITE AND RECEIVER L1/L2 DIFFERENTIAL DELAYS	
5.1 Introduction	97
5.2 Methods to Estimate GPS Satellite and Receiver L1/L2 Differential Delay	97
5.2.1 Definition of GPS Satellite and Receiver L1/L2 Differential Delay	97
5.2.2 Satellite Differential Delays	98
5.2.3 Receiver Differential Delays	100
5.3 A Proposed Algorithm to Estimate GPS Satellite and Receiver L1/L2 Differential Delay	102
5.3.1 Estimation Assumption	103
5.3.2 Estimation Procedure	104
5.4 Test Results and Discussion	108
5.4.1 Description of Test Data	108
5.4.2 Methods to Verify the Algorithm	110
5.4.2.1 Daily Variation of the Satellite-Plus-Receiver Differential Delay	110
5.4.2.2 Comparison with the Results of Other Organisations	116
5.4.2.3 Variability of the Standard Deviation of the TEC Prediction Residuals in Regional Ionosphere Modelling	119
5.5 Concluding Remarks	120
6. AN ALTERNATIVE GRID-BASED ALGORITHM TO IMPROVE THE ACCURACY OF REAL-TIME IONOSPHERE MODELLING	
6.1 Introduction	121
6.2 Conventional Grid-Based Ionospheric Delay Estimation Algorithm	122
6.2.1 Introductory Remarks	122
6.2.2 Ionospheric Pierce Point Location Determination	123

6.2.3 Slant TEC Estimation Using Dual-Frequency GPS	
Measurements.....	124
6.2.3.1 Basic GPS Pseudo-Range and Carrier	
Phase Observables	124
6.2.3.2 Slant TEC Estimation Using Dual-Frequency	
GPS Measurements	125
6.2.3.3 Concluding Remarks.....	126
6.2.4 Vertical TEC Estimation.....	128
6.2.5 Grid Point TEC Determination	128
6.2.6 Ionospheric Pierce Point TEC Interpolation.....	129
6.3 UNSW Grid-Based Ionospheric Delay Estimation Algorithm	133
6.4 Program “POSTEC”	136
6.5 Test Results and Discussion	147
6.5.1 Data Description.....	147
6.5.1.1 Small Region - PGGGA Data Set.....	147
6.5.1.2 Medium Region - GSI Data Set.....	149
6.5.1.3 Large Region - ARGN Data Set.....	150
6.5.2 Data Processing.....	152
6.5.3 Test Result Comparisons Between UNSW Algorithm	
and Conventional Algorithm.....	154
6.5.3.1 Using Different Weighting Functions	154
6.5.3.2 Using Different Ionosphere Models	156
6.5.3.3 Performance of the UNSW Grid-Based Algorithm.....	157
6.5.4 Test Result Comparisons Between UNSW Algorithm	
and Polynomial Algorithm.....	171
6.5.4.1 Polynomial Algorithms	171
6.5.4.2 Test Results and Discussion.....	172
6.6 Concluding Remarks	178
7. SUMMARY, CONCLUSIONS, AND RECOMMENDATIONS	
7.1 Summary of the Research.....	179

7.2 Conclusions of the Research.....	181
7.2.1 Multipath Template.....	182
7.2.2 Real-Time Failure Detection and Repair.....	182
7.2.3 GPS Instrumental L1/L2 Differential Delay Estimation.....	183
7.2.4 UNSW Grid-Based Algorithm	184
7.3 Recommendations	185
REFERENCES.....	187
VITA.....	197

LIST OF FIGURES

Figure	page
2.1. The geographic regions of the ionosphere.....	14
2.2. Observed TEC versus predicted TEC from broadcast model for single-frequency GPS users at location (-20°S, 140°E), ARGN region, from day 182 to 186, 1995	33
2.3. Pseudo-range derived TEC, carrier phase derived TEC, and phase levelled TEC (before correcting the GPS satellite and receiver L1/L2 differential delay) of GPS satellite PRN 24, over site “alic”, ARGN region, on day 181, 1995.....	38
2.4. Time series of PRN 24’s elevation angle, at site “alic”, on day 181, 1995.....	38
2.5. Corrected phase levelled TEC, phase levelled TEC, and pseudo-range derived TEC of PRN 24, over site “alic”, ARGN region, on day 181, 1995.....	39
3.1. The multipath effect is a result of signals from a satellite reaching the receiver’s antenna via more than one path.	43
3.2. A block diagram of computation procedure for K_1 for satellite PRN 1.....	53
3.3. A block diagram of computation procedure for multipath MP1 for satellite PRN 1.....	54
3.4. Time series of multipath MP1 for PRN 1 at site “blyt”, PGGA on day 012, 1996.....	55
3.5. Time series of multipath MP2 for PRN 1 at site “blyt”, PGGA on day 012, 1996.....	55
3.6. Multipath MP1 statistics of the 12 single-day multipath templates.....	60
3.7. The statistical comparison between the percentages of group A, for multipath MP1 (ie. “Day 12”, before applying multipath template) and multipath residual $\Delta MP1$ (ie. “Day 12 -Day 11”, after applying multipath template generated from the data of day 11) for each GPS satellite, for day 12, from the results of Table 3.6.....	65

3.8.	The statistical comparison between the percentages of group A, for multipath MP1 (ie. “Day 12”, before applying multipath template) and multipath residual Δ MP1 (ie. “Day 12 -Day 11”, after applying multipath template generated from the data of day 11), for day 12, according to satellite elevation.....	66
3.9.	The statistical comparison between the percentages of group A, for multipath MP1 (ie. “Day 12”, before applying multipath template) and multipath residual Δ MP1 (ie. “Day 12 -Day 11”, after applying multipath template generated from the data of day 11), for day 12, according to satellite azimuth.....	67
3.10.	The performance of the multi-day multipath template compared to that of the single-day multipath template.....	71
4.1.	A block diagram of the robust Kalman filter of Masreliez-Martin	79
4.2.	Main steps of the real-time failure detection and repair algorithm.....	85
4.3.	A block diagram of program “REALTEC”	88
4.4.	The phase-derived TEC (a) and phase-levelled TEC (b) of PRN 21 for day 121, 1995.	90
4.5.	Post-processing TEC estimates versus real-time TEC estimates of PRN 21 for day 121, 1995.....	92
4.6.	Post-processed TEC estimates versus real-time TEC estimates of PRN 21 for day 119, 1995.....	93
4.7.	Real-time TEC estimates, comparison of different types of multipath template, for PRN 21 for day 121, 1995.....	94
4.8.	Comparison of the means of the TEC estimate difference for each PRN at site “blyt”, PGGA data, day 12, 1996.....	95
4.9.	Comparison of the standard deviations of the TEC estimate difference for each PRN at site “blyt”, PGGA data, day 12, 1996.....	96
5.1.	Ionospheric pierce point (IPP) geometry.....	105

5.2.	Satellite differential delay differences between the UNSW solution and solutions from DLR and PL. ‘+’ represents ‘UNSW - DLR’, ‘o’ represents ‘UNSW - PL’.	117
5.3.	Satellite differential delay differences between the UNSW solution and solutions from JPL and NRCan. ‘+’ represents ‘UNSW - JPL’, ‘o’ represents ‘UNSW - NRCan’.	118
5.4.	Satellite differential delay differences between the UNSW solution and solutions from IAG and IfE. ‘+’ represents ‘UNSW - IAG’, ‘o’ represents ‘UNSW - IfE’.	118
5.5.	TEC prediction residual distribution of ionosphere modelling, with mean value -0.11 TECU, standard deviation 0.991 TECU.	120
6.1.	Schematic showing some nodes of the imaginary grid and 4 Ionospheric Pierce Points (IPPs).	131
6.2.	Schematic showing interpolation geometry for User Pierce Point (UPP).	132
6.3.	Main functions of the POSTEC program.	140
6.4.	Standard deviation comparisons of TEC prediction residuals using different weighting functions for day 119, 1996, for the GSI data.	155
6.5.	Standard deviation comparisons of TEC prediction residuals using different ionosphere models for day 119, 1996, for the GSI data.	157
6.6.	Comparison between UNSW grid-based algorithm and conventional algorithm at site “crfp”, PGGGA data, from day 002 to 012, 1996.	159
6.7.	Comparison between UNSW grid-based algorithm and conventional algorithm at PGGGA region (excluding site “crfp”), from day 002 to 012, 1996.	160
6.8.	Comparison between UNSW grid-based algorithm and conventional algorithm at site “2110”, GSI data, from day 112 to 119, 1996.	161

6.9.	Comparison between UNSW grid-based algorithm and conventional algorithm at GSI region (excluding site “2110”), from day 112 to 119, 1996.	162
6.10.	Comparison between UNSW grid-based algorithm and conventional algorithm at site “alic”, ARGN data, from day 182 to 195, 1995.	163
6.11.	TEC prediction residual comparison between UNSW grid-based algorithm and conventional algorithm, at PGGGA region (excluding site “crfp”), for day 012, 1996	164
6.12.	TEC prediction residual versus cumulative probability using UNSW grid-based algorithm and conventional algorithm, at PGGGA region (excluding site “crfp”), for day 012, 1996.....	165
6.13.	TEC prediction residual comparison between UNSW grid-based algorithm and conventional algorithm, at site “crfp”, PGGGA data, for day 012, 1996	166
6.14.	TEC prediction residual versus cumulative probability using UNSW grid-based algorithm and conventional algorithm, at site “crfp”, PGGGA data, for day 012, 1996	166
6.15.	TEC prediction residual comparison between UNSW grid-based algorithm and conventional algorithm, at GSI region (excluding site “2110”), for day 118, 1996.....	167
6.16.	TEC prediction residual versus cumulative probability using UNSW grid-based algorithm and conventional algorithm, at GSI region (excluding site “2110”), for day 118, 1996	168
6.17.	TEC prediction residual comparison between UNSW grid-based algorithm and conventional algorithm, at site “2110”, GSI data, for day 118, 1996.....	169
6.18.	TEC prediction residual versus cumulative probability using UNSW grid-based algorithm and conventional algorithm, at site “2110”, GSI data, for day 118, 1996	169

6.19.	TEC prediction residual comparison between UNSW grid-based algorithm and conventional algorithm, at site “alic”, ARGN data, for day 195, 1995	170
6.20.	TEC prediction residual versus cumulative probability using UNSW grid-based algorithm and conventional algorithm, at site “alic”, ARGN data, for day 195, 1995	171
6.21.	Comparison between 6-term, 10-term, and 15-term polynomial algorithms at site “alic”, ARGN data, from day 182 to 195, 1995	174
6.22.	Comparison between UNSW grid-based algorithm, conventional grid-based algorithm, and 10-term polynomial algorithm at site “alic”, ARGN data, from day 182 to 195, 1995	174
6.23.	TEC prediction residual comparison between various polynomial algorithms, at site “alic”, ARGN data, for day 195, 1995	175
6.24.	TEC prediction residual versus cumulative probability using various polynomial algorithms, at site “alic”, ARGN data, for day 195, 1995	176
6.25.	TEC prediction residual comparison between UNSW grid-based algorithm, conventional grid-based algorithm, and 10-term polynomial algorithm, at site “alic”, ARGN data, for day 195, 1995	176
6.26.	TEC prediction residual versus cumulative probability using UNSW grid-based algorithm, conventional grid-based algorithm, and 10-term polynomial algorithm, at site “alic”, ARGN data, for day 195, 1995	177

LIST OF TABLES

Table	page
3.1. An example of multipath MP1 computation of PRN 1 at site “blyt”, PGGGA, day 12, 1996.	55
3.2. The multipath MP1 statistics of the 12 single-day multipath templates.....	59
3.3. The multipath MP2 statistics of the 12 single-day multipath templates.	59
3.4. The multipath residual Δ MP1 statistics, for day 12, after applying single-day multipath template generated from various day’s data.	62
3.5. The multipath residual Δ MP2 statistics, for day 12, after applying single-day multipath template generated from various day’s data.	62
3.6. Statistical comparison between the multipath MP1 (before applying multipath template) and the multipath residual Δ MP1 (after applying single multipath template generated from the data of day 11), for day 12, according to GPS satellite PRNs.....	64
3.7. The multipath residual Δ MP1 statistics, for day 12, after applying various multi-day multipath templates	70
3.8. The multipath residual Δ MP2 statistics, for day 12, after applying various multi-day multipath templates	71
4.1. Post-processing derived phase correction, Δ TS, versus real-time derived Δ TS.....	92
4.2. Real-time TEC estimate difference statistics of Figure 4.7.....	94
5.1. PGGGA stations used in this study.....	109
5.2. Mean SPR differential delay (Mean SPR) estimation, in units of TECU, for each tracked GPS satellite at the five PGGGA stations, over the period day 001 to 012, 1996.....	112

5.3.	Standard deviation (std dev) of the mean SPR differential delay, for each tracked GPS satellite at the five PGGA stations, over the period day 001 to 012, 1996.	113
5.4.	Daily averages of the SPR differential delay estimates over all 25 GPS satellites, in units of TECU, at the five PGGA sites, over the period day 001 to 012, 1996.	114
5.5.	The average values of SAT estimates for each satellite, in units of TECU, at the five PGGA stations, over the period day 001 to 012, 1996.	115
5.6.	The standard deviation (std dev) of the mean SAT estimate for each satellite, in units of TECU, at the five PGGA stations, over the period day 001 to 012, 1996.	116
5.7.	The standard deviation (std dev) of the “TEC prediction residuals” of PGGA regional ionosphere modelling, in units of TECU, for day 001 to 012, 1996.	120
6.1.	Welcome page of the POSTEC program.	137
6.2.	Main menu of the POSTEC program.	138
6.3.	Interactive files input request once the “Multipath & Slant Phase-derived TEC Est.” option was chosen.	138
6.4.	File “ALIC1810.95T” was chosen.	139
6.5.	“Multipath and slant phase-derived TEC estimation” program running after “ALIC1810.95T” was input.	139
6.6.	PGGA stations and their coordinates.	148
6.7.	RINEX data sample of site “blyt”, PGGA, for day 001, 1996.	148
6.8.	GSI stations used in these analyses.	149
6.9.	RINEX data sample of site “2002”, GSI, for day 111, 1996.	149
6.10.	RINEX data sample of site “2110”, GSI, for day 111, 1996.	150
6.11.	ARGN stations used in these analyses.	151
6.12.	RINEX data sample of site “tidb”, ARGN, for day 181, 1995.	151
6.13.	RINEX data sample of site “alic”, ARGN, for day 181, 1995.	152

6.14.	Mean and standard deviation comparisons of TEC prediction residuals using different weighting functions for day 119, 1996, for the GSI data.	155
6.15.	Mean and standard deviation comparisons of TEC prediction residuals of using different ionosphere models for day 119, 1996, for the GSI data.	156
6.16.	Comparison between UNSW grid-based algorithm and conventional algorithm at site “crfp”, PGGGA data, from day 002 to 012, 1996.	159
6.17.	Comparison between UNSW grid-based algorithm and conventional algorithm at PGGGA region (excluding site “crfp”), from day 002 to 012, 1996.	160
6.18.	Comparison between UNSW grid-based algorithm and conventional algorithm at site “2110”, GSI data, from day 112 to 119, 1996.	161
6.19.	Comparison between UNSW grid-based algorithm and conventional algorithm at GSI region (excluding site “2110”), from day 112 to 119, 1996.	162
6.20.	Comparison between UNSW grid-based algorithm and conventional algorithm at site “alic”, ARGN data, from day 182 to 195, 1995.	163
6.21.	Statistical data comparison between UNSW grid-based algorithm and conventional algorithm, at PGGGA region (excluding site “crfp”), for day 012, 1996.	164
6.22.	Statistical data comparison between UNSW grid-based algorithm and conventional algorithm, at site “crfp”, PGGGA data, for day 012, 1996.	165
6.23.	Statistical data comparison between UNSW grid-based algorithm and conventional algorithm, at GSI region (excluding site “2110”), for day 118, 1996.	167

6.24. Statistical data comparison between UNSW grid-based algorithm and conventional algorithm, at site “2110”, GSI data, for day 195, 1995	168
6.25. Statistical data comparison between UNSW grid-based algorithm and conventional algorithm, at site “alic”, ARGN data, for day 195, 1995	170
6.26. Comparison of standard deviation of TEC prediction residuals among UNSW grid-based algorithm, conventional algorithm, and various polynomial algorithms at site “alic”, ARGN data, from day 182 to 195, 1995	175
6.27. Statistical data comparison between UNSW grid-based algorithm and 10-term polynomial algorithm, at site “alic”, ARGN data, for day 195, 1995	177

CHAPTER 1

INTRODUCTION

1.1 The Global Positioning System as a Tool for Ionosphere Modelling and Monitoring

The Navstar Global Positioning System (*GPS*) is an all-weather, space-based navigation system developed by the U.S. Department of Defense (DoD) to satisfy the requirements of the military forces for accurate position, velocity, and time, in a common reference system, anywhere on or near the earth, on a continuous basis. Due to the tremendous accuracy potential of this system, and recent improvements in receiver technology, there is a growing community which utilises the GPS for a variety of civilian applications.

The GPS system can be conveniently divided into three segments: (1) the space segment, (2) the control segment, and (3) the user segment (Rizos, 1997). The space segment comprises the satellites in orbit. The control segment consists of facilities required for satellite health monitoring, telemetry, tracking, command and control, ephemeris computations and uplinking. The user segment is the final link in the chain of system components. It comprises the GPS receiver, consisting of an antenna, signal tracking circuitry, user interface, power, and a microcomputer to control the operation of the receiver.

There are two main types of observables that can be made on the GPS signals: pseudo-ranges ("biased" ranges) and carrier phase (or "ambiguous" ranges) (eg. *ibid*, 1997; Langley, 1993).

The ionising action of the sun's radiation on the earth's upper atmosphere produces free electrons. Above about 60 km the number of these free electrons is sufficient to affect the propagation of electromagnetic waves. This "ionised" region of the atmosphere is a

plasma and is referred to as the “*ionosphere*”. Shorter wavelength radio signals, such as GPS signals, pass through the ionosphere but are affected by it.

Ionospheric scientists used radio transmissions from the first Sputnik satellite launched in 1957 to measure the number of electrons in the ionosphere (Coco, 1991). Ever since those first measurements, they have continued to take advantage of radio transmissions from a wide variety of satellites to gain a better understanding of the ionosphere. Ionospheric scientists often call satellites whose main objectives are not ionospheric research “*satellites of opportunity*”, because they present a convenient opportunity to investigate the ionosphere at a relatively low cost (ibid, 1991). GPS satellites represent the latest generation of satellites of opportunity for ionospheric scientists, and a number of groups are using these satellites to monitor the ionosphere (eg. Lanyi and Roth, 1988; Clynych et al., 1989; Bishop et al., 1992; Coco et al., 1993; Mannucci et al., 1993; Bishop et al., 1994a; Wanninger, 1994; Wild, 1994; Feltens, 1995a, 1995b; Wilson et al., 1995; Feltens et al., 1996; Langley & Komjathy, 1996; Jakowski, 1996).

In GPS positioning and navigation, the ionosphere can be the largest source of error in the absence of Selective Availability (SA) (Klobuchar, 1991). The main ionospheric effects on GPS signals are phase advance and group delay (ibid, 1991). The ionospheric delay is a function of the Total Electron Content (TEC) along the signal path and the frequency of the propagated signal. Since the ionosphere is a dispersive medium for radio waves (eg. Langley, 1992; Langley, 1996; Rizos, 1997), a dual-frequency GPS receiver can eliminate (to the first order) the ionospheric delay through a linear combination of L1 and L2 observables (Hofmann-Wellenhof et al., 1994). On the other hand, taking advantage of this, the dual-frequency GPS receiver can be used to estimate the TEC along the path from the receiver to each tracked GPS satellite. These TEC estimates can be used to: (1) study the ionosphere, or (2) generate an ionosphere model for single-frequency GPS users.

However, low-cost, single-frequency GPS receivers cannot use this option. They can either ignore the ionospheric delay or correct for approximately 50 to 60 percent of the rms range error using the Klobuchar model coefficients transmitted as part of the satellite messages (eg. Feess and Stephens, 1987; Coco, 1991; Klobuchar, 1991).

Consequently, it is beneficial for supporting single-frequency GPS positioning and navigation applications, in real-time, to estimate ionospheric delays over a region of interest using a network of GPS dual-frequency receivers (eg. Campbell et al., 1986; Coco et al., 1990; Coco, 1991; Klobuchar, 1991; Bishop et al., 1992; Coco et al., 1993; Bishop et al., 1994b; Conker et al., 1995; El-Arini et al., 1995; Engler et al., 1995; Komjathy & Langley, 1996b, 1996c; Lin et al., 1996a, 1996b).

1.2 Motivations for the Investigations

This research was motivated by the following:

- There is a growing community which utilises the GPS for a variety of civilian applications, such as surveying and mapping, land, sea and air navigation, search and rescue operations, etc.
- There are a number of permanent GPS networks using dual-frequency receivers around the world, such as the International GPS Service for Geodynamics (IGS) network, the Australian Regional GPS Network (ARGN) network, etc. Dual-frequency GPS data from these networks are valuable for studying and monitoring the ionosphere.
- This solar cycle maximum will occur around the year 2000, and hence it is necessary to develop a good algorithm to mitigate the ionospheric delay effects on GPS positioning and navigation applications.
- Real-time ionosphere modelling is an ideal method to provide ionospheric delay corrections to single-frequency users so that they may reduce ionospheric delay effect.
- In real-time ionosphere modelling using GPS measurements, some challenging problems, such as real-time failure detection and repair, pseudo-range multipath mitigation, etc., must be solved.

1.3 Research Objectives

Based on the above-mentioned motivations, the main research objectives of this thesis are to fulfil the following two requirements: (1) to develop algorithms to obtain accurate absolute TEC estimates from dual-frequency GPS observables in real-time, and (2) to develop an algorithm for improving the accuracy of real-time ionosphere modelling.

a) To Develop Algorithms to Obtain Accurate Absolute TEC Estimates from Dual-Frequency GPS Observables in Real-Time

When radio waves such as the GPS signals propagate through the ionosphere they suffer an extra time delay. This time delay is related to the TEC of the ionosphere. The TEC is defined as the total number of electrons that are contained in a column with cross-sectional area of 1 m^2 along the signal path between the satellite and the receiver. The unit of measurement is (el / m^2) . The Total Electron Content Unit (TECU) is defined as: one $TECU = 1 \cdot 10^{16} \text{ el} / \text{m}^2$.

The TEC value along the path from the receiver to GPS satellite can be estimated from dual-frequency GPS observables. There are two types of TEC estimates from dual-frequency GPS receiver, namely, *pseudo-range derived TEC*, and *carrier phase derived TEC*. Pseudo-range derived TEC gives an *absolute* measure of the TEC. However, this estimated TEC is “noisy” due to the effect of multipath and measurement noise. On the other hand, carrier phase derived TEC gives the *relative* measure of the TEC due to the existence of the integer ambiguities on the L1 and L2 signals.

In order to obtain accurate absolute TEC estimates, the pseudo-range derived TEC estimates and the carrier phase derived TEC estimates must be combined somehow. There are two options. In the *post-processing* option, the “phase levelling” procedure (eg. Coster & Gaposchkin, 1989; Wilson & Mannucci, 1993, 1994; Bishop et al., 1994a; Klobuchar, 1996; Lin, et al., 1996a) is commonly used. This is accomplished by “fitting” the carrier phase derived TEC estimates to the unambiguous, but noisy, pseudo-range derived TEC estimates. The outputs are then the so-called “phase levelled TEC” estimates. The multipath effects on the pseudo-range derived TEC estimates will be

mitigated after “phase levelling” and the cycle slip(s) in the carrier phase can be detected and repaired in a prior step.

In the *real-time* option, a recursive process such as a Kalman filter is typically used to estimate TEC. Unlike the post-processing mode, carrier phase measurement failures must be detected, identified and repaired in real-time. Since the pseudo-range derived TEC is used to estimate the linear combination of the integer ambiguities on L1 and L2 signals, a special multipath mitigation technique must be implemented to overcome the pseudo-range multipath effects.

In addition, the GPS satellite and receiver L1/L2 differential delays must be subtracted from the estimated TEC values to generate unbiased absolute TEC estimates.

Hence, the first objective of this research is to develop algorithms in order to obtain real-time, accurate, and absolute TEC estimates from dual-frequency GPS observables.

Three issues should be addressed. Firstly, the multipath effects on pseudo-range derived TEC estimates should be mitigated, secondly, the carrier phase data failures must be detected and repaired, promptly and correctly, and finally, the GPS satellite transmitter and receiver L1/L2 differential delay should be estimated effectively and reliably.

b) To Develop an Algorithm for Improving the Accuracy of Real-Time Ionosphere Modelling

In order to support single-frequency GPS positioning and navigation applications, in real-time, a network of GPS dual-frequency receivers could be distributed over the region of interest. Each receiver measures the TEC for each ionospheric pierce point (defined in chapter 5). These TEC estimates are sent to a master station in real-time. The master station collects the TEC data from all receivers and generates an ionosphere model using, for example, grid-based algorithm. In the case of a grid-based algorithm, the vertical TEC at each node of an imaginary fixed grid is estimated from the collected TEC estimates. The master station sends the vertical TEC value at each node of the grid, as well as the node latitude and longitude (or an identification number), to all users via a geostationary communications satellite, or other telemetry means. Then, the user receiver

computes the latitude and longitude of its ionospheric pierce points. For each of the user's ionospheric pierce point, the receiver computes its vertical delay, interpolated from the grid using the vertical delays of the four nodes of the cell that contains the pierce point.

The “*grid-based algorithm*” is an example of a real-time regional ionosphere modelling method. Typically, a simple weighting function, such as “*inverse distance*” (eg. Conker et al., 1995) is used, and the “*Klobuchar Model*” (Klobuchar, 1987) is used to predict the ionospheric delay ratios between the grid point and reference points. It is recognised that the accuracy of the real-time regional ionosphere modelling is related to: (1) the type of weighting function, and (2) the ionosphere model used to predict the ionospheric delay ratio between the grid point and reference points. Hence, another objective of this research is to develop an alternative grid-based algorithm that improves the accuracy of real-time ionosphere modelling. Two issues should be addressed. That is: (1) the chosen weighting function, and (2) the ionosphere model used to predict the ionospheric delay ratio between the grid point and reference points should minimise the errors of the grid point's vertical TEC estimations.

1.4 Methodology and Scope of the Research

As mentioned in the earlier sections, the scope of this research includes two aspects: (1) to develop algorithms to obtain accurate absolute TEC estimates from dual-frequency GPS observables in real-time, and (2) to design algorithms that improve the accuracy of real-time ionosphere modelling. The research objectives were described in section 1.3. In order to fulfil these objectives, several algorithms were proposed and tested. The proposed algorithms and their functions are summarised below:

1) In order to obtain accurate absolute TEC estimates from dual-frequency GPS observables in real-time the following algorithms were proposed and tested:

⇒ A “*Multi-day multipath template technique*” was proposed to mitigate the pseudo-range multipath effects on the pseudo-range derived TEC in real-time.

⇒ A “*real-time failure detection and repair algorithm*” was proposed to detect and repair the GPS carrier phase “failures”, such as the occurrence of cycle slip(s), to assure the accuracy of carrier phase derived TEC in real-time.

⇒ An “*alternative L1/L2 differential delay estimation algorithm*” was proposed to estimate GPS satellite transmitter and receiver L1/L2 differential delays to obtain reliable absolute ionospheric delay estimation.

2) In order to improve the accuracy of real-time ionosphere modelling, for both the “single-frequency GPS positioning and navigation applications” and the “ionosphere community”, the following algorithm was proposed and tested:

⇒ A “*modified grid-based algorithm*” was proposed to improve the accuracy of real-time ionosphere modelling.

In order to facilitate the necessary testing of these proposed algorithms, a considerable amounts of computer software was developed in the C++ computer language. These softwares were integrated into several packages, such as “MULTIPAT” for multipath template generation, “REALTEC” for real-time TEC estimation, and “POSTEC” for post-processing TEC estimation, including “L1/L2 differential delay estimation”, “modified grid-based algorithm”, etc.

In order to study the performance of these algorithms and computer packages, as well as simulating the performance of real-time regional ionosphere modelling, many dual-frequency GPS data sets from different networks, such as the Australian Regional GPS Network (ARGN), the Japanese Geographical Survey Institute (GSI) GPS network, and the Permanent GPS Geodetic Array (PGGA) in Southern California were processed and analysed.

1.5 Outline of the Thesis

This thesis consists of seven chapters.

Chapter 1 - Introduction. This chapter introduces the research topic, the background studies, the motivation for the research, the research objectives, and the anticipated contributions from it.

Chapter 2 - Ionosphere and GPS. An introduction to that part of the atmosphere called the ionosphere. The Global Positioning System (GPS), its observables and main error sources are briefly addressed. Issues concerning the ionospheric effects on GPS, ionospheric delay estimation using GPS, and the dominant factors affecting the accuracy of ionospheric delay estimation using GPS are discussed.

Chapter 3 - Using multipath template technique to improve the real-time ionospheric delay estimation accuracy. Here, methods to mitigate GPS multipath effects are reviewed. Then the concept and methodology of a novel approach, the so-called “multi-day multipath template”, which can mitigate the pseudo-range multipath effect, is introduced. The “MULTIPAT” program developed by the author, which can generate multipath template for a static station, is described. The experimental results and comments are given. Emphasis is placed on the application for real-time ionospheric delay estimation to mitigate the multipath effect on the pseudo-range derived Total Electron Content (TEC).

Chapter 4 - Real-time failure detection and repair in TEC estimation using GPS by robust and conventional Kalman filter state estimates. The concept of conventional and robust Kalman filters is briefly reviewed. The methodology and procedure of real-time failure detection and repair in TEC estimation by robust and conventional Kalman filter state estimates are presented. The program “REALTEC”, based on the proposed methodology and procedure, is described. Experimental results from different data sets are reported. Emphases are placed on: (1) real-time detection and repair of the failure(s) caused by carrier phase cycle slip(s), and (2) real-time pseudo-range multipath mitigation

applying the “multi-day multipath template”. The performance of “REALTEC” is demonstrated by the experimental results that were obtained.

Chapter 5 - An algorithm to estimate GPS satellite and receiver L1/L2 differential delays. Firstly, the definitions of GPS satellite and receiver L1/L2 differential delay are given. Then, an algorithm developed at UNSW which can estimate the sum of the GPS satellite transmitter and receiver L1/L2 differential delay is introduced. Test results and comparisons with the results of other organisations are presented.

Chapter 6 - An alternative grid-based algorithm to improve the accuracy of real-time ionosphere modelling. A description of the principles of the conventional real-time grid-based ionosphere modelling algorithm (called conventional algorithm) is given. Then, in order to improve the accuracy of real-time ionosphere modelling, an alternative grid-based algorithm (referred to as the UNSW algorithm) is introduced. The major differences between these two algorithms are highlighted. A brief description of the features and functions of the real-time ionosphere modelling package “POSTEC” is presented. Data over different periods from different networks, such as the Australian Regional GPS Network (ARGN), the Japanese Geographical Survey Institute (GSI) GPS network, and the Permanent GPS Geodetic Array (PGGA) in Southern California were processed and analysed using the POSTEC package. Test results and a performance analysis of the UNSW algorithm, the conventional algorithm, and the polynomial algorithm are presented.

Chapter 7 - Summary, conclusions and recommendations. This is the final chapter of the thesis. Here, the summary, conclusions on the results presented are drawn and recommendations for further work are given.

1.6 Contributions of this Research

The contributions of this research can be summarised as follows:

- 1) A “multi-day multipath template” algorithm has been developed. Test results confirm that the multipath effects on GPS pseudo-ranges are effectively mitigated. Consequently, the accuracy of real-time ionospheric delay estimation can be improved significantly.
- 2) A novel “real-time failure detection and repair procedure” for ionospheric delay estimation using robust and conventional Kalman filters has been implemented and tested. Test results confirm that the GPS carrier phases failures, such as the occurrence of cycle slips, are successfully detected and repaired.
- 3) An algorithm to estimate GPS satellite and receiver L1/L2 differential delays has been proposed and tested. Test results confirm that the sum of the GPS satellite and receiver L1/L2 differential delays can be estimated effectively using this algorithm, even in a single-site case.
- 4) A new real-time, grid-based ionosphere modelling algorithm has been developed and tested. Extensive tests on data from different networks, such as the Australian Regional GPS Network (ARGN), the Japanese Geographical Survey Institute (GSI) GPS network, and the Permanent GPS Geodetic Array (PGGA) in Southern California confirm that the accuracy of real-time ionosphere modelling can be improved significantly.
- 5) A suite of computer software, “REALTEC”, “POSTEC”, etc., has been developed, implementing the above-mentioned algorithms. These programs are useful for both routine real-time ionospheric delay estimation, and for future research after minor modifications.

CHAPTER 2

IONOSPHERE AND GPS

2.1 Introduction to Ionosphere

The ionising action of the sun's radiation on the earth's upper atmosphere produces free electrons. Above about 60 km the number of these free electrons is sufficient to affect the propagation of electromagnetic waves. This "ionised" region of the atmosphere is a plasma and is referred to as the "ionosphere". Shorter wavelength radio signals, such as GPS signals, pass through the ionosphere but are affected by it.

The ionosphere has been studied for more than one hundred years. A brief history of ionospheric physics and radio communications is presented below (see eg. Davies, 1969; Hargreaves, 1992; Håkergård, 1995; Rishbeth et al., 1996). In 1839 Gauss speculated that the small daily variations of the geomagnetic field are due to electric currents flowing in a conducting layer in the Earth's upper atmosphere. In 1882 Stewart suggested that upper atmospheric currents are produced by the dynamo action of winds blowing the Earth's magnetic field. The "reflecting layer" in the upper atmosphere was in effect discovered by Marconi when he sent radio signals across the Atlantic in 1901. The idea of a "conducting layer" having the property of reflecting electromagnetic waves was taken up by Kennelly and Heaviside in 1902. The real beginning of ionospheric science came with the experiment of 1924-1925 that measured the height of the layer and revealed its stratified nature. In 1925 Breit and Tuve used a pioneering radar technique, in which the measurement of the travel time of a photoelectrically produced radio pulse gave the height of reflection. In 1925 Appleton and Barnett used BBC transmitters for a frequency-changing experiment that demonstrated the interference between the ground wave and sky wave. This was the starting point of electromagnetic probing of the ionosphere. The term "*ionosphere*" was coined in 1926, apparently independently by R.A. Watson-Watt and E.V. Appleton, though it didn't appear in the literature till later.

In 1957 the first satellite was launched (Sputnik I), and ionospheric scientists used signals from the satellite to measure the number of electrons in the ionosphere. Ever since those first measurements, signals from a wide variety of instruments, space borne or ground based, have been used to gain a better understanding of the ionosphere.

The letters E and F, and later D, used to denote the different ionospheric layers, were introduced by Appleton. The reason for this nomenclature is described by Sir Edward Appleton in a reply to a letter from Dr. J.H. Dellinger (Davies, 1969). The letter, dated March 20, 1943, runs:

“I was very interested to have your question on the early history of the nomenclature for the ionospheric layers. The story of how I came to give them the names D, E, and F is really a very simple one. In the early work with our broadcasting wavelengths, I obtained reflections from the Kennelly-Heaviside layer, and on my diagrams I used the letter E for the electric vector of the down coming waves. When therefore in the winter of 1925, I found that I could get reflections from a higher and completely different layer, I used the term F for the electric vector of the wave reflected from it. Then at about the same time I got occasional reflections from a very low height and so naturally used the letter D for the electric vector of the return waves. Then I suddenly realised that I must name these discrete strata and being rather fearful of assuming any finality about my measurements I felt I ought not to call them A, B, and C since there might be undiscovered layers both below and above them. I therefore felt that the original designation for the electric vector D, E, and F might be used for the layers themselves since there was considerable latitude for the naming of any layers that might come to light as a result of further work. I am afraid that that is all there is in the story.”

One should note that the terms “layer” and “region” are often used interchangeably, but the official terminology defines “region” in terms of range of height within the atmosphere, and uses “layer” to refer to ionisation within a given region (Rishbeth et al., 1996). The major characteristics of each region of the ionosphere, in terms of their

potential effects on GPS signals, are summarised below (note that heights given are only approximate) (Klobuchar, 1996):

D-Region, 50-90 km: This region, produced by ionisation of several molecular species from hard x rays and solar Lyman α radiations, causes absorption of radio signals at frequencies up to the low VHF band, and has no measurable effect on GPS frequencies.

E-Region, 90-140 km: The normal E region, produced by solar soft x rays, has a minimal effect on GPS. An intense E region, with irregular structure, produced by solar particle precipitation in the auroral region, might cause minor scintillation effects. Sporadic E, still of unknown origin, is very thin and also has a negligible effect at GPS frequencies.

F1, 140-210 km: The normal F1 region, combined with the E region, can account for up to 10% of the ionospheric delay encountered by GPS. Diffusion is not important at F1 region heights and, as with the normal E region, it has a highly predictable density from known solar emissions. The F1 region is produced through ionisation of molecular species, and its electron density merges into the bottom-side of the F2 region.

F2, 210-1000 km: The F2 region is the most dense and also has the highest variability, causing most of the observed effects on GPS receivers. The height of the peak of the electron density of the F2 region generally varies from 250 to 400 km, but it can be even much higher or somewhat lower under extreme conditions. The F2 region is produced mainly from ionisation of atomic oxygen, which is the principal constituent of the neutral atmosphere at those heights. The F2, and to some extent the F1, regions, cause most of the problems for radio-wave propagation at GPS frequencies.

H⁺>1000 km: The protonosphere, is a region of ionised hydrogen, with a lesser contribution from helium gas. It is of low density, but extends out to approximately the orbital height of GPS satellites. It can be a significant source of unknown electron density and consequent variability of time delay for GPS users. Estimates of the contribution of the protonosphere vary from 10% of the total ionospheric time delay during daytime hours, when electron density of the F2 region is highest, to approximately

50% during the night-time, when the F2 region is low. The electron content of the protonosphere does not change by a large amount during the day, but is depleted during major magnetic storms and can take several days to recover to pre-storm values.

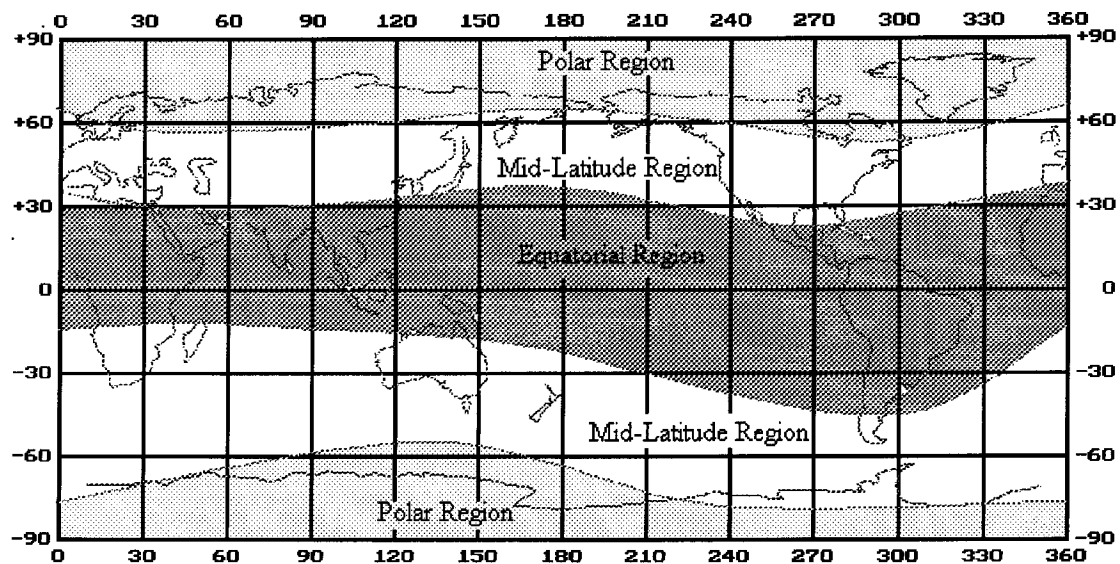


Figure 2.1. The geographic regions of the ionosphere (after Wanninger, 1994).

The geographic regions of the ionosphere are approximately indicated in Figure 2.1 (after Wanninger, 1994). However, it should be noted that these regions vary in their exact boundaries with local time and prevailing geographical conditions (eg. Bishop et al., 1991; *ibid*, 1994; Håkegård, 1995).

2.2 The Global Positioning System

2.2.1 General Description of the GPS System

The Navstar Global Positioning System is an all-weather, space-based navigation system developed by the U.S. Department of Defense (DoD) to satisfy the requirements of the military forces for accurate position, velocity, and time, in a common reference system, anywhere on or near the earth, on a continuous basis. Due to the tremendous accuracy potential of this system, and recent improvements in receiver technology, there is a growing community which utilises the GPS for a variety of civilian applications.

The system can be conveniently divided into three segments: (1) the space segment, (2) the control segment, and (3) the user segment (Rizos, 1997).

The Space Segment comprises the satellites in orbit. The basic functions of the satellites are to: (1) receive and store data transmitted by the Control Segment, (2) maintain accurate time, and (3) transmit information and signals to users. The Block I satellites were built by the Rockwell International corporation. The follow-on operational satellites are separated into four series: II, IIA, IIR and IIF. The Block II and IIA satellites were also built by the Rockwell corporation and are massive, weighing over 900 kg each. 28 Block II/IIA satellites have been built, of which 26 have been launched and activated, with the remainder to be launched between now and the end of the century. However, the replacement Block IIR satellites are being built by the General Electric Corporation (now the Lockheed-Martin Corporation), and the entire constellation of 21 satellites will be launched from 1997 through 2001. The Block IIF series are still in the design phase and may, for example, incorporate an additional civilian transmission frequency. Rockwell International was awarded the contract to build the satellites, which are to be launched between 2001 and 2015.

The Block II are maintained on a once per day upload. The Block IIA satellites incorporate features that permit the navigation message to be up to 180 days in length compared to the Block II's 14 days. The Block IIR satellites incorporate the autonomous (180 days) navigation feature based on cross link ranging between satellites. The Block IIF satellites will have the same capability. The Navstar GPS system consists of 24 satellites (21+3 active spares) at an altitude of about 20,000km. The satellites are distributed in 6 orbital planes in a manner which ensures the visibility of four or more satellites at all locations on the earth's surface at any time.

There are a number of satellite numbering conventions in use, the two most widely used are:

-
- **Navstar (or SVN) number.** The Block II satellites are numbered SVN 13 through SVN21, the Block IIA satellites are designed SVN 22 through SVN 40, and the Block IIR will be designated SVN 41 and above.
 - **PRN number,** being the number of the segment of the available 37 seven-day sections of the P-code pseudo-random-noise (PRN) code, 5 of which are associated with ground stations, and each of the remaining 32 with a different satellite (Wells et al., 1986).

The Control Segment consists of facilities required for satellite health monitoring, telemetry, tracking, command and control, ephemeris computations and uplinking. There are five ground facility stations: Hawaii, Colorado Springs, Ascension Is., Diego Garcia and Kwajalein. They perform the following functions:

- All five stations are **monitor stations**, tracking the satellites and sending the tracking data to the Master Control Station.
- Colorado Springs is the **Master Control Station (MCS)**, where the tracking data is processed in order to compute the satellite ephemerides and satellite clock corrections. It is also the station that initiates all operations of the Space Segment, such as satellite manoeuvring, signal encryption, satellite clock keeping, etc.
- Three of the stations (Ascension Is., Diego Garcia, and Kwajalein) are **upload stations** allowing for the uplink of data to the satellites (eg. Wells et al., 1986; Seeber, 1993). The data includes the ephemerides and clock correction information transmitted within the navigation message, as well as command telemetry from the MCS.

Each of the upload stations can view all the satellites once a day. All satellites can therefore be viewed by an upload station three times a day. New navigation messages and command telemetry can be transmitted to GPS satellites approximately every 8 hours, if necessary. At present the upload rate is once (and sometimes twice) per day.

The User Segment is the final link in the chain of system components. It comprises the GPS receiver, consisting of an antenna, signal tracking circuitry, user interface, power, and a microprocessor to control the operation of the receiver. There are at present over 100 manufacturers of GPS receivers of varying types ranging from low-cost, single-frequency sets to expensive dual-frequency receivers for surveying applications.

GPS satellites broadcast signals on two L-band carrier frequencies: an L1 frequency of 1575.42 MHz and an L2 frequency of 1227.60 MHz. The corresponding wavelengths are about 19 cm for L1 and 24 cm for L2. Both frequencies are modulated by so-called Pseudo-Random Noise (PRN) Codes. The L1 carrier is modulated by the C/A code, whereas both carrier frequencies are modulated by the P-code. Both signals contain the navigation message which is transmitted at a data rate of 50 bits per second. The navigation message contains information such as ephemerides, satellite clock corrections, satellite status and health flags.

2.2.2 GPS Observables

There are two main types of observables that can be made on the GPS signals: **pseudo-ranges** ("biased" ranges), and **carrier phase** (or "ambiguous" ranges).

A **pseudo-range** is the difference between the signal transmission time at the satellite and reception time at the receiver. It is scaled to units of length using the speed of light. The equation for the pseudo-range observation is (Erickson, 1992; Langley, 1993; *ibid*, 1997):

$$P = \rho + c(dT - dt) + d_{ion} + d_{trop} + d_p + \varepsilon_p \quad (2.1)$$

where P is the observed pseudo-range, ρ is the geometric range from the receiver to the satellite, c is the speed of light, dt is the satellite clock error, dT is the receiver clock error, d_{ion} is the delay due to the ionosphere, d_{trop} is the delay due to the troposphere, d_p is the orbital error, and ε_p is the pseudo-range measurement noise.

The pseudo-range measurement noise is a function of the code receiver noise ε_{prx} , and multipath ε_{mult} :

$$\varepsilon_P = f(\varepsilon_{prx}, \varepsilon_{mult}) \quad (2.2)$$

The satellite-receiver range, ρ , when expanded has the form:

$$\rho = \sqrt{(X^S - x_R)^2 + (Y^S - y_R)^2 + (Z^S - z_R)^2} \quad (2.3)$$

where X^S , Y^S , and Z^S are the satellite coordinates (which may be computed using the broadcast ephemeris data) and x_R , y_R , and z_R are the receiver's antenna coordinates.

The carrier phase observation is more complex than the pseudo-range observation. At epoch t_0 when a satellite signal is "locked on", the carrier phase observation is a measure of the misalignment between an incoming signal and that generated by the receiver oscillator. Assuming continuous signal lock, during subsequent epochs this measurement is the sum of the initial phase misalignment at epoch t_0 and the whole number of integer cycles from epoch t_0 to the current epoch t . Accordingly, from Wells et al. (1986), the measured carrier phase, $\Phi_{measured}$, can be written as:

$$\Phi_{measured} = \text{fraction}(\Phi) + \text{integer}(\Phi; t_0, t) \quad (2.4)$$

Carrier phase measurements are scaled by their wavelength to convert them from cycles to units of length. For a carrier phase measurement to represent a satellite-receiver range, one needs to add an ambiguity term to account for the unknown number of integer cycles between the satellite and receiver at epoch t_0 . Then the equation for a carrier phase observation is:

$$\Phi = \rho + c(dT - dt) + \lambda N - d_{ion} + d_{trop} + d_{\rho} + \varepsilon_{\Phi} \quad (2.5)$$

where Φ is the carrier phase observation in units of length, N is the integer cycle ambiguity, λ is the carrier phase wavelength, ε_Φ is the carrier phase measurement noise.

The carrier phase measurement noise ε_Φ is also a function of the receiver noise, ε_{prx} and multipath, ε_{mult} :

$$\varepsilon_\Phi = f(\varepsilon_{prx}, \varepsilon_{mult}) \quad (2.6)$$

Note the similarities between the pseudo-range observation equation and the carrier phase observation equation. The only differences between the two are the addition of an ambiguity term, λN , for carrier phase observations and the reversal of sign for the ionospheric delay term d_{ion} .

2.2.3 Error Sources

2.2.3.1 Satellite Clock Errors

The satellite clock error is the difference between the satellite clock time and true GPS time. The relationship between a specific satellite clock time and GPS time is transmitted by the Control Segment via a three parameter model:

$$\Delta t_{sv} = a_0 + a_1(t - t_0) + a_2(t - t_0)^2 \quad (2.7)$$

where Δt_{sv} is the difference between the satellite clock time and true GPS time, t is the measurement transmit time, t_0 is the reference time, a_0 is the satellite clock time offset, a_1 is the frequency offset, a_2 is the frequency drift.

GPS satellites carry atomic clocks which maintain highly accurate GPS time in orbit. However, the accuracy is degraded by Selective Availability (SA). SA includes satellite clock dithering which is implemented through the injection of errors in the a_1 term and

reduces the accuracy from the sub-100 nanosecond level to over 300 nanoseconds. When the difference from a satellite to two simultaneously observing receivers is performed, the satellite clock error is eliminated.

2.2.3.2 Orbital Errors

The orbital error arises from uncertainties of the predicted broadcast ephemerides affected by SA and the true orbit. The broadcast ephemerides of the satellite are updated regularly by the GPS Control Segment. In order to generate the navigation messages of the satellites, monitoring stations distributed around the world are required to continuously track all satellites in view. This data is then transmitted to the MCS and processed to create up-to-date navigation parameters. It is estimated that broadcast ephemerides error are less than 20 metres. When post-mission precise ephemerides are used in place of the broadcast ephemerides, the orbital errors are at the few decimetre level.

In addition to satellite clock dithering, SA is also implemented by degrading orbital information to deny unauthorised real-time access to the full GPS position and velocity accuracy. The consequent horizontal accuracy is less than 100 m (2drms) 95% of the time when SA is on. Orbital errors can be reduced by differential GPS.

2.2.3.3 Ionospheric Delay

The atmospheric layer from about 60 km upwards is the ionosphere and can retard GPS signals from their velocity in free space by more than 300 ns in the worst case, corresponding to a range delay of 100 metres. The ionospheric delay is a function of the Total Electron Content (TEC) along the signal path, and the frequency of the propagated signal. TEC is a function of the solar ionising flux, magnetic activity, user location and view location. Dual-frequency receivers make use of the fact that the L1 and L2 signals experience different propagation delays in the ionosphere. However, the GPS receivers used by the majority of civilian users will be of the inexpensive, single-frequency variety, which do not provide measurements to eliminate this delay.

2.2.3.4 Tropospheric Delay

The effect of tropospheric refractivity can be estimated with an accuracy of a few decimetres in most cases when the mask angle is set at 5° or greater. The vertical distribution of water vapour is less predictable than that of dry temperature and pressure, and is the major cause of the prediction error. Water vapour radiometers and stochastic modelling have been successfully used in static positioning application, but is of limited use for kinematic applications. DGPS over distances of 20 km or less appears to be the most cost effective method to limit the effect of the troposphere to below the few cm-level.

2.2.3.5 Receiver Clock Errors

Receiver clock error is the offset of the receiver clock time with respect to GPS time. In general, all receivers are synchronised with GPS time during observation sessions, but the synchronisation is accurate to the 0.1 microsecond level under Selective Availability (SA), and perhaps to the 0.01 microsecond level with SA off (Rizos, 1997). The receiver clock drift continuously and hence must be synchronised. Since the error is dependent on receiver hardware, it can be estimated as an unknown parameter or eliminated by differencing of data at one receiver to two satellite signals.

2.2.3.6 Receiver Measurement Errors

These errors consist mostly of thermal noise intercepted by the antenna or produced by the internal components of the receiver. Their magnitude depends on parameters such as tracking bandwidth, carrier-to-noise density ratio, code and code tracking mechanisation parameters. The accuracy of carrier phase measurement, although affected by the tracking bandwidth, is generally better than 1 cm. Major improvements have been made in receiver design through the 80's and manufacturers now claimed an accuracy of the order of 1 m for C/A code pseudo-range in static mode when the tracking bandwidth can be maintained at a level of one Hz. The ratio of 10 between C/A and P-code chipping rates will increase the measuring accuracy of the P-code pseudo-range substantially.

Modern receiver technology tends to bring the internal phase noise below 1 mm, and to reduce the code noise to the decimetre level (Qiu, 1993).

2.2.3.7 Multipath

Multipath affects both code and carrier measurements. Carrier multipath does not exceed 0.25λ , but can result in a large position error if the GDOP is poor (Georgiadou & Kleusberg, 1989). For C/A code pseudo-range multipath, in a test involving a TI4100 receiver in a high multipath environment in static mode, multipath of an amplitude of 20 m was observed, with systematic effects having periods of up to several minutes (Lachapelle et al., 1989). The subsequent use of an absorption ground plane reduced multipath substantially. In kinematic mode, multipath is more random in nature. The degree of randomness will obviously depend on the dynamics of the platform.

Multipath errors affect not only the accuracy of the position, but also the site occupation time necessary to resolve the carrier phase ambiguities. Possible measures to mitigate the effect are: improve the receiver performance (eg. Van Nee et al., 1994), model and calibrate the multipath error (eg. Kee & Parkinson, 1994), select an antenna site distant from reflecting objects, and design antenna/backplane combinations to further isolate the antenna from surroundings, such as the use of choke-ring ground plane and RF absorbing material.

2.2.3.8 L1/L2 Differential Delay

The P-codes transmitted from GPS satellites at the two frequencies show a synchronisation bias due to different hardware paths inside the transmitter. Similar effects are also known for the receiver hardware. The bias caused by a GPS satellite is called the “satellite L1/L2 differential delay” (or simply, satellite differential delay), and the bias caused by GPS receiver is called the “receiver L1/L2 differential delay” (or simply, receiver differential delay) (Coco, 1991; Wanninger, 1992). Some authors refer to the “satellite L1/L2 differential delay” as “satellite inter-frequency bias”, and the “receiver L1/L2 differential delay” as “receiver inter-frequency bias” (eg. Chao et al., 1995;

Håkergård, 1995). The satellite and receiver differential delays are transparent to GPS navigation and surveying users as they are simply absorbed unnoticed into the satellite receiver clock error. However, these delays introduce error in the estimation of ionospheric delay using dual-frequency GPS receivers. This error can be as large as 15 ns at L1, which is larger than a typical mid-latitude nighttime value of ionospheric delay (Coco, 1991). Thus, these differential delay cannot be ignored. **Further study and discussion on this issue will be given in chapter 5.**

2.2.3.9 Phase Centre Offsets and Imaging

The physical centre of a GPS antenna does not generally coincide with the point at which the signal is received. The point to which the radio measurements are referred, the phase centre, is the apparent electrical centre of the antenna. The phase centres of the two GPS frequencies are independent of each other and will coincide only by chance. Moreover, the apparent phase centre position will be a function of the signal incidence direction due to the non-spherical phase pattern of the antenna. The antenna patterns of the two frequencies are independent of each other.

Phase centre locations for copies of a single model of antenna tend to be consistent (Wanninger, 1992). They can be determined in laboratory experiments and then be used to correct the ionospheric observable. Schupler & Clark (1991) determined phase centre offsets and phase centre variations for 5 standard GPS antennas, and found that L1/L2 offsets can reach 0 - 5 cm ($0.0 - 0.5 \cdot 10^{16} \text{ el} / \text{m}^2$) (ibid, 1992). The full bias propagates to the ionospheric observable when the L1/L2 offset direction coincides with the signal incidence direction.

Antenna imaging is caused by conducting material in the vicinity of the antenna. An antenna "image" in the conductor interferes with the phase pattern of the antenna (Tranquilla, 1986). It causes environmental-induced phase centre variations. This effect diminishes with increasing distance between antenna and conducting body. Antenna imaging has to be avoided by careful attention to antenna siting.

2.3 Major Ionospheric Effects on GPS

The major effects the ionosphere can have on GPS are the following: (1) group delay of the signal modulation, or absolute range error, (2) carrier phase advance, or relative range error, (3) Doppler shift, or range-rate errors, (4) Faraday rotation of linearly polarised signals, (5) refraction or bending of the radio wave, (6) distortion of pulse waveforms, (7) signal amplitude fading or amplitude scintillation, and (8) phase scintillation (Klobuchar, 1996). However, only group delay and carrier phase advance effects are discussed in this section. Discussions on other effects, such as the influence of ionospheric disturbances on precise GPS measurements, can be found in the literature, such as Wanninger et al. (1992), Wanninger (1993a, 1993b, 1993c, 1993d), Klobuchar (1996), Knight & Finn (1996), etc.

When radio waves propagate through the ionosphere they suffer an extra time delay. This time delay is characterised by the Total Electron Content (TEC).

The TEC is defined as :

$$TEC = \int_S^R n_e(s) ds. \quad (2.8)$$

where n_e is the electron density in units of “number of electrons/ m^3 ”.

Equation (2.8) defines the total number of electrons that are contained in a column with cross-sectional area of 1 m^2 , along the signal path s between the satellite S and the receiver R . The unit of measurement is el / m^2 . The TECU (Total Electron Content Unit) is defined as:

$$TECU = 1 \cdot 10^{16} \text{ el} / m^2 \quad (2.9)$$

The ionosphere is a dispersive medium for radio waves. For an index of refraction n , in ionised gas, the formula for the dispersion (Seeber, 1993) is:

$$n^2 = 1 - n_e \frac{C^2 \cdot e^2}{\pi f^2 m_e} \quad (2.10)$$

where e is elementary mass; m_e is electron mass.

Rearranging, and neglecting higher order terms, gives :

$$n = 1 - \frac{C \cdot n_e}{f^2} \quad (2.11)$$

The coefficient C (=40.3) contains all the constant parameters. Equation (2.11) indicates that the index of refraction, and thus the time delay of signal propagation, is proportional to the inverse of the squared frequency.

Note that the refractive index of the ionosphere, n , was derived by Appleton and Hartree (Davies, 1969; Ajayi et al., 1980; Klobuchar, 1996; Langley, 1996). The ionospheric refractive index is the basis for the effects on GPS signals, and the first-order form, such as equation (2.11), is sufficient for most purposes. GPS users who require ionospheric corrections to centimetre or millimetre accuracy should refer to the work of Brunner & Gu (1991), and Bassiri & Hajj (1993), for additional details on higher-order ionospheric effects on GPS.

The refraction coefficient, describing the propagation of phase, can be written as a power series:

$$n_p = 1 + \frac{c_2}{f^2} + \frac{c_3}{f^3} + \frac{c_4}{f^4} + \dots \quad (2.12)$$

The coefficients c_i are independent of the carrier frequency f , however, through the electron density n_e , they depend on the state of the ionosphere. The coefficient c_2 is estimated with equation (2.11) to be $c_2 = -40.3n_e$. An approximate relation is therefore :

$$n_p = 1 - \frac{C \cdot n_e}{f^2} \quad (2.13)$$

$$n_g = n_p + f \frac{dn}{df} \quad (2.14)$$

The refraction coefficient of the group delay, n_g , follows equation (2.14), and with the first derivative of equation (2.12):

$$\frac{dn}{df} = -\frac{2c_2}{f^3} - \frac{3c_3}{f^4} - \frac{4c_4}{f^5} - \dots \quad (2.15)$$

as :

$$n_g = n_p - \frac{2c_2}{f^2} - \frac{3c_3}{f^3} - \frac{4c_4}{f^4} - \dots \quad (2.16)$$

and with equation (2.12) as:

$$n_g = 1 - \frac{c_2}{f^2} - \frac{2c_3}{f^3} - \frac{3c_4}{f^4} - \dots \quad (2.17)$$

Truncating after the first order term, it follows that :

$$n_g = 1 + \frac{C \cdot n_e}{f^2} \quad (2.18)$$

A comparison with equation (2.13) makes it clear that the effect of the ionosphere on the phase and on group velocity is equal in magnitude, but has a different sign.

Integration along the entire propagation path s yields the total effect of ionospheric refraction on the pseudo-range R :

$$d_{ion} = \int_s (n_g - 1) ds \quad (2.19)$$

$$d_{ion} \approx \frac{C}{f^2} \int_s n_e ds = \frac{C}{f^2} TEC \quad (2.20)$$

The corresponding expression for phase measurements is :

$$d_{ion} \approx -\frac{C}{f^2} \int_s n_e ds = -\frac{C}{f^2} TEC \quad (2.21)$$

where d_{ion} is the ionospheric delay in units of metres; f is the carrier frequency in Hz; TEC is total electron content in units of el/m^2 ; C is a constant equal to $40.3 m \cdot Hz^2 \cdot (el/m^2)^{-1}$ (Coco et al., 1991).

The ionospheric delay can be expressed in units of seconds as:

$$\delta_{ion} \approx \frac{C}{c \cdot f^2} \int_s n_e ds = \frac{C}{c \cdot f^2} TEC \quad (2.22)$$

where c is the speed of light in m/s; δ_{ion} is the ionospheric delay in seconds.

Equations (2.20) to (2.22) establish the relationship between the ionospheric delay and TEC. From these equations, one can find that 1 metre of ionospheric range delay at L1 signal corresponds to about 6.16 TECU, and 1 nanosecond of ionospheric time delay at L1 represents 1.85 TECU.

Equations (2.8) to (2.22) provide the physical and mathematical basis for the determination of the ionospheric delay from GPS measurements.

2.4 Total Electron Content

The parameter of the ionosphere that produces most of the effects on GPS signals is the TEC. Values of TEC from 1 to 1000 TECU, along the radio wavepath, represent the extremes of observed values in the Earth's ionosphere (Klobuchar, 1996). No value of

TEC greater than 1000 TECU has ever been measured, even along a slant path in the Earth's ionosphere during a high solar maximum period, hence that represents a safe maximum design value for system designers.

Studies of the diurnal, seasonal, and solar cycle behaviour of TEC have been conducted by numerous observers, using various measurement techniques, over more than 30 years (ibid, 1996). Although TEC measurements are generally made from satellite radio signals of opportunity, observed at arbitrary elevation angles, the TEC usually is expressed as an equivalent vertical TEC by dividing the slant TEC by the secant of the elevation angle at a mean ionospheric height, normally taken between 350 and 400 km.

The day-to-day variability of the ionosphere has a standard deviation of $\pm 20\%$ to 25 % about monthly average conditions. The deviations from monthly average conditions are more-or-less normally distributed, but there are occasional days in which the monthly average ionospheric range error is exceeded by a factor of 2 or more. A "worst case" slant range error caused by the Earth's ionosphere, including the factor of 3 conversion from vertical to low-elevation angle viewing of a GPS satellite, during solar maximum conditions, could be as high as 300 ns, or 100 m.

2.4.1 Dependence of Total Electron Content on Solar Flux

The sun's UV flux produces the ionisation found in the various regions of the ionosphere. The sun varies in its UV energy output with an approximate 11-year cycle. Direct measurements of solar UV flux only can be made above the ionosphere, which absorbs all of the UV flux in producing the ionosphere. Only a limited number of direct measurements of solar UV flux have been made, but a useful surrogate measure of solar ultraviolet activity is the number of sunspots observed on the solar disk. Sunspots have been observed since the early 1700s.

Beginning in 1947, changes in solar UV activity also have been inferred by measurements of the solar flux at a radio wavelength of 10.7 cm, or a radio frequency of approximately 2.8 GHz. Solar 10.7-cm radio wavelength flux measurements are a better quantitative

measure of solar activity than the sunspot number, which is a more subjective, manual measure of solar variability. Both the observed sunspot activity on the surface of the sun and the 10.7-cm solar radio flux are approximate measures of solar UV activity, but they are the only continuous measures of solar variability that are available.

The art of predicting long-term solar activity is not precise; thus, the best guess concerning the next solar cycle peak, expected to occur near the turn of the century, is that it will be an average one, certainly lower than four of the last five cycles (Klobuchar, 1996).

Results of studies of the correlation of solar 10.7-cm wavelength flux against the day-to-day variability of the ionosphere show poor short-term, but good long-term, agreement. Over an 11-year solar cycle, the monthly average daytime TEC correlates well with the monthly average solar radio flux, but TEC variations for individual days during most months do not correlate well with day-to-day changes in solar 10.7-cm radio flux (ibid, 1996). *Thus, the day-to-day values of TEC cannot be predicted by knowing the solar radio flux.*

2.4.2 Ionospheric Models

2.4.2.1 Empirical and Physical Models of the Ionosphere

Because of the complicated nature of the ionosphere, there have been numerous approaches to ionospheric modelling over the years. These approaches include (Schunk & Sojka, 1996): (1) Empirical models based on extensive world-wide data sets; (2) Three-dimensional, time-dependent physical models including self-consistent coupling to other solar-terrestrial regions; (3) Analytical model based on orthogonal function fits to the output obtained from numerical models; and (4) Models driven by real-time ionospheric inputs.

Empirical Models: By definition, an empirical model is dependent on measurements. Typically, the data are collected over an extended period of time via remote (ionosondes,

topside sounders, incoherent scatter radars) or in situ (rockets and satellites) techniques. The data are synthesised, binned with the aid of appropriate indices, and then fitted with simple analytical expressions. Because of this approach, the empirical models represent “average” not “instantaneous” conditions, and therefore they describe the “climatology” of the system. One of the empirical models is the *Bent Model* (Bent et al., 1972), which was developed for ground-to-satellite communications. The model provides the TEC and electron density profile in the altitude range from 150-2000 km as a function of latitude, longitude, time, season and the 10.7-cm solar flux. The Bent model has been widely used for ionospheric refraction corrections in satellite tracking. Another comprehensive empirical model of the ionosphere is the *International Reference Ionosphere* (IRI), which has been under development and revision for more than a decade (Rawer & Bilitza, 1989). The IRI provides information on the global distribution of the electron density, the ion composition, and the ion and electron temperature. The information is obtained by specifying the date, time, position, and solar activity level (sunspot number), as well as the parameters desired.

Physical Models: Physical models are very effective for elucidating the mechanisms that control ionospheric behaviours. With this approach, one tries to model the physical and chemical processes that are thought to be relevant to a given ionospheric domain, with the hope that the calculated plasma parameters actually describe the real ionosphere. These numerical models have a distinct advantage over the empirical models in that the response of the system to geomagnetic storms and sub-storms can be modelled. However, they also have the disadvantage in that the calculated response depends on solar, interplanetary, and magnetospheric drivers, which may not be well known. For example, the “Sodankyla Ion Chemistry” (SIC) model (Burns et al., 1991) was developed to model the chemical reaction of the D and E regions of the ionosphere.

Analytical and Parameterised Models: In an effort to disseminate the information obtained from the physical models, a new brand of analytical model has recently been developed. Basically, the new approach is to fit the extensive output of the physical models with relatively simple analytical functions so that the “theoretical data” can be quickly and easily accessed. Models of this type have been developed for the low,

middle, and high latitude regions of the ionosphere. For example, the Fully Analytic Ionospheric Model (FAIM) was developed for use at low and middle latitudes (Anderson et al., 1989).

Real-Time, Data-Driven Models: In recent years there has been a strong interest in developing real-time, data-driven specification and forecast models for the different regions of the solar-terrestrial system. One of the models under development is the Parameterised Real-time Ionospheric Specification Model (PRISM) (Daniell et al., 1995). PRISM is composed of two parts: (1) The PIM model is used to provide a global distribution of electron densities for a given geophysical situation, and (2) A Real Time System (RTS) then adjusts the PIM electron densities until the calculated ionospheric parameters match, in a least squares sense, all relevant real-time data.

Note that the day-to-day variability of the TEC from the monthly mean value, at any given time and location, is approximately 20-25 %, 1 sigma (Klobuchar, 1996). None of the ionospheric models presently available has been very successful in predicting the day-to-day variability of the ionosphere. In fact, the existing models are considered to be excellent if the bias between the prediction of the monthly mean TEC and the actual monthly mean TEC is within $\pm 10\%$. With a model bias of at least 10%, and a day-to-day variability that cannot yet be modelled of 20-25%, the overall error in estimating the ionospheric range error for GPS using only an ionospheric model is approximately 22-27%, 1 sigma.

2.4.2.2 Single-Frequency User Ionospheric Algorithm

In the mid-1970s, a simple algorithm was developed for the GPS single-frequency user to correct for approximately 50% of the ionospheric range error (Klobuchar, 1987). The 50% correction goal was established because the GPS satellite message had space for only eight coefficients to describe the worldwide behaviour of the Earth's ionosphere. Furthermore, these coefficients could not be updated more often than once per day, and

generally not even then. Finally, simple equations had to be used to implement the algorithm to avoid causing undue computational stress on the GPS user.

A function, namely a “half cosine” term, was used to represent the diurnal variation of TEC in the single-frequency GPS user algorithm. This half cosine (ibid, 1987) is:

$$T_{iono} = F \times \{DC + A \cos[2\pi(T - \phi) / P]\} \quad (2.23)$$

There are four potential variables in the cosine representation of diurnal TEC: (1) the amplitude, A ; (2) the period, P ; (3) The DC offset term; and (4) the phase of the maximum with respect to local noon, ϕ . Realising that only eight coefficients could be used to represent these four variables, that describe the diurnal variation of TEC over the entire globe, a study was made to determine which of the four cosine coefficients could be simplified to best use the total of eight terms available in the GPS message. When the original single-frequency GPS user ionospheric correction algorithm was proposed in 1975, the Bent Model was the best available model of worldwide TEC (Klobuchar, 1996). Thus, the Bent model was used to produce model diurnal curves of a large range of latitudes using a longitude in the approximate middle of the Contiguous United States (CONUS) region. The variation of the DC and the phase terms in the equivalent cosine representation of diurnal TEC over a large range of latitudes was much smaller than the variation of the amplitude and the period terms. Accordingly, the DC term was chosen to have a constant of 5 ns, largely because little data were available on the contribution to TEC from the Earth’s protonosphere, that region of electron above a vertical height of approximately 1000 km. The phase term was given a constant value of 14 h local time, however, the range of values found for the diurnal peak in TEC varied from 11-17 h for certain seasons, latitudes, and conditions of solar activity. The remaining terms, the amplitude and the period of the equivalent positive “half cosine”, were then each allowed to have four coefficients to represent their behaviour over the entire globe. The functional form chosen to represent the behaviour of the amplitude and the period terms was simply a cubic polynomial in geomagnetic latitude, rather than in geographic latitude, because it had been found many years before that the electron density at the peak of the F region could be fit better by using geomagnetic latitude.

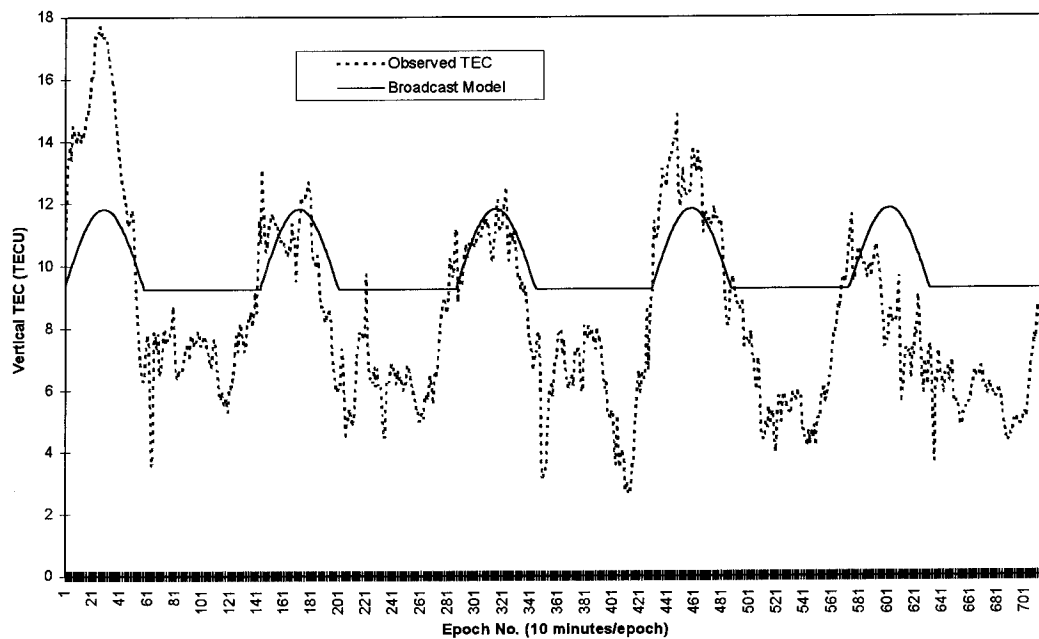


Figure 2.2. Observed TEC versus predicted TEC from broadcast model for single-frequency GPS users at location (-20°S , 140°E), ARGN region, from day 182 to 186, 1995.

There are several significant limitations of this algorithm. For example, Feess & Stephens (1987) have shown that the residual ionospheric error in comparisons they made against actual GPS dual-frequency ionospheric data, was approximately 40%. Thus, the correction for ionospheric time delay/range error was approximately 60% rms. There are certainly much better ionospheric models available than the simple, single-frequency GPS user ionospheric correction algorithm. However, going from the simple algorithm accurate to approximately 50-60%, to a state-of-the-art, complex ionospheric models that cannot beat the approximately 75% barrier of the inherent, unknown, (and presently unmodellable) day-to-day variability of the ionosphere, is hardly worth the additional trouble. If the GPS user really needs a better correction algorithm, serious consideration should be given to using either differential GPS, or a dual-frequency receiver to actually measure the first-order ionospheric differential group delay and differential carrier phase advance.

Figure 2.2 shows the observed TEC versus predicted TEC from the broadcast model for single-frequency GPS users at location (-20°S , 140°E), ARGN region, from day 182 to

186, 1995 (after Lin & Rizos, 1996b). Note that the observed TEC values were estimated by the grid-based ionosphere model described in chapter 6. From Figure 2.2 it is obvious that the broadcast ionosphere model cannot predict the day-to-day variability of the real ionosphere very well. Further details on testing of “single-frequency user ionospheric algorithm” (Klobuchar model) can be found in Feess & Stephens (1987), Håkergård (1995), Komjathy (1997), etc.

2.5 Ionospheric Delay Estimation Using GPS Measurements

2.5.1 Observation Equations

As discussed in *section 2.3*, the determination of the ionospheric delay for the GPS signals is equivalent to estimating the ionospheric TEC. Because the ionosphere is a dispersive media, differencing the measurements made at two different frequencies gives a measure of the ionospheric delay. This difference also has all the frequency-independent effects removed, such as satellite motion, tropospheric effects and clocks errors. For pseudo-range measurements, the difference is directly proportional to the slant columnar content in the ideal case. However, one must consider other issues, such as multipath, receiver and satellite L1/L2 differential delays, if we want to estimate TEC using pseudo-range measurements. Note that further discussion of the multipath issue will be given in chapter 3. The issue of GPS satellite and receiver L1/L2 differential delays will be dealt with in chapter 5.

According to equation (2.1), the L1/L2 pseudo-range measurements (in units of m) can be expressed as:

$$P_1 = \rho + c(dT - dt) + d_{ion1} + d_{trop} + d_{\rho} + \varepsilon_{P1} \quad (2.24)$$

$$P_2 = \rho + c(dT - dt) + d_{ion2} + d_{trop} + d_{\rho} + \varepsilon_{P2} \quad (2.25)$$

where P_1 , P_2 are the pseudo-ranges measured on L1 and L2 respectively, d_{ion1} , d_{ion2} are the ionospheric delays at L1 and L2 respectively, ε_{P1} , ε_{P2} are the measurement noises at

L1 and L2 respectively, and the other frequency-independent biases are defined in section 2.2.3.

From equations (2.20), (2.24), and (2.25), after rearrangement:

$$P_2 - P_1 = 40.3 \times TEC \times \left(\frac{f_1^2 - f_2^2}{f_1^2 f_2^2} \right) + \varepsilon_{P_2} - \varepsilon_{P_1} \quad (2.26)$$

Neglecting the random noise terms in equation (2.26), the TEC term derived from pseudo-ranges can be expressed as:

$$\begin{aligned} TEC &= \frac{1}{40.3} \times \left(\frac{f_1^2 - f_2^2}{f_1^2 f_2^2} \right)^{-1} \times (P_2 - P_1) \\ &= 9.5196 \times 10^{16} \times (P_2 - P_1) \quad [\text{el} / \text{m}^2] \\ &= 9.5196 \times (P_2 - P_1) \quad [\text{TECU}] \end{aligned} \quad (2.27)$$

From equation (2.27), it can be seen that 30 cm (or 1 ns) differential ionospheric delay corresponds to approximately 2.85 TECU.

Carrier phase data have less measurement noise than pseudo-range measurements. However, the carrier phase measurements contain an unknown bias, the initial integer ambiguity, hence it is not possible to estimate the absolute TEC directly.

From equation (2.5), the carrier phase measurements (in units of m) can be expressed as:

$$\Phi_1 = \rho + c(dT - dt) + \lambda_1 N_1 - d_{ion1} + d_{trop} + d_\rho + \varepsilon_{\Phi_1} \quad (2.28)$$

$$\Phi_2 = \rho + c(dT - dt) + \lambda_2 N_2 - d_{ion2} + d_{trop} + d_\rho + \varepsilon_{\Phi_2} \quad (2.29)$$

where Φ_1 , Φ_2 are carrier phase measurements at L1, L2 respectively, λ_1 , λ_2 are carrier wavelengths (in m) of L1, L2 respectively, N_1 , N_2 are integer ambiguity parameters (in cycles) at L1, L2 respectively, and ε_{Φ_1} , ε_{Φ_2} are the carrier phase noise terms.

From equations (2.21), (2.28), and (2.29), after arrangement, the TEC term derived from carrier phases without considering the noise terms, is:

$$\begin{aligned}
 TEC &= 9.5196 \times 10^{16} \times [(\Phi_1 - \Phi_2) - (\lambda_1 N_1 - \lambda_2 N_2)] \quad [\text{el} / \text{m}^2] \\
 &= 9.5196 \times [(\Phi_1 - \Phi_2) - (\lambda_1 N_1 - \lambda_2 N_2)] \quad [\text{TECU}] \\
 &= 9.5196 \times (\Phi_1 - \Phi_2) + D \quad [\text{TECU}]
 \end{aligned} \tag{2.30}$$

$$D = -9.5196 \times (\lambda_1 N_1 - \lambda_2 N_2) \quad [\text{TECU}] \tag{2.31}$$

Equation (2.30) gives only the relative measure of the TEC. To obtain accurate absolute values of TEC, the pseudo-range and carrier phase measurements must be combined. This is accomplished by fitting the carrier phase data to the unambiguous, but noisy, pseudo-range measurements.

Define:

$$TR = 9.5196 \times (P_2 - P_1) \quad [\text{TECU}] \tag{2.32}$$

$$TS = 9.5196 \times (\Phi_1 - \Phi_2) \quad [\text{TECU}] \tag{2.33}$$

Let TR_i be the i th measurement of the frequency-differenced pseudo-range using equation (2.32) in a carrier phase connected data arc consisting of M points. If TS_i is the i th frequency-differenced carrier phase measurement using equation (2.33), then equations (2.27) and (2.30) can be re-written for the i th TEC estimate:

$$TEC_i = TR_i \quad [\text{TECU}] \tag{2.34}$$

$$TEC_i = TS_i + D \quad [\text{TECU}] \tag{2.35}$$

Then a levelling constant D , for the arc, is computed as follows:

$$D = \frac{1}{M} \sum_{i=1}^M (TR_i - TS_i) \tag{2.36}$$

The TEC observable, TEC_i , is formed by adding this constant to the carrier phase measurements TS_i :

$$TEC_i = TS_i + D \quad (2.37)$$

2.5.2 Potential Limitations in Absolute TEC Estimation Using GPS

As discussed in the previous section, the principle of absolute TEC estimation from dual-frequency GPS observables is rather simple. However, since the remaining uncertain GPS satellite and receiver L1/L2 differential delays, multipath effects and noise may exceed the expected TEC values, special estimation techniques are needed to derive reliable TEC estimates (eg. Klobuchar et al., 1993; Mannucci et al., 1993; Wanninger et al., 1994; Jakowski et al., 1995; Jakowski, 1996).

Although satellite L1/L2 differential delays have been measured before launch, these values are not reliable and have to be redetermined in flight (eg. Lanyi & Roth, 1988; Wilson & Mannucci, 1993). Recently a lot of effort has been invested in estimating the level and stability of GPS satellite and receiver differential delays, as a basis for subsequent TEC estimations (eg. Wilson & Mannucci, 1994; Gao et al., 1994; Sardon et al., 1994; Wanninger et al., 1994; Chao et al., 1995; Komjathy & Langley, 1996a; Lin & Rizos, 1996a).

Sardon et al. (1994) found that the variation of the GPS satellite differential delays (relative to its mean) was below 1 ns (2.85 TECU), using different sessions of data during a 1-year period (September 1990 to September 1991).

Probably the most important error in absolute TEC estimation is caused by multipath effects on the absolute pseudo-range derived TEC (eg. Klobuchar et al., 1993; Wanninger et al., 1994; Jakowski, 1996). To reduce multipath and noise errors in the pseudo-range derived TEC, the pseudo-range and carrier phase measurements must be combined using the procedure described in the last section.

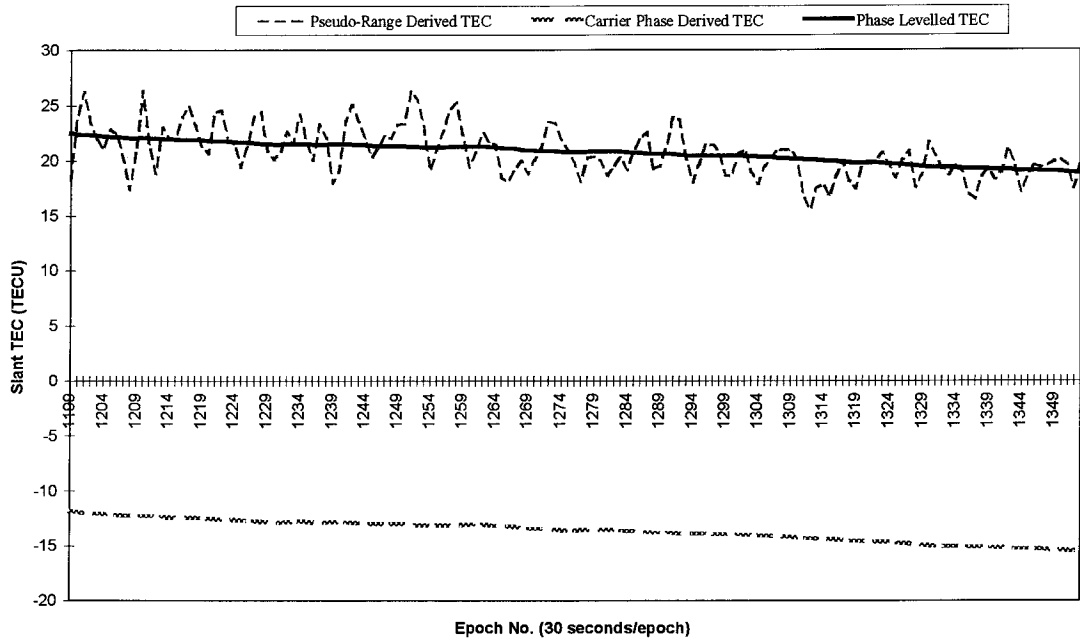


Figure 2.3. Pseudo-range derived TEC, carrier phase derived TEC, and phase levelled TEC (before correcting for the GPS satellite and receiver L1/L2 differential delay) of GPS satellite PRN 24, over site “alic”, ARGN region, on day 181, 1995.

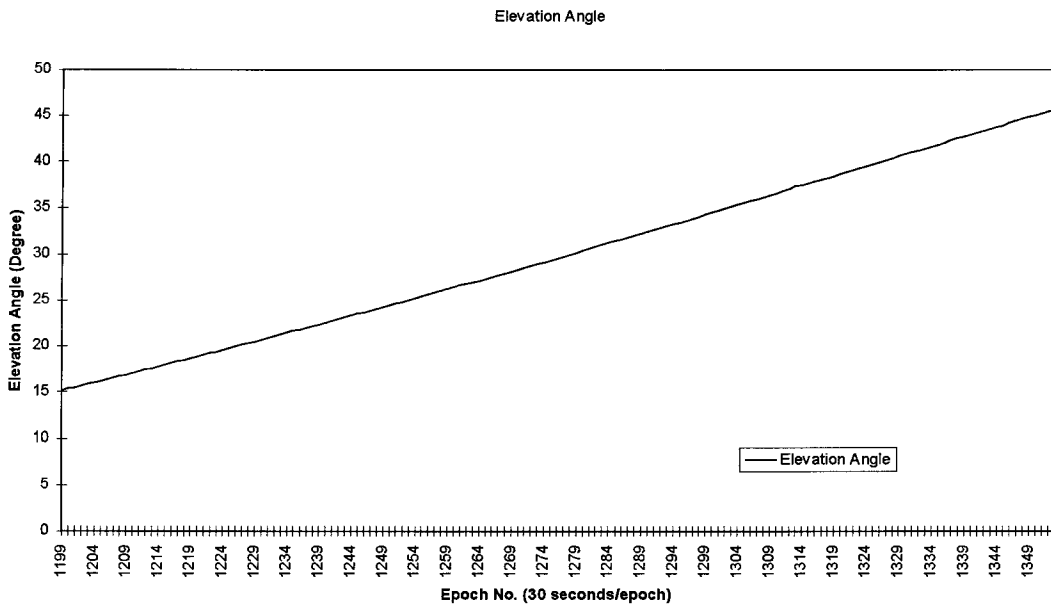


Figure 2.4. Time series of PRN 24’s elevation angle, at site “alic”, on day 181, 1995.

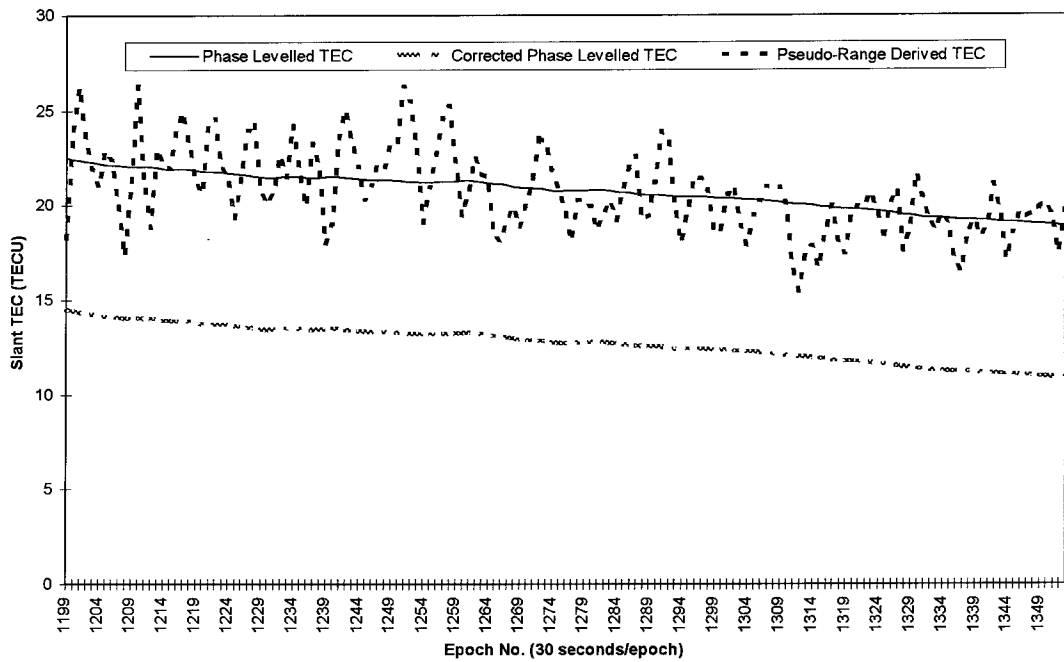


Figure 2.5. Corrected phase levelled TEC, phase levelled TEC, and pseudo-range derived TEC of PRN 24, over site “alic”, ARGN region, on day 181, 1995.

The time series of pseudo-range derived TEC, carrier phase derived TEC, and phase levelled TEC (before correcting for the GPS satellite and receiver L1/L2 differential delay) of GPS satellite PRN 24, over site “alic”, ARGN region, on day 181, 1995 are shown in Figure 2.3. The corresponding elevation angle of PRN 24 is shown Figure 2.4. Figure 2.5 shows the time series of corrected phase levelled TEC, phase levelled TEC, and pseudo-range derived TEC of PRN 24, over site “alic”, ARGN region, on day 181, 1995. The “corrected phase levelled TEC” is defined as the difference between the phase levelled TEC and the sum of GPS satellite and receiver L1/L2 differential delay. From Figure 2.5, it can be seen that the sum of GPS satellite and receiver L1/L2 differential delay of PRN 24 at site “alic”, ARGN region, on day 181, 1995 is approximately 8.0 TECU. Note that the sum of GPS satellite and receiver L1/L2 differential delay of PRN 24 was obtained using the proposed algorithm described in chapter 5.

2.5.3 Potential Limitations in Real-Time TEC Estimation Using GPS

The ionospheric effects on GPS have been discussed in previous sections. Also, it was mentioned that the ionosphere varies from day to day (cf. Figure 2.2). For single-

frequency GPS users, they can either ignore the ionospheric effects or apply the broadcast ionosphere model to correct approximately 50-60% of the ionospheric delay. For precise GPS navigation and positioning applications, such as Wide Area Differential GPS, Wide Area Augmentation System, it is beneficial to estimate ionospheric delays, in real-time, over a region of interest using a network of GPS dual-frequency receivers.

From the point view of data processing, there are several potential limitations in real-time TEC estimation using GPS, namely: (1) multipath effect on pseudo-range derived TEC, (2) carrier phase failure(s), such as the occurrence of cycle slips, and (3) GPS satellite and receiver L1/L2 differential delays. Apart from these limitations, there are certainly other limitations, such as data transmission from the reference stations to the base (or control station), data links, data latency, etc. However, this thesis will concentrate on the issues of data processing, such as (1) multipath mitigation, (2) carrier phase failure detection and repair, and (3) GPS satellite and receiver L1/L2 differential delay estimation.

CHAPTER 3
USING MULTIPATH TEMPLATE TECHNIQUE TO
IMPROVE THE REAL-TIME IONOSPHERIC DELAY
ESTIMATION ACCURACY

3.1 Introduction

With the advent of new GPS hardware and software the quality of GPS measurements has been significantly improved. Consequently, GPS multipath is the dominant error source for many precise GPS applications. Various methods for reducing multipath have been developed. The “multipath template technique” has been proposed for the reduction of the effects of multipath on a real-time GPS ionospheric monitoring system (Coco et al., 1993; Bishop et al., 1994a). The authors used single-day data to generate a “template”, and demonstrated that it was an effective way of mitigating multipath effects for ionospheric monitoring applications.

In this chapter, a “multi-day multipath template technique” (Lin & Rizos, 1997b) is introduced which uses dual-frequency GPS receivers at known stations to estimate and reduce the multipath for each pseudo-range measurement, on an epoch-by-epoch basis. This generated multipath template can be applied to successive days of data to reduce the pseudo-range multipath errors. This technique has the potential to reduce multipath effects in both geodetic and ionospheric applications. According to test results, the performance of the “multi-day multipath template technique” is superior to that of the single-day technique. The methodology is described below, followed by the test results using multi-day data from the Permanent GPS Geodetic Array (PGGA), Southern California, USA. Further test results on the application of the multipath template in the context of real-time ionospheric delay estimation are presented in chapter 4.

3.2 Methods to Mitigate GPS Multipath Effects

Multipath is the phenomenon whereby a signal arrives at an antenna via two or more different paths (Wells et al., 1986). Multipath is mainly caused by reflecting surfaces, such as metallic objects, ground or water surfaces, near the antenna (Hofmann-Wellenhof et al., 1994; Langley, 1996; Rizos, 1997). Figure 3.1 illustrates the multipath effect. Multipath has a number of effects: it may cause signal interference between the direct and indirect (reflected) signal leading to noisier measurement, or it may confuse the tracking electronics of the hardware resulting in a biased measurement that is the sum of the satellite-to-reflector (reflecting surface) and the reflector-to-antenna distance.

Multipath affects both code and carrier measurements. Carrier multipath does not exceed 0.25λ , but can result in a large position error if the GDOP is poor (Georgiadou & Kleusberg, 1989). In static mode, multipath is systematic in nature and difficult to detect or reduce using filtering techniques. For C/A code pseudo-range multipath, in a test involving a TI4100 receiver in a high multipath environment in static mode, multipath of an amplitude of 20 m was observed, with systematic effects having periods of up to several minutes (Lachapelle et al., 1989). The subsequent use of an absorption ground plane reduced multipath substantially. In kinematic mode, multipath is more random in nature. The degree of randomness will obviously depend on many factors including the dynamics of the antenna.

Multipath errors affect not only the accuracy of the position determination, but also the site occupation time needed to resolve the carrier phase ambiguities. It is hence important to avoid or mitigate multipath. Possible measures to mitigate the multipath (Lin, 1995b; Lin & Rizos, 1996b; Lin & Rizos, 1997b) are:

- 1) **Improve the receiver performance.** The narrow Early-Late (E/L) correlation spacing technique used in the NovAtel GPSCard receiver reduces the multipath error and noise level in pseudo-range measurements. However, the multipath errors in carrier phase measurements are not reduced. Meehan & Young (1992) described several techniques to reduce the code and carrier multipath developed at the Jet Propulsion Laboratory (JPL). Some of them have been tested with the Turbo Rogue

GPS receiver. Townsend & Fenton (1994) introduced a new tracking loop which took full advantage of the narrow correlator spacing design but in addition was much more resistant to multipath effects on the correlation function, and thereby reducing the multipath bias on the pseudo-range measurements. Van Nee et al. (1994) demonstrated that it was possible to largely reduce GPS code and carrier multipath errors by using a specific receiver architecture which simultaneously eliminated the parameters of line-of-sight plus multipath signals.

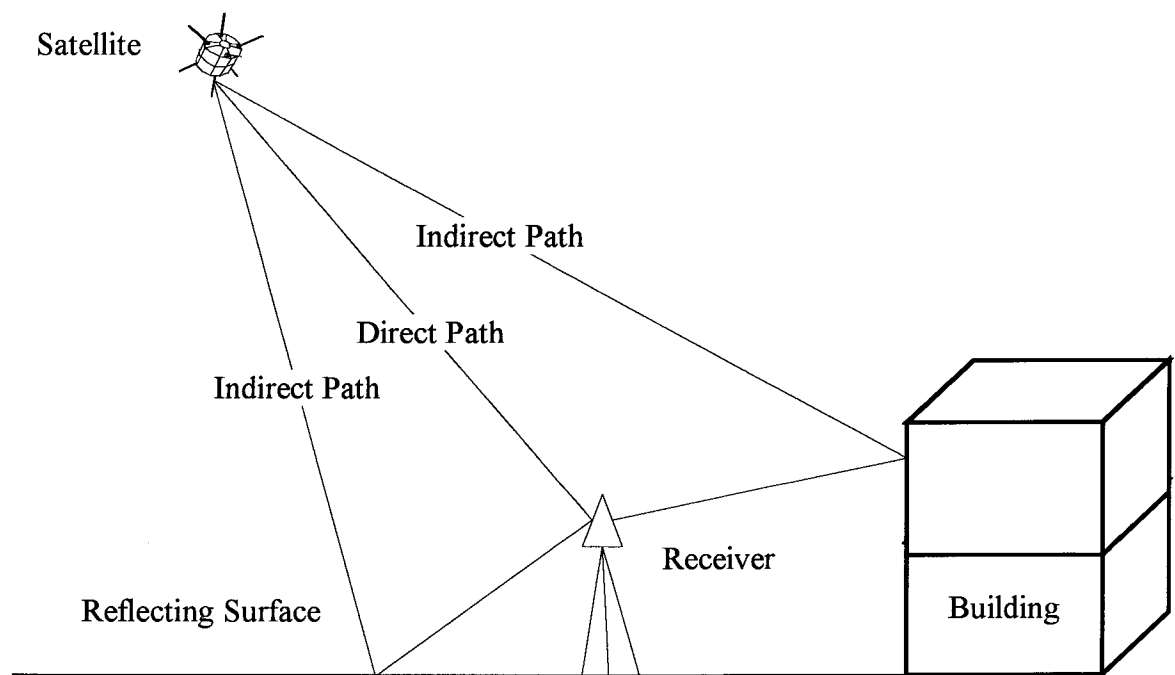


Figure 3.1. The multipath effect is a result of signals from a satellite reaching the receiver's antenna via more than one path.

- 2) **Mitigate the multipath error in code and carrier phase measurements with mathematical models.** Cohen & Parkinson (1991) used a spherical harmonic function of satellite elevation and azimuth to represent the multipath error. They successfully calibrated the relative multipath error in continuous carrier phase between two antenna for attitude determination but the same technique cannot be used for positioning. Kee & Parkinson (1994) proposed a technique to calibrate the multipath errors on the pseudo-range measurements without a change of receiver hardware, using the fact that multipath is dependent on the geometry of surfaces surrounding the GPS antenna. The technique is applicable for a static user.

- 3) **Minimise multipath effects using special operational procedures.** Select an antenna site distant from reflecting objects, and design antenna/backplane combinations to further isolate the antenna from its surroundings, such as the use of choke ring ground plane and RF absorbing material. Lachapelle et al. (1989) discussed two multipath counter-measures, that is, the use of a RF absorbent ground plane at the monitor station and the use of parallel filters at monitor station and mobile station, for marine DGPS applications. Tranquilla et al. (1989) described the performance of several antenna/ground plane configurations developed at the Jet Propulsion Laboratory for TOPEX, which might be used for improved ground station operation. Axelrad et al. (1994) described a technique which used the signal-to-noise (SNR) information to correct multipath errors in differential phase observations.
- 4) **Mitigate the pseudo-range multipath using the generated multipath template.** The multipath effects on GPS measurements depend on the physical environment and the receiver-satellite geometry. As the GPS satellites are in nearly circular orbits, at an approximate altitude of 20200 km, they will again be over the same position on the surface of the earth at the end of a sidereal day (approximately 23 hrs 56 mins in length). Thus, the viewing geometry is the same each day, but with a shift of about four minutes per day. When the physical environment about a GPS receiver remains unchanged from day to day, then the multipath effect will mostly be constant. Based on this assumption, the “multipath template technique” (Coco et al., 1993; Bishop et al., 1994a; Lin & Rizos, 1997b) has been developed and used to mitigate GPS pseudo-range multipath at static GPS reference stations. The effect of the slow day-to-day changes in satellite orbits on the performance of the multipath template technique will be further addressed in the following sections.

The above mentioned techniques are only some of the multipath mitigation approaches that are possible. In the following sections only the “multi-day multipath template” generation methodology and test results are presented.

3.3 Multi-Day Multipath Template Generation Methodology

3.3.1 Pseudo-Range Multipath Detection Equations

The simplest method of estimating the multipath error in pseudo-range measurements is to compute the differences between pseudo-range and carrier phase measurements (Evans, 1986). The pseudo-range is obtained by multiplying propagation time from satellite to receiver by the propagation velocity of the GPS signal. Pseudo-range measurements are influenced by a number of error sources. The carrier phase contains the same geometric information and is subject to the same error sources as the pseudo-range except for the ionospheric effect. The ionosphere advances the carrier phase and delays the pseudo-range. So a correction for the ionospheric effect using dual-frequency measurements has to be made.

Since the range information contained in the pseudo-range and carrier phase is highly correlated, when we subtract the carrier range measurements from the pseudo-range measurements we are eliminating the geometric information. Systematic errors, such as orbital errors, receiver clock errors and tropospheric errors will cancel as they have similar effects on the pseudo-range and carrier phase. As the multipath error in carrier phase measurements is approximately two order of magnitudes smaller than that in pseudo-range measurements this leaves, for the most part, pseudo-range multipath, receiver measurement noise and a constant bias caused by the unknown cycle ambiguity from the carrier phase.

The equations used to detect pseudo-range multipath (Rocken et al., 1994; Rizos, 1997) using a dual-frequency GPS receiver will be derived here.

According to equation (2.1), the L1/L2 pseudo-range measurements (in units of m) after considering the multipath effects can be expressed as:

$$P_1 = \rho + c(dT - dt) + d_{ion1} + d_{trop} + d_{\rho} + MP_{(P1)} + \varepsilon_{P1} \quad (3.1)$$

$$P_2 = \rho + c(dT - dt) + d_{ion2} + d_{trop} + d_{\rho} + MP_{(P2)} + \varepsilon_{P2} \quad (3.2)$$

where P_1 , P_2 are the pseudo-ranges measured on L1 and L2 respectively; ρ is the geometric range from the receiver to the satellite; c is the speed of light; dt is the satellite clock error; dT is the receiver clock error; d_{ion1} , d_{ion2} are the ionospheric delays at L1 and L2 respectively; d_{trop} is the delay due to the troposphere; d_p is the orbital error; $MP_{(P1)}$, $MP_{(P2)}$ are the pseudo-range multipath at L1 and L2 respectively; ε_{P1} , ε_{P2} are the pseudo-range measurement noise at L1 and L2 respectively.

From equation (2.5), the carrier phase measurements (in units of m), after considering the multipath effects, can be expressed as:

$$\Phi_1 = \rho + c(dT - dt) + \lambda_1 N_1 - d_{ion1} + d_{trop} + d_p + mp_{(\Phi1)} + \varepsilon_{\Phi1} \quad (3.3)$$

$$\Phi_2 = \rho + c(dT - dt) + \lambda_2 N_2 - d_{ion2} + d_{trop} + d_p + mp_{(\Phi2)} + \varepsilon_{\Phi2} \quad (3.4)$$

where Φ_1 , Φ_2 are carrier phase measurements at L1, L2 respectively; λ_1 , λ_2 are carrier wavelengths (in m) of L1, L2 respectively; N_1 , N_2 are integer ambiguity parameters (in cycles) at L1, L2 respectively; $mp_{(\Phi1)}$, $mp_{(\Phi2)}$ are the carrier phase multipath at L1, L2 respectively; $\varepsilon_{\Phi1}$, $\varepsilon_{\Phi2}$ are the carrier phase noise terms.

Define:

$$R = \rho + c(dT - dt) + d_{trop} + d_p \quad (3.5)$$

$$I1 = d_{ion1} \quad (3.6)$$

$$I2 = d_{ion2} \quad (3.7)$$

$$B1 = \lambda_1 N_1 \quad (3.8)$$

$$B2 = \lambda_2 N_2 \quad (3.9)$$

$$MP1 = MP_{(P1)} + \varepsilon_{P1} \quad (3.10)$$

$$MP2 = MP_{(P2)} + \varepsilon_{P2} \quad (3.11)$$

$$mp1 = mp_{(\Phi1)} + \varepsilon_{\Phi1} \quad (3.12)$$

$$mp2 = mp_{(\Phi2)} + \varepsilon_{\Phi2} \quad (3.13)$$

The simplified pseudo-range measurement model is:

$$P_1 = R + I1 + MP1 \quad (3.14)$$

$$P_2 = R + I2 + MP2 \quad (3.15)$$

The simplified carrier phase measurement model is:

$$\Phi_1 = R - I1 + B1 + mp1 \quad (3.16)$$

$$\Phi_2 = R - I2 + B2 + mp2 \quad (3.17)$$

We assume that carrier phase noise plus multipath is small in comparison with pseudo-range noise plus multipath and can therefore be neglected. Further, we define:

$$\alpha \equiv \frac{I2}{I1} = \left(\frac{f_1}{f_2} \right)^2 \approx 1.646944 \quad (3.18)$$

where f_1 is the L1 frequency 1.57542 GHz; f_2 is the L2 frequency 1.22760 GHz.

Find MP1 by forming the appropriate linear combination of equations (3.14) and (3.16):

$$P_1 - \Phi_1 = 2I1 + MP1 - B1 \quad (3.19)$$

$$MP1 - B1 = P_1 - \Phi_1 - 2I1 \quad (3.20)$$

And from equations (3.16), (3.17), and (3.18):

$$\Phi_1 - \Phi_2 = I2 - I1 + B1 - B2 = I1 \times (\alpha - 1) + B1 - B2 \quad (3.21)$$

$$2I1 = \frac{2}{\alpha - 1} \times (\Phi_1 - \Phi_2) - 2 \times \frac{(B1 - B2)}{\alpha - 1} \quad (3.22)$$

Thus we can write the following expression for MP1:

$$MP1 - B1 = P_1 - \Phi_1 - \frac{2}{\alpha - 1} \times (\Phi_1 - \Phi_2) + \frac{2}{\alpha - 1} \times (B1 - B2) \quad (3.23)$$

or

$$MP1 - [B1 + \frac{2}{\alpha - 1} \times (B1 - B2)] = P_1 - (1 + \frac{2}{\alpha - 1}) \times \Phi_1 + \frac{2}{\alpha - 1} \times \Phi_2 \quad (3.24)$$

Define:

$$K_1 = -[B1 + \frac{2}{\alpha - 1} \times (B1 - B2)] \quad (3.25)$$

The equation (3.24) is rewritten as:

$$\begin{aligned} MP1 + K_1 &= P_1 - (1 + \frac{2}{\alpha - 1}) \times \Phi_1 + \frac{2}{\alpha - 1} \times \Phi_2 \\ &= P_1 - 4.0915 \times \Phi_1 + 3.0915 \times \Phi_2 \end{aligned} \quad (3.26)$$

Where the second term on the left hand side of equation (3.26), ie. K_1 , is a constant. Since MP1 is assumed to be zero-mean this constant can be computed by averaging over all values of MP1 and then subtracting this average from the MP1 values computed at each epoch. Thus the multipath (after the constant K_1 has been removed) can be written as :

$$MP1 = P_1 - 4.0915 \times \Phi_1 + 3.0915 \times \Phi_2 \quad (3.27)$$

A similar derivation for MP2 yields:

$$MP2 - [B2 + \frac{2\alpha}{\alpha - 1} \times (B1 - B2)] = P_2 - (\frac{2\alpha}{\alpha - 1}) \times \Phi_1 + (\frac{2\alpha}{\alpha - 1} - 1) \times \Phi_2 \quad (3.28)$$

Define:

$$K_2 = -[B2 + \frac{2\alpha}{\alpha - 1} \times (B1 - B2)] \quad (3.29)$$

The equation (3.28) is rewritten as:

$$\begin{aligned} MP2 + K_2 &= P_2 - \left(\frac{2\alpha}{\alpha-1}\right) \times \Phi_1 + \left(\frac{2\alpha}{\alpha-1} - 1\right) \times \Phi_2 \\ &= P_2 - 5.0915 \times \Phi_1 + 4.0915 \times \Phi_2 \end{aligned} \quad (3.30)$$

or if we rearrange some terms and remove the constant term, K_2 , caused by the carrier phase biases:

$$MP2 = P_2 - 5.0915 \times \Phi_1 + 4.0915 \times \Phi_2 \quad (3.31)$$

The two equations (3.27) and (3.31) can now be used to compute L1 and L2 pseudo-range multipath.

An alternative technique for the detection of pseudo-range multipath was proposed by Lachapelle (1990). An estimate of the combined magnitude of pseudo-range multipath and pseudo-range measurement accuracy may be found by subtracting the double-differenced carrier phase observations from the double-differenced pseudo-range observations:

$$\delta = \nabla\Delta P - (\nabla\Delta\Phi + \nabla\Delta N) \quad (3.32)$$

This technique is valid for short baselines where ionospheric errors are expected to be negligible. The errors remaining in the difference quantity, δ , include receiver noise and multipath from both pseudo-range and carrier phase measurements. With receiver noise and multipath of carrier phase measurements usually being less than a few cm, the combination of carrier phase errors compared to the pseudo-range errors is negligible. This leaves pseudo-range receiver measurement noise and pseudo-range multipath errors. If the double-differenced pseudo-range measurement is known, the remaining errors in δ are likely to be a product of multipath (Erickson, 1992).

3.3.2 Multipath Template Generation

The multipath contribution to GPS measurements depends on the physical environment and the receiver-satellite geometry. The GPS satellites will again be over the same position on the earth's surface at the end of a sidereal day (approximately 23 hrs 56 mins in length). Thus the viewing geometry is the same each day, but with a shift of about four minutes per day. When the physical environment remains unchanged from day to day, then the multipath disturbance will be constant (Coco et al., 1993; Bishop et al., 1994a; Lin & Rizos, 1997b).

With these assumptions the “**multipath template**” at static GPS reference stations has been developed using the following procedure. Note that, for simplicity, only MPI for a single GPS satellite is considered. The data rate is 30 seconds, that is, 2880 epochs for a 24-hour data. The procedure is summarised below (after Lin & Rizos, 1997b):

Step 1: Pre-processing: including data loss detection (eg. how many epochs data lost?), GPS measurement outlier detection, carrier phase cycle-slip detection and repair, satellite azimuth and elevation angle computation, etc.

Step 2: Compute constant K_1 for each continuous GPS satellite arc using equation (3.26) (cf. Figure 3.2).

Step 3: Compute MPI (cf. Figure 3.3) using equation (3.27), after removing K_1 , so that the general form of MPI for any epoch can be expressed as:

$$MPI(i, j, k) \tag{3.33}$$

where $i(= 1,2,\dots,365)$ denotes the day number; $j(= 1,2,\dots,2880)$ denotes the epoch number; and $k(= 1,2,\dots,31)$ denotes the GPS satellite PRN number.

Step 4: Convert the MPI file from 2880 epochs in length to 2872 epochs. The new data sequence is expressed as (8 epochs corresponds to a 4-minute shift):

$$\begin{aligned} MP1'(i, j, k) &= 0.5 \cdot [MP1(i, j, k) + MP1(i, j + 2872, k)] \quad \text{when } j \leq 8 \\ MP1'(i, j, k) &= MP1(i, j, k) \quad \text{when } 9 \leq j \leq 2872 \end{aligned} \quad (3.34)$$

Step 5: Transfer the $MP1'$ of the current day i to $MP1''$, referring to a reference day i_0 , using the following relation:

$$MP1''(i, j, k) = MP1'(i, temp, k) \quad (3.35)$$

where $temp = (j + 2872 - (i - i_0) \cdot 8)$, if $temp \geq 2873$ then $temp = temp - 2872$; i_0 is the reference day chosen to be several days earlier than the current day i .

Step 6: Generate the “multipath template” for a static reference station:

$$MP1'''(j, k) = \sum_{i=1}^n MP1''(i, j, k) / n \quad (3.36)$$

where:

- (1) if $n = 1$, the $MP1'''(j, k)$ is a “single-day multipath template”
- (2) if $n > 1$, the $MP1'''(j, k)$ is a “multi-day multipath template”

Once the “multipath template” for $MP1$ is generated it can be used to predict the pseudo-range multipath quantity if the parameters i, j, k are given. The following equation describes the relationship between the predicted multipath and the “multipath template”:

$$\overline{MP1}(i, j, k) = MP1'''(temp1, k) \quad (3.37)$$

where:

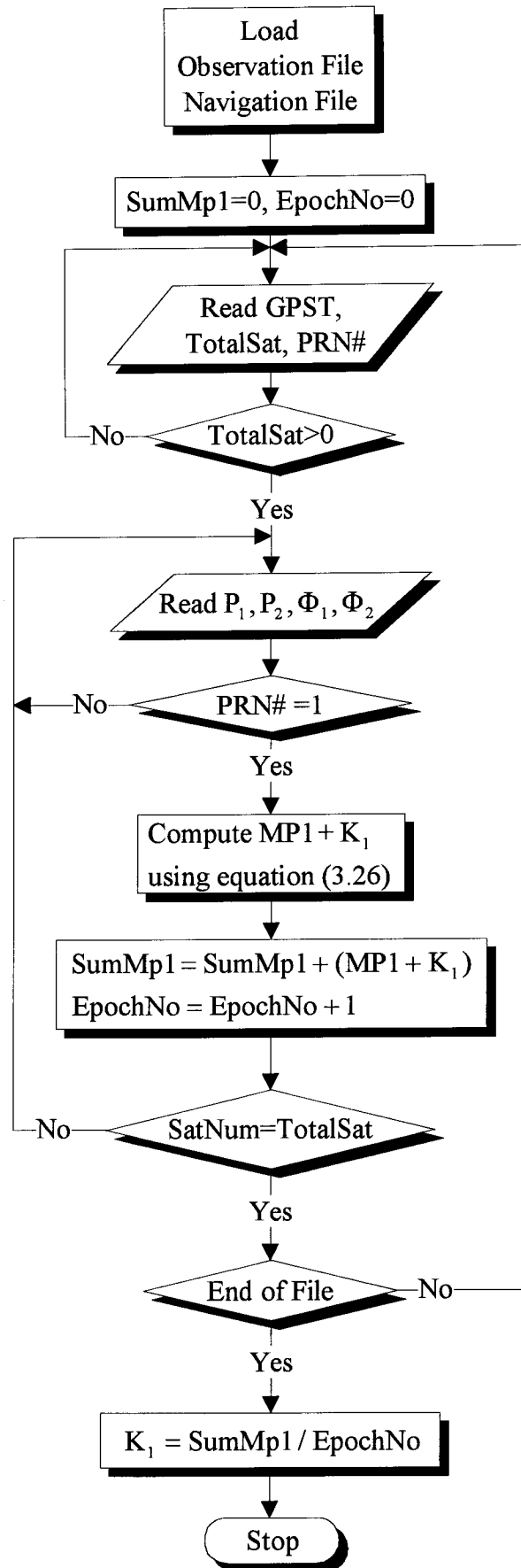
$\overline{MP1}(i, j, k)$ is the predicted multipath

$temp1 = [j + (i - i_0) \cdot 8]$, if $temp1 \geq 2880$ then $temp1 = temp1 - 2880$

The above procedure is also applicable for the prediction of MP2. In addition, it can be used to predict multipath for pseudo-range with varied data rate. However, the $j, temp, temp1$ terms in equations (3.33) to (3.37) must be modified accordingly.

Figure 3.2 shows the main steps required to compute the constant K_1 for satellite PRN 1. The main steps for computing multipath MP1 for satellite PRN 1 are illustrated in Figure 3.3. For reasons of clarity, it is assumed that there is only one arc for the tracked GPS satellite PRN 1 in this example. Symbols “SumMp1” and “EpochNo” refer to “Sum of PRN 1’s $MP1 + K_1$ values over the whole arc” and “Total epoch number of PRN1 over the whole arc” respectively. “GPST” refers to the GPS time. “TotalSat” is the total tracked GPS satellite number for that epoch. “PRN#” is the PRN number of the tracked satellite. “SatNum” refers to how much of the satellite’s data have been read.

An example of multipath MP1 computation for PRN 1 at site “blyt”, of the Permanent GPS Geodetic Array (PGGA), USA (PGGA, 1996), on day 12, 1996 is presented in Table 3.1. The Ashtech Z-12 GPS receiver was used to collect 24 hours of GPS measurements each day. The data rate was 30 seconds with a cut-off angle of 10 degrees. GPS satellite PRN 1 was tracked continuously for 6.4 hours (totally 768 epochs, that is, from epoch number 1371 to epoch 2138) on day 12, 1996, at site “blyt”. Note that the constant “ K_1 ” in Table 3.1 is computed by averaging over 768 epochs of “ $MP1 + K_1$ ” (cf. equation (3.26)). The minimum and maximum of elevation angles are 9.952° and 85.200° respectively. Time series of multipath MP1 and MP2 for PRN 1 at site “blyt”, PGGA on day 012, 1996, are plotted in Figures 3.4 and 3.5 respectively.

Figure 3.2. A block diagram of computation procedure for K_1 for satellite PRN 1.

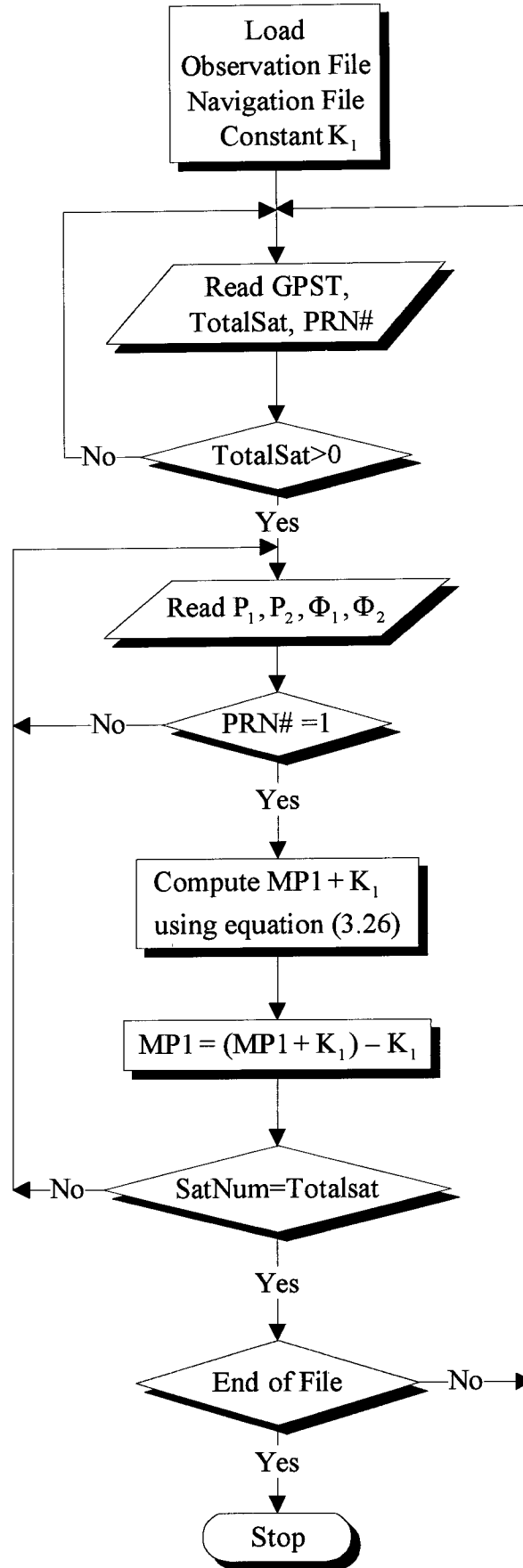
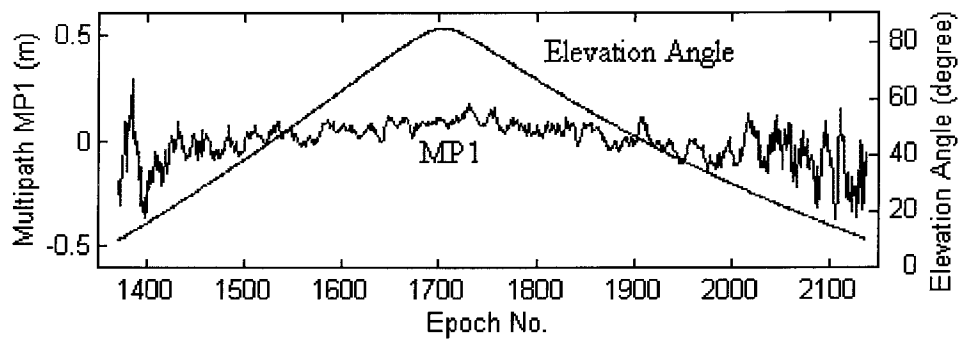
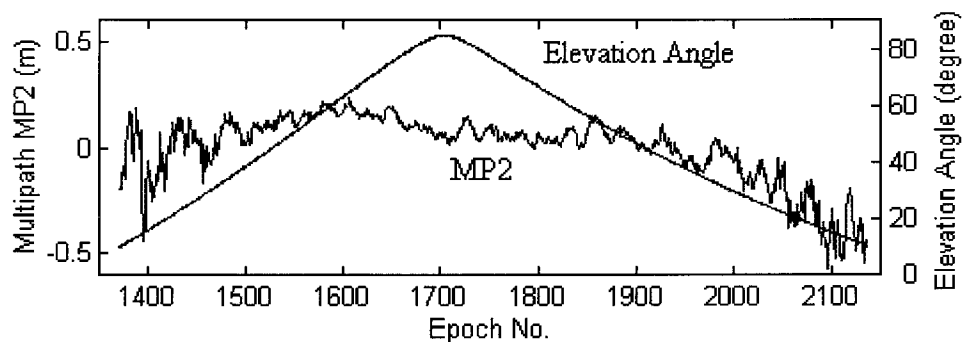


Figure 3.3. A block diagram of computation procedure for multipath MP1 for satellite PRN 1.

Table 3.1. An example of multipath $MP1$ computation of PRN 1 at site “blyt”, PGGA, day 12, 1996.

Epoch No.	$MP1 + K_1$ (m)	K_1 (m)	$MP1$ (m)	Elevation ($^\circ$)
1371	17370622.896	17370623.094	-0.198	9.952
1372	17370622.785	17370623.094	-0.309	10.157
1373	17370622.843	17370623.094	-0.251	10.363
1374	17370622.990	17370623.094	-0.104	10.569
1375	17370623.010	17370623.094	-0.040	10.775
1376	17370623.054	17370623.094	0.020	10.982
1377	17370623.114	17370623.094	0.092	11.189
1378	17370623.186	17370623.094	-0.142	11.396
1379	17370622.952	17370623.094	0.080	11.604

Figure 3.4. Time series of multipath $MP1$ for PRN 1 at site “blyt”, PGGA on day 012, 1996.Figure 3.5. Time series of multipath $MP2$ for PRN 1 at site “blyt”, PGGA on day 012, 1996.

3.4 Program “MULTIPAT”

Based on the procedure described in section 3.3, a multipath template generation software package, known as “MULTIPAT”, was developed. The main features of “MULTIPAT” are:

- 1) Generate a “multi-day multipath template” for a static reference station on an epoch-by-epoch basis using the procedures described in section 3.3.
- 2) Predict the pseudo-range multipath quantity using equation (3.37) if a multipath template data file is available.

Generally speaking, program “MULTIPAT” consists of the following parts:

- Input:

- a) GPS observation file (in RINEX format)
- b) GPS navigation file (in RINEX format)

- Processing:

- a) Detecting the arc numbers for each tracked GPS satellite in a 24 hours data
- b) Computing constants K_1 , K_2 for each arc of each tracked satellite
- c) Estimating pseudo-range multipath MP1, MP2 for each satellite on an epoch-by-epoch basis
- d) Data manipulation of the generated multipath files using equations (3.33) to (3.36)

- Output:

- a) Multi-day multipath template file
- b) Report on multipath template generation, such as the arc numbers for each tracked satellite, the constants K_1 , K_2 for each arc of each tracked satellite, etc.

c) Predicted pseudo-range multipath for a specific time

3.5 Experimental Results and Discussion

In order to test the proposed “multipath template technique”, a 12-day segment of data from site “blyt” (from day 001 to 012, 1996), of the Permanent GPS Geodetic Array, USA (PGGA, 1996) were used. Ashtech Z-12 dual-frequency GPS receivers were used to collect 24 hours of GPS measurements each day. The data rate was 30 seconds with a cut-off angle of 10 degrees.

Following the procedure described in section 3.3, the MP1 and MP2 values for each GPS satellite, at each epoch, were estimated and the “multipath template” for each day was generated. There were 12 single-day multipath templates. Day 001, 1996, was chosen as the reference day i_0 .

The multipath residual (the difference between the observed multipath and predicted multipath) for L1 pseudo-range, $\Delta MP1(i, j, k)$, is defined as:

$$\Delta MP1(i, j, k) = MP1(i, j, k) - \overline{MP1}(i, j, k) \quad (3.38)$$

where $MP1(i, j, k)$ is the observed multipath (equation (3.33)); $\overline{MP1}(i, j, k)$ is the predicted multipath (equation (3.37)); and the parameters i, j, k were defined in section 3.3.

Similarly, the multipath residual for L2 pseudo-range, $\Delta MP2(i, j, k)$, is defined as:

$$\Delta MP2(i, j, k) = MP2(i, j, k) - \overline{MP2}(i, j, k) \quad (3.39)$$

In order to analyse the test results, the multipath quantities (both MP1 and MP2) and the multipath residuals (both $\Delta MP1$ and $\Delta MP2$) are classified into four groups:

group A: -0.05 to +0.05 m;
 group B: -0.15 to +0.15 m;
 group C: -0.25 to +0.25 m;
 group D: -0.35 to +0.35 m

In this data set, there were approximately 20300 multipath observations (note, 2872 epochs for the generated multipath template). The percentage of multipath (or multipath residual) belonging to each group, for each day, was computed, as well as the standard deviations.

3.5.1 Daily Repetition of Single-Day Multipath Templates

In theory, if the physical environment around a static GPS station remains unchanged the predicted multipath effect for each single-day “multipath template” should be almost identical. As discussed in section 3.3.2, the GPS satellites will again be over approximately the same position on the earth’s surface at the end of a sidereal day (approximately 23 hrs 56 mins in length). Thus the viewing geometry is the same each day, but with a shift of about four minutes per day. Equations 3.34 to 3.37 are used to correct for the effect of GPS satellite orbit period on the multipath repetition period.

The statistics for multipath MP1 and MP2 of the 12 single-day multipath templates are shown in Tables 3.2 and 3.3 respectively. “Day No. n” ($n = 1, 2, \dots, 12$) indicates that the single-day multipath template generated from the data of day “n” was applied to compute the multipath MP1 and MP2. Over the 12-day period, for MP1, the average percentages and their standard deviations of group A, B, C and D were $41.2 \pm 1.1\%$, $87.0 \pm 0.6\%$, $95.9 \pm 0.3\%$ and $98.6 \pm 0.2\%$ respectively. In the case of MP2, the average percentages and their standard deviations of group A, B, C and D were $35.3 \pm 1.3\%$, $79.7 \pm 1.3\%$, $93.1 \pm 0.6\%$ and $97.1 \pm 0.3\%$ respectively. The average standard deviations, over the 12-day period, for MP1 and MP2 were 0.116m and 0.141m respectively.

Figure 3.6 illustrates the behaviour of each single-day multipath template for MP1, where the X-axis indicates the day number, the Y-axis denotes the multipath category (group A to D), and the Z-axis indicates the MP1 percentage.

From these test results it can be seen that: (1) for L1 pseudo-range, there is a 98.6% probability that the absolute value of MP1 is less than 0.35m, (2) for L2 pseudo-range, there is a 97.1% probability that the absolute value of MP2 is less than 0.35m, and (3) the day-to-day variations of the percentages of group A, B, C, and D for MP1 and MP2 are less than 1.3% (maximum value) that confirms the assumption of daily constancy.

Table 3.2. The multipath MP1 statistics of the 12 single-day multipath templates.

Day No.	Group				Standard deviation (m)
	A (%)	B (%)	C (%)	D (%)	
1	42.3	86.9	95.4	98.4	0.121
2	42.5	86.1	95.5	98.5	0.120
3	42.5	86.2	95.6	98.3	0.116
4	43.7	86.6	96.1	98.7	0.119
5	44.6	87.3	96.2	98.6	0.124
6	44.6	87.6	96.3	98.9	0.108
7	43.5	87.8	96.1	98.7	0.119
8	42.1	86.5	95.6	98.5	0.117
9	41.8	86.9	95.6	98.4	0.116
10	44.2	87.4	96.2	98.8	0.114
11	44.2	88.1	96.2	98.7	0.108
12	41.9	87.0	96.2	98.8	0.111

Table 3.3. The multipath MP2 statistics of the 12 single-day multipath templates.

Day No.	Group				Standard deviation (m)
	A (%)	B (%)	C (%)	D (%)	
1	34.2	77.8	92.2	96.7	0.147
2	32.8	77.0	91.9	96.8	0.149
3	34.1	78.3	93.1	97.2	0.143
4	37.1	79.6	92.8	97.1	0.141
5	36.5	79.8	93.1	97.2	0.140
6	35.4	80.5	93.4	97.3	0.139
7	35.2	79.9	93.1	97.2	0.140
8	36.4	80.8	93.6	97.4	0.136
9	34.2	80.2	92.8	96.9	0.142
10	35.8	80.7	93.1	96.7	0.142
11	36.5	80.9	93.8	97.4	0.136
12	35.2	81.0	93.8	97.4	0.135

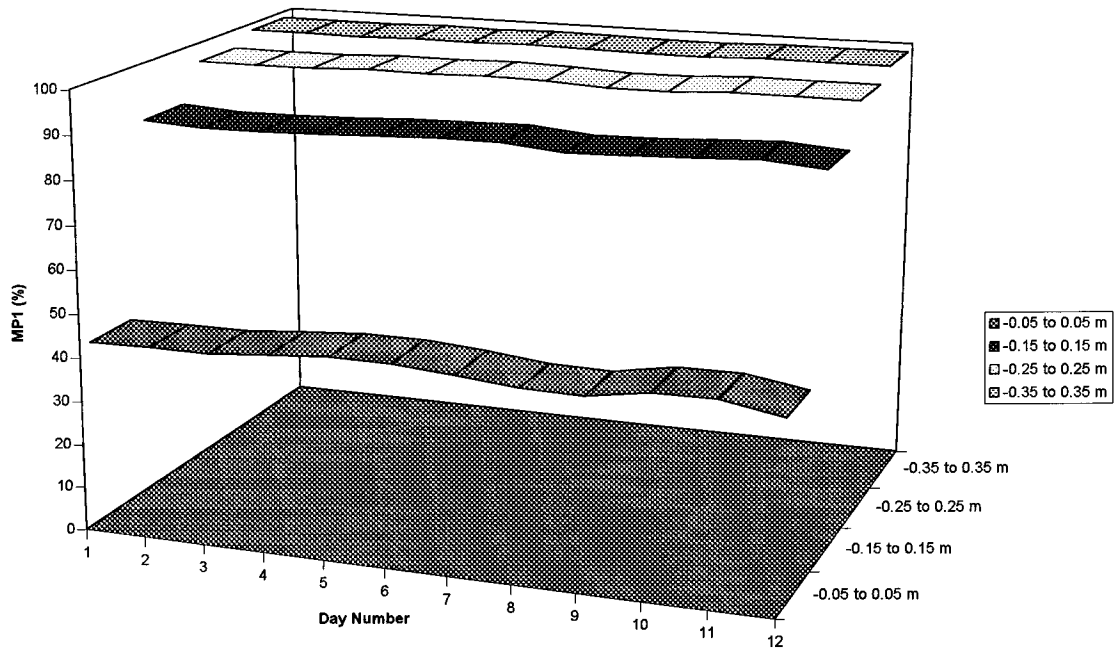


Figure 3.6. Multipath MP1 statistics of the 12 single-day multipath templates.

3.5.2 Performance of Single-Day Multipath Templates

In order to test the performance of the generated multipath template from a different day, the multipath template generated from day 012 (denoted as Day 12) was chosen as the “checking multipath template”. The multipath values predicted from the “checking multipath template” were assumed to be the true values. The other single-day multipath templates, generated from day 001 to 011, were used to predict the multipath values for Day 12. Then the multipath residuals, $\Delta MP1$ and $\Delta MP2$, were computed using equations (3.38) and (3.39) respectively. The “performance” of the generated single-day multipath template was judged according to the percentage of the computed multipath residuals belonging to each group (A, B, C, and D), for each day.

3.5.2.1 Performance Characteristics of Single-Day Multipath Templates

The statistics for multipath residuals $\Delta MP1$ and $\Delta MP2$, for day 12, after applying the single-day multipath template generated from various day’s data are summarised in Tables 3.4 and 3.5 respectively. “Day No. j ” ($j = 1, 2, \dots, 11$) indicates that the single-day

multipath template generated from the data of day “j” was applied to compute the multipath residuals.

From Tables 3.4 and 3.5, it is found that the percentages of multipath residuals, $\Delta MP1$ and $\Delta MP2$, belonging to group A to D, from “Day No. 7” to “Day No. 11” are larger than that from “Day No. 1” to “Day No. 6”. For example, for *multipath residual $\Delta MP1$* , the percentages for groups A, B, C and D were 58.2%, 90.3%, 96.5% and 98.5% respectively, if the multipath template from “day 1” was applied. On the other hand, for $\Delta MP1$, the percentages for groups A, B, C and D were 63.6%, 91.7%, 97.2% and 99.0% respectively, if the multipath template from “day 11” was applied. From Table 3.2 the percentages for groups A, B, C and D of *multipath $MP1$* for day 12 were 41.9%, 87.0%, 96.2% and 98.8% respectively, without applying any multipath template. Note that the percentage of group A for multipath residual $\Delta MP1$ (eg. 63.6% for applying the single-day multipath of day 11) is much larger than that for multipath $MP1$ (eg. 41.9% for without applying any multipath template). That is most of the multipath effects were mitigated which caused the percentage of the multipath residual belonging to group A to D increase if the multipath template was applied.

Hence, it is concluded that the performances of single-day multipath templates generated from the data of “day 7 to 11” are better than that from the data of “day 1 to 6”. Bishop et al. (1994a) also reported a similar finding. They found that a multipath template yielded good results for about 7 days. However, in all cases, the multipath template can mitigate most multipath disturbance (compared Tables 3.4 and 3.5 to Tables 3.2 and 3.3).

Table 3.4. The multipath residual $\Delta MP1$ statistics, for day 12, after applying single-day multipath template generated from various day's data.

Day No.	Group				Standard deviation (m)
	A (%)	B (%)	C (%)	D (%)	
1	58.2	90.3	96.5	98.5	0.100
2	55.6	89.7	96.3	98.6	0.103
3	58.2	90.7	96.8	98.9	0.097
4	57.2	89.3	96.6	98.8	0.099
5	58.2	90.6	96.7	98.8	0.098
6	59.9	91.1	96.8	98.7	0.098
7	63.2	91.7	97.0	98.9	0.092
8	64.1	91.9	97.3	99.0	0.090
9	64.5	92.1	97.1	98.9	0.092
10	64.5	91.8	97.1	98.9	0.091
11	63.6	91.7	97.2	99.0	0.092

Table 3.5. The multipath residual $\Delta MP2$ statistics, for day 12, after applying single-day multipath template generated from various day's data.

Day No.	Group				Standard deviation (m)
	A (%)	B (%)	C (%)	D (%)	
1	51.2	86.4	94.8	98.0	0.118
2	47.0	85.5	94.3	97.6	0.124
3	50.7	87.5	95.4	98.1	0.113
4	50.9	86.7	95.3	98.2	0.115
5	50.7	87.0	95.2	97.8	0.119
6	53.7	87.8	95.6	98.5	0.109
7	56.1	88.2	95.8	98.3	0.107
8	56.7	89.0	95.8	98.4	0.105
9	57.8	88.9	95.6	98.3	0.109
10	57.3	88.9	95.5	98.3	0.108
11	59.1	89.0	95.9	98.4	0.104

3.5.2.2 Performance Comparisons as a Function of Satellite PRNs

From the results of the previous section, the multipath template can mitigate most of the multipath disturbance. In other words, the percentages of multipath residuals, $\Delta MP1$ and $\Delta MP2$, belonging to groups A to D with applying multipath template are much larger than the percentages of multipath quantities, MP1 and MP2, belonging to groups A to D without applying any multipath template. In order to further study the performance of the

single-day multipath template, the percentages of multipath MP1 before applying multipath template (ie. the “observed” multipath of day 12) and the percentages of multipath residual Δ MP1 after applying the single-day multipath template generated from the data of day 11 were analysed on a satellite by satellite basis.

The statistical comparison between the multipath MP1 (before applying multipath template) and the multipath residual Δ MP1 (after applying single multipath template generated from the data of day 11) for day 12, as a function of GPS satellite PRN number is summarised in Table 3.6. “Day 12” represents that the multipath MP1 statistics for day 12 without applying any multipath template. “Day 12 - Day 11” represents that the multipath residual Δ MP1 statistics for day 12 after applying the single-day multipath template derived from the data of day 11. “PRN No. k” ($k = 1, 2, \dots, 31$) means that the GPS satellite PRN number is “k”. It can be seen that the percentages of Δ MP1 belonging to groups A and B of “Day 12 - Day 11” are much larger than the percentages of MP1 belonging to A and B of “Day 12” for each PRN. Note that there is a big difference between the percentages for MP1 and Δ MP1, belonging to group A (ie. -0.05 to +0.05 m). This confirms the finding of the previous section that the multipath template technique is an effective procedure for mitigating multipath.

In order to further illustrate the performance of the multipath template, the statistical comparison between the percentages of group A, for MP1 and Δ MP1, for each GPS satellite, from the results of Table 3.6, are plotted in Figure 3.7. The minimum and maximum values of the percentages of group A for MP1 were 19.3% (PRN 29) and 64.4% (PRN 25) respectively. On the other hand, the minimum and maximum values of the percentages of group A for Δ MP1 were 42.3% (PRN 31) and 88.0% (PRN 28) respectively. The percentages belonging to group A, of the multipath residual Δ MP1, for most (92%) of the PRNs increased significantly when the single-day multipath template was applied. For example, for PRN 12, the percentages belonging to group A of MP1 and Δ MP1 were 24.8% and 82.2% respectively. In other words, there was only 24.8% of the multipath quantities, MP1, whose absolute values were less than 0.05m. However, for Δ MP1, the percentage became 82.2%. That is, most of the multipath disturbance had

been mitigated after applying the multipath template. Note that in the case of satellites 26 and 31, the technique is not so successful, possibly due to their low elevation angles and the existence of multiple arcs during the 24-hour period.

Table 3.6. Statistical comparison between the multipath MP1 (before applying multipath template) and the multipath residual Δ MP1 (after applying single multipath template generated from the data of day 11) for day 12, according to GPS satellite PRNs.

PRN No.	Day 12				Day 12 - Day 11			
	MP1 of Group				Δ MP1 of Group			
	A (%)	B (%)	C (%)	D (%)	A (%)	B (%)	C (%)	D (%)
1	43.4	92.3	96.9	99.5	74.8	93.6	97.5	99.1
2	39.7	87.5	98.4	99.7	62.7	92.3	97.9	99.6
4	46.6	87.9	97.1	99.5	64.5	91.8	97.7	99.2
5	50.1	92.8	98.7	99.6	79.4	97.3	99.3	99.7
6	44.6	91.6	96.0	97.9	67.5	90.7	95.9	97.0
7	31.8	78.7	92.7	96.8	49.6	90.0	96.4	98.2
9	41.8	78.3	91.6	96.4	49.7	89.0	97.6	99.8
12	24.8	80.8	93.9	98.9	82.2	98.9	99.6	99.9
14	31.6	85.7	96.9	98.7	56.8	91.6	97.7	99.3
15	43.0	84.8	94.7	97.9	53.8	84.3	92.7	95.9
16	42.3	84.5	95.6	99.1	54.3	84.5	95.2	99.2
17	35.7	88.1	96.3	97.9	75.6	97.1	99.1	99.5
18	47.2	90.4	98.4	99.7	66.6	93.4	97.2	98.7
19	40.1	91.1	98.6	99.9	59.2	92.4	97.2	98.8
20	46.3	85.5	95.4	98.3	57.5	85.1	90.9	94.5
21	33.8	87.0	95.9	98.2	73.7	93.1	98.2	99.9
22	35.0	85.4	94.1	97.2	46.3	84.4	96.3	98.9
23	52.6	88.5	94.9	99.6	72.5	95.8	99.3	99.8
24	51.4	91.4	97.4	98.5	67.5	93.8	98.0	99.6
25	64.4	94.5	99.3	100.0	66.5	94.5	98.4	99.4
26	44.4	84.3	94.7	98.6	46.4	86.4	95.7	98.6
27	50.4	93.6	96.8	99.1	72.2	94.0	97.4	99.5
28	49.5	91.2	99.1	99.9	88.0	99.2	99.9	100.0
29	19.3	83.0	96.2	99.3	65.6	94.8	97.8	99.2
31	42.0	81.0	93.8	98.1	42.3	85.0	95.5	98.3

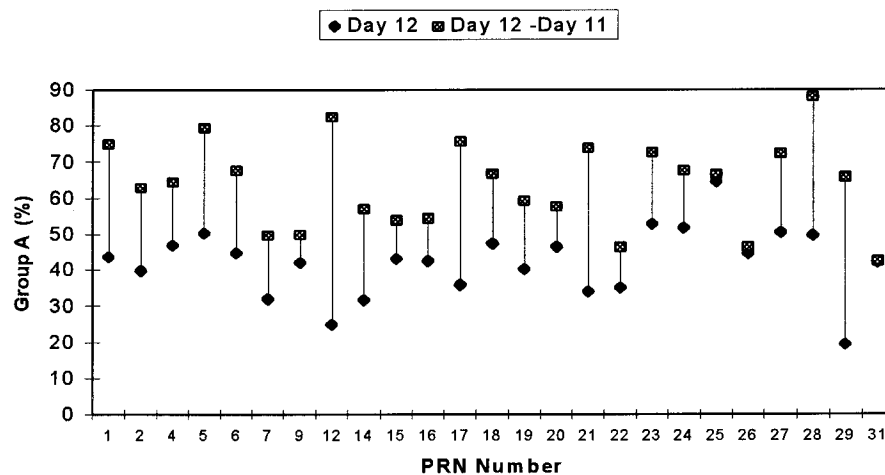


Figure 3.7. The statistical comparison between the percentages of group A, for multipath MP1 (ie. “Day 12”, before applying multipath template) and multipath residual Δ MP1 (ie. “Day 12 -Day 11”, after applying multipath template generated from the data of day 11) for each GPS satellite, for day 12, from the results of Table 3.6.

3.5.2.3 Performance Comparisons as a Function of Satellite Elevation

In order to study the effect of satellite elevation angle on the performance of the multipath template, the same data set was processed and analysed again, but on a satellite elevation by satellite elevation basis. The satellite elevation angles, during the 24-hour period, were grouped into six elevation bands, each 15° wide.

From the analysis of previous sections, the major impact of applying the multipath template is to increase the percentages for multipath residual, Δ MP1 and Δ MP2, belonging to group A. Hence, only the statistical comparison between the percentages of group A, for multipath MP1 and multipath residual Δ MP1, for day 12, according to satellite elevation, is plotted in Figure 3.8. “Day 12” represents the percentage of “multipath” MP1 belonging to group A, for day 12, before applying any multipath template, for each elevation band. “Day 12 - Day 11” represents the percentage of “multipath residual” Δ MP1 belonging to group A, for day 12, after applying the single-day multipath template generated from the data of day 11, for each elevation band. “Obs. Num. % per Band” means that there is “m%” of the total observation number, during the 24-hour period, belonging to elevation band “n”.

It can be seen from Figure 3.8 that: (1) about 90% of the observations related to elevation angles larger than 15°, and (2) the difference between the percentages belonging to group A, for multipath MP1 and multipath residual Δ MP1, increased as the elevation angles increased (for example, the differences for elevation band “00 - 15” to “75 - 90” were 3.4%, 10.5%, 18.1%, 23.6%, 49.8% and 60.6% respectively; that is, more multipath disturbance were mitigated as the elevation angle increased by applying the multipath template). Hence, from Figure 3.8, it can be concluded that the performance of the multipath template is correlated with elevation angle.

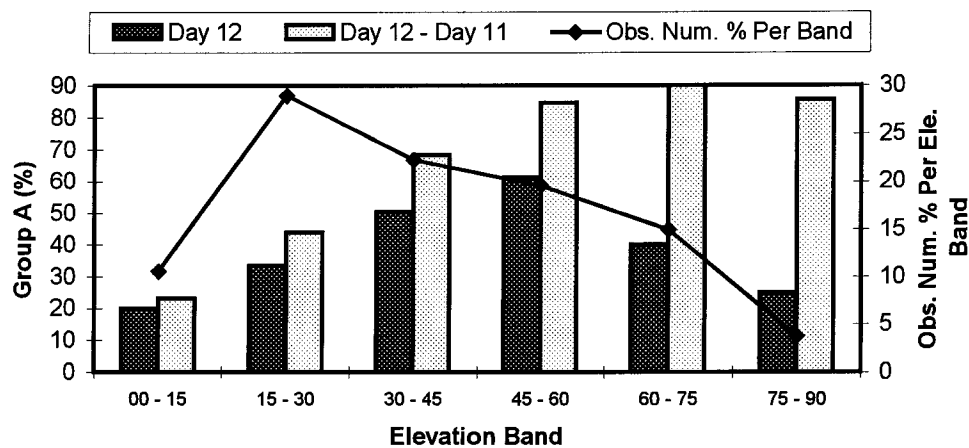


Figure 3.8. The statistical comparison between the percentages of group A, for multipath MP1 (ie. “Day 12”, before applying multipath template) and multipath residual Δ MP1 (ie. “Day 12 -Day 11”, after applying multipath template generated from the data of day 11), for day 12, according to satellite elevation.

3.5.2.4 Performance Comparisons as a Function of Satellite Azimuth

In order to study the effect of satellite azimuth on the performance of the multipath template, the same data set was processed and analysed again, but on a satellite azimuth by satellite azimuth basis. The satellite azimuth, during the 24-hour period, were grouped into six segmented bands each with 60° width.

The statistical comparison between the percentages of group A, for multipath MP1 and multipath residual Δ MP1, for day 12, according to satellite azimuth, is plotted in Figure

3.9. “Day 12” represents the percentages of multipath MP1 belonging to group A, for day 12, before applying any multipath template, for each azimuth band. “Day 12 - Day 11” represents the percentage of the “multipath residual” Δ MP1 belonging to group A, for day 12, after applying the single-day multipath template generated from the data of day 11, for each azimuth band. “Obs. Num. % per Band” means that there is “m%” of the total observation number, during the 24-hour period, belonging to azimuth band “n”.

From Figure 3.9 it can be seen that the group A MP1 percentages of day 12 for the six azimuth bands are similar (from 38.9% to 43.3%). However, after applying the multipath template, the percentages of multipath residual Δ MP1 belonging to group A increases noticeably. The reasons for this band-difference could be: (1) it includes observations from different elevation bands, (2) varying environmental conditions in the different azimuth bands.

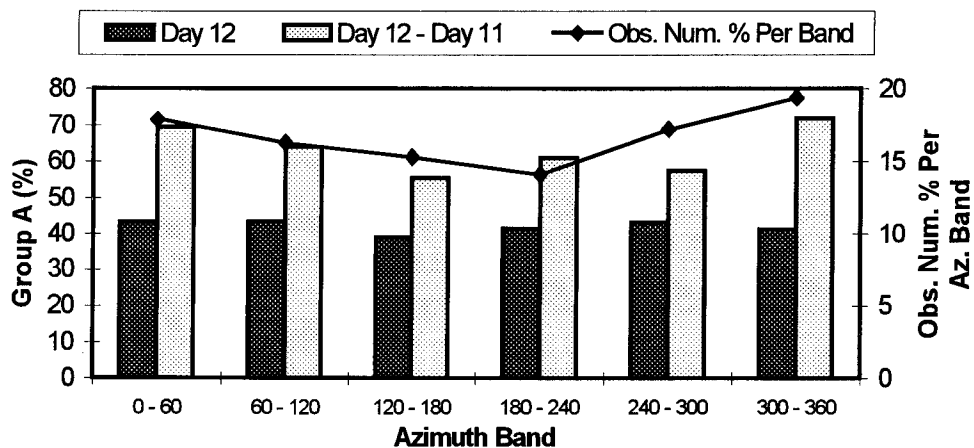


Figure 3.9. The statistical comparison between the percentages of group A, for multipath MP1 (ie. “Day 12”, before applying multipath template) and multipath residual Δ MP1 (ie. “Day 12 -Day 11”, after applying multipath template generated from the data of day 11), for day 12, according to satellite azimuth.

3.5.3 Performance of Multi-Day Multipath Templates

Different “multi-day multipath templates” were generated using equation (3.36), starting from day 011 plus day 010, then adding day 009, and so on. As before, the multipath template generated from day 012 is chosen as the “checking multipath template”. The “multipath residuals”, $\Delta MP1$ and $\Delta MP2$, were computed using equations (3.38) and (3.39) respectively. The “performance” of the generated multi-day multipath template was judged according to the percentages of the computed multipath residuals belonging to each group (A, B, C, and D).

The multipath residual statistics of $\Delta MP1$ and $\Delta MP2$, for day 12, after applying various multi-day multipath templates are summarised in Tables 3.7 and 3.8 respectively. The “Day ID” in these two Tables denotes the various multi-day multipath templates, where the codes from “A” to “L” refer to:

Day ID A: without applying any multipath template, ie. the original data of day 12

Day ID B: applying multipath template from day 11 data

Day ID C: applying multipath template from data of (day 11 plus day 10)

Day ID D: applying multipath template from data of (day 11 to day 09)

Day ID E: applying multipath template from data of (day 11 to day 08)

Day ID F: applying multipath template from data of (day 11 to day 07)

Day ID G: applying multipath template from data of (day 11 to day 06)

Day ID H: applying multipath template from data of (day 11 to day 05)

Day ID I: applying multipath template from data of (day 11 to day 04)

Day ID J: applying multipath template from data of (day 11 to day 03)

Day ID K: applying multipath template from data of (day 11 to day 02)

Day ID L: applying multipath template from data of (day 11 to day 01)

Note that the results of “Day ID A”, actually represent the “multipath” of MP1 and MP2, for day 12, without applying any multipath template. The results of “Day ID B” represent the “multipath residual” of $\Delta MP1$ and $\Delta MP2$, for day 12, after applying the “single-day multipath template” generated from the data of day 11. The results of “Day

ID C” and so on, represent the “multipath residual” of $\Delta MP1$ and $\Delta MP2$, for day 12, after applying the various “multi-day multipath templates”.

From Tables 3.7 and 3.8, it is found that: (1) the percentages belonging to group A of “multipath” MP1 and MP2, for “Day ID A” (41.9% and 35.2%), are smaller than the percentages belonging to group A of “multipath residual” $\Delta MP1$ and $\Delta MP2$, for “Day ID B” (63.6% and 59.1%) to “Day ID L” (71.1% and 64.2%), (2) the percentages belonging to group A of “multipath residual” $\Delta MP1$ and $\Delta MP2$ (63.6% and 59.1%), for “Day ID B” (ie. the single-day multipath template of day 11), are smaller than the percentages belonging to group A of “multipath residual” $\Delta MP1$ and $\Delta MP2$, for “Day ID C” (68.8% and 62.5%) to “Day ID L” (71.1% and 64.2%) (Note that “Day ID C” to “Day ID L” represent the various multi-day multipath template), and (3) the maximum percentages belonging to group A of “multipath residual” $\Delta MP1$ and $\Delta MP2$, occur at “Day ID F”.

Note that the “performance” of the generated multipath template (both single-day and multi-day) was judged according to the percentage of the computed multipath residuals belonging to each group (A, B, C, and D). Hence from the above analysis, it can be concluded that: (1) both single-day and multi-day multipath template can mitigate most of the multipath disturbance, (2) the performance of the multi-day multipath template is better than that of the single-day multipath template, and (3) the performance of the multi-day multipath template of “Day ID F” (ie. multi-day multipath generated from the data of day 11 to day 07) is better than that of other multi-day multipath templates.

Figure 3.10 illustrates an example of performance comparisons of “Day 12” values, “Day 12 - Day 11” values, and applying the multi-day multipath template. The X-axis indicates the “multipath bands” (from M1 to M7), and the Y-axis denotes the percentage of multipath (or multipath residual) for each multipath band, for “Day 12”, “Day 12 - Day 11”, and “Day 12 - Day (11...7)”. “Day 12” refers to the statistics of “multipath” MP1, for day12, without applying any multipath template. “Day 12 - Day 11” refers to the statistics of “multipath residual” $\Delta MP1$, for day12, after applying the “single-day multipath template” generated from the data of day 11. “Day 12 - Day (11...7)” refers to

the statistics of “multipath residual” $\Delta MP1$, for day12, after applying the “multi-day multipath template” generated from the data of day 11 to day 7.

The “multipath bands” (from M1 to M7) are defined as:

M1: -0.35 to -0.25 m; M2: -0.25 to -0.15 m; M3: -0.15 to -0.05 m;
M4: -0.05 to +0.05 m; M5: +0.05 to +0.15 m; M6: +0.15 to +0.25 m;
M7: +0.25 to +0.35 m;

From Figure 3.10 it can be seen that: (1) the percentage of multipath residual $\Delta MP1$, for “Day 12 - Day (11...7)”, for multipath band “M4” is much larger than that for “Day 12” and “Day 12 - Day 11”, and (2) the percentage of the multipath residual (or multipath) belonging to multipath band “M3” to “M5”, ie. within $\pm 0.15m$, for “Day 12”, “Day 12 - Day 11”, and “Day 12 - Day (11...7)”, are 87.1%, 91.7%, and 95.0% respectively. These results further confirm that: (1) the multipath template can mitigate most of the multipath disturbance, and (2) the multi-day multipath template is superior to that of the single-day multipath template.

Table 3.7. The multipath residual $\Delta MP1$ statistics, for day 12, after applying various multi-day multipath templates.

Day ID	Group				Standard deviation (m)
	A (%)	B (%)	C (%)	D (%)	
A	41.9	87.0	96.2	98.8	0.111
B	63.6	91.7	97.2	99.0	0.092
C	68.8	93.8	98.0	99.3	0.079
D	71.3	94.5	98.4	99.6	0.074
E	71.9	94.8	98.7	99.6	0.071
F	72.4	95.1	98.8	99.7	0.070
G	72.1	95.0	98.8	99.7	0.070
H	71.8	94.9	98.8	99.7	0.071
I	71.5	95.0	98.8	99.7	0.070
J	71.4	95.1	98.8	99.7	0.070
K	71.0	95.2	98.8	99.7	0.070
L	71.1	95.0	98.8	99.7	0.070

Table 3.8. The multipath residual $\Delta MP2$ statistics, for day 12, after applying various multi-day multipath templates.

Day ID	Group				Standard deviation (m)
	A (%)	B (%)	C (%)	D (%)	
A	35.2	81.0	93.8	97.4	0.135
B	59.1	89.0	95.9	98.4	0.104
C	62.5	90.9	96.9	99.1	0.093
D	64.6	91.6	97.3	99.2	0.088
E	65.1	92.0	97.5	99.3	0.086
F	65.3	92.2	97.7	99.4	0.084
G	65.2	92.2	97.7	99.4	0.083
H	64.3	92.2	97.7	99.3	0.085
I	64.3	92.3	97.8	99.3	0.084
J	64.4	92.3	97.8	99.4	0.084
K	64.1	92.2	97.9	99.4	0.084
L	64.2	92.3	97.9	99.3	0.084

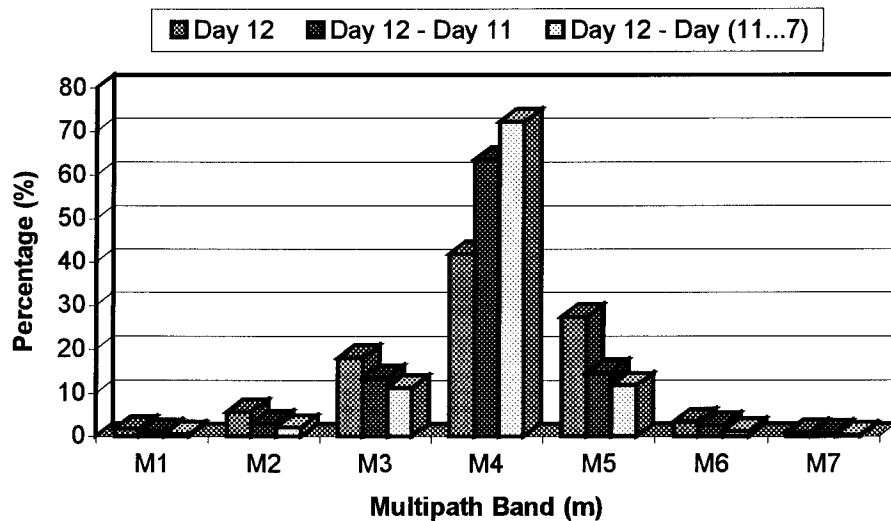


Figure 3.10. The performance of the multi-day multipath template compared to that of the single-day multipath template.

3.5.4 Comments on Multipath Template Technique

As discussed in section 3.3.2, the multipath contribution to GPS measurements depends on the physical environment and the receiver-satellite geometry. That is, the multipath is a kind of *site-dependent* and *satellite-dependent* error to GPS measurements. The data

from site “blyt” (Blythe) of PGGA were used to test the proposed “multipath template technique” due to their data availability over a 12-day period. According to the test results, it is demonstrated that the proposed multipath template technique, either single-day or multi-day multipath template, is useful for mitigating the multipath effects on GPS pseudo-range measurements at a static site.

Other examples of applying the proposed multipath template technique in real-time TEC estimation are presented in section 4.5.3. The UNSW data and PGGA data (cf. Section 4.5.1) were processed and analysed. According to the test results, the proposed multi-day multipath template works well at sites “ec05” (UNSW) and “blyt” (PGGA). Hence, it can be concluded that the proposed multipath template technique is suitable for mitigating pseudo-range multipath at static reference stations.

3.6 Application in Real-Time Ionospheric Delay Estimation

Referring to equation (2.27), the pseudo-range derived TEC is:

$$TEC = 9.5196 \times (P_2 - P_1) \text{ [TECU]} \quad (3.40)$$

However, if the multipath MP1 and MP2 are considered, from equations (2.20), (3.1), (3.2), (3.10), and (3.11), after rearrangement:

$$P_2 - P_1 = 40.3 \times TEC \times \left(\frac{f_1^2 - f_2^2}{f_1^2 \cdot f_2^2} \right) + MP2 - MP1 \quad (3.41)$$

Therefore, the TEC term (in units of TECU) derived from the pseudo-range measurements can be expressed as:

$$\begin{aligned} TEC &= 9.5196 \times [(P_2 - P_1) - (MP2 - MP1)] \\ &= 9.5196 \times (P_2 - P_1) - 9.5196 \times (MP2 - MP1) \end{aligned} \quad (3.42)$$

From equation (2.32), equation (3.42) can be rewritten as:

$$TEC = TR - 9.5196 \times (MP2 - MP1) \quad (3.43)$$

The multipath template can be generated from the GPS measurements of the previous days. In a real-time TEC estimation application, the current day's multipath for MP1 and MP2 can be predicted beforehand by the generated multipath template using equation (3.37) and stored in a file. This multipath file is then input to the real-time TEC estimation software, such as program "REALTEC" (described in chapter 4). Using equation (3.43), the multipath effect on pseudo-range derived TEC estimate is therefore mitigated for each tracked GPS satellite on an epoch-by-epoch basis (Lin, 1997). The test results of applying the multipath template technique for real-time ionospheric delay estimation are presented in chapter 4.

3.7 Concluding Remarks

A "multi-day multipath template" algorithm has been implemented and tested. The algorithm can be used to generate either a "single-day multipath template" or a "multi-day multipath template". From the test results over 12 days, it can be concluded that: (1) both single-day and multi-day multipath templates are useful for mitigating the multipath effects on GPS pseudo-range measurements at a static site, (2) the performance of the multi-day multipath template is superior to that of the single-day multipath template, (3) the performance of the multi-day multipath template of "Day ID F" (ie. multi-day multipath generated from the data of previous 5 days, day 11 to day 07) is better than that of other multi-day multipath templates, and (4) the performances of single-day multipath templates generated from the data of "day 7 to 11" are better than that from the data of "day 1 to 6". Note that the multipath template generated from day 012 (denoted as Day 12) was chosen as the "checking multipath template" (cf. Section 3.5.2). This technique is suitable for mitigating pseudo-range multipath at reference stations for LADGPS (eg. Lin, 1995a), WADGPS and WAAS networks, GPS deformation monitoring networks, etc.

CHAPTER 4

REAL-TIME FAILURE DETECTION AND REPAIR IN TEC ESTIMATION USING GPS BY ROBUST AND CONVENTIONAL KALMAN FILTER STATE ESTIMATES

4.1 Introduction

As described in chapter 2, when radio waves such as the GPS signals propagate through the ionosphere they suffer an extra time delay. This time delay is related to the Total Electron Content (TEC) of the ionosphere.

If dual-frequency GPS measurements are available, the absolute measure of the TEC can be computed from the L1/L2 pseudo-range measurements using equation (2.27). However, this estimated TEC is “noisy” due to the effect of multipath and measurement noise (cf. equation (3.42)). In addition, there is the effect of other biases due to the GPS satellite and receiver L1/L2 differential delays. On the other hand, the relative measure of the TEC can be calculated from the L1/L2 carrier phase measurements using equation (2.30). These have the virtue of being less noisy than those derived using pseudo-range data.

In order to obtain accurate absolute TEC estimates, the pseudo-range derived TEC estimates and the carrier phase derived TEC estimates must be combined somehow. There are two options. In the post-processing option, the “phase levelling” procedure (eg. Coster & Gaposchkin, 1989; Bishop et al., 1994a; Klobuchar, 1996; Lin et al., 1996a) is commonly used. This is accomplished by “fitting” the carrier phase derived TEC estimates to the unambiguous, but noisy, pseudo-range derived TEC estimates (cf. section 2.5.1). The outputs are then the so-called “phase levelled TEC” estimates. The multipath effects on the pseudo-range derived TEC estimates will be mitigated after “phase levelling” and the cycle slip(s) in the carrier phase can be detected and repaired in a prior step (eg. Blewitt, 1990; Han, 1995).

In the real-time option, a recursive process such as a Kalman filter is typically used to estimate TEC. Unlike the post-processing mode, carrier phase measurement failures, such as the occurrence of cycle slips, must be detected, identified and repaired in real-time (eg. Coster et al., 1992; Coco et al., 1993; Jungstand et al., 1995; Engler et al., 1995; Lin, 1997).

For the estimation of the D term, an unknown bias due to the integer ambiguity of carrier phase measurements, in equation (2.31), in post-processing mode a complete arc of data (a period without cycle slips, or with corrected cycle slips) can be used. But in real-time, only the data (pseudo-ranges and carrier phases) from the first several epochs per arc are used, a special multipath mitigation technique must be implemented to overcome the pseudo-range multipath effects on the estimation of D term (eg. Coco et al., 1993; Bishop et al., 1994a; Wanninger et al., 1994; Engler et al., 1995; Jakowski, 1996; Klobuchar, 1996; Lin & Rizos, 1997b; Lin, 1997).

In addition, the GPS satellite and receiver L1/L2 differential delays must be subtracted from the estimated TEC values to generate unbiased absolute TEC estimates. There are several algorithms which can be used to derive the GPS instrumental L1/L2 differential delays in the post-processing mode. It has been noted that the instrumental L1/L2 differential delays are stable over a period of several days (eg. Engler et al., 1995; Lin & Rizos, 1996a). The determination of instrumental L1/L2 differential delays will be considered further in chapter 5.

Hence, in order to obtain accurate absolute TEC estimates in real-time if the post-processed GPS instrumental L1/L2 differential delays are used, two issues should be addressed. Firstly, the multipath effects on pseudo-range derived TEC estimates should be mitigated, and secondly, the carrier phase data failures must be detected and repaired, promptly and correctly. In order to overcome these problems, a novel approach (after Lin, 1997) is presented in this chapter.

The proposed approach involves two algorithms: (1) applying a “multipath template” procedure to mitigate the pseudo-range multipath, and (2) applying a statistical test to the state difference estimated from robust and conventional Kalman filters in order to

detect (and repair) carrier phase failure. The concept and methodology of the multipath template has been introduced in chapter 3. The proposed real-time failure detection and repair algorithm uses two procedures: (1) application of a statistical test on the state difference estimated from robust and conventional Kalman filters in order to detect and identify the carrier phase failure, and (2) application of a Kalman filter algorithm to repair the “identified carrier phase failure”.

In this chapter, the concept and methodology is first introduced. Then, test results from the UNSW and the Permanent GPS Geodetic Array (PGGA) data are presented to demonstrate the improved performance of this approach for real-time ionospheric delay estimation.

4.2 Conventional and Robust Kalman Filter

The Kalman filter, as a recursive estimation procedure, solves the state vector estimation problem for a linear dynamic system with the linear observation model (Gelb, 1974):

$$\underline{x}_k = \Phi_{k-1} \underline{x}_{k-1} + \underline{w}_{k-1}, \quad \underline{w}_k \sim N(\underline{0}, Q_k) \quad (4.1)$$

$$\underline{z}_k = H_k \underline{x}_k + \underline{v}_k, \quad \underline{v}_k \sim N(\underline{0}, R_k) \quad (4.2)$$

where $k=1,2,\dots$, is the epoch number; \underline{x}_k is the m -dimensional state vector at time k ; Φ_{k-1} is the known (m,m) transition matrix describing the state transition from time $k-1$ to k ; H_k is the (n,m) design matrix; and \underline{w}_k and \underline{v}_k are system and observation noise processes, $E(\underline{w}_k \underline{w}_k^T) = Q_k$, $E(\underline{v}_k \underline{v}_k^T) = R_k$ respectively. It is well known that under the assumption of the initial state $\hat{\underline{x}}_0$ and its variance P_0 being known, \underline{w}_k and \underline{v}_k being white noise processes uncorrelated with \underline{x}_k and with each other, the Kalman filter for model (4.1) and (4.2) gives by the time update solution:

$$\hat{\underline{x}}_k(-) = \Phi_{k-1} \hat{\underline{x}}_{k-1}(+) \quad (4.3)$$

$$P_k(-) = \Phi_{k-1} P_{k-1}(+) \Phi_{k-1}^T + Q_{k-1} \quad (4.4)$$

and the measurement update solution:

$$\hat{\underline{x}}_k(+) = \hat{\underline{x}}_k(-) + K_k [z_k - H_k \hat{\underline{x}}_k(-)] \quad (4.5)$$

$$P_k(+) = [I - K_k H_k] P_k(-) \quad (4.6)$$

$$K_k = P_k(-) H_k^T [H_k P_k(-) H_k^T + R_k]^{-1} \quad (4.7)$$

The symbols, (-) and (+) indicate the best estimate before and after measurement update.

For such a linear discrete-time stochastic system with Gaussian white noises, it is known that the conventional Kalman filter produces the minimum variance estimate of the states. However, when the noise processes are non-Gaussian the filter is very sensitive and will respond immediately, yielding poor performance for the accuracy of its estimates. In order to obtain a robust estimate of states a “robust Kalman filter” of the Masreliez-Martin type (Mertikas & Rizos, 1996c) is adopted. Only the basic principles of the robust Kalman filter are presented here. Further details can be found in *ibid* (1996c), Wang & Kubik (1993), etc.

To obtain the robust Kalman filter estimates, the distribution of the m-dimensional state vector \underline{x} is assumed to be Gaussian, whereas the n-dimensional measurement error \underline{v} is assumed to follow a non-Gaussian symmetric, but heavy-tailed distribution. Further, a linear transformation, through the (n,n) matrix T, is applied to equation (4.1) at time k. Therefore the new transformed measurements will be:

$$T z_k = T \{ H_k \underline{x}_k + \underline{v}_k \} \quad (4.8)$$

The time update solution is:

$$\hat{\underline{x}}_k^*(-) = \Phi_{k-1} \hat{\underline{x}}_{k-1}^*(+) \quad (4.9)$$

$$P_k^*(-) = \Phi_{k-1} P_{k-1}^*(+) \Phi_{k-1}^T + Q_{k-1} \quad (4.10)$$

and the measurement update solution is:

$$\hat{\underline{x}}_k^*(+) = \hat{\underline{x}}_k^*(-) + K_k^* \underline{\Psi}(\underline{v}') \quad (4.11)$$

with the vector transformed measurement innovations:

$$\underline{v}' = T\{\underline{z} - H\underline{x}(-)\} \quad (4.12)$$

$$P_k^*(+) = P_k^*(-) - K_k^* H P_k^*(-) E_0\{\Psi'(\underline{v}')\} \quad (4.13)$$

$$K_k^* = P_k^*(-) H^T T^T \quad (4.14)$$

The notation $(\hat{\underline{x}}(\cdot), P^*(\cdot))$ indicates robust estimates of the states and their covariance in the min-max sense, and K_k^* is the gain matrix of the robust Kalman filter. While the vector of the Ψ -functions is represented by:

$$\underline{\Psi}(\underline{v}') = [\Psi_1(\underline{v}'), \Psi_2(\underline{v}'), \dots, \Psi_n(\underline{v}')]^T = [\Psi(v'_1), \Psi(v'_2), \dots, \Psi(v'_n)]^T \quad (4.15)$$

The Ψ -function is an odd symmetric scalar function that gives the best estimates; that is, giving estimates which have a minimum variance over the least-favourable distributions. For example, if the ε -contaminated Gaussian family is chosen, then the Ψ -function becomes that of Huber's (Huber, 1981) with the following formulation:

$$\Psi_\varepsilon(v') = \begin{cases} v' & \text{if } |v'| \leq b \\ \text{sign}(v')b & \text{if } |v'| > b \end{cases} \quad (4.16)$$

where b is a cut-off value; ε is a fixed number with $0 < \varepsilon < 1$, representing the gross-error contamination.

The notation $\Psi'(v')$ in equation (4.13) is the derivative of the Ψ -function and the symbol $E_0\{\Psi'(v')\}$ denotes the Ψ' function for the least-favourable distribution F_0 . For example, when the ε -contaminated Gaussian family is chosen, then this expected value of the Ψ -function is given by the expression:

$$E_0\{\Psi_\varepsilon\} = (1 - \varepsilon)\{\Phi(b) - \Phi(-b)\} = (1 - \varepsilon)\{2\Phi(b) - 1\} \quad (4.17)$$

where $\Phi(b)$ is the standard Gaussian distribution evaluated for the cut-off value b . A block diagram showing the functional components of the robust Kalman filter of Masreliez-Martin is illustrated in Figure 4.1.

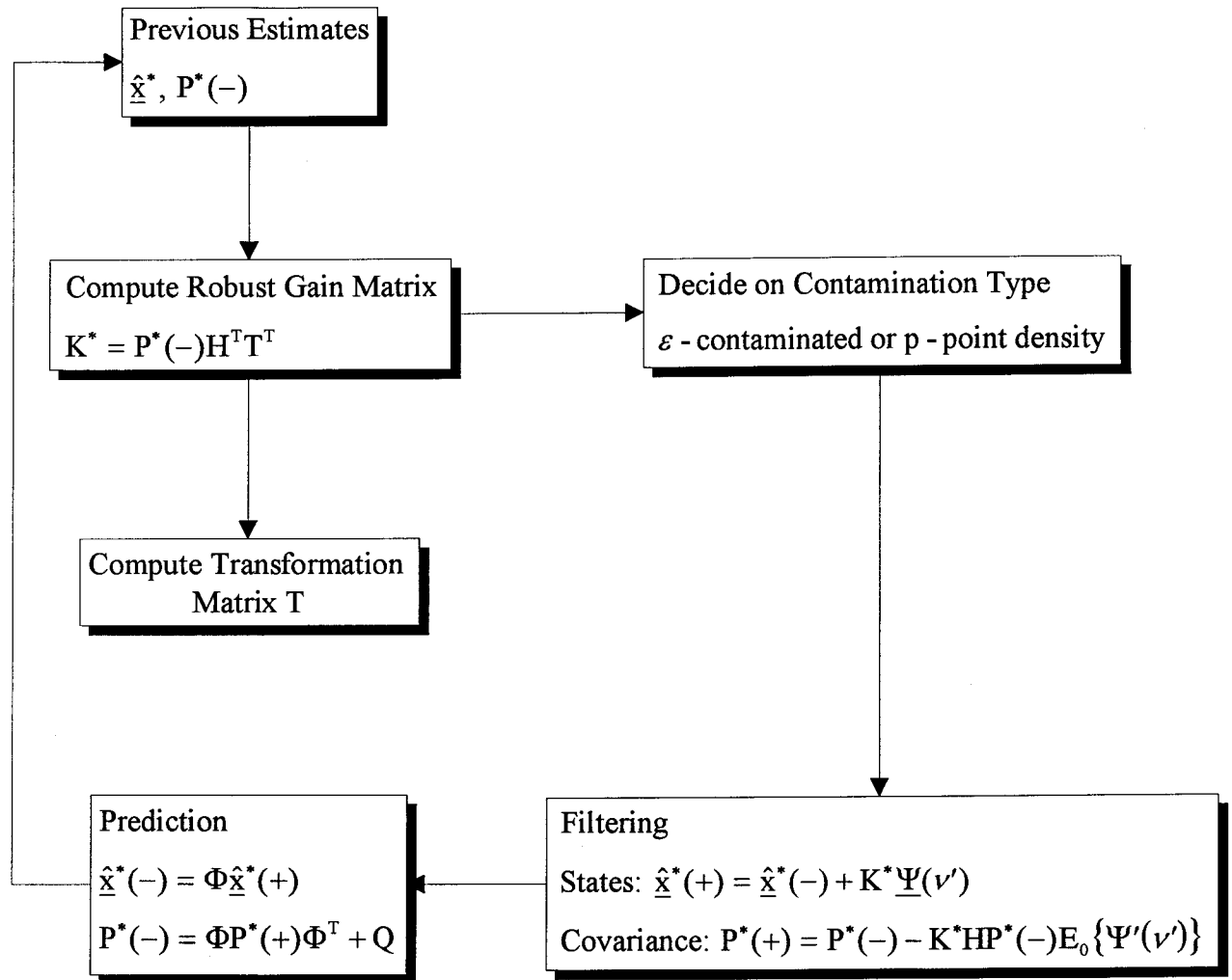


Figure 4.1. A block diagram of the robust Kalman filter of Masreliez-Martin (after Mertikas & Rizos, 1996c).

In this chapter, the following matrices and values are used to estimate real-time TEC. Those common to both the robust and conventional Kalman filters are:

$$\begin{aligned} \underline{x} &= [TEC, TEC', D]^T; \underline{z} = [TR, TS]^T; H = \begin{bmatrix} 1 & 0 & 0 \\ 1 & 0 & 1 \end{bmatrix} \\ \Phi &= \begin{bmatrix} 1 & \Delta t & 0 \\ 0 & 1 & 0 \\ 0 & 0 & 1 \end{bmatrix}; Q = \begin{bmatrix} \frac{1}{3} \Delta t^3 q & \frac{1}{2} \Delta t^2 q & 0 \\ \frac{1}{2} \Delta t^2 q & \Delta t q & 0 \\ 0 & 0 & 0 \end{bmatrix} \\ R &= \begin{bmatrix} 2500 & 0 \\ 0 & 1 \end{bmatrix} (TECU^2) \end{aligned} \quad (4.18)$$

where TR denotes the pseudo-range derived TEC (cf. equation (2.32)); TS is the carrier phase derived TEC (cf. equation (2.33)); TEC' is the first derivative of the TEC estimate; q is the spectral density of the random process; Δt is the time difference from epoch i to epoch $i+1$. Note that the value for q was established based on the following assumption that the values for the variation of the vertical TEC in a period of 3 minutes are 0.3 TECU (Wang, 1995). Then the vertical TEC was modeled as random walk stochastic process with the power spectral density $q (=0.0005 \text{ TECU}^2/\text{sec})$.

For the robust Kalman filter, the cut-off value b is taken as 1.945 and the contaminating proportion ϵ is 1% (Mertikas & Rizos, 1996c).

4.3 Real-Time Failure Detection and Repair in Ionospheric Delay Estimation

Real-time failure detection and repair in the GPS measurements is one of the challenge issues in GPS positioning and navigation community (eg. Coster et al., 1992; Coco et al., 1993; Jungstand et al., 1995; Engler et al., 1995; Klobuchar, 1996; Mertikas & Rizos, 1996a, 1996b, 1996c, 1997). By “failure”, we refer to “changes” in the information of the measurements that are: (1) of unknown magnitude, and (2) occur at unknown

instants of time (Mertikas & Rizos, 1996c). In this section, the real-time failure detection and repair algorithm in TEC estimation is described.

4.3.1 Concept

The difference between the conventional (non-robust) and the robust Kalman filter estimates of the states are considered “failure-indicating signals” (ibid, 1996c). These signals are assumed to follow a normal distribution with mean value μ and variance σ^2 , provided the assumptions underpinning the Kalman filter are satisfied. Measurement departures from a conforming class (process “in-control”) will be indicated as shifts in the mean value μ and the standard deviation σ of the process. Further, when a gross error is present in the measurements this can be detected by readily implementing an outlier screening procedure in a sequential form. The following steps describe the method of detecting failure of TEC estimates in real-time.

The failure-indicating signals X are defined as:

$$X_i = TEC_i - TEC_i^*, \quad i = 1, 2, \dots \quad (4.19)$$

where TEC_i and TEC_i^* are the TEC states estimated by the conventional and robust Kalman filter at time i respectively.

The sample mean value \bar{X}_r and the sample variance S_r^2 of the first r observations $\{X_1, X_2, \dots, X_r\}$ can be obtained sequentially using the following expressions:

$$\begin{aligned} \bar{X}_r &= \frac{1}{r}[(r-1)\bar{X}_{r-1} + X_r]; \\ S_r^2 &= \frac{r-2}{r-1}S_{r-1}^2 + \frac{1}{r}(X_r - \bar{X}_{r-1})^2 \end{aligned} \quad (4.20)$$

In order to downgrade the influence of outliers on the estimation of the mean and standard deviation of the process, the Winsorization process (Huber, 1981) is used to

“robustify” the estimation procedure. In this case the raw measurements X_r have been replaced by pseudo-observations X_r^* such that:

$$X_r^* = \begin{cases} X_r & \text{if } \frac{|X_r - \bar{X}_r|}{S_r} < c \\ \bar{X}_r + cS_r & \text{if } \frac{X_r - \bar{X}_r}{S_r} > c \\ \bar{X}_r - cS_r & \text{if } \frac{X_r - \bar{X}_r}{S_r} < -c \end{cases} \quad (4.21)$$

These truncated data values X^* are then used to produce estimates of the mean \bar{X}_r^* and the standard deviation S_r^* of the process. The constant c regulates the amount of “robustness” in the Winsorization. That is, quantity c plays as the role of a regulator provided that the data are normal (Mertikas, 1994; Mertikas & Rizos, 1996c). If, for example, $c=1$ then 68% of the data is expected to be good and the rest are to be bad data or outliers, if $c=2$ then 95% of the data is expected to be good, and if $c=3$ then 99% of the data is expected to be good. Taking a conservative approach, the value of 3 was adopted for c in this thesis. To test the compatibility of the new random variable X_r^* with its predecessors $\{X_1^*, X_2^*, \dots, X_{r-1}^*\}$, the standardised variate t , which is a good approximate to the Student’s t distribution, is defined as:

$$t_r = \sqrt{\frac{(r-1)}{r}} \left[\frac{(X_r^* - \bar{X}_{r-1}^*)}{S_{r-1}^*} \right] \quad (4.22)$$

The Studentised variables are then transformed to a more convenient standard normal variable $u(t_r)$ using the following approximation (Wallace, 1959):

$$u(t_r) = \text{sign}(X_r^* - \bar{X}_{r-1}^*) \left[\frac{8(r-2)+1}{8(r-2)+3} \right] \sqrt{(r-2) \log \left(1 + \frac{t_r^2}{(r-2)} \right)} \sim N(0,1) \quad (4.23)$$

To screen the outliers in this sequential data set, a discordance test using the well-known three-sigma (99% confidence level) identification rule is used:

$$\text{Declare } X_r \text{ as failure if } |u(t_r)| > 3 \quad (4.24)$$

A disagreement between the conventional state estimates and its robust ones indicates that a failure has been detected. The following section describes the operation of the failure detection and repair algorithm.

4.3.2 Detection and Identification Step

Two Kalman filters, one conventional and one robust, are used to estimate the TEC for each tracked GPS satellite (in this example, only one GPS satellite, PRN 1, is considered). If the $|u(t_r)|$ value of PRN 1 is greater than 3, then it is assumed that a carrier phase failure has occurred.

4.3.3 Repair Step

Let “ ΔTS ” be the failure correction to TS , the phase derived TEC, “ \overline{TS} ” the corrected TS , and “ CN ” the cycle slip number. ΔTS and CN are set to zero at the initial tracking of PRN 1. The relationship between TS and \overline{TS} is:

$$\overline{TS} = TS + \Delta TS \quad (4.25)$$

Let “ $\text{Inno}(TS)$ ” be the innovation of TS , which can be computed from the conventional Kalman filter as:

$$\text{Inno}(TS) = \overline{TS} - [TEC(-) + D(-)] \quad (4.26)$$

where $TEC(-)$ and $D(-)$ are estimates of TEC and D before measurement update (cf. equations (4.3) and (4.18)).

Let “ dN_1 ” and “ dN_2 ”, in units of cycles, be the carrier phase cycle slips on the L1 and L2 signals respectively. The combined effect of dN_1 and dN_2 on TS is:

$$dT_S = 9.5196 \times (\lambda_1 dN_1 - \lambda_2 dN_2) \quad (4.27)$$

Considering the fact that the minimum possible value of “ dTS ” is ± 0.24 TECU (Wanninger, 1994), when $dN_1 = -5$ and $dN_2 = -4$, or $dN_1 = 5$ and $dN_2 = 4$, the critical value of 0.25 TECU was selected as the criteria for invoking the repair action. The main steps of the failure detection and repair algorithm are shown in Figure 4.2. For example, if the failure occurred at epoch k , then the innovation $Inno(TS)$ is computed by equation (4.26) and the failure correction ΔTS is determined according to the steps listed in Figure 4.2. The predicted states from equations (4.3) and (4.9) are adopted as estimated states. From epoch $k+1$ on, the TS is corrected by equation (4.25).

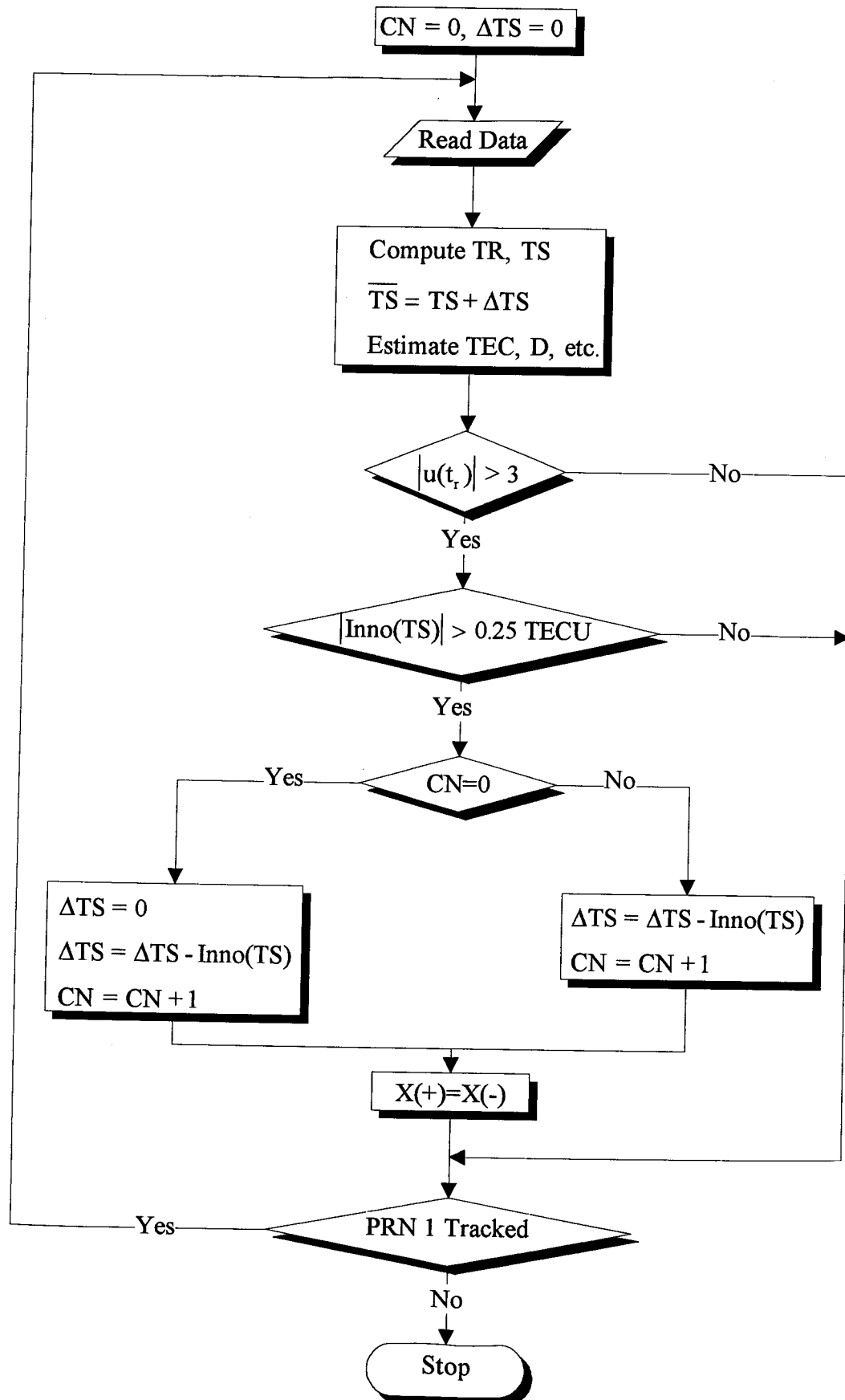


Figure 4.2 Main steps of the real-time failure detection and repair algorithm.

4.4 Program “REALTEC”

Based on the algorithm described in section 4.3, a real-time TEC estimation software package, known as “REALTEC”, was developed. The main features of REALTEC are:

- 1) apply a statistical test on the state, ie. TEC in equation (4.18), difference estimated from robust and conventional Kalman filters in order to “detect and identify” the carrier phase failure(s) in real-time,
- 2) apply a Kalman filter algorithm to repair the “identified carrier phase failure(s)” in real-time,
- 3) apply a multipath template to mitigate the pseudo-range multipath effect on pseudo-range derived TEC (ie. TR) to improve the accuracy of real-time TEC estimation.

A block diagram of program REALTEC is shown in Figure 4.3. Generally speaking, REALTEC consists of three parts:

- Input:

- a) GPS observation file
- b) GPS navigation file
- c) GPS satellite and receiver L1/L2 differential delays
- d) Multipath template

- Processing:

- a) Compute TR, TS
- b) Mitigate pseudo-range multipath effect on TR using multipath template if the multipath template is available
- c) Calibrate GPS satellite and receiver L1/L2 differential delays on TR (this issue will be addressed in Chapter 5)

d) Detect, identify, and repair the carrier phase failure(s) in order to get accurate TS estimate

- Output:

a) Accurate vertical TEC estimates on an epoch-by-epoch basis

b) Report of real-time failure detection and repair

c) Accuracy report of TEC estimates

Some symbols which appear in Figure 4.3 are defined as follows:

“GPST” is the GPS time, “TotalSat” is the total number of tracked GPS satellites at an epoch, “PRN#” is the PRN number of the tracked GPS satellite, “Prn.Epoch” is the epoch number of the tracked GPS satellite, “SumTR” is the sum of TR for a specific PRN, “SumTRS” is the sum of “TR-TS” for a specific PRN, “SatNum” means how many PRNs’ data belonging to the same epoch are read.

The weight matrices, such as R, Q matrices of equation (4.18), the epoch number required to estimate the initial value of each state at the beginning for each tracked GPS satellite, the cut-off value b, etc., are entered in the “Load Processing Parameters” part of Figure 4.3. For example, the first twelve epochs of data for each PRN are used to estimate TEC initial value, as shown in Figure 4.3.

Note that the program REALTEC is developed to simulate the real-time TEC estimation. After minor modification, this program can be implemented as a “real-time TEC estimation system”. In this case, the observation file and navigation file shown in Figure 4.3 will be replaced by real-time input directly from the GPS receiver. However, the multipath template and GPS satellite and receiver biases can be generated from the previous day’s data. In addition, the “End of File” condition in Figure 4.3 will be replaced by other conditions, such as “Data Available”, etc.

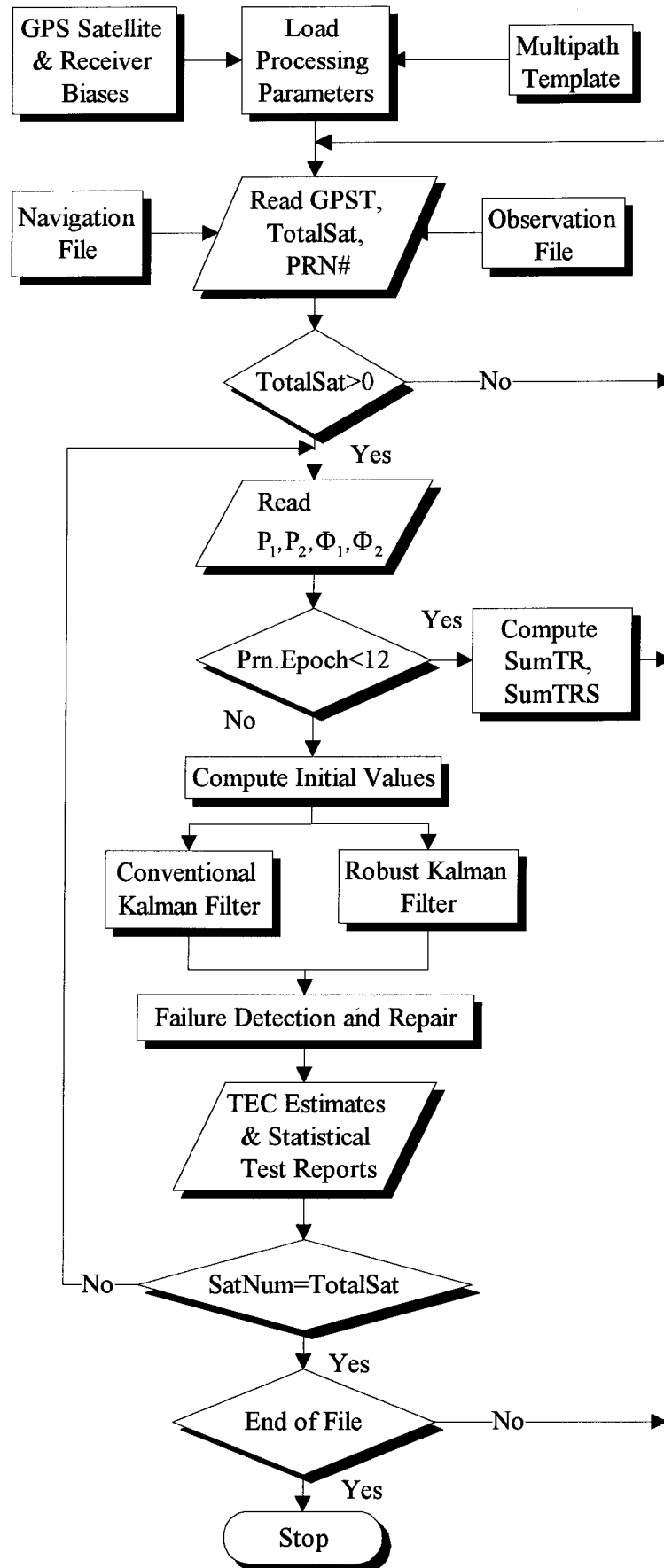


Figure 4.3 A block diagram of program “REALTEC”.

4.5 Experimental Results and Discussion

4.5.1 Data Description

a) The UNSW Data

The UNSW data set was collected from 28 April, 1995 (day 118, 1995) to 01 May, 1995 (day 121, 1995) on the roof of the Geography and Surveying Building of The University of New South Wales, using Leica System 200 GPS receivers. The Leica receiver can track up to 9 satellites, and measure L1 and L2 carrier phases, C/A and P2 pseudo-ranges. Four astronomical pillars, EC02, EC05, EC14 and EC19, were selected as station sites. Each GPS receiver collected 2 hours of data on four consecutive days. The data rate was 1 second and the elevation cut-off angle was set to 20 degrees.

From earlier tests (Lin, 1995b; Lin & Rizos, 1996b), it was found that there were measurement failures in the data sets collected from site EC05. Therefore, the data sets from site EC05 were selected to test the performance of the proposed algorithm.

b) The PGGA Data

A number of data sets from station Blythe (blyt), day 001 to 012, 1996, from the Permanent GPS Geodetic Array (PGGA), in Southern California, USA (PGGA, 1996) were also processed and analysed to test the proposed algorithm. The “blyt” station is equipped with an ASHTECH Z-12 geodetic receiver, and collects C/A, P1 and P2 pseudo-ranges and L1 and L2 carrier phase data, from all visible GPS satellites every 30 seconds. The cut-off angle was 10 degrees.

4.5.2 Test I --- Cycle Slip Detection and Repair

4.5.2.1 UNSW Case -- Post-Processing Mode

In order to verify the performance of the proposed procedure, the post-processing algorithm involving the widelane and $\Phi_{-7,9}$ phase combinations (Han, 1995) is used to detect and repair the carrier phase cycle slips. The data before and after the cycle slip repair process are processed using the carrier “phase levelling” process (cf. section 2.5.1).

The computed carrier phase derived TEC, TS, and carrier phase levelled TEC for PRN 21 on day 121, 1995, are shown in Figures 4.4(a) and 4.4(b) respectively. Line A and B represent the TEC estimates after and before the cycle slip repair was carried out respectively. From this Figure, it is evident that there is one cycle slip in the observed data. The carrier phase levelled TEC derived from cycle slip free data are used to verify the performance of the proposed procedure.

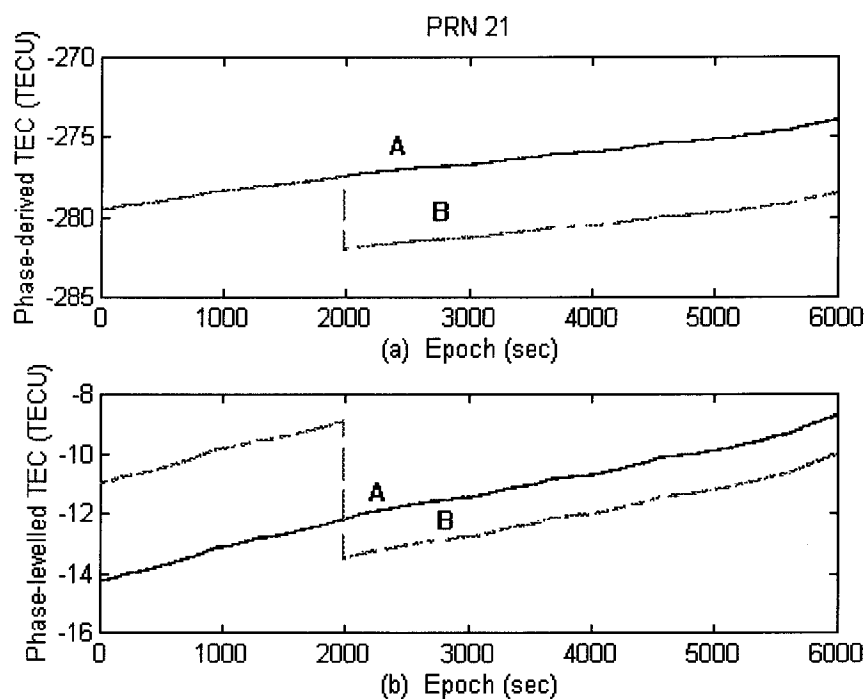


Figure 4.4. The phase-derived TEC (a) and phase-levelled TEC (b) of PRN 21 for day 121, 1995.

Note that the values of phase-derived TEC (cf. Figure 4.4(a)) in this experiment are negative due to the integer ambiguity of carrier phase measurements (cf. Equation (2.31)). In addition, the values of phase-levelled TEC (cf. Figure 4.4(b)) or slant TEC (cf. Figures 4.5 to 4.7) in this experiment are negative due to the effect of the GPS satellite and receiver L1/L2 differential delays. As discussed in section 4.1, the GPS satellite and receiver L1/L2 differential delays are stable over a period of several days. Hence, in order to obtain accurate absolute TEC estimates in real-time, the post-processed GPS satellite and receiver L1/L2 differential delays (eg. -30.73 TECU for PRN 21 over site EC05) must be subtracted from the phase-levelled TEC values (cf. Equation 5.1).

4.5.2.2 UNSW Case -- Real-Time Mode

The real-time TEC estimation software package REALTEC was used to process the raw data from day 121, 1995. The test results are shown in Figure 4.5. The real-time TEC estimates without applying the multipath template are represented by line A. The post-processed TEC estimates with cycle slip free data are represented by line B. Line C represents the real-time TEC estimates after applying the multipath template generated from current day's data. Line D indicates the post-processed TEC estimates from the raw data. The range of elevation angle of PRN 21 is also shown in this Figure. Note that line C has been shifted by +0.5 TECU from line B for clarity. Details of the failure detection and repair process from post-processing, and from the REALTEC software, for PRN 21 are shown in Table 4.1. ReT means "real-time mode", and PoP stands for "post-processing". The GPS time, indicating the time of occurrence of the cycle slip, is in units of seconds. The other parameters were defined in section 4.3. From these test results it is concluded that: (1) REALTEC is capable of detecting and repairing the carrier phase cycle slips in real-time, and (2) the achieved TEC accuracy from REALTEC is identical to that obtained from post-processing if the multipath template is used.

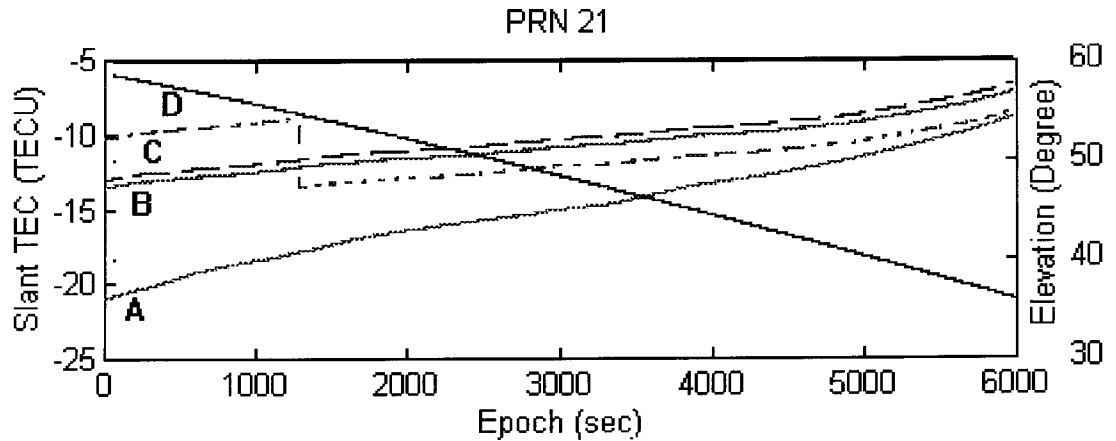


Figure 4.5. Post-processing TEC estimates versus real-time TEC estimates of PRN 21 for day 121, 1995.

Table 4.1. Post-processing derived phase correction, ΔTS , versus real-time derived ΔTS .

Mode	Time	dN_1	dN_2	ΔTS
PoP	93350.0	-18	-16	4.614
ReT	93350.0	N/A	N/A	4.615

In order to further demonstrate the performance of REALTEC, data from day 119, 1995, were processed. The test results are shown in Figure 4.6. The post-processing result indicates that there are three cycle slips on PRN 21, as shown by line C. The post-processed TEC estimates with cycle slip free data are indicated by line A. The real-time TEC estimates using REALTEC with raw data are indicated by line B. Again, line B has been shifted from line A by +0.5 TECU. The current day's multipath template is applied. From this Figure it is concluded that REALTEC is able to generate good quality TEC estimates (compared to post-processed TEC estimates) in real-time, even though there are multiple cycle slips in the raw data.

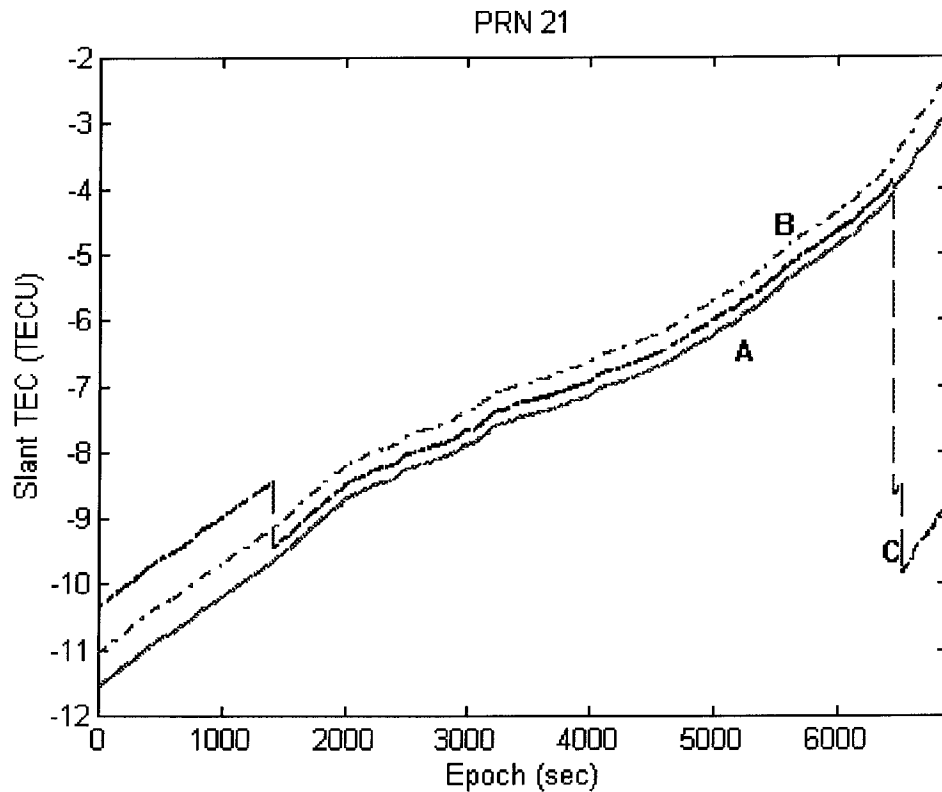


Figure 4.6. Post-processed TEC estimates versus real-time TEC estimates of PRN 21 for day 119, 1995.

4.5.3 Test II --- Effectiveness of the Multipath Template

In order to demonstrate the effectiveness of using the multipath template for real-time TEC determination, the same two data sets were again processed.

4.5.3.1 UNSW Case

The test results of processing the UNSW data are shown in Figure 4.7. The raw data from day 121, 1995, was processed using REALTEC. Line A represents the TEC estimates without applying any multipath template. Line B represents the TEC estimates after applying the single-day multipath template of day 121, 1995 (Note that line B is identical the result from post-processing according to the test results of section 4.5.2.2.). Line C represents the TEC estimates after applying the multi-day multipath template generated from the data of days 118 to 120, 1995. Line D expresses the TEC estimates

after applying the single-day multipath of day 118, 1995 (i.e. using data from 3 days earlier). The statistics of these tests (in units of TECU) are summarised in Table 4.2. From these tests, it is obvious that the multipath will degrade the real-time TEC estimation if the multipath template is not used. Conversely, the accuracy of TEC estimation can be appreciably improved if a multipath template is applied.

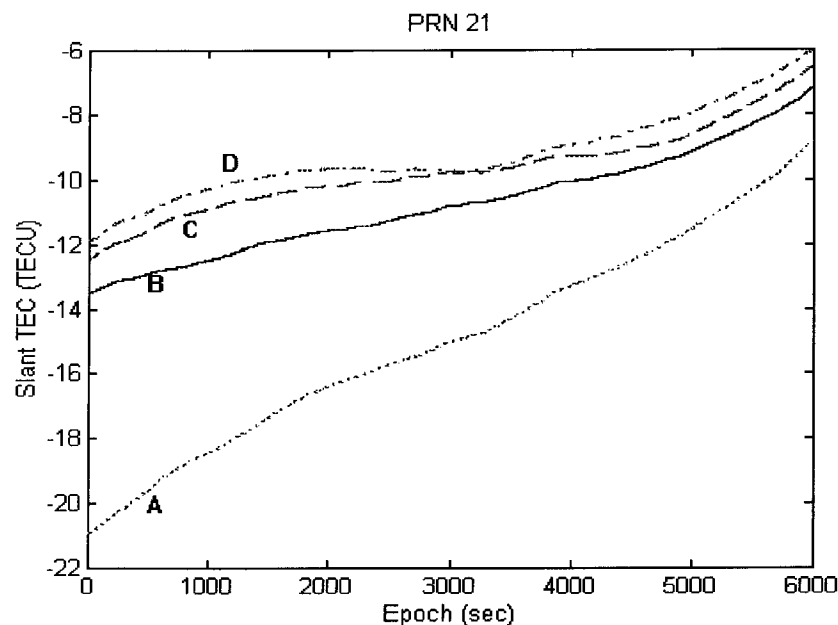


Figure 4.7. Real-time TEC estimates, comparison of different types of multipath template, for PRN 21 for day 121, 1995.

Table 4.2. Real-time TEC estimate difference statistics of Figure 4.7.

	Mean	Std.	Max.	Min.
B-A	4.15	1.61	7.4	1.61
B-C	-1.03	0.36	-0.51	-1.64
B-D	-2.24	0.42	-0.99	-2.24

4.5.3.2 PGGGA Case

In order to further test the performance of the proposed procedure, the PGGGA data were also processed in both the post-processed and real-time mode. Multi-day multipath template performance was studied in Lin & Rizos (1997b) using the same data set.

The post-processed TEC estimates of day 012, 1996, at site “blyt”, for each PRN, are assumed to be the true values. The various multipath templates, and the raw GPS observation file, were input to REALTEC, and used to generate real-time TEC estimates. For each PRN, the estimated TEC differences between post-processing and real-time processing were computed. The mean values and standard deviations of these differences were calculated and plotted in Figures 4.8 and 4.9 respectively. In this test period, 25 GPS satellites were tracked.

In these two Figures, “MP12c Cali.” means that the single-day multipath of day 012, 1996, was used. “MP11-6 Cali.” means that the multi-day multipath template generated from days 006 to 011, 1996, was used. “No MP Cali.” indicates that no multipath template was used. In Figure 4.8, it can be seen that: (1) the current day (i.e. day 012) multipath template gives the minimum mean values of TEC estimate differences for each PRN, and (2) compared to “No MP Cali”, the mean values of TEC estimate differences are reduced significantly for most (84%) of the PRNs if the multi-day multipath template was used. On the other hand, the standard deviations of the TEC estimate differences are reduced significantly for most (92%) of the PRNs if the multi-day multipath template was used (Figure 4.9).

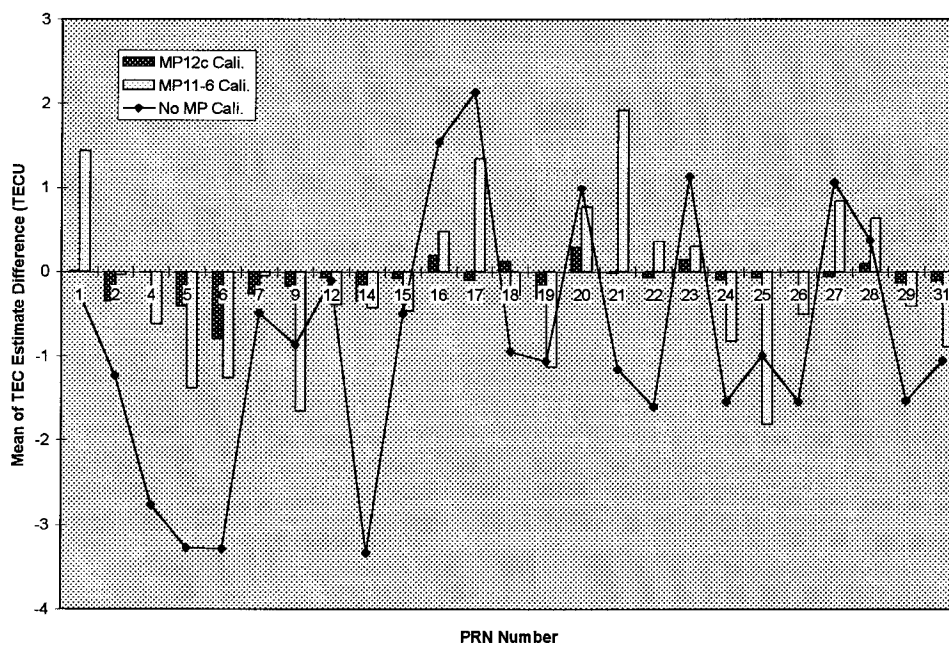


Figure 4.8. Comparison of the means of the TEC estimate difference for each PRN at site “blyt”, PGGA data, day 12, 1996.

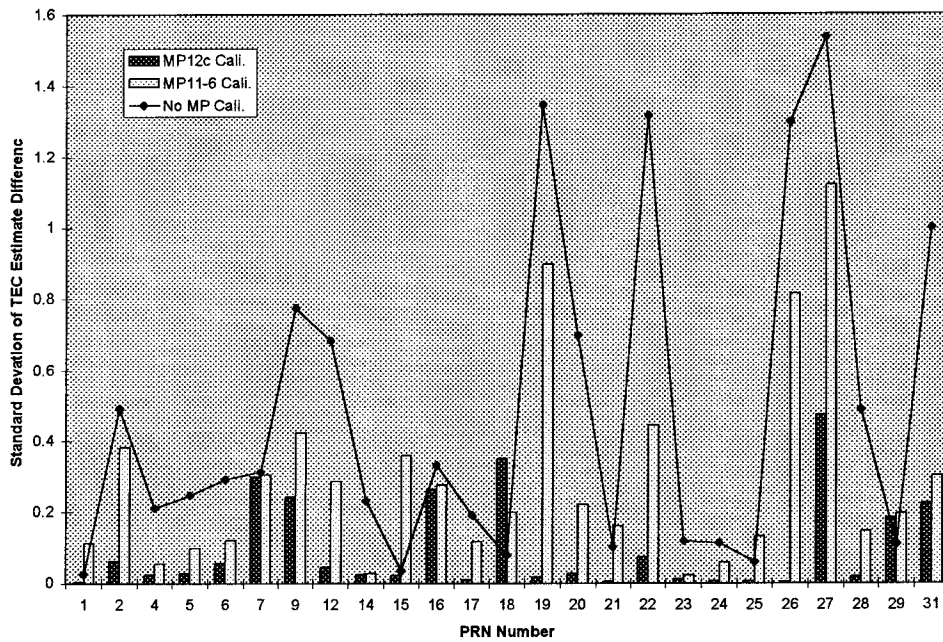


Figure 4.9. Comparison of the standard deviations of the TEC estimate difference for each PRN at site “blyt”, PGGA data, day 12, 1996.

4.6 Concluding Remarks

In order to improve the accuracy of real-time ionospheric delay estimation, a novel approach to the processing of phase and pseudo-range data was developed. From the test results, it has been demonstrated that the carrier phase derived TEC “failure” caused by cycle slips can be detected and repaired promptly and correctly in real-time. In addition, the proposed multipath template technique can effectively mitigate the multipath effect on pseudo-range derived TEC.

CHAPTER 5

AN ALGORITHM TO ESTIMATE GPS SATELLITE AND RECEIVER L1/L2 DIFFERENTIAL DELAYS

5.1 Introduction

As discussed in section 2.5.2, one of the challenging problems in making absolute ionospheric measurements using dual-frequency observations of the GPS satellites is to estimate the satellite and receiver L1/L2 differential delays (Coco, 1991; Bishop et al., 1992; Klobuchar et al., 1993; Wanninger et al., 1994; Jakowski et al., 1995; Jakowski, 1996). Both the satellite and receiver L1/L2 differential delays stem from hardware delays in the L1 and L2 signal paths (Wilson & Mannucci, 1993).

Firstly, the definition of GPS satellite and receiver L1/L2 differential delay is introduced in section 5.2. Methods to estimate GPS satellite and receiver L1/L2 differential delay are briefly reviewed. Then the major features, the basic assumptions, and the estimation procedure for a proposed algorithm are described in section 5.3. Methods of verifying the estimation methods, the experimental results and discussion are given in section 5.4. Finally, some conclusions are drawn based on the experimental results.

5.2 Methods to Estimate GPS Satellite and Receiver L1/L2 Differential Delay

5.2.1 Definition of GPS Satellite and Receiver L1/L2 Differential Delay

The codes transmitted by GPS satellites at the two L-band frequencies (L1 and L2) are carefully synchronised so that they are broadcast simultaneously. Absolute simultaneity is not possible, however, so the time difference between the transmitted time at the two frequencies is called the “*satellite L1/L2 differential delay*” or “*satellite differential*”

delay” (Coco, 1991), designated as T_{gd} . Each GPS satellite has a unique satellite differential delay.

Differential frequency delays may also be present in GPS receivers. These are called the “*receiver L1/L2 differential delay*” or “*receiver differential delay*”, because the L1 and L2 signals must travel through different hardware paths or electronic circuitry inside the receiver (ibid, 1991). Each GPS receiver has its individual receiver differential delay.

The satellite and receiver differential delays are transparent to GPS navigation and surveying users as they are simply absorbed unnoticed into the satellite and receiver clock biases (ibid, 1991). However, these delays introduce error in the measurement of Total Electron Content (TEC). According to Wilson & Mannucci (1994), ignoring the *satellite differential delays* when computing line-of-sight TEC measurements from GPS observables may result in an error of ± 3 ns (± 9 TECU). On the other hand, ignoring the *receiver differential delays* when computing line-of-sight TEC measurements from GPS observables may result in an error of ± 10 ns (± 30 TECU). Note that 1 ns of differential delay is 2.852 TEC units (TECU) (Klobuchar, et al., 1993), and that one TECU is 1×10^{16} el / m² which will cause about 16.2 cm group delay at the L1 frequency.

5.2.2 Satellite Differential Delays

The requirements on the GPS satellites demand that the satellite differential delay shall not exceed 15 ns (43 TECU) and random variations shall not exceed 3 ns (9 TECU) (Wanninger, 1992). Actual satellite differential delays were determined in prelaunch factory tests. These values are less than 3 ns for the Block I satellites (Coco et al., 1991). Prelaunch testing values are also included in the satellite broadcast message. They have been broadcast for all satellites since the autumn of 1990. Maximum values are about 4 ns (12 TECU) (Wanninger, 1992, 1994). However, these values do not agree with those reported in the literature (eg. Coco et al., 1991; Klobuchar et al., 1993; Wanninger, 1994). Hence, several working groups, or computation centres, have made attempts to measure the satellite differential delay from various GPS satellites, including the Phillips Laboratory (PL) (Klobuchar et al., 1993), Jet Propulsion Laboratory (JPL) (Wilson et al., 1993), DLR

(DLR, 1996), ESOC (Feltens et al., 1996), UNB (Komjathy & Langley, 1996b), and others.

Basically there are two different methods for estimating the satellite differential delays: (1) the single-site modelling technique (Lanyi & Roth, 1988; Coco et al., 1991; Bishop et al., 1994b), and (2) the multi-site modelling technique (Wilson & Mannucci 1993; Gao et al., 1994; Sardon et al., 1994; Wilson & Mannucci, 1994; Chao et al., 1995; Komjathy & Langley, 1996b; Feltens et al., 1996).

The first method, for example, suggested by Lanyi & Roth (1988), uses only nighttime GPS data from a single-site, and assumes that: (1) the ionospheric TEC is constant for a period of 4-6 hours, (2) the slant and vertical TEC are related by a constant obliquity factor, and (3) the satellite and receiver differential delays are constant over several hours. Then, GPS differential group delay measurements from a mid-latitude nighttime observation period are input to a least squares estimation process to estimate the coefficients of a local two-dimensional quadratic model of the vertical TEC and the combined satellite and receiver differential delays for each tracked GPS satellite (cf. section 5.3). If the receiver differential delay can be calibrated, the satellite differential delay can be determined using this method.

The second method, for example, suggested by Wilson & Mannucci (1993), uses 12-24 hours of GPS data from 30-40 sites to model the global ionosphere and estimate the satellite and receiver differential delays. A thin spherical model, similar to that described in Lanyi & Roth (1988), is assumed. Two available techniques, such as “HARM” (for *harmonics*) and “TRIN” (for *triangular interpolation*) (Wilson & Mannucci, 1993), can be used to model the global/regional ionosphere. Again, at least one of the receiver must be calibrated beforehand. Then, all satellite differential delays and all (uncalibrated) receiver differential delays can be estimated.

The problem of estimating the satellite differential delays using the GPS data itself is difficult because one must simultaneously estimate the TEC assuming a model of the ionosphere. That is the major reason for the disagreement between the reported satellite differential delay values. For example, Feltens et al. (1996) report a comparison of the

results of the estimated satellite and receiver differential delays from three International GPS for Geodynamics Service (IGS) analysis centres (DLR, UNB and ESOC). They found that the agreement between these analysis centres is at the 1 ns level. The disagreement has led to some discussion of the possibility that the satellite differential delays are varying in time (Wilson & Mannucci, 1993).

In addition, the stability of the satellite differential delays is another important issue regarding to estimate the ionospheric delay using GPS data. If the variation of the differential delays is too big, or for as long as they are not calibrated, the differential delay must be determined from existing GPS observations together with a simple ionospheric model. The satellite (and receiver) differential delays are known to be very sensitive to temperature changes (eg. Coco et al., 1991; Wanninger, 1992; Chao et al., 1996).

Coco et al. (1991) reported that the day-to-day variations of the Block I satellite differential delays was less than 0.3 ns (0.9 TECU) over a five week time span. Sardon et al. (1994) found that the variation of the GPS satellite differential delays (relative to its mean) was below 1 ns (2.85 TECU), using different sessions of data during a 1-year period (September 1990 to September 1991). Jungstand et al. (1995) reported that the stability of the satellite differential delays over 1.5 years was below 1.5 ns (4.3 TECU). Results of other investigations can be found in the literature (eg. Gao et al., 1994; Wilson & Mannucci, 1994; Komjathy & Langley, 1996b; Feltens et al., 1996).

5.2.3 Receiver Differential Delays

The receiver differential delays originate in the antenna and preamp unit, coaxial cable, and the band-pass filters in the GPS receivers (Chao et al., 1996). It is known that receiver differential delays are very sensitive to temperature changes (eg. Coco et al., 1991; Wanninger, 1992; Chao et al., 1996). Chao et al. (1996) reported that a deliberate heating of a Stanford's receiver by 30° F showed a receiver differential delay increase of more than 0.5 m relative to the differential delay of the other receivers in the network.

There are three possible methods to measure (or estimate) the receiver differential delays (eg. Wilson & Mannucci, 1993):

- **Using the internal calibration capability of the receiver.** The geodetic GPS receivers, such as the Rogue SNR-8 and MiniRogue, have an internal calibration capability (Wanninger et al., 1994). For example, the Rogue receiver developed at JPL has a hardware calibration mode in which one connects jumper cables so that the same radio frequency signal is sent through both frequency (L1 & L2) paths in the receiver (Wilson & Mannucci, 1993). By averaging the difference of the two delays over 20 minutes or longer, one can directly measure the receiver differential delay introduced by a particular component of the receiver hardware.
- **Collocating with a calibrated receiver (such as a Rogue receiver) and running the same antenna feed into both receivers.** GPS receivers that do not have a calibration mode can be calibrated against a receiver that has by running the same antenna feed into both receivers. Differencing the two data sets and averaging yields the difference of the receiver differential delays.
- **Estimating by fitting multi-site GPS data.** One can also estimate the receiver differential delays by fitting multi-site data from a regional (or global) network of GPS receivers, that is the receiver and satellite differential delays can be estimated simultaneously. Only one calibrated receiver is required to define the absolute level of the differential delays.

As the receiver differential delays are sensitive to temperature changes, the stability of the receiver differential delays are questionable. Wilson & Mannucci (1993) reported that the receiver differential delay calibration for the Goldstone receiver (Rogue) had three reproducible values: -2.5, -7.7, and -4.9 ns, due to hardware changes, for the period of 1/16/90 to 7/21/93. These calibration values were stable at the level of 0.1 ns (0.3 TECU). Note that the receiver at Goldstone was in a temperature-controlled environment. A receiver in a less controlled environment may exhibit diurnal, or other, variations in the calibration value (ibid, 1993).

Wanninger (1992) reported that the day-to-day variations of the receiver differential delay for the Ashtech P-code receivers (beta version) were up to 3 ns (9 TECU). Wanninger et

al. (1994) reported other experiment results on the stability of the receiver differential delays. They used the data sets from two Ashtech Z-12 receivers on a zero baseline to analyse the daily variation of the difference of the receiver differential delays of these two receivers. They found that the day-to-day variability of the difference of the receiver differential delay was at the 0.2 ns (0.5 TECU) level. However, there was a 2.3 ns (6.5 TECU) difference over the two month period. It was concluded that pre-determined calibration values for those receivers would be of little value after just a few weeks.

5.3 A Proposed Algorithm to Estimate GPS Satellite and Receiver L1/L2 Differential Delays

As discussed in the previous section, the ionospheric delay estimates derived from dual-frequency GPS observables are corrupted by both the satellite and receiver differential delays. Although the prelaunch testing values of satellite differential delays are included in the satellite broadcast message, in practice these values do not agree with those reported in the literature. Hence, several groups of investigators have attempted to measure the satellite differential delays from various GPS satellites using different approaches. The agreement of the estimated satellite differential delays between different groups is at the 1 ns level. In addition, the variation in time of the satellite differential delay is about 1 to 1.5 ns level over 1 year.

Only two types of geodetic GPS receivers offered an internal calibration capability, the Rogue SNR-8 and the MiniRogue. Both receivers are no longer in production (Wanninger et al., 1994). Other geodetic GPS receivers such as the Ashtech Z-12, Trimble SSi, and TurboRogue, can be used to estimate ionospheric delay, but they do not have an internal calibration capability. Hence, their differential delays must be estimated. In addition, the receiver differential delays are sensitive to temperature changes.

Some research centres, such as the DLR (Germany), provide GPS satellite and receiver differential delays for each day on the Internet. However, the data used to estimate the satellite and receiver differential delays are from the GPS sites (about 18 sites) in the European area. In other words, the DLR provides the receiver differential delays for those 18 receivers only. In this thesis, several data sets from different regions, over different

periods, such as the PGGGA, GSI, ARGN (further described in chapter 6), were processed and analysed. The collected GPS data came from several types of receivers which do not have an internal calibration capability. Hence, in order to obtain accurate absolute TEC estimates from dual-frequency GPS data and so fulfil the research objectives of this thesis, an algorithm to estimate GPS satellite and receiver differential delays was developed and tested (Lin & Rizos, 1996a, 1996b).

The proposed algorithm is similar to the procedure described in Coco et al. (1991). However, some modifications were made to the algorithm. The major modifications were: (1) the ionosphere height was changed from 350 km to 400 km (since most of the data set used in this study were from Australia region, and it was recommended that the height of ionosphere shell be taken to be 400 km in this region (eg. Wang, 1995)), (2) the terms of the polynomial used to model the ionosphere was changed from 6-term to 15-term, (3) 24-hour data sets were processed instead of only nighttime data, and (4) the procedure was modified to handle multi-site data. The underlying assumptions and estimation procedure are described in the following sections. Note that only the results from single-site data are presented in this chapter, since most of the receivers (in the collected data sets) did not have internal calibration capability, although the proposed algorithm is capable of processing multi-site data.

5.3.1 Estimation Assumption

The proposed estimation procedure is a single-site modelling technique implemented in post-processed mode. This technique is based on the following assumptions:

- 1) The time dependence of the ionosphere is handled by representing the observations in a reference frame, “co-rotating reference frame”, that rotates with respect to an Earth-fixed reference frame, so that the direction of the sun is always fixed at 180° co-rotating longitude (Coco et al., 1991). The relationship between the longitude in the co-rotating reference frame and that in the earth-fixed frame is expressed by equation (5.8).

- 2) A single-layer (or thin-shell) model is adopted for the ionosphere. It is assumed that the vertical TEC can be approximated by a thin spherical shell which is located at an altitude of 400 km above the earth's surface, and that all electrons encountered along the signal path from GPS satellite to receiver are contained within this shell. The geometry of a single ionosphere layer model and the ionospheric pierce point (IPP) are illustrated in Figure 5.1.
- 3) The ionosphere can be modelled well by a 15-term polynomial in the solar-magnetic coordinate system for a period of 3 hours. (Four types of polynomials were tested in this study: 4-term, 6-term, 10-term, and 15-term. In addition, various observation session lengths, such as 2-hour, 3-hour, 6-hour, 12-hour, etc., were tested. Note that the choice of the number of polynomial terms and the observation session length is based on the criterion that they provide good estimates of TEC and satellite plus receiver differential delay (detailed verification schemes see section 5.4.2))
- 4) The satellite and receiver differential delays are assumed to be constant over the observation session. The slant and vertical TEC are assumed to be related by a constant obliquity factor (or mapping function).

5.3.2 Estimation Procedure

The estimation procedure, based on the above-mentioned assumptions, is:

Step 1: A dual-frequency GPS receiver measures pseudo-range and carrier phase data at L1/L2 and its observables are used to compute TEC. The “phase levelling” technique described in chapter 2 (eg. Coco et al., 1991; Komjathy & Langley, 1996b; Lin et al., 1996a, 1996b) is used to compute the precise phase-levelled slant TEC for each tracked satellite at each observation epoch. The equations involved can also be found in section 2.5.1. These slant TEC measurements are the sum of the true slant TEC, the GPS satellite differential delay b^S and the receiver differential delay b_R . They can therefore be expressed as:

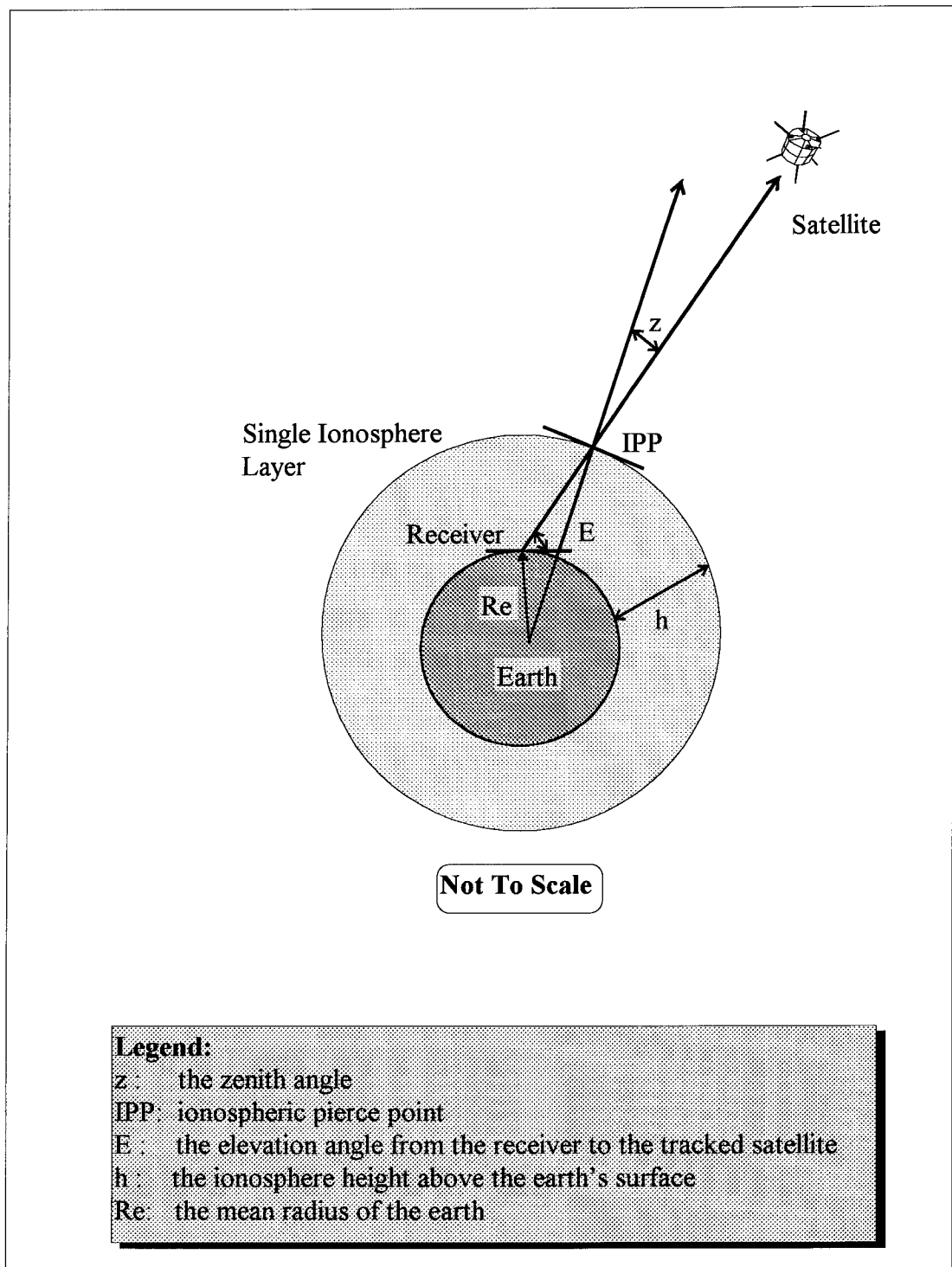


Figure 5.1. Ionospheric pierce point (IPP) geometry.

$$TEC_m = S(E) \times TEC_v + b_R + b^S \quad (5.1)$$

where TEC_m (in units of TECU) is the slant TEC measurement, E (in degrees) is the elevation angle from the receiver to the tracked satellite, $S(E)$ is the obliquity factor with zenith z at the *ionospheric pierce point* (IPP) and TEC_v (in units of TECU) is the vertical TEC at the IPP. The IPP is the intersection of the user's line-of-sight to the tracked satellite with the centre of the ionosphere slab (ie. the single-layer is located at an altitude of 400 km above the earth's surface). (cf. Figure 5.1)

Since it is assumed that the ionospheric electron density is concentrated on a thin shell of height 400 km above the earth, all slant TEC measurements are converted to an equivalent vertical value by using the shell elevation mapping function, the obliquity factor, $S(E)$ of equation (5.1), which may be defined as (Mannucci et al., 1993):

$$S(E) = \frac{1}{\cos z} = \left[1 - \left(\frac{R_e \cos E}{R_e + h}\right)^2\right]^{-0.5} \quad (5.2)$$

where R_e is the mean radius of the earth in km, h is the height of the ionosphere above the earth's surface, here, assumed to be 400 km, and z is the zenith angle. The use of a mapping function is clearly an approximation, and can lead to errors of several TECU when applied to regions of large horizontal electron density gradients (eg. Klobuchar et al., 1993). There are other mapping functions. For example, Clynch et al. (1989) used a 4-term polynomial as a function of elevation angle as the mapping function (ionosphere height was assumed to be 250 km) to monitor polar region ionosphere. Sardon et al. (1995) adopted the mapping function derived by Sovers & Faselow (1987) to study the GPS satellite and receiver L1/L2 differential delays.

TEC_v at the IPP is represented by the following polynomial:

$$\begin{aligned} TEC_v(\phi_m, \lambda_{cr}) = & a_0 + a_1 \cdot \phi_m + a_2 \cdot \lambda_{cr} + a_3 \cdot \phi_m^2 + a_4 \cdot \lambda_{cr}^2 + a_5 \cdot \phi_m \cdot \lambda_{cr} \\ & + a_6 \cdot \phi_m^3 + a_7 \cdot \lambda_{cr}^3 + a_8 \cdot \phi_m^2 \cdot \lambda_{cr} + a_9 \cdot \phi_m \cdot \lambda_{cr}^2 + a_{10} \cdot \phi_m^4 \\ & + a_{11} \cdot \lambda_{cr}^4 + a_{12} \cdot \phi_m^3 \cdot \lambda_{cr} + a_{13} \cdot \phi_m^2 \cdot \lambda_{cr}^2 + a_{14} \cdot \phi_m \cdot \lambda_{cr}^3 \end{aligned} \quad (5.3)$$

where ϕ_m is the geomagnetic latitude of the IPP, λ_{cr} (defined below), is the longitude of the IPP in the co-rotating reference frame, and a_0, \dots, a_{14} are ionosphere model coefficients.

If the geographic latitude and longitude of the GPS receiver (ϕ_u, λ_u) are known, the geographic latitude and longitude of an IPP can be computed (eg. Klobuchar, 1987; Lin et al., 1996a) according to the observed azimuth and elevation angle to the tracked satellite, and the geometry of the single-layer ionosphere model. The latitude of a pierce point ϕ_{pp} is computed from:

$$\phi_{pp} = \sin^{-1}(\sin \phi_u \cdot \cos \psi_{pp} + \cos \phi_u \cdot \sin \psi_{pp} \cos A) \quad (5.4)$$

where ψ_{pp} is the angle subtended at the centre of the earth between the user position vector and the earth projection of the pierce point, computed from:

$$\psi_{pp} = \frac{\pi}{2} - E - \sin^{-1}\left(\frac{R_e}{R_e + h} \cos E\right) \quad (5.5)$$

A is the azimuth angle of the satellite at the user's location. The longitude of the pierce point λ_{pp} is:

$$\lambda_{pp} = \lambda_u + \sin^{-1}\left(\frac{\sin \psi_{pp} \sin A}{\cos \phi_{pp}}\right) \quad (5.6)$$

The geomagnetic coordinate system with its dipole axis intersecting the geographic sphere, or Boreal pole (ϕ_p, λ_p) , at approximately $78.7^\circ N$ latitude and $290.1^\circ E$ longitude (Biel, 1990), is used to compute the geomagnetic latitude, ϕ_m , of the IPP:

$$\sin \phi_m = \sin \phi_{pp} \sin \phi_p + \cos \phi_{pp} \cos \phi_p \cos(\lambda_{pp} - \lambda_p) \quad (5.7)$$

The longitude of the IPP in the co-rotating reference frame depends on both the IPP longitude in an earth-fixed frame and the rotation of the earth-fixed frame relative to the sun (Coco et al., 1991):

$$\lambda_{cr} = \lambda_{ef} + T_e \cdot \omega_e \quad (5.8)$$

where λ_{cr} is the longitude of the IPP in the co-rotating reference frame; λ_{ef} is the longitude of the IPP in an earth-fixed reference frame; T_e is Universal Time (UT); and ω_e is the angular velocity of the earth. Hence, in co-rotating reference frame, the direction of the sun is always fixed at 180° (λ_{cr}) (ibid, 1991).

Step 2: A 24-hour data set at a site is divided into eight 3-hour sessions (note that the reason for selecting a 3-hour session length was discussed in section 5.3.1). For each session, the Satellite-Plus-Receiver (SPR) differential delay ($b_R + b^S$), for each tracked satellite, and the 15 terms of the ionosphere model of equation (5.3), are estimated by a least squares procedure. The SPR term is a lumped estimate of the satellite and receiver differential delays, as it is impossible to separate b^S from b_R unless the internal hardware calibration value for the receiver differential delay b_R is available.

Step 3: Finally, a weighted average procedure is used to compute the mean SPR differential delay for each tracked GPS satellite. These SPR differential delays can be used to calibrate the measured slant TEC in order to provide precise TEC measurements.

5.4 Test Results and Discussion

5.4.1 Description of Test Data

In order to verify this estimation technique, a number of data sets from the *Permanent GPS Geodetic Array* (PGGA), in Southern California, USA (PGGA, 1996), were processed and analysed.

Five stations: Blythe (blyt), China Lake (coso), Yucaipa (crfp), Scripps (sio3), and Vandenberg (vndp) were selected for the tests. The main reason for selecting this 5-station network as a test field was to further validate the UNSW estimation algorithm for regional ionosphere modelling applications. Four sites (located approximately at the vertexes of a quadrilateral), “blyt”, “coso”, “sio3”, and “vndp” were chosen as reference stations used to generate the regional ionosphere model, and site “crfp” (located approximately at the centre of the quadrilateral formed by the 4 reference stations) was designated the “user”, permitting the “standard deviation” of the “TEC prediction residuals” of the ionosphere model to be computed (cf. section 5.4.2.3). The coordinates of these PGGA sites, and their approximate distances from the “crfp” site, are shown in Table 5.1. These stations were equipped with Ashtech Z-XII3 geodetic receivers, and collected data from all visible GPS satellites every 30 seconds. Data from day 001 to 012, 1996, were processed.

Table 5.1. PGGA stations used in this study.

Site Name	Latitude N	Longitude W	Dist. to User	Notes
blyt	33.43 degree	114.71 degree	225.64 km	Remote Site
coso	35.98 degree	117.81 degree	225.78 km	Remote Site
crfp	34.04 degree	117.10 degree	0.0 km	User
sio3	32.87 degree	117.25 degree	131.47 km	Remote Site
vndp	34.55 degree	120.48 degree	328.48 km	Remote Site

Before estimating the satellite-plus-receiver differential delay and the ionosphere parameters of equation (5.3), some pre-processing steps are followed, such as the slant TEC computation, phase levelling, etc. (Lin et al., 1996a). The elevation cut off angle was set to 15°.

5.4.2 Methods to Verify the Algorithm

Several methods were used to verify the performance of this algorithm.

5.4.2.1 Daily Variation of the Satellite-Plus-Receiver Differential Delay

The Satellite-Plus-Receiver (SPR) differential delay ($b_R + b^S$), for the 25 GPS satellites at the five PGGGA sites, during the period from day 001 to 012, 1996, were estimated. Then, the mean SPR differential delay for each satellite over the 12-day period was computed for each site. The results are shown in Table 5.2. It is obvious from Table 5.2 that each GPS satellite has a different SPR differential delay at each site. The maximum SPR differential delay in this experiment is about 49 TECU (which is about 5 m in differential delay, or 8 m group delay at the L1 frequency) for PRN 12 at site “vndp”. Without calibrating for these SPR differential delays it is impossible to obtain precise TEC estimation from GPS measurements.

The standard deviation of the mean SPR differential delay for the 12-day period were computed and are given in Table 5.3. These standard deviation values indicate the day-to-day variability of the SPR differential delay estimates. The average value of the standard deviations of the SPR differential delay estimates for the whole experiment is 1.24 TECU (or 0.43 ns in differential delay), with a maximum of 1.52 TECU, and a minimum of 0.81 TECU.

The mean standard deviation of 1.24 TECU represents an error estimate of the lumped satellite-plus-receiver differential delays. This value also provides an upper bound for the day-to-day variation of the lumped satellite-plus-receiver differential delays.

The estimated SPR differential delay, SPR_j , for a certain receiver to a tracked GPS satellite j , can be expressed as (Coco et al., 1991):

$$SPR_j = b_j^S + b_R + M_j + I_j + I_c \quad (5.9)$$

where b_j^s is the differential delay from satellite j , M_j is the bias (unique to an individual satellite) attributed to multipath, I_j is the bias (unique to an individual satellite) due to mismodelling of the ionosphere, I_c is the bias (common to all satellites) due to mismodelling of the ionosphere, and b_R is the receiver differential delay (common to all satellites).

According to equation (5.9), the receiver differential delay, b_R , and the bias due to mismodelling of the ionosphere, I_c , are common to all satellites and cause the estimated SPR differential delays of a common satellite to vary across different sites (cf. Table 5.2). In order to remove these common biases, b_R and I_c , the daily average of the SPR differential delay estimates over all 25 GPS satellites, for a specific site, is first computed. The results are shown in Table 5.4. The mean of the daily average of the SPR differential delay estimates over all 25 GPS satellites for each site provides an estimate of the receiver differential delay for that site. From Table 5.4 it is found that the receiver differential delays of the five PGGGA sites range from 22 to 36 TECU (7.7 to 12.6 ns in differential delay). The standard deviations of the means are shown in the bottom row of Table 5.4. The mean value is 0.85 TECU (0.29 ns in differential delay).

In the next step, the difference between the estimate of SPR differential delay and its daily average, SAT, is computed for each satellite. The average value of these SAT estimates over the 12-day period for each satellite are summarised in Table 5.5. These average values represent the biases from each satellite, including the b_j^s , M_j , and I_j terms of equation (5.9). The mean satellite biases for each satellite from the five PGGGA sites are given in the 7th column of Table 5.5. It can be seen that the GPS satellite biases, including the b_j^s , M_j , and I_j terms of equation (5.9), are in the range -8.87 to +12.67 TECU (-3.11 to 4.44 ns). The standard deviation of the satellite bias estimates from the five sites are given in the 8th column of Table 5.5. The standard deviation (std dev) of the mean SAT estimate for each satellite, at the five PGGGA sites, over the 12-day period are given in Table 5.6. The mean standard deviation of the mean SAT estimate is the precision of the satellite differential delay estimate from applying this algorithm. It is 1.00 TECU (0.35 ns).

On the basis of these experimental results, it is concluded that: (1) the day-to-day variation of the combined satellite and receiver differential delay is ± 1.24 TECU (± 0.43 ns), (2) the receiver differential delays are in the range of 22 to 36 TECU (7.7 to 12.6 ns) with a mean standard deviation of ± 0.85 TECU (± 0.29 ns), and (3) the GPS satellite differential delays are in the range of -8.87 to +12.67 TECU (-3.11 to 4.44 ns) with a mean standard deviation of ± 1.00 TECU (0.35 ns).

Table 5.2. Mean SPR differential delay (Mean SPR) estimation, in units of TECU, for each tracked GPS satellite at the five PPGA stations, over the period day 001 to 012, 1996.

PRN	Mean SPR at blyt	Mean SPR at coso	Mean SPR at crfp	Mean SPR at sio3	Mean SPR at vndp
1	30.24	23.07	24.48	29.45	36.47
2	33.05	27.31	28.42	32.24	40.83
4	24.64	18.28	20.28	25.30	32.12
5	28.48	20.81	22.91	28.63	35.55
6	26.24	18.74	19.59	25.58	32.66
7	33.01	26.89	28.53	33.14	40.71
9	26.98	20.69	21.65	26.80	34.02
12	41.25	33.62	36.98	41.81	48.95
14	29.44	21.90	24.76	28.22	37.27
15	31.70	25.54	26.32	30.14	38.94
16	33.15	25.74	27.65	32.50	39.77
17	32.30	25.94	25.77	31.49	38.35
18	24.65	17.16	20.78	23.86	33.10
19	29.28	23.30	25.14	28.21	37.72
20	32.07	24.21	26.47	31.66	38.82
21	32.50	26.29	26.04	31.12	38.38
22	25.29	20.08	19.20	23.27	32.28
23	31.30	25.34	25.14	31.02	37.84
24	33.50	26.70	28.20	34.04	40.51
25	20.65	14.22	16.29	20.07	28.26
26	24.22	18.25	17.72	22.40	31.06
27	27.69	20.13	23.49	26.62	35.24
28	24.46	16.87	18.26	23.09	30.98
29	19.97	12.23	15.65	18.38	27.76
31	28.96	18.40	20.75	23.47	32.75

Table 5.3. Standard deviation (std dev) of the mean SPR differential delay, for each tracked GPS satellite at the five PGGGA stations, over the period day 001 to 012, 1996.

PRN	std dev at blyt	std dev at coso	std dev at crfp	std dev at sio3	std dev at vndp
1	1.48	1.35	1.94	1.54	1.27
2	1.28	0.85	1.23	1.67	1.25
4	1.07	0.64	1.15	1.37	0.79
5	0.86	0.82	0.90	1.26	0.89
6	1.19	1.38	1.09	0.99	0.38
7	1.52	0.90	1.40	1.71	1.20
9	1.46	1.31	1.93	2.31	1.54
12	1.44	0.97	1.51	1.12	1.27
14	1.44	1.69	1.28	1.36	1.44
15	1.55	1.24	1.47	1.34	1.18
16	0.98	1.59	0.79	1.35	1.09
17	1.57	1.21	1.01	1.06	0.59
18	1.01	1.39	1.17	1.01	1.48
19	0.87	1.09	1.03	1.21	0.96
20	0.81	0.76	0.83	1.05	0.60
21	1.64	0.55	1.32	1.61	0.69
22	1.56	0.54	1.33	1.00	1.35
23	1.84	0.91	0.90	1.57	0.63
24	0.74	0.75	0.92	1.27	0.75
25	1.34	1.62	1.52	1.52	1.56
26	2.09	1.79	1.20	1.73	1.04
27	1.21	0.85	1.41	1.87	1.45
28	1.42	0.72	1.34	2.06	1.42
29	1.23	1.53	1.01	0.96	1.39
31	1.37	0.86	1.34	1.97	1.49

Table 5.4. Daily averages of the SPR differential delay estimates over all 25 GPS satellites, in units of TECU, at the five PGGGA sites, over the period day 001 to 012, 1996.

	Blyt	coso	crfp	sio3	vndp
day 001	28.14	21.95	23.22	26.53	35.57
day 002	29.16	22.71	25.06	28.58	36.46
day 003	31.12	22.54	25.65	29.92	36.94
day 004	29.09	n/a	n/a	n/a	n/a
day 005	29.71	21.38	23.36	27.96	35.98
day 006	29.41	22.35	23.85	28.61	36.11
day 007	28.11	22.31	23.93	29.05	36.29
day 008	28.30	21.44	23.22	27.63	35.94
day 009	28.30	21.48	23.58	n/a	36.24
day 010	28.41	21.77	22.63	n/a	34.90
day 011	27.53	22.04	23.12	27.69	35.67
day 012	30.91	22.31	22.73	26.65	34.90
arithmetic mean	29.02	22.03	23.67	28.07	35.93
standard deviation	1.12	0.46	0.94	1.09	0.654

(n/a = data not available for that particular day)

Table 5.5. The average values of SAT estimates for each satellite, in units of TECU, at the five PGGA stations, over the period day 001 to 012, 1996.

PRN	blyt	coso	crfp	sio3	vndp	Mean	std dev
1	1.23	1.05	0.81	1.38	0.54	1.00	0.33
2	4.03	5.28	4.75	4.18	4.90	4.62	0.52
4	-4.12	-3.56	-3.38	-2.77	-3.55	-3.48	0.48
5	-0.28	-1.22	-0.45	0.56	-0.39	-0.58	0.37
6	-2.77	-3.29	-4.08	-2.49	-3.41	-3.21	0.62
7	4.00	4.87	4.87	5.08	4.78	4.72	0.42
9	-1.68	-1.34	-2.02	-1.00	-1.92	-1.59	0.42
12	12.22	11.60	13.31	13.29	12.91	12.67	0.74
14	0.83	-0.13	1.09	0.16	1.34	0.66	0.62
15	2.68	3.47	2.65	2.07	3.00	2.77	0.51
16	4.13	3.62	3.78	3.82	3.84	3.84	0.18
17	3.28	3.91	2.10	3.42	2.22	2.99	0.79
18	-4.07	-4.87	-2.89	-4.20	-2.84	-3.77	0.88
19	0.48	1.12	1.47	0.14	1.53	0.95	0.61
20	3.30	2.18	3.05	3.59	3.05	3.03	0.52
21	3.49	4.42	2.37	3.06	2.24	3.12	0.89
22	-3.24	-2.37	-4.48	-4.80	-3.66	-3.71	0.97
23	2.28	3.31	1.73	2.95	1.66	2.38	0.73
24	4.68	4.67	4.80	5.97	4.80	4.98	0.55
25	-7.98	-7.81	-7.38	-8.00	-7.68	-7.77	0.25
26	-4.79	-3.78	-5.95	-5.67	-5.19	-5.08	0.85
27	-1.33	-1.90	-0.18	-1.45	-0.70	-1.11	0.67
28	-4.22	-5.16	-5.03	-4.98	-4.95	-4.87	0.37
29	-8.68	-9.80	-8.02	-9.69	-8.17	-8.87	0.83
31	-3.06	-3.62	-2.93	-4.60	-3.18	-3.48	0.68

Table 5.6. The standard deviation (std dev) of the mean SAT estimate for each satellite, in units of TECU, at the five PGGGA stations, over the period day 001 to 012, 1996.

PRN	blyt	coso	crfp	sio3	vndp
1	0.75	1.20	1.29	0.99	0.94
2	0.93	0.84	0.71	0.88	0.82
4	0.82	0.80	0.64	0.63	0.70
5	0.80	0.70	0.92	0.44	0.60
6	0.51	1.38	0.69	0.55	0.65
7	1.08	1.00	0.94	0.85	0.76
9	1.24	1.30	1.36	1.60	1.13
12	1.09	1.02	0.96	0.94	0.78
14	1.69	1.43	0.96	1.59	1.31
15	0.99	0.93	1.01	1.15	0.90
16	0.71	1.42	0.94	1.62	0.81
17	0.72	1.35	0.66	0.60	0.98
18	1.24	1.10	1.22	0.94	1.16
19	0.78	1.19	0.58	0.72	0.76
20	0.77	0.78	0.53	0.50	0.70
21	0.79	0.70	0.64	0.91	0.70
22	1.80	2.03	1.43	1.38	1.48
23	0.92	1.04	0.72	0.82	0.92
24	0.75	0.61	0.79	0.53	0.65
25	1.64	1.38	1.36	1.70	1.51
26	1.28	1.97	0.76	0.97	1.48
27	1.09	0.75	1.07	1.25	1.01
28	0.78	0.55	1.21	1.25	0.92
29	1.60	1.31	1.06	1.33	1.21
31	1.02	0.62	1.13	1.44	1.10
Mean std dev	1.03	1.09	0.94	1.02	0.96

5.4.2.2 Comparison with the Results of Other Organisations

The results from the DLR Neustrelitz (DLR) tests (DLR, 1996), and the USAF Phillips Laboratory (PL) tests (Bishop et al., 1994b) are compared with these results. Since these two organisations provide results for the satellite differential delays with the daily average removed, it is possible to directly make a comparison. Single-site technique was used by PL to process eleven sets of data, one day each, from an Ashtech Z-12 receiver at Hanscom AFB (PL) and from the JPL Westford site (Bishop et al., 1994b). DLR used the multi-site technique (Sardon et al., 1994) to process the data from 20 GPS stations.

Eighteen of them are in Europe, one in Australia and one in the USA. All of these stations are equipped with Rogue or Turbo-Rogue receivers, except Mendeleevo which is equipped with a Trimble receiver. Note that PL's results are referred to 1994 and DLR's results refer to day 001 to 012, 1996 (ie. the same period as this experiment).

Satellite differential delay differences between the UNSW solutions and those from PL and DLR are given in Figure 5.2. The standard deviations for "UNSW - DLR" and "UNSW - PL" are 0.96 TECU (0.33 ns) and 1.13 TECU (0.39 ns) respectively. The satellite differential delay differences are in the range ± 0.66 ns for "UNSW - DLR", and ± 0.88 ns for "UNSW - PL".

In order to further validate the UNSW estimation algorithm, comparisons were also made with other organisations. The following comparisons are based on the data quoted by Gao et al. (1994), including the following organisations: Natural Resources Canada (NRCan), Canada; Instituto de Astronomia y Geodesia (IAG), Spain; Institut fuer Erdmessung (IfE), Germany and the Jet Propulsion Laboratory (JPL), USA. Before making the comparisons, the average of all satellite biases of each organisation is first computed (Coco et al., 1991; Bishop et al., 1994b). Then, the average is removed from each satellite bias estimate. These averages are, for JPL, NRCan, IAG and IfE, -1.776 ns, -0.14 ns, -1.9196 ns, and -1.6156 ns respectively.

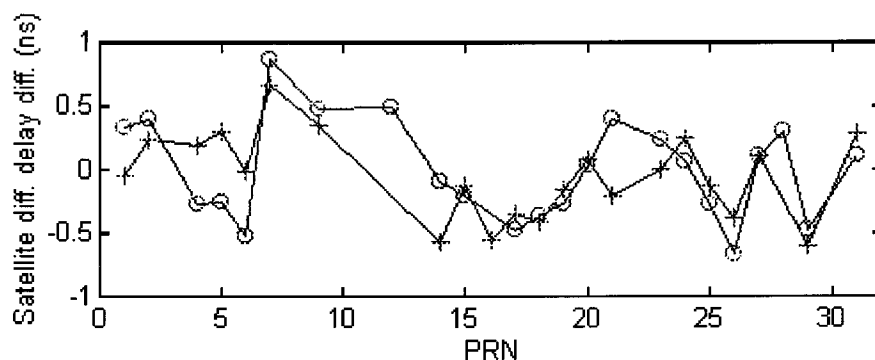


Figure 5.2. Satellite differential delay differences between the UNSW solution and solutions from DLR and PL. '+' represents 'UNSW - DLR', 'o' represents 'UNSW - PL'.

The satellite differential delay differences between the UNSW solutions and those of JPL, NRCan, IAG and IfE are shown in Figures 5.3 and 5.4. The standard deviations for

“UNSW - JPL”, “UNSW - NRCan”, “UNSW - IAG”, and “UNSW - IfE” are 1.38 TECU (0.48 ns), 3.72 TECU (1.31 ns), 3.00 TECU (1.05 ns) and 3.05 TECU (1.07 ns) respectively. Note that NRCan’s solution has a 1 ns bias (Gao et al., 1994) which causes the standard deviation of “UNSW - NRCan” to be 1.31 ns. If this bias is removed, then the UNSW algorithm can estimate satellite differential delays which are in agreement with those of other organisations at the 1 ns level.

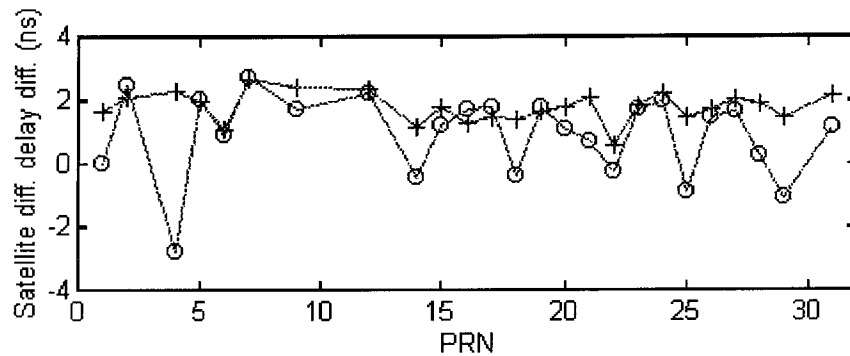


Figure 5.3. Satellite differential delay differences between the UNSW solution and solutions from JPL and NRCan. ‘+’ represents ‘UNSW - JPL’, ‘o’ represents ‘UNSW - NRCan’.

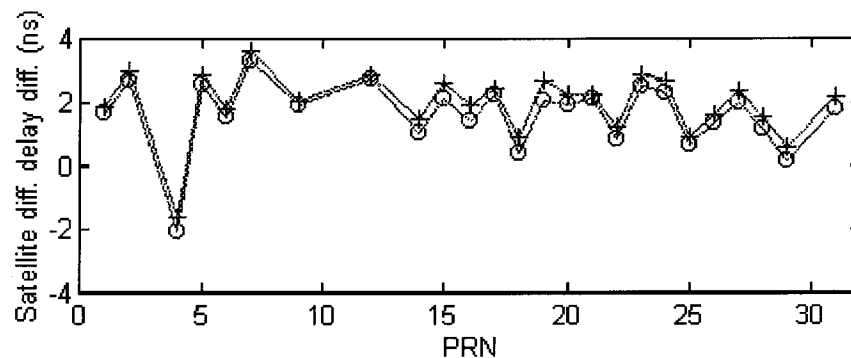


Figure 5.4. Satellite differential delay differences between the UNSW solution and solutions from IAG and IfE. ‘+’ represents ‘UNSW - IAG’, ‘o’ represents ‘UNSW - IfE’.

From the estimated satellite differential delay comparisons shown in Figures 5.2 to 5.4, it can be concluded that: (1) the estimated satellite differential delay values using UNSW algorithm agreed with that estimated by PL, DLR and JPL to within 0.5 nanosecond, and (2) the estimated satellite differential delay values using UNSW algorithm agreed with those estimated by NRCan, IAG and IfE to within 1.1 nanosecond.

5.4.2.3 Variability of the Standard Deviation of the TEC Prediction Residuals in Regional Ionosphere Modelling

In order to further validate the UNSW estimation algorithm, five sites of the PGGGA (cf. Table 5.1) are selected in order to check the “standard deviation” of the “TEC prediction residuals” for PGGGA regional ionosphere modelling. “*TEC prediction residual*” is defined as the difference between the vertical TEC value derived from GPS observables at a user site and that derived from regional ionosphere modelling. Four sites, “blyt”, “coso”, “sio3”, and “vndp” were chosen as reference stations used to generate the regional ionosphere model, and site “crfp” was designated the “user”, permitting the “standard deviation” of the “TEC prediction residuals” of the ionosphere model to be computed. These five sites were equipped with dual-frequency GPS receivers. The UNSW algorithm was used to estimate the combined GPS satellite-plus-receiver differential delays (SPRs) for each satellite, for each site, each day. Then, these SPR differential delays were used to calibrate the TEC measurements. A grid-based ionosphere model was generated. Details of the generation of such ionosphere models will be presented in chapter 6.

The “standard deviation” of the “TEC prediction residuals” for the ionosphere modelling of the PGGGA area over an 11-day period are shown in Table 5.7. (Note that there was no result for day 004 due to there being no data available.) Figure 5.5 is an example of the “TEC prediction residual” distribution based on a 24-hour data set (13,760 observations). From Table 5.7 it can be seen that the average standard deviation of the TEC prediction residuals over a 12-day period is at the 1 TECU level (which is at the GPS receiver measurement noise level).

The UNSW algorithm has also been used for wide-area ionosphere modelling. Data from Australian Regional GPS Network stations, as well as the GSI GPS network in Japan, were used to generate a wide-area ionosphere model. The test results from these data sets will be summarised in chapter 6.

Table 5.7. The standard deviation (std dev) of the “TEC prediction residuals” of PGGA regional ionosphere modelling, in units of TECU, for day 001 to 012, 1996.

(n/a = data not available for that particular day)

Day No.	001	002	003	004	005	006	007	008	009	010	011	012
std dev	0.99	1.31	1.04	n/a	1.07	0.90	1.14	0.92	0.95	0.93	1.06	0.98

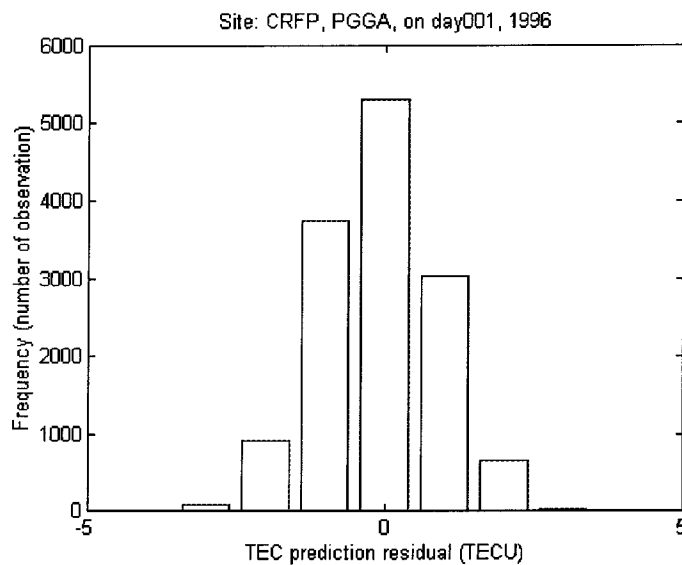


Figure 5.5. TEC prediction residual distribution of ionosphere modelling, with mean value -0.11 TECU, standard deviation 0.991 TECU.

5.5 Concluding Remarks

In order to obtain accurate absolute ionospheric delay estimates using dual-frequency GPS measurements, the GPS satellite and receiver differential delays must be calibrated reliably. Test results from the literature strongly suggest that the satellite and receiver differential delays vary from day-to-day. Hence, the satellite and receiver differential delays must be calibrated periodically. In addition, many permanent sites are equipped with GPS receivers which do not have an internal calibration capability. Consequently, an estimation procedure was developed to estimate the sum of satellite and receiver differential delays. Test results confirm that the proposed algorithm was able to effectively calibrate the satellite and receiver differential delays. The proposed algorithm was then applied to regional ionosphere modelling. Detailed results of the regional ionosphere modelling are presented in chapter 6.

CHAPTER 6

AN ALTERNATIVE GRID-BASED ALGORITHM
TO IMPROVE THE ACCURACY OF
REAL-TIME IONOSPHERE MODELLING

6.1 Introduction

One real-time regional ionosphere modelling method is the so-called “*grid-based algorithm*”, or “conventional grid-based algorithm”. Typically, a simple weighting function, such as “*inverse distance*” (eg. Conker et al., 1995), is applied, and the “*Klobuchar model*” (Klobuchar, 1987) is used to predict the ionospheric delay ratios between the grid point and reference points. In order to improve the real-time regional ionosphere modelling performance, an alternative grid-based algorithm, referred to here as the “UNSW grid-based algorithm”, was proposed (Lin & Rizos, 1997a, 1997c). In this new algorithm, an “*exponential function*” is adopted as the weighting function and the “*grid-based ionosphere model*” estimated from the previous day is used to predict the ionospheric delay ratios between the grid point and reference points.

Firstly, the basic concept and methodology of the conventional grid-based algorithm is introduced. The fundamental equations used in the conventional grid-based algorithm, such as ionospheric pierce point (IPP) location determination, slant TEC estimation using dual-frequency GPS measurements, etc., are reviewed and summarised. Then, the UNSW grid-based algorithm is introduced. A suite of computer software called “POSTEC” developed by the author is described. Test results from different GPS networks, such as PGGGA, GSI, ARGN, are summarised and discussed to demonstrate the performance of UNSW grid-based algorithm to improve the accuracy of real-time ionosphere modelling.

6.2 Conventional Grid-Based Ionospheric Delay Estimation Algorithm

6.2.1 Introductory Remarks

Several real-time ionospheric estimation algorithms, such as the grid-based, least-squares fit, spherical harmonic analysis, spherical cap harmonic analysis, and adjusted spherical harmonic analysis, have been proposed to generate ionospheric delay corrections to support single-frequency GPS users (El-Arini et al., 1995). However, only the grid-based algorithm was investigated in this thesis.

A summary of the grid-based ionospheric correction procedure is presented below (ibid, 1995):

- 1) Several Wide-area Reference Stations (WRSs) are located around a region. Each WRS measures the ionospheric delay (TEC), for each ionospheric pierce point (IPP), using a dual-frequency GPS receiver. These TEC measurements are sent to the Wide-area Master Station (WMS).
- 2) The WMS collects the TEC data from all WRSs. Combining the data from all the satellites, it estimates the vertical ionospheric delay (vertical TEC) at each node of an imaginary fixed grid (eg. 5 degree in latitude and longitude) on the ionospheric shell.
- 3) The WMS sends the vertical delay estimate of each node of the grid as well as the node latitude and longitude (or an identification number), to all users via a geostationary communication satellite, or other telemetry means.
- 4) The user receiver computes the latitude and longitude of its ionospheric pierce points. For each of the user's ionospheric pierce points, the receiver computes its vertical delay, interpolated from the grid using the vertical delays of the four nodes of the cell that contains the pierce point, using one of many possible interpolation techniques, such as the weighting function approach, bilinear, bicubic, inverse distance, etc.

One grid-based algorithm that could be used at the WMS to estimate the vertical TEC at each grid node is the “*inverse distance*” algorithm (eg. Conker et al., 1995). This algorithm is referred to as the “*conventional grid-based algorithm*” in this thesis.

In order to present the overall concept of the “conventional grid-based algorithm”, a summary of the equations from previous chapters is given in the following sections.

6.2.2 Ionospheric Pierce Point Location Determination

In order to model the regional ionosphere, the ionosphere is usually described by a so-called “*thin-shell model*” (Lanyi & Roth, 1988). The height of this idealised “*shell*” is usually set at an altitude of between 300 and 400 km above the earth. The intersection of the line-of-sight from the GPS satellite to receiver with this thin-shell is the “*ionospheric pierce point*” (IPP). The IPP geometry is shown in Figure 5.1.

If the geographic latitude and longitude of the GPS receiver, (ϕ_u, λ_u) , are known, the geographic latitude and longitude of an IPP can be computed (eg. Klobuchar, 1987; Lin et al., 1996a) according to the observed azimuth, A , and elevation angle, E , to the tracked satellite, and the single-layer ionosphere model. The latitude of a pierce point ϕ_{pp} is computed as:

$$\phi_{pp} = \sin^{-1}(\sin \phi_u \cdot \cos \psi_{pp} + \cos \phi_u \cdot \sin \psi_{pp} \cos A) \quad (6.1)$$

where ψ_{pp} is the earth’s central angle between the user position and the earth projection of the pierce point, computed from:

$$\psi_{pp} = \frac{\pi}{2} - E - \sin^{-1}\left(\frac{R_e}{R_e + h} \cos E\right) \quad (6.2)$$

The longitude of the pierce point λ_{pp} is:

$$\lambda_{pp} = \lambda_u + \sin^{-1} \left(\frac{\sin \psi_{pp} \sin A}{\cos \phi_{pp}} \right) \quad (6.3)$$

6.2.3 Slant TEC Estimation Using Dual-Frequency GPS Measurements

6.2.3.1 Basic GPS Pseudo-Range and Carrier Phase Observables

From equations (3.1) and (3.2), the L1/L2 pseudo-range measurements (in units of m) after considering the multipath effects are expressed as:

$$P_1 = \rho + c(dT - dt) + d_{ion1} + d_{trop} + d_\rho + MP_{(P1)} + \varepsilon_{P1} \quad (6.4)$$

$$P_2 = \rho + c(dT - dt) + d_{ion2} + d_{trop} + d_\rho + MP_{(P2)} + \varepsilon_{P2} \quad (6.5)$$

where P_1 , P_2 are the pseudo-ranges measured on L1 and L2 respectively; ρ is the geometric range from the receiver to the satellite; c is the speed of light; dt is the satellite clock error; dT is the receiver clock error; d_{ion1} , d_{ion2} are the ionospheric delays at L1 and L2 respectively; d_{trop} is the delay due to the troposphere; d_ρ is the orbital error; ε_{P1} , ε_{P2} are the pseudo-range measurement noise at L1 and L2 respectively; $MP_{(P1)}$, $MP_{(P2)}$ are the pseudo-range multipath at L1 and L2 respectively.

From equations (3.3) and (3.4), the carrier phase measurements (in units of m) after considering the multipath effects are expressed as:

$$\Phi_1 = \rho + c(dT - dt) + \lambda_1 N_1 - d_{ion1} + d_{trop} + d_\rho + mp_{(\Phi1)} + \varepsilon_{\Phi1} \quad (6.6)$$

$$\Phi_2 = \rho + c(dT - dt) + \lambda_2 N_2 - d_{ion2} + d_{trop} + d_\rho + mp_{(\Phi2)} + \varepsilon_{\Phi2} \quad (6.7)$$

where Φ_1 , Φ_2 are carrier phase measurements at L1, L2 respectively; λ_1 , λ_2 are carrier wavelengths (in m/cycle) of L1, L2 respectively; N_1 , N_2 are integer ambiguity parameters (in cycle) at L1, L2 respectively; $mp_{(\Phi1)}$, $mp_{(\Phi2)}$ are the carrier phase multipath at L1, L2 respectively; $\varepsilon_{\Phi1}$, $\varepsilon_{\Phi2}$ are the carrier phase noise terms.

Define:

$$MP1 = MP_{(P1)} + \varepsilon_{P1} \quad (6.8)$$

$$MP2 = MP_{(P2)} + \varepsilon_{P2} \quad (6.9)$$

$$mp1 = mp_{(\Phi1)} + \varepsilon_{\Phi1} \quad (6.10)$$

$$mp2 = mp_{(\Phi2)} + \varepsilon_{\Phi2} \quad (6.11)$$

The simplified pseudo-range measurements are:

$$P_1 = \rho + c(dT - dt) + d_{ion1} + d_{trop} + d_{\rho} + MP1 \quad (6.12)$$

$$P_2 = \rho + c(dT - dt) + d_{ion2} + d_{trop} + d_{\rho} + MP2 \quad (6.13)$$

The simplified carrier phase measurements are:

$$\Phi_1 = \rho + c(dT - dt) + \lambda_1 N_1 - d_{ion1} + d_{trop} + d_{\rho} + mp1 \quad (6.14)$$

$$\Phi_2 = \rho + c(dT - dt) + \lambda_2 N_2 - d_{ion2} + d_{trop} + d_{\rho} + mp2 \quad (6.15)$$

6.2.3.2 Slant TEC Estimation Using Dual-Frequency GPS Measurements

From equations (2.20), (6.12), and (6.13), after rearrangement:

$$P_2 - P_1 = 40.3 \times TEC \times \left(\frac{f_1^2 - f_2^2}{f_1^2 \cdot f_2^2} \right) + MP2 - MP1 \quad (6.16)$$

Therefore, the TEC term derived from the pseudo-range measurements can be expressed as (cf. equations (2.32) and (3.42)):

$$\begin{aligned} TEC &= 9.5196 \times [(P_2 - P_1) - (MP2 - MP1)] && [\text{TECU}] \\ &= TR - 9.5196 \times (MP2 - MP1) && [\text{TECU}] \end{aligned} \quad (6.17)$$

From equations (2.21), (2.31), (2.33), (6.14), and (6.15), after arrangement, the TEC term derived from carrier phases without considering the multipath and noise terms, is:

$$\begin{aligned} TEC &= 9.5196 \times [(\Phi_1 - \Phi_2) - (\lambda_1 N_1 - \lambda_2 N_2)] && [\text{TECU}] \\ &= TS + D && [\text{TECU}] \end{aligned} \quad (6.18)$$

Let TR_i be the i th measurement of the frequency-differenced pseudo-range using equation (2.32) in a carrier phase connected data arc consisting of M points. If TS_i is the i th frequency-differenced carrier phase measurement using equation (2.33), then equations (6.17) and (6.18) can be re-written for the i th TEC estimate:

$$TEC_i = TR_i - 9.5196 \times (MP2 - MP1)_i \quad [\text{TECU}] \quad (6.19)$$

$$TEC_i = TS_i + D \quad [\text{TECU}] \quad (6.20)$$

Then a levelling constant D , for the arc, is computed as follows (further discussion is given in section 6.2.3.3):

$$D = \frac{1}{M} \sum_{i=1}^M (TR_i - TS_i) \quad (6.21)$$

The TEC observable, TEC_i , is formed by adding this constant to the carrier phase measurements TS_i :

$$TEC_i = TS_i + D \quad (6.22)$$

6.2.3.3 Concluding Remarks

If dual-frequency GPS measurements are available, the absolute measure of the TEC can be computed from the L1/L2 pseudo-range measurements using equation (6.17). However, this estimated TEC is “noisy” due to the effect of multipath and measurement noise. In addition, there is the effect of other biases due to the GPS satellite and receiver L1/L2 differential delays. On the other hand, the relative measure of the TEC, TS , can be

calculated from the L1/L2 carrier phase measurements using equation (2.33). These have the virtue of being less noisy than those derived using pseudo-range data.

In order to obtain accurate absolute TEC estimates, the pseudo-range derived TEC estimates, TR , and the carrier phase derived TEC estimates, TS , must be combined somehow. There are two options. In the post-processing option, the “phase levelling” procedure is commonly used (cf. section 2.5.1). This is accomplished by “fitting” the carrier phase derived TEC estimates to the unambiguous, but noisy, pseudo-range derived TEC estimates. The outputs are then the so-called “phase levelled TEC” estimates. The multipath effects on the pseudo-range derived TEC estimates will be mitigated after “phase levelling” and the cycle slip(s) in the carrier phase can be detected and repaired in a prior step.

In the real-time option, a recursive process such as a Kalman filter is typically used to estimate TEC. Unlike the post-processing mode, carrier phase measurement failures must be detected, identified and repaired in real-time. Since the pseudo-range derived TEC is used to estimate the D term in equation (6.18), a special multipath mitigation technique must be implemented to overcome the pseudo-range multipath effects.

The “multi-day multipath template” technique has been introduced in chapter 3. The multipath template generated from the previous day’s GPS data is used to mitigate the pseudo-range multipath effect (cf. equation (6.17)) on TEC estimates. A real-time failure detection and repair algorithm in TEC estimation was described in chapter 4. The main purpose of this algorithm is to detect and repair the TS failure(s) in real-time. Test results presented in these two chapters demonstrate that multipath effects on TR are mitigated significantly and the TS failure(s) can be detected and repaired promptly and reliably.

In addition, the GPS satellite and receiver L1/L2 differential delays must be subtracted from the estimated TEC values to generate unbiased absolute TEC estimates. There are several algorithms which can be used to derive the GPS instrumental L1/L2 differential delays in the post-processing mode. It has been noted that the instrumental L1/L2 differential delays are stable over a period of several days (eg. Engler et al., 1995; Lin &

Rizos, 1996a). An alternative algorithm for the determination of the GPS instrumental L1/L2 differential delays was introduced in chapter 5.

6.2.4 Vertical TEC Estimation

Because the measured TEC is along the line-of-sight to the tracked GPS satellite, the vertical TEC at pierce point TEC_v is modelled using the following expression:

$$TEC_m = S(E) \times TEC_v + b_R + b^S \quad (6.23)$$

where TEC_m is the slant TEC measurement using equation (6.22); b_R is the GPS L1/L2 receiver differential delay; b^S is the GPS L1/L2 satellite differential delay and $S(E)$ is the obliquity factor (or mapping function) with zenith z at the IPP:

$$S(E) = \frac{1}{\cos z} = \left[1 - \left(\frac{R_e \cos E}{R_e + h} \right)^2 \right]^{-0.5} \quad (6.24)$$

where E is the elevation angle of the satellite from the user's location; R_e is the mean radius of the earth; and h is the height of the ionosphere layer ($h=400$ km in this thesis). The use of a mapping function is clearly an approximation, and can lead to errors of several TECU when applied to regions of large horizontal electron density gradients (eg. Klobuchar et al., 1993). There are other mapping functions. For example, Clynch et al. (1989) used a 4-term polynomial as a function of elevation angle as the mapping function (ionosphere height was assumed to be 250 km) to monitor polar region ionosphere. Sardon et al. (1995) adopted the mapping function derived by Sovers & Faselow (1987) to study the GPS satellite and receiver L1/L2 differential delays.

6.2.5 Grid Point TEC Determination

One grid-based algorithm that could be used at the WMS to estimate the vertical TEC at each grid node is the “*inverse distance*” algorithm (eg. Conker et al., 1995). That is, for a grid point p , the vertical TEC is estimated by:

$$\hat{\tau}_{vp} = \sum_{i=1}^n \left(\frac{\tau_p}{\tau_i} \right) \frac{\left[\frac{\sin(e_i)}{d_{ip}} \right]}{\left[\sum_{k=1}^n \frac{\sin(e_k)}{d_{kp}} \right]} \tau_{vi} \quad \text{when } d_{ip} \neq 0$$

(6.25)

$$\hat{\tau}_{vp} = \tau_{vj} \quad \text{when } d_{jp} = 0, j \in \{1, 2, \dots, n\}$$

where τ_{vi} is the TEC_v at the i th “reference point”; $\hat{\tau}_{vp}$ is the estimated TEC_v at “grid point” p ; d_{ip} is the distance (measured at the single ionosphere layer) between the i th “reference point” and grid point p ; τ_p is the predicted TEC_v at grid point p from an ionospheric model such as the “Klobuchar model”; τ_i is the predicted TEC_v at the i th reference point as estimated by the ionospheric model; e_i is the elevation angle from the receiver to the GPS satellite. Figure 6.1 is a schematic showing some nodes of the imaginary grid and 4 ionospheric pierce points.

Let the coordinates of i th reference point and grid point p be $(\phi_{pp}, \lambda_{pp})$ and (ϕ_p, λ_p) respectively, then the distance d_{ip} can be calculated as:

$$d_{ip} = (R_e + h) \times \cos^{-1}[\sin \phi_{pp} \sin \phi_p + \cos \phi_{pp} \cos \phi_p \cos(\lambda_{pp} - \lambda_p)]$$

(6.26)

6.2.6 Ionospheric Pierce Point TEC Interpolation

The user receiver computes the latitude and longitude of its pierce points. For each of the user’s pierce points, the receiver computes its vertical delay, interpolated from the grid using the vertical delays of the four nodes of the cell that contains the pierce point, using one of many possible interpolation techniques, such as the weighting function approach, bilinear, bicubic, inverse distance, etc. The weighting function approach is introduced as follows (Junkins et al., 1973; FAA, 1994). The mathematical formulation for the interpolated vertical ionospheric pierce point delay $\tau_{vpp}(\phi_{pp}, \lambda_{pp})$, as a function of ionospheric pierce point latitude ϕ_{pp} and longitude λ_{pp} , is:

$$\tau_{vpp}(\phi_{pp}, \lambda_{pp}) = \sum_{i=1}^4 W_i(x_{pp}, y_{pp}) \times \tau_{vi} \quad (6.27)$$

where $i=1,2,3,4$, represents the sequence of 4 nodes of the cell, starting from the right-top node, and in counter-clockwise direction, and the general equation for the weighting function is:

$$W(x, y) = x^2 y^2 (9 - 6x - 6y + 4xy) \quad (6.28)$$

and τ_{vi} are the broadcast pierce point vertical delay values at the four corners of the grid. The output value at a desired pierce point pp is τ_{vpp} , with its geographical coordinates ϕ_{pp} and λ_{pp} . Figure 6.2 is a schematic showing the interpolation geometry for a user pierce point (UPP). The other quantities are:

$$W_1(x, y) = W(x, y) \quad (6.29)$$

$$W_2(x, y) = W(1 - x, y) \quad (6.30)$$

$$W_3(x, y) = W(1 - x, 1 - y) \quad (6.31)$$

$$W_4(x, y) = W(x, 1 - y) \quad (6.32)$$

$$\Delta\lambda_{pp} = \lambda_{pp} - \lambda_1 \quad (6.33)$$

$$\Delta\phi_{pp} = \phi_{pp} - \phi_1 \quad (6.34)$$

$$x_{pp} = \frac{\Delta\lambda_{pp}}{\lambda_2 - \lambda_1} = \frac{\Delta\lambda_{pp}}{\text{longitude grid interval}} \quad (6.35)$$

$$y_{pp} = \frac{\Delta\phi_{pp}}{\phi_2 - \phi_1} = \frac{\Delta\phi_{pp}}{\text{latitude grid interval}} \quad (6.36)$$

where (ϕ_1, λ_1) is the latitude and longitude of the left-bottom node of the cell and (ϕ_2, λ_2) is the latitude and longitude of the right-top node of the cell (cf. Figure 6.2).

As can be seen from equations (6.27) and (6.28), this interpolation technique involves only simple algebra, and provides a continuous surface (Junkins et al., 1973).

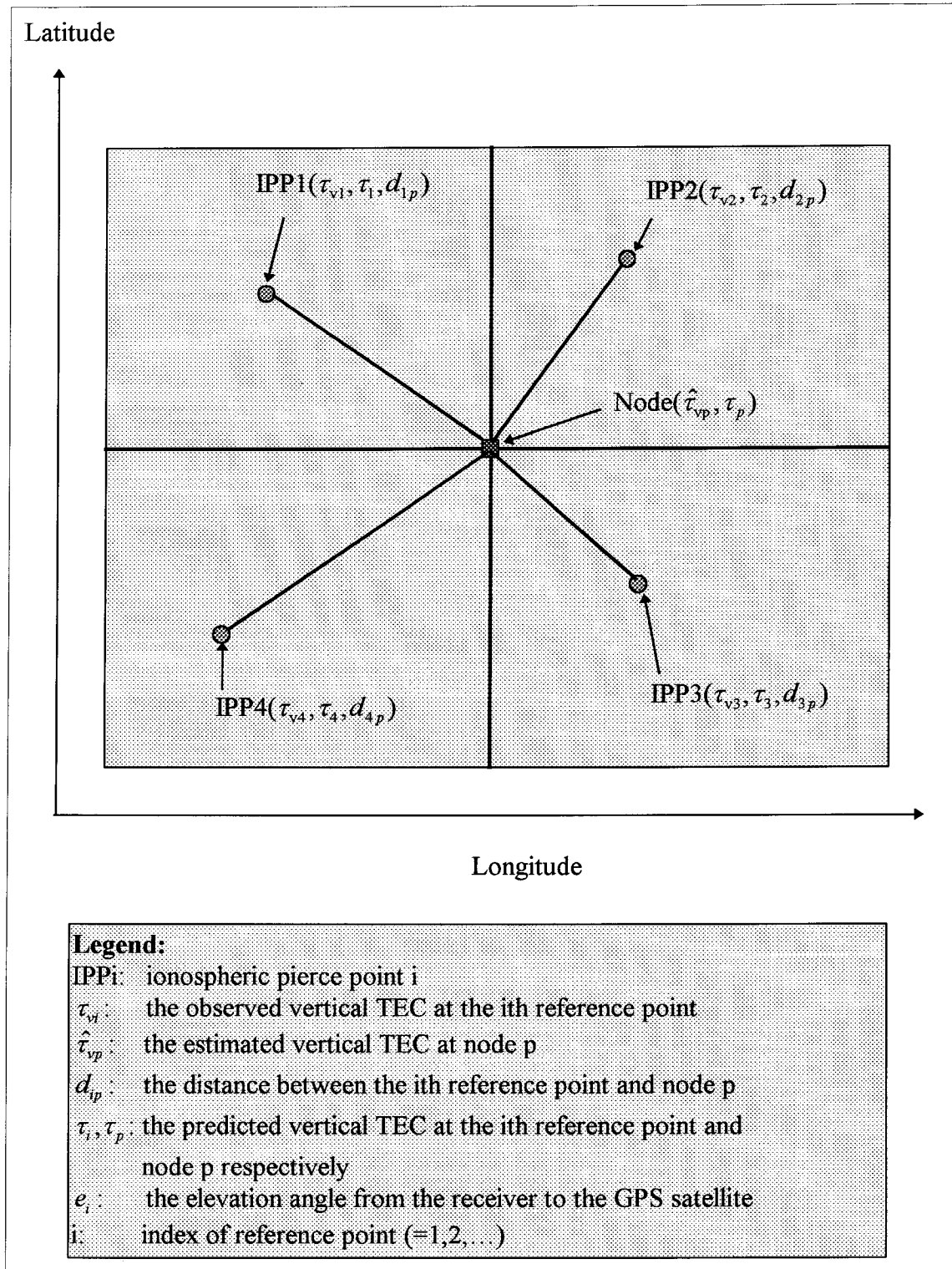


Figure 6.1. Schematic showing some nodes of the imaginary grid and 4 Ionospheric Pierce Points (IPPs).

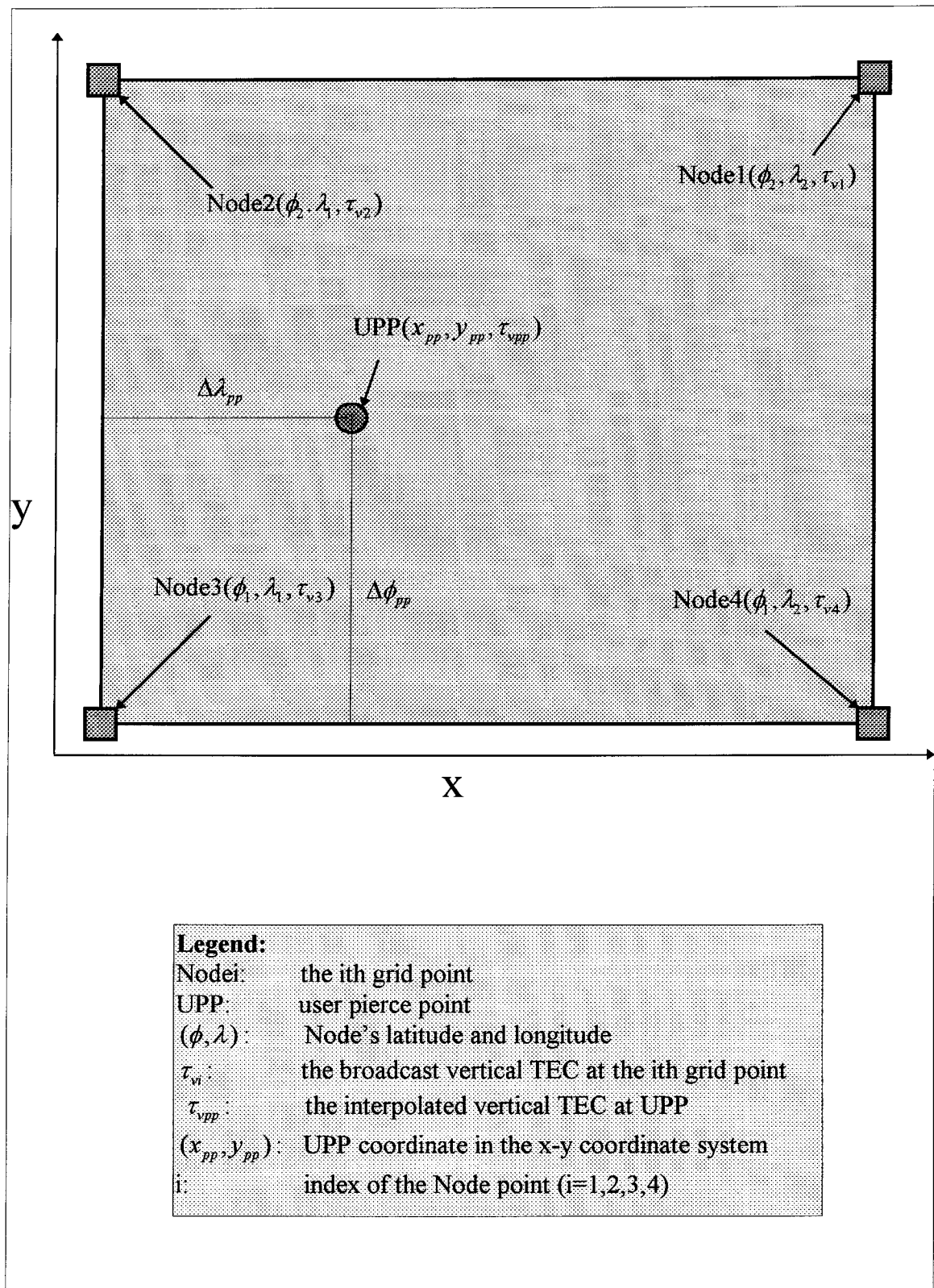


Figure 6. 2. Schematic showing interpolation geometry for User Pierce Point (UPP).

Once the user establishes the vertical delay at the pierce point, the user can then multiply that vertical delay by the obliquity factor $S(E)$ to obtain the slant delay τ_{spp} , to be subtracted from his pseudo-range measurement:

$$\tau_{spp}(\phi_{pp}, \lambda_{pp}) = S(E) \times \tau_{vpp}(\phi_{pp}, \lambda_{pp}) \quad (6.37)$$

where τ_{vpp} is the interpolated vertical delay at the user-to-satellite ionospheric pierce point derived as described above, and $S(E)$ is derived from equation (6.24).

6.3 UNSW Grid-Based Ionospheric Delay Estimation Algorithm

In order to improve the real-time regional ionosphere modelling performance, an improved grid-based algorithm, referred to here as the “UNSW grid-based algorithm”, was developed. The UNSW grid-based algorithm is similar to the algorithm described in Conker et al. (1995). However, some modifications were made to the algorithm. The major modifications were: (1) an “*exponential function*” is adopted as the weighting function, and (2) the “*grid-based ionosphere model*” estimated from the previous day is used to predict the ionospheric delay ratios between the grid point and reference points.

Define:

$$f_i = \frac{\tau_p}{\tau_i} \quad (6.38)$$

$$g_i = \frac{\sin(e_i)}{d_{ip}} \quad (6.39)$$

$$h = \sum_{k=1}^n \frac{\sin(e_k)}{d_{kp}} = \sum_{k=1}^n g_k \quad (6.40)$$

The conventional grid-based algorithm of equation (6.25) can be simplified as:

$$\hat{\tau}_{vp} = \sum_{i=1}^n f_i \frac{g_i}{h} \tau_{vi} \quad \text{when } d_{ip} \neq 0, \quad \hat{\tau}_{vp} = \tau_{vj} \quad \text{when } d_{jp} = 0, j \in \{1, 2, \dots, n\} \quad (6.41)$$

From equation (6.41), it is evident that “ f_i ” is the ratio of the predicted TEC values using an ionosphere model, such as the Klobuchar Model, between the grid point p and the i th reference point, “ g_i ” is the weight given to the i th reference point, and “ h ” is the sum of the “ g_i ” of the n reference points. The “ f_i ” value is a function of the ionospheric model used, and the locations of the grid point and reference points. The “ g_i ” and “ h ” values are functions of the weighting function used, the distance d_{ip} and the elevation angle e_i .

In order to improve the accuracy of the vertical TEC estimates of the grid point, an alternative grid-based algorithm was developed. This algorithm is referred to here as the “*UNSW grid-based algorithm*” (Lin & Rizos, 1997a, 1997c). That is, for a grid point p , the vertical TEC is estimated by:

$$\hat{\tau}_{vp}^* = \sum_{i=1}^n \left(\frac{\tau_p^*}{\tau_i^*} \right) \frac{\{ \sin(e_i) \times \exp[-20.0 \times (\frac{d_{ip}}{M})^2] \}}{\{ \sum_{k=1}^n \sin(e_k) \times \exp[-20.0 \times (\frac{d_{kp}}{M})^2] \}} \tau_{vi} \quad \text{when } d_{ip} \neq 0$$

(6.42)

$$\hat{\tau}_{vp}^* = \tau_{vj} \quad \text{when } d_{jp} = 0, j \in \{1, 2, \dots, n\}$$

where τ_{vi} is the TEC_v at the i th “reference point”; $\hat{\tau}_{vp}^*$ is the estimated TEC_v using the “*UNSW grid-based algorithm*” at “grid point” p ; d_{ip} is the distance (at the single ionosphere layer) between the i th “reference point” and grid point p ; e_i is the elevation angle from the receiver to the GPS satellite; τ_p^* and τ_i^* are the estimated TEC_v at the grid point p and the i th reference point respectively (using the “regional grid-based ionosphere model” generated from the data from the previous day); and the M value is defined as a maximum distance beyond which reference points are not used. Note that τ_p^* and τ_i^* are estimated using equation (6.27) and the “regional grid-based ionosphere model” is generated from the data from the previous day, however, τ_p and τ_i in equation (6.25) are estimated from the Klobuchar Model (see chapter 2).

Define:

$$f_i^* = \frac{\tau_p^*}{\tau_i^*} \quad (6.43)$$

$$g_i^* = \sin(e_i) \times \exp[-20.0 \times (\frac{d_{ip}}{M})^2] \quad (6.44)$$

$$h^* = \sum_{k=1}^n g_k^* \quad (6.45)$$

Then equation (6.42) is simplified to:

$$\hat{\tau}_{vp}^* = \sum_{i=1}^n f_i^* \frac{g_i^*}{h^*} \tau_{vi} \quad \text{when } d_{ip} \neq 0, \quad \hat{\tau}_{vp}^* = \tau_{vj} \quad \text{when } d_{jp} = 0, j \in \{1, 2, \dots, n\} \quad (6.46)$$

Note that the “regional grid-based ionosphere model” of the first day should be generated using the “conventional grid-based algorithm”, if the “UNSW grid-based algorithm” is used for the first time. From the second day on, the “UNSW grid-based algorithm” is used to generate a regional ionosphere model, however, f_i^* of equation (6.43) is computed from the “regional grid-based ionosphere model” generated by the conventional algorithm. From the third day on, f_i^* is also computed using the “regional grid-based ionosphere model” generated by the UNSW algorithm.

In order to verify the performance of the “UNSW grid-based algorithm”, GPS dual-frequency data sets from different regions, such as the ARGN, GSI, etc., networks (section 6.5) were processed and analysed. The “TEC prediction residual” is defined as the difference between the vertical TEC value derived from GPS observables (from the dual-frequency receivers) at a “User” site and that derived from regional ionosphere modelling, from either the “UNSW grid-based algorithm” or the “conventional grid-based algorithm”.

Test results of the grid-based algorithms using different weighting functions are presented in section 6.5.3.1. Test results of the grid-based algorithms using different ionosphere models, such as the Klobuchar Model, the grid-based ionosphere model generated from the previous day’s GPS data, etc., are presented in section 6.5.3.2. It is considered that the grid-based algorithm works well if the standard deviation of the TEC prediction residual is

small. Based on this consideration, and the test results of sections 6.5.3.1 and 6.5.3.2, the weighting function “ $we(1)$ ” and the “grid-based ionosphere model generated from the previous day’s data” were selected as the basis of the “*UNSW grid-based algorithm*”. Test results of the performance of the “UNSW grid-based algorithm” are given in sections 6.5.3.3 and 6.5.4.

6.4 Program “POSTEC”

In order to test the performance of the proposed algorithm, a data post-processing version of the grid-based ionosphere modelling software package, known as “*POSTEC*”, was developed, to simulate real-time regional ionosphere modelling. The characteristics of the POSTEC program are :

- 1) At each Wide-area Reference Station (WRS), the carrier “*phase levelling procedure*” (cf. section 6.2.3) is used to estimate the slant TEC for each IPP on an epoch-by-epoch basis.
- 2) The “phase levelled” slant TEC estimates are calibrated by the estimated *GPS satellite and receiver L1/L2 differential delays* using the UNSW algorithm described in chapter 5, to generate an accurate unbiased slant TEC. The slant TEC estimates are then converted to vertical TEC values at the IPPs (cf. section 6.2.4).
- 3) The conventional and UNSW grid-based algorithms (cf. sections 6.2.5 and 6.3) are used to generate the ionosphere model for the region of interest. The grid spacing is about 5 degrees in both the latitude and longitude directions. Note that the “M” value of equation (6.42) is set to 830 km which corresponds to the maximum diagonal length of the $5^\circ \times 5^\circ$ grid cell over the ionosphere layer with height $h=400$ km.
- 4) The weighting function approach (cf. section 6.2.6) is used to compute the vertical TEC estimate for each IPP defined by the arbitrary location of a user.

- 5) The TEC prediction residuals are computed and analysed in order to verify the performance of an ionosphere modelling algorithm.
- 6) The POSTEC is a collocation of programs that run independently from a main menu program. The main menu lists the functions (each implemented within a separate program).

The “welcome page” and the “main menu” of the POSTEC program are shown in Tables 6.1 and 6.2. For example, if the “Multipath & Slant Phase-derived TEC Est.” function was chosen, then the program asks the operator to choose the input file(s) as shown in Table 6.3. Table 6.4 shows that file “ALIC1810.95T” was chosen. Note that the “ALIC1810.95T” is the TEC data file of site “alic”, ARGN region, for day 181, 1995 (cf. section 6.5.1.3). Table 6.5 shows the executing status of “Multipath and slant phase-derived TEC estimation” program after file “ALIC1810.95T” was input.

Table 6.1. Welcome page of the POSTEC program.

Sun 27 Apr 1997 17:19:16
----- Welcome -----
Post-Processing TEC (POSTEC) Estimation Package
For ARGN, Version 3.01
Satellite Navigation and Positioning
Geomatic Engineering, The University of New South Wales
Written by Lao-Sheng Lin
Satellite Navigation and Positioning, Geomatic Engineering
The University of New South Wales, Sydney, Australia.
Copyright (C) 1997
OK _

F1 Help

Table 6.2. Main menu of the POSTEC program.

```

Sun 27 Apr 1997 17:23:59
----- Main Menu -----
( ) Multipath & Slant Phase-Derived TEC Est.
( ) GPS Sat. & Rec. L1/L2 Diff. Delay Est.
( ) GPS Sat. & Rec. L1/L2 Diff. Delay Compu.
( ) Vertical TEC Estimation
( ) Read TEC Files from Reference Sites
( ) Conventional Grid-Based Ionosphere Modelling
( ) UNSW Grid-Based Ionosphere Modelling
( ) Polynomial Ionosphere Modelling
( ) Grid-Based User TEC Estimation
( ) Poly-Based User TEC Estimation
( ) Polynomial TEC Prediction Residuals Sorting
( ) Grid-based TEC Prediction Residuals Sorting

Exit _ OK _

F1 Help ; TAB to activate

```

Table 6.3. Interactive files input request once the “Multipath & Slant Phase-derived TEC Est.” option was chosen.

```

Sun 27 Apr 1997 18:34:46
----- Utilities -----
Input Files
E:\POSTEC\PROGRAMS\*.??T _[]! OK _

Files
ALIC1810.95T | Cancel _
GDMS.BAT |
..\ |

[]

E:\POSTEC\PROGRAMS\E:\POSTEC\PROGRAMS\*.??T
ALIC1810.95T 1636231 Oct 04,1995 12:51p

F1 Help ; Hit <enter> for file list

```

Table 6.4. File "ALIC1810.95T" was chosen.

```

Sun 27 Apr 1997 18:50:33
-----
+----- Utilities -----+
|
| Input Files
| ALIC1810.95T      _□;      OK      _
|
| Files
| ALIC1810.95T      |
| GDMS.BAT          |
| ..\               |
|
| □ _____ □
|
| E:\POSTEC\PROGRAMS\E:\POSTEC\PROGRAMS\*.??T
| ALIC1810.95T 1636231   Oct 04,1995 12:51p
|
+-----+
-----
F1 Help | Hit <enter> for file list

```

Table 6.5. "Multipath and slant phase-derived TEC estimation" program running after
"ALIC1810.95T" was input.

```

*****
* Carrier Phase Levelling Software (Ionomula) Version 1.1*
*   Developed by Lao-Sheng (David) Lin at UNSW           *
*   24 February, 1997                                   *
*****
Obs file: E:\POSTEC\PROGRAMS\ALIC1810.95T
TEC file: E:\POSTEC\PROGRAMS\ALIC1810.TEC
STA file: E:\POSTEC\PROGRAMS\ALIC1810.STA
Maximum Observation age is 30 seconds

j= 500
j= 1000
j= 1500
j= 2000
j= 2500
finish computing mean values
jj= 0
jj= 500
jj= 1000
jj= 1500
jj= 2000
jj= 2500

```

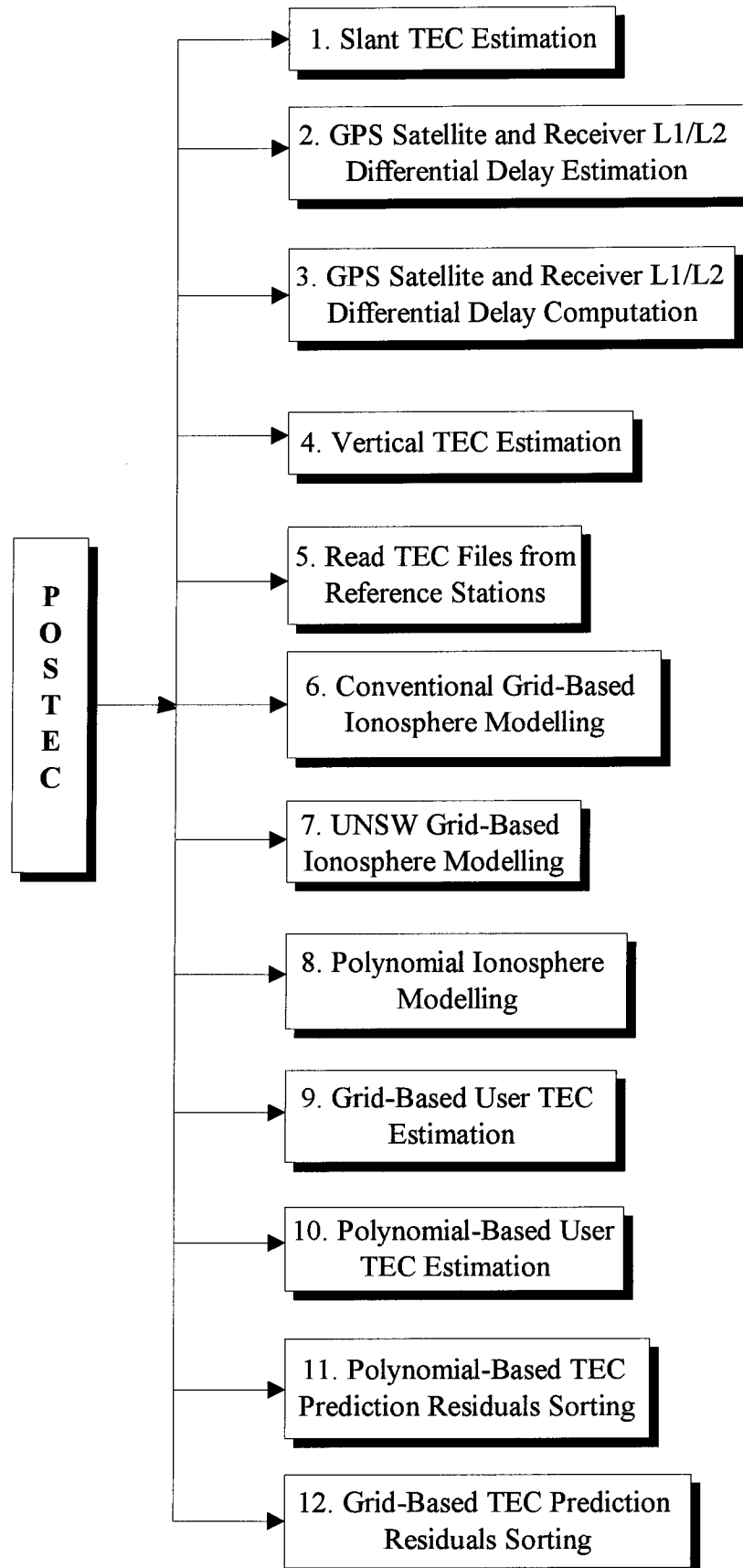


Figure 6.3. Main functions of the POSTEC program.

The main functions of the POSTEC program are shown in Figure 6.3. Each function is implemented within a separate program. Below the input/output file(s) and processing strategy for each function are briefly described (cf. Figure 6.3).

1) *Slant TEC Estimation (Program 1)*

- Input:
 - a) GPS navigation file
 - b) GPS observation file (either raw data or TEC data)

- Processing:
 - a) Slant TEC estimation using dual-frequency GPS measurements (cf. section 6.2.3)
 - b) Pseudo-range multipath estimation for generating “multipath template” (cf. chapter 3)
 - c) Azimuth and elevation angles computation for each tracked satellite

- Output:
 - a) Slant TEC and pseudo-range multipath MP1, MP2 estimates for each tracked GPS satellite on an epoch-by-epoch basis
 - b) Statistical data, such as how many arcs for each tracked satellite, levelling constant D for each arc (cf. equation (6.21)), etc.
 - c) Azimuth and elevation angles for each satellite

2) *GPS Satellite and Receiver L1/L2 Differential Delay Estimation (Program 2)*

- Input:
 - a) Slant TEC file from Program 1
 - b) Program parameters, such as site’s geographic coordinate, session number , etc.

- Processing:
 - a) GPS L1/L2 satellite and receiver differential delay estimation (cf. chapter 5) for each tracked satellite, for each session
- Output:
 - a) GPS L1/L2 satellite and receiver differential delay estimate for each tracked satellite for each session

3) *GPS Satellite and Receiver L1/L2 Differential Delay Computation (Program 3)*

- Input:
 - a) Estimated satellite and receiver differential delays from Program 2
- Processing:
 - a) Compute the daily estimates of the satellite and receiver differential delay using the weighted average algorithm (cf. chapter 5)
- Output:
 - a) Daily estimate of the sum of the satellite plus receiver differential delay for each satellite

4) *Vertical TEC Estimation (Program 4)*

- Input:
 - a) Slant TEC estimates from Program 1
 - b) Estimated satellite and receiver differential delays from Program 3

c) Geographic coordinate of the site

• Processing:

a) Ionospheric pierce point (IPP) location determination (cf. section 6.2.2)

b) Vertical TEC estimation (cf. section 6.2.4)

• Output:

a) Vertical TEC estimate for each IPP

b) Geographical coordinate for each IPP

5) Read TEC Files from Reference Stations (Program 5)

• Input:

a) Files (including vertical TEC estimate and geographical coordinate for each IPP) from reference stations

• Processing:

a) Data from different files are combined to a single file on an epoch-by-epoch basis

• Output:

a) Single file (including vertical TEC estimate and geographical coordinate for each IPP)

6) Conventional Grid-Based Ionosphere Modelling (Program 6)

• Input:

a) File generated from Program 5

- b) Program parameters, such as the grid size, grid node number, etc.
- c) Ionosphere coefficients of Klobuchar Model

- Processing:
 - a) Grid point TEC determination using “Conventional grid-based algorithm” (cf. section 6.2.5)

- Output:
 - a) Region ionosphere model (file including the vertical TEC estimates on the grid nodes of a region) on an epoch-by-epoch basis

7) UNSW Grid-Based Ionosphere Modelling (Program 7)

- Input:
 - a) File generated from Program 5
 - b) Program parameters, such as the grid size, grid node number, the value of M, etc.
 - c) File including the “regional grid-based ionosphere model” of the previous day

- Processing:
 - a) Grid point TEC determination using “UNSW grid-based algorithm” (cf. section 6.3)

- Output:
 - a) Region ionosphere model (file including the vertical TEC estimates on the grid nodes of a region) on an epoch-by-epoch basis

8) Polynomial Ionosphere Modelling (Program 8)

- Input:
 - a) File generated from Program 5
 - b) Program parameters, such as the order of the selected polynomial, etc.

- Processing:
 - a) Determining the polynomial coefficients (Lin et al., 1996a; section 6.5.4)

- Output:
 - a) Estimated polynomial coefficients on an epoch-by-epoch basis

9) Grid-Based User TEC Estimation (Program 9)

- Input:
 - a) Files (including vertical TEC estimate and geographical coordinate for each IPP) from user site
 - b) Region ionosphere model (either from the output of Program 6 or from the output of Program 7)

- Processing:
 - a) Ionospheric pierce point TEC interpolation (cf. section 6.2.6)

- Output:
 - a) Ionospheric pierce point vertical TEC estimates on the epoch-by-epoch basis
 - b) TEC prediction residual estimate for each IPP

10) Polynomial-Based User TEC Estimation (Program 10)

- Input:
 - a) Files (including vertical TEC estimate and geographical coordinate for each IPP) from user site
 - b) Region ionosphere model (from the output of Program 8)
- Processing:
 - a) Ionospheric pierce point TEC interpolation using the estimated polynomial coefficients (cf. *ibid*, 1996a; section 6.5.4)
- Output:
 - a) Ionospheric pierce point vertical TEC estimates on an epoch-by-epoch basis
 - b) TEC prediction residual estimate for each IPP

11) Polynomial-Based TEC Prediction Residuals Sorting (Program 11)

- Input:
 - a) File including the TEC prediction residuals from Program 10
- Processing:
 - a) Computing the mean and standard deviation of the TEC prediction residuals of a user site (24-hour data)
 - b) Classifying the TEC prediction residuals into a certain number of groups and computing the frequency of each group
- Output:

- a) The daily mean and standard deviation of the TEC prediction residuals
- b) Statistical report on the classification of the TEC prediction residuals

12) *Grid-Based TEC Prediction Residuals Sorting (Program 12)*

- Input:

- a) File from the output of Program 9

- Processing:

- a) Computing the mean and standard deviation of the TEC prediction residuals of a user site (24-hour data)
- b) Classifying the TEC prediction residuals into a certain number of groups and computing the frequency of each group

- Output:

- a) The daily mean and standard deviation of the TEC prediction residuals
- b) Statistical report on the classification of the TEC prediction residuals

6.5 Test Results and Discussion

6.5.1 Data Description

6.5.1.1 Small Region - PGGA Data Set

In order to verify the UNSW estimation technique, a number of data sets from the *Permanent GPS Geodetic Array (PGGA)*, in Southern California, USA (PGGA, 1996), were processed and analysed.

Five stations: Blythe (blyt), China Lake (coso), Yucaipa (crfp), Scripps (sio3), and Vandenberg (vndp) were selected for the tests. The coordinates of these PPGA sites, and their distances from the “crfp” site, are shown in Table 6.6. These stations were equipped with ASHTECH Z-XII3 geodetic receivers, and collect data from all visible GPS satellites every 30 seconds. A RINEX data sample of site “blyt”, PPGA, for day 001, 1996, is shown in Table 6.7. Data from day 001 to 012, 1996, were processed.

Table 6.6. PPGA stations and their coordinates.

Site Name	Latitude N	Longitude W	Dist. To User	Notes
blyt	33.43 degree	114.71 degree	245.92 km	Remote Site
coso	35.98 degree	117.81 degree	239.59 km	Remote Site
crfp	34.04 degree	117.10 degree	0.0 km	User
sio3	32.87 degree	117.25 degree	139.20 km	Remote Site
vndp	34.55 degree	120.48 degree	335.78 km	Remote Site

Table 6.7. RINEX data sample of site “blyt”, PPGA, for day 001, 1996.

2	OBSERVATION DATA G (GPS)					RINEX VERSION / TYPE	
	ASRINEXO V2.5.4 LH SOPAC/IGPP/SIO/UCSD 02-JAN-96 20:07					PGM / RUN BY / DATE	
	PPGA Data [Permanent GPS Geodetic Array - S. California]					COMMENT	
	SOPAC (Scripps Orbit and Permanent Array)					COMMENT	
	IGPP [Institute of Geophysics and Planetary Physics]					COMMENT	
	SIO [Scripps Institution of Oceanography]					COMMENT	
	UCSD [University of California, San Diego]					COMMENT	
	questions: ppga@ppga.ucsd.edu					COMMENT	
	GPS data archive anonymous login: toba.ucsd.edu					COMMENT	
	BLYT					MARKER NAME	
	JAB					OBSERVER / AGENCY	
435	ASHTECH Z-XII3		1E00		REC # / TYPE / VERS		
973	DORNE MARGOLIN ASH					ANT # / TYPE	
	-2223206.8900	-4830352.7500	3510605.1000		APPROX POSITION XYZ		
	0.0000	0.0000	0.0000		ANTENNA: DELTA H/E/N		
	1	1				WAVELENGTH FACT L1/2	
	5	C1	L1	L2	P1 P2	# / TYPES OF OBSERV	
	30						INTERVAL
	1996	1	1	0	0	30.000000	TIME OF FIRST OBS
						END OF HEADER	
96	1	1	0	0	30.0000000	0 8 12 16 27 18 19 31 2 29	
	24475621.653	-6852874.694	6	-4375960.418	8	24475620.582	24475627.738
	24272522.537	-11022843.13846	-8571349.11447	24272520.6714	24272526.2484		
	21232233.388	-34155328.20546	-26592036.73248	21232232.5344	21232236.5714		
	21940279.566	-26636985.18046	-20736308.15248	21940278.4984	21940282.6804		
	20710329.214	-41948262.97946	-32666108.46648	20710328.1474	20710332.1724		
	22185402.919	-27619526.98946	-21505451.90748	22185401.4804	22185405.0794		
	22363591.094	-24826545.27546	-19301177.79048	22363589.7454	22363594.6594		
	24477901.489	-34166715.52046	-26607973.36747	24477901.0624	24477905.8684		

6.5.1.2 Medium Region - GSI Data Set

A number of data sets from stations of the GSI, Japan, GPS network, from day 111 to 119, 1996, were processed and analysed to test the proposed algorithm. The GSI stations used, together with their coordinates, are listed in Table 6.8. All GSI stations were equipped with Ashtech Z-12 GPS receivers (except site "2110"). Station "2110" was equipped with a Trimble 4000SSE GPS receiver. Note that Ashtech Z-12 collects L1, L2, C1, P1, P2 data (cf. Table 6.9), but the Trimble 4000SSE collects L1, L2, C1, P2 data (cf. Table 6.10) (P1 is not available). The data rate was 30 seconds.

Table 6.8. GSI stations used in these analyses.

Site Name	Latitude N	Longitude E	Dist. To User	Notes
2110	36.11 degree	140.09 degree	0.0 km	User
2002	36.11 degree	140.09 degree	0.0 km	Remote Site
0029	39.11 degree	141.20 degree	369.82 km	Remote Site
0073	35.49 degree	131.70 degree	808.08 km	Remote Site
2001	43.53 degree	141.85 degree	892.16 km	Remote Site
2004	31.43 degree	130.88 degree	1060.74 km	Remote Site

Table 6.9. RINEX data sample of site "2002", GSI, for day 111, 1996.

2	OBSERVATION DATA							RINEX VERSION / TYPE
ASHTORIN	22 - APR - 96 01:38							PGM / RUN BY / DATE
2002								MARKER NAME
101	Z-XII3	1E891D0						OBSERVER / AGENCY
							REC # / TYPE / VERS	
							ANT # / TYPE	
-3957161.8129	3310183.4761	3737762.7934						APPROX POSITION XYZ
0.0001	0.0000	0.0000						ANTENNA: DELTA H/E/N
1	1							WAVELENGTH FACT L1/2
7	L1	L2	C1	P1	P2	D1	D2	# / TYPES OF OBSERV
30								INTERVAL
1996	4	20	0	0	30.000000			TIME OF FIRST OBS
1996	4	20	23	59	30.000000			TIME OF LAST OBS
								END OF HEADER
96	4	20	0	0	30.0000000	0	5 6 22 20 1 25	0.000000000
-18646345.302	9	-14511539.91948	21721187.502		21721187.6554		21721191.3714	
-0.000		-0.000						
-18661999.633	9	-14273420.55148	21864967.818		21864967.1984		21864972.1644	
-0.000		-0.000						
-12143445.435	9	-9446270.57147	23192415.579		23192415.5854		23192420.9644	
-0.000		-0.000						
-19988763.668	9	-15546643.36048	21586132.839		21586132.8814		21586137.9944	
-0.000		-0.000						
-26758233.144	9	-20826617.56949	20622524.758		20622525.0034		20622528.4344	
-0.000		-0.000						

Table 6.10. RINEX data sample of site “2110”, GSI, for day 111, 1996.

2	OBSERVATION DATA					RINEX VERSION / TYPE
DAT2RIN 2.00c	GARD		06MAY96 5:42:40		GMTPGM / RUN BY / DATE	
COSMOS	GSI				OBSERVER / AGENCY	
5386	TRIMBLE 4000SSE		Nav 7.06 Sig 3.03		REC # / TYPE / VERS	
0	PERMANENT L1/L2				ANT # / TYPE	
92110	MARKER NAME					
2762	MARKER NUMBER					
-3957160.0775	3310203.2825	3737752.9810			APPROX POSITION XYZ	
0.0000	0.0000	0.0000			ANTENNA: DELTA H/E/N	
1	1	0			WAVELENGTH FACT L1/2	
5	L1	C1	P1	L2	P2	
30	# / TYPES OF OBSERV					
1996	4	20	0	0	30.000000	
1996	4	20	23	59	0.000000	
25	INTERVAL					
TIME OF FIRST OBS						
TIME OF LAST OBS						
# OF SATELLITES						
END OF HEADER						
96	4	20	0	0	30.0000000 0 5 1 6 20 22 25	
-1916048.19810	21505759.89800		2071460.15850		21505762.07840	
-6337292.67610	21640798.45300		-4807895.63250		21640799.64840	
7910500.14010	23112021.01600		6342239.95450		23112022.63340	
-7751151.18110	21784571.50000		-5893895.55650		21784573.18840	
-11939355.12110	20542126.08600		-9202371.33250		20542126.19140	

6.5.1.3 Large Region - ARGN Data Set

The Australian Regional GPS Network (ARGN) is an extension of the Australian Fiducial Network (AFN) with 13 stations in continental Australia and its offshore and Antarctic territories, and one station in New Zealand. The ARGN stations and their coordinates are listed in Table 6.11. The data sets, from day 181 to 195, 1995, were processed and analysed. “yar1” and “tidb” stations were equipped with Rogue SNR-8 receivers (cf. Table 6.12), with the rest of the ARGN stations were equipped with Rogue ICS-4000Z GPS receivers (cf. Table 6.13). The data rate was also 30 seconds.

Table 6.11. ARGN stations used in these analyses.

Site Name	Latitude S	Longitude E	Dis To User	Notes
alic	23.67 degree	133.89 degree	0.00 km	User
cedu	31.87 degree	133.81 degree	969.67 km	Remote Site
darw	12.84 degree	131.13 degree	1317.41 km	Remote Site
tow2	19.35 degree	146.78 degree	1507.16 km	Remote Site
karr	20.98 degree	117.10 degree	1863.29 km	Remote Site
yar1	29.05 degree	115.35 degree	2062.62 km	Remote Site
tidb	35.40 degree	148.98 degree	2078.43 km	Remote Site
hob2	42.80 degree	147.44 degree	2623.20 km	Remote Site
mac1	54.50 degree	158.94 degree	4262.76 km	Remote Site
wel2	41.28 degree	174.78 degree	4526.92 km	Remote Site

Table 6.12. RINEX data sample of site "tidb", ARGN, for day 181, 1995.

2	OBSERVATION DATA	GPS							RINEX VERSION / TYPE
srx/v1.8.1.3	5/19/95BAI		95/07/01	08:15:17					PGM / RUN BY / DATE
dsc40									MARKER NAME
dsc40									MARKER NUMBER
DSN	JPL								OBSERVER / AGENCY
(DSCC40)	ROGUE SNR-8	0.0							REC # / TYPE / VERS
	DORNE MARGOLIN R								ANT # / TYPE
0.000	0.0000	0.0000							ANTENNA: DELTA H/E/N
30									INTERVAL
1	1	0							WAVELENGTH FACT L1/2
4	L1	L2	P1	P2					# / TYPES OF OBSERV
	SNR is mapped to signal strength [0,1,4-9]								COMMENT
	SNR: >500 >100 >50 >10 >5 >0 bad n/a								COMMENT
	sig: 9 8 7 6 5 4 1 0								COMMENT
	1995	06	30	00	00	00.000000			TIME OF FIRST OBS
	1995	06	30	23	59	30.000000			TIME OF LAST OBS
	25								# OF SATELLITES
									END OF HEADER
95	06	30	00	00	00.0000000	0	7	01	14 15 20 21 25 29
	-9304504.86208		-7250263.76108		22981004.63108		22981005.41208		
	-12086945.75508		-9418397.15408		22418163.24508		22418163.92608		
	-22488845.22908		-17523778.28508		20827195.63508		20827196.21908		
	-181202.25606		-141195.87606		24861227.51306		24861229.43006		
	-1554824.32807		-1211554.43607		24071681.44307		24071683.72407		
	-20503563.92608		-15976797.39708		20420173.37108		20420172.95808		
	-3146669.21007		-2451948.99607		24354384.02007		24354384.69907		

Table 6.13. RINEX data sample of site "alic", ARGN, for day 181, 1995.

2	IONOSPHERIC TEC DATA G						RINEX VERSION / TYPE
	ROGUETEC V1.0.0 UX AUSLIG 01-JUL-95 14:39						PGM / RUN BY / DATE
	GPS Network Australis (GNA) - ALICE SPRINGS Australia						COMMENT
	-0.000000000083 HARDWARE CALIBRATION (S)						COMMENT
	0.000000067007 CLOCK OFFSET (S)						COMMENT
	TEC DATA CALCULATED BY ROGUE ICS-4000Z RECEIVER						COMMENT
	AZ = AZIMUTH, EL = ELEVATION						COMMENT
	TR = TEC FROM PSEUDORANGES, TS = TEC FROM CARRIER PHASE						COMMENT
	S1,S2 = SIGNAL TO NOISE RATIOS on L1,L2						COMMENT
	ALIC						MARKER NAME
	AU12						MARKER NUMBER
	mrh	auslig					OBSERVER / AGENCY
	126	ROGUE ICS-4000Z 93.05.25 / 2.8.33.2					REC # / TYPE / VERS
	222	DORNE MARGOLIN T					ANT # / TYPE
	-4052053.6361 4212836.6703 -2545107.5865						APPROX POSITION XYZ
	0.0070 0.0000 0.0000						ANTENNA: DELTA H/E/N
	1 1						WAVELENGTH FACT L1/2
	6 AZ EL TR TS S1 S2						# / TYPES OF OBSERV
	30						INTERVAL
	1995 6 30 0 0 30.000000						TIME OF FIRST OBS
	1995 6 30 23 59 30.000000						TIME OF LAST OBS
							END OF HEADER
	95 6 30 0 0 30.0000000 2 29 31						
	284.6 30.0 14.5413 -6.0744 244 214						
	330.5 18.9 24.1769 13.0244 181 118						
	95 6 30 0 1 0.0000000 3 29 31 21						
	284.4 30.1 15.0343 -6.1477 244 214						
	330.7 18.8 21.5179 13.0986 177 111						
	85.0 8.1 36.7302 19.9192 142 72						

6.5.2 Data Processing

In order to test the performance of the proposed grid-based algorithm, data sets from different region over different periods, as described in last section, were processed and analysed using the package "POSTEC".

In brief, the data processing included the following steps:

- 1) At each station, the carrier "*phase levelling procedure*" is used to estimate the slant TEC for each IPP on an epoch-by-epoch basis.
- 2) The "phase levelled" slant TEC estimates are calibrated by the estimated *L1/L2 GPS satellite and receiver differential delays* using the UNSW algorithm described in

chapter 5 to generate accurate unbiased slant TECs. The slant TEC estimates are then converted to vertical TEC values at the IPPs.

- 3) The grid-based algorithm is used to generate the ionosphere model for the region of interest. The grid spacing is about 5 degrees in both the latitude and longitude directions.
- 4) The weighting function approach (eg. Junkins et al., 1973; FAA, 1994; Lin et al., 1996a) is used to compute the vertical TEC estimate for each IPP defined by the arbitrary location of a user.

6.5.3 Test Result Comparisons between UNSW Algorithm and Conventional Algorithm

6.5.3.1 Using Different Weighting Functions

In order to test the effect of different weighting functions, “ g_i ” in equation (6.41), on the accuracy of the grid node’s vertical TEC estimates, the weighting functions expressed in equation (6.47) (Schut, 1976) were studied using the GSI data:

$$\begin{aligned}
 we(1) &= \exp(-20 \cdot r^2), \quad we(2) = \exp(-14 \cdot r^2), \quad we(3) = (1-r)^3(1-r^2)^3 / r \\
 we(4) &= (1-r)^3(1-r^2)^3 / r^2, \quad we(5) = (1-r)^2 / r^2, \quad we(6) = 1/r \\
 we(7) &= 1/r^2, \quad we(8) = 1/r^3, \quad we(9) = 1/r^4, \quad we(10) = 1 - 0.9 \cdot r^2
 \end{aligned} \tag{6.47}$$

where the variable “ r ” is defined as the ratio of distance d_{ip} and a quantity M (both d_{ip} and M were defined in section 6.3).

The weighting functions in equation 6.47 have been used in various methods of height interpolation for digital terrain models in photogrammetric community. Further details can be found in *ibid* (1976).

Here, the “ f_i ” value is computed using the “Klobuchar Model”. The test results are summarised in Table 6.14 and Figure 6.4. In Table 6.14, “Std Dev” means “Standard Deviation”. “Site 2110” is designated as the “User” (c.f. Table 6.8). Five of the GSI stations (excluding site “2110”) are treated as reference stations. The “GSI Region” represents the results of all reference stations.

Table 6.14. Mean and standard deviation comparisons of TEC prediction residuals using different weighting functions for day 119, 1996, for the GSI data.

Weighting Function	Site "2110"		GSI Region	
	Mean (TECU)	Std Dev (TECU)	Mean (TECU)	Std Dev (TECU)
we(1)	-0.06	1.980	-0.08	1.509
we(2)	-0.05	2.010	N/A	N/A
we(3)	-0.05	1.988	-0.07	1.525
we(4)	-0.05	1.974	-0.06	1.558
we(5)	-0.06	1.996	-0.06	1.548
we(6)	-0.09	2.175	-0.07	1.639
we(7)	-0.08	2.062	-0.06	1.579
we(8)	-0.06	2.007	-0.06	1.575
we(9)	-0.05	1.988	-0.05	1.590
we(10)	-0.07	2.249	-0.08	1.683

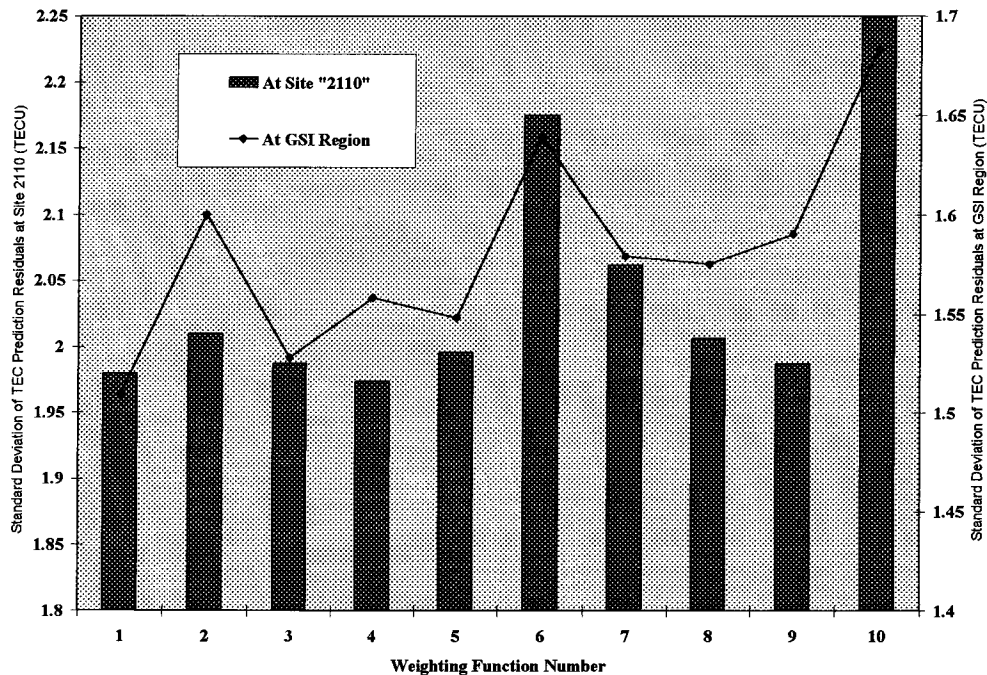


Figure 6.4. Standard deviation comparisons of TEC prediction residuals using different weighting functions for day 119, 1996, for the GSI data.

From Table 6.14 and Figure 6.4 it can be concluded that the weighting function "we(1)" gives the best TEC estimation accuracy on grid nodes. Note that the weighting function "we(1)" is used in equation (6.42) of the "proposed grid-based algorithm", and "we(6)" is used in equation (6.25) of the "conventional grid-based algorithm".

6.5.3.2 Using Different Ionosphere Models

As described in section 6.3, the “ f_i ” value in equation (6.41) depends on the “ionosphere model” used. Several “ionosphere models” were used to study their impact on the accuracy of the grid node’s vertical TEC estimates. The weighting function “we(6)”, that is the inverse distance algorithm, was used for all tests. The results using the GSI data are summarised in Table 6.15 and Figure 6.5. “Klob. D119” and “Klob. D118” refer to the “Klobuchar Model” of day 119 and 118 respectively. “Klob. D001” refers to the “Klobuchar Model” of day 001, 1996. “Grid D118” means that the “grid-based ionosphere model” generated from the data of day 118 was used. From Table 6.15 and Figure 6.5 it can be concluded that: (1) the accuracy of grid node’s TEC estimation can be improved if “Grid D118” is used, and (2) the accuracy of TEC estimation will be degraded if an outdated ionosphere model such as “Klob. D001” is used.

Table 6.15. Mean and standard deviation comparisons of TEC prediction residuals of using different ionosphere models for day 119, 1996, for the GSI data.

Ionosphere Model	Site “2110”		GSI Region	
	Mean (TECU)	Std Dev (TECU)	Mean (TECU)	Std Dev (TECU)
Klob. D119	-0.09	2.175	-0.07	1.639
Klob. D118	-0.07	2.164	-0.06	1.630
Klob. D001	2.34	4.565	N/A	N/A
Grid D118	-0.11	2.127	-0.04	1.582

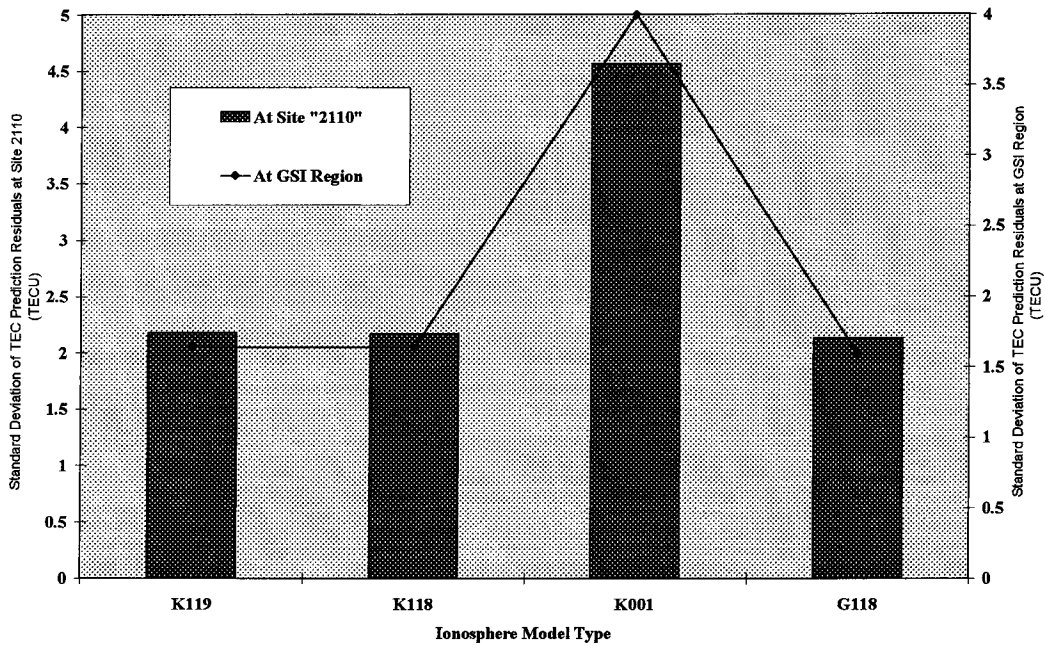


Figure 6.5. Standard deviation comparisons of TEC prediction residuals using different ionosphere models for day 119, 1996, for the GSI data.

6.5.3.3 Performance of the UNSW Grid-Based Algorithm

From the test results presented in sections 6.5.3.1 and 6.5.3.2, it is apparent that the accuracy of the grid node's vertical TEC estimates of a regional ionosphere model depends on: (1) the weighting function, and (2) the ionosphere model which is used to compute the predicted TEC ratio, " f_i " of equation (6.41), between the grid point and the reference points. Hence, an improved grid-based algorithm was proposed in section 6.3 to estimate the grid node's vertical TEC values. In order to test the performance of the proposed algorithm, the data sets described in section 6.5.1 were processed using the "POSTEC" software.

The test results from the PGG region are given in Tables 6.16 and 6.17 as well as Figures 6.6 and 6.7. The test results from the GSI region are given in Tables 6.18 and 6.19 as well as Figures 6.8 and 6.9. The test results from the ARG region are given in Table 6.20 and Figure 6.10. The "*Conv.*" and "*UNSW*" columns represent the "conventional grid-based algorithm" and "UNSW proposed grid-based algorithm" results

respectively. The “*Impro. (%)*” value is defined as $\{[(\text{“Conv.”} - \text{“UNSW”}) / \text{“Conv.”}] \times 100\}$.

From the test results it is evident that the standard deviations of the TEC prediction residuals can be reduced significantly in all cases, *approximately 29% to 31% in the case of the PGGA data, 10% to 20% in the case of the GSI data, and 36% for the ARGN data, if the UNSW algorithm is used.* Note that site “2110” and other GSI stations are equipped with different types of GPS receivers (c.f. section 6.5.1.2). Nevertheless the standard deviation of TEC prediction residuals can be reduced to around 10%.

In order to further demonstrate the performance of the UNSW algorithm, the detailed statistical reports of a single day from each region are given below. The results for the PGGA region (excluding site “crfp”) for day 012, 1996, are given in Table 6.21, and Figures 6.11 and 6.12. The results for site “crfp”, PGGA data for day 012, 1996, are given in Table 6.22, and Figures 6.13 and 6.14. The results for the GSI region (excluding site “2110”) for day 118, 1996, are given in Table 6.23, and Figures 6.15 and 6.16. The results for site “2110”, GSI data, for day 118, 1996, are given in Table 6.24, and Figures 6.17 and 6.18. The results for site “alic”, ARGN data for day 195, 1995, are given in Table 6.25, and Figures 6.19 and 6.20.

Tables 6.21 to 6.25, summarise the daily statistical report comparison of the TEC prediction residuals between using the UNSW grid-based algorithm and using the conventional grid-based algorithm. “TPR” is an abbreviation of “TEC Prediction Residual”, “Fre” refers to “Frequency”, “Pro.” is “Probability”, and “Cum. Pro.” is “Cumulative Probability”. From the results shown in Tables 6.21 to 6.25, and Figures 6.11 to 6.20, it is evident that the performance of the UNSW grid-based algorithm is much better than that of the conventional grid-based algorithm. The TEC prediction residuals of UNSW grid-based algorithm and conventional algorithm are approximately less than ± 2.5 TECU and ± 3.5 TECU respectively at the 99% probability level in the case of PGGA data. In the cases of the GSI data and ARGN data, the TEC prediction residuals of the UNSW grid-based algorithm and conventional algorithm are approximately less than ± 4.5 TECU and ± 5.5 TECU respectively at the 99% probability level.

Table 6.16. Comparison between UNSW grid-based algorithm and conventional algorithm
at site “crfp”, PGGGA data, from day 002 to 012, 1996.

Day	Mean (TECU)		Standard Deviation (TECU)		
	Conv.	UNSW	Conv.	UNSW	Impro. (%)
002	0.01	0.08	1.309	0.934	28.8
003	0.01	0.08	1.043	0.642	38.4
004	N/A	N/A	N/A	N/A	N/A
005	0.08	0.15	1.068	0.762	28.7
006	-0.05	0.02	0.897	0.618	31.1
007	0.09	0.15	1.135	0.829	27.0
008	-0.05	0.01	0.918	0.548	40.3
009	0.09	0.06	0.952	0.704	26.1
010	0.14	0.10	0.930	0.717	22.9
011	0.03	0.07	1.057	0.764	27.7
012	-0.01	0.00	0.976	0.606	37.9
Average	0.03±0.06	0.07±0.05	1.03±0.12	0.71±0.12	30.89±5.9

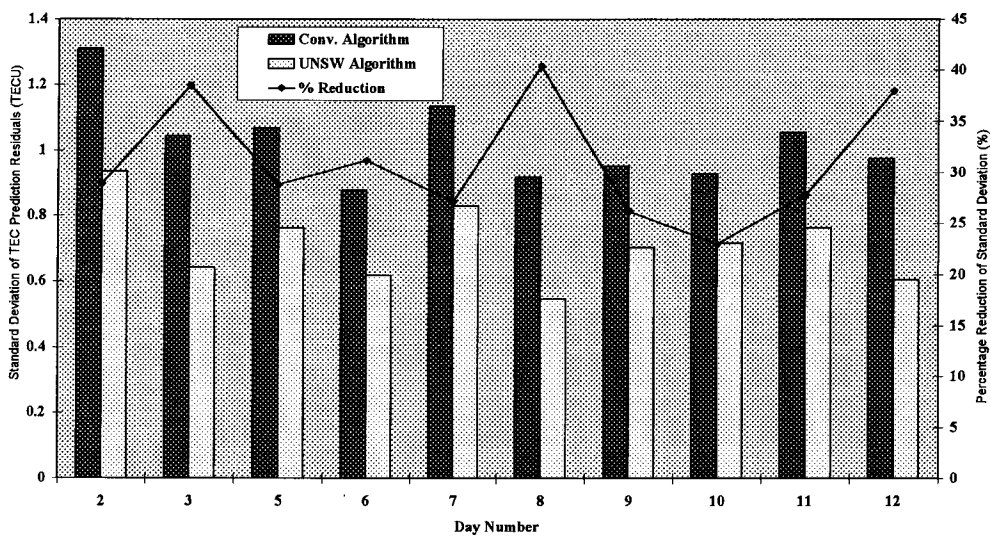
Figure 6.6. Comparison between UNSW grid-based algorithm and conventional algorithm
at site “crfp”, PGGGA data, from day 002 to 012, 1996.

Table 6.17. Comparison between UNSW grid-based algorithm and conventional algorithm at PGGa region (excluding site “crfp”), from day 002 to 012, 1996.

Day	Mean (TECU)		Standard Deviation (TECU)		
	Conv.	UNSW	Conv.	UNSW	Impro. (%)
002	-0.02	0.06	1.466	1.186	19.1
003	-0.05	0.05	1.148	0.83	27.7
004	N/A	N/A	N/A	N/A	N/A
005	-0.07	0.02	1.040	0.762	26.7
006	-0.05	0.02	0.924	0.675	26.9
007	-0.08	0.01	1.188	0.862	27.4
008	-0.07	0.02	1.006	0.710	29.4
009	-0.11	-0.03	1.019	0.704	30.9
010	-0.07	0.00	0.781	0.488	37.5
011	-0.09	0.00	1.076	0.744	30.9
012	-0.02	0.05	0.889	0.597	32.8
Average	-0.06±0.03	0.02±0.03	1.05±0.19	0.76±0.19	28.93±4.8

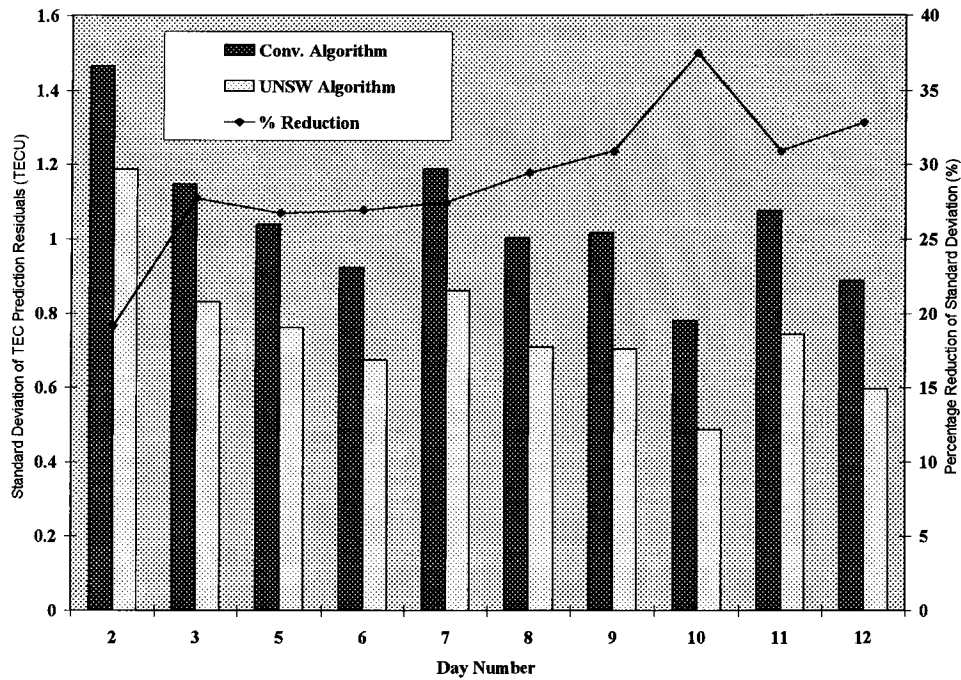


Figure 6.7. Comparison between UNSW grid-based algorithm and conventional algorithm at PGGa region (excluding site “crfp”), from day 002 to 012, 1996.

Table 6.18. Comparison between UNSW grid-based algorithm and conventional algorithm
at site “2110”, GSI data, from day 112 to 119, 1996.

Day	Mean (TECU)		Standard Deviation (TECU)		
	Conv.	UNSW	Conv.	UNSW	Impro. (%)
112	-0.12	-0.03	1.301	1.253	03.6
113	-0.11	-0.03	1.152	1.100	04.5
114	0.11	0.10	1.176	0.997	15.2
115	0.12	0.09	1.332	1.224	08.1
116	0.11	0.09	2.194	1.882	14.1
117	-0.32	-0.12	1.431	1.256	12.2
118	-0.53	-0.44	1.861	1.633	12.2
119	-0.09	0.02	2.175	1.887	13.0
Average	-0.11±0.23	-0.04±0.18	1.58±0.43	1.40±0.35	10.4±4.4

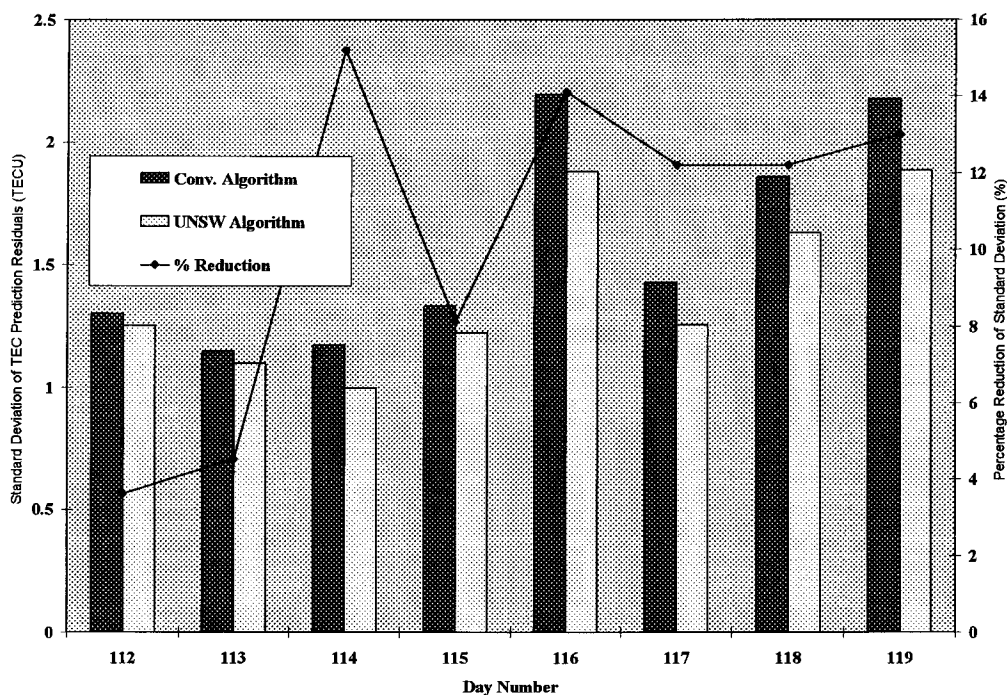
Figure 6.8. Comparison between UNSW grid-based algorithm and conventional algorithm
at site “2110”, GSI data, from day 112 to 119, 1996.

Table 6.19. Comparison between UNSW grid-based algorithm and conventional algorithm at GSI region (excluding site “2110”), from day 112 to 119, 1996.

Day	Mean (TECU)		Standard Deviation (TECU)		
	Conv.	UNSW	Conv.	UNSW	Impro. (%)
112	-0.09	-0.03	1.212	0.962	20.6
113	-0.05	-0.05	1.199	0.983	18.0
114	-0.10	-0.08	1.313	1.082	17.6
115	-0.05	-0.05	1.236	1.008	18.4
116	-0.15	-0.06	2.100	1.640	21.9
117	-0.07	-0.02	1.395	1.074	23.0
118	-0.10	-0.06	1.587	1.272	19.8
119	-0.07	-0.07	1.639	1.326	19.1
Average	-0.09±0.03	-0.05±0.02	1.46±0.31	1.17±0.23	19.8±1.9

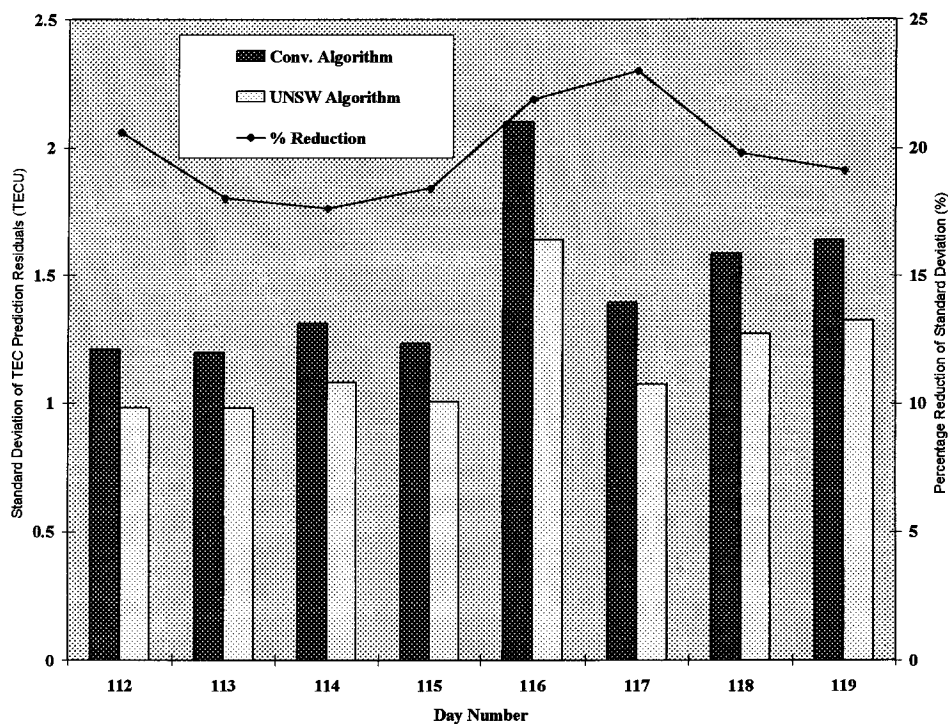


Figure 6.9. Comparison between UNSW grid-based algorithm and conventional algorithm at GSI region (excluding site “2110”), from day 112 to 119, 1996.

Table 6.20. Comparison between UNSW grid-based algorithm and conventional algorithm at site “alic”, ARGN data, from day 182 to 195, 1995.

Day	Mean (TECU)		Standard Deviation (TECU)		
	Conv.	UNSW	Conv.	UNSW	Impro. (%)
182	-0.35	-0.23	1.475	1.171	20.5
183	0.51	0.28	1.550	1.108	28.5
184	0.42	0.10	1.469	1.038	29.3
185	0.53	0.22	1.531	1.008	34.2
186	0.11	0.09	1.087	0.709	34.8
187	0.19	0.10	1.117	0.677	39.4
188	0.25	0.15	1.181	0.764	35.3
189	0.68	0.40	1.558	1.014	36.1
190	0.46	0.22	1.358	0.830	38.9
191	0.50	0.25	1.525	0.954	38.8
192	0.46	0.18	1.525	0.818	46.4
193	0.38	0.16	1.278	0.806	37.2
194	0.31	0.13	1.161	0.650	44.0
195	0.23	-0.03	1.594	0.960	40.0
Average	0.29±0.24	0.14±0.15	1.39±0.19	0.89±0.16	36.0±6.6

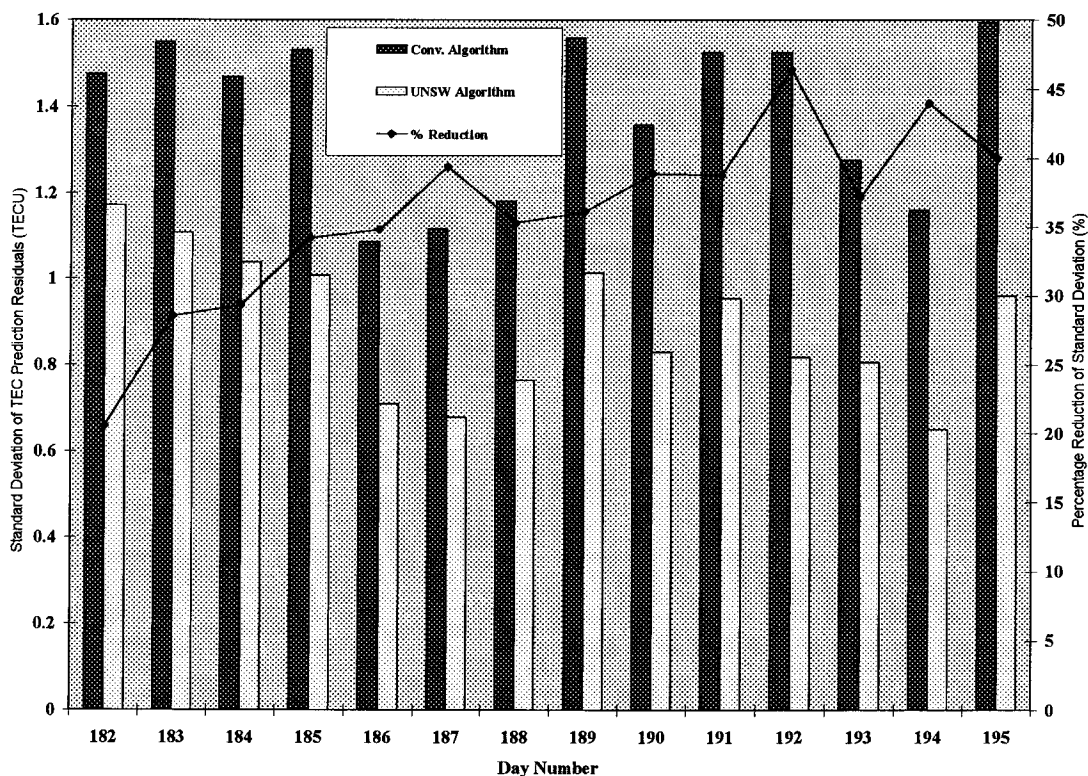


Figure 6.10. Comparison between UNSW grid-based algorithm and conventional algorithm at site “alic”, ARGN data, from day 182 to 195, 1995.

Table 6.21. Statistical data comparison between UNSW grid-based algorithm and conventional algorithm, at PGGa region (excluding site “crfp”), for day 012, 1996.

TPR (TECU)	UNSW Grid-Based Algorithm			Conventional Grid-Based Algorithm		
	Fre.	Pro. (%)	Cum. Pro. (%)	Fre.	Pro. (%)	Cum. Pro. (%)
-3.0	0	0.00	0.00	176	0.34	0.34
-2.0	328	0.62	0.62	1993	3.80	4.14
-1.0	7813	14.90	15.52	13453	25.66	29.80
0.0	34389	65.60	81.12	22906	43.69	73.49
1.0	8784	16.76	97.88	11366	21.68	95.17
2.0	1073	2.05	99.92	2307	4.40	99.57
3.0	37	0.07	100.00	223	0.42	100.00

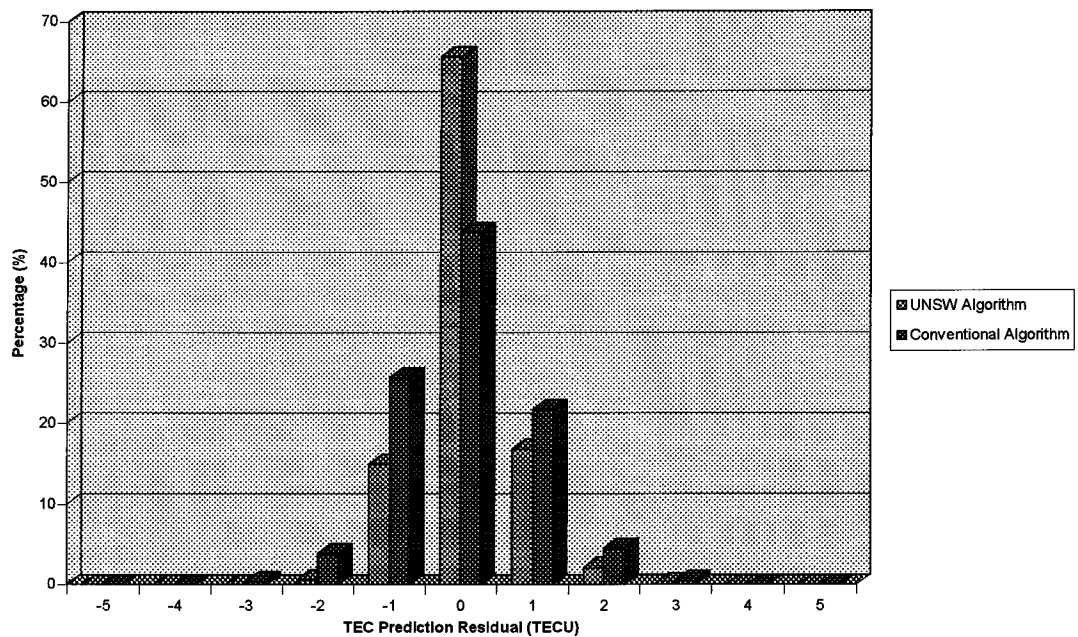


Figure 6.11. TEC prediction residual comparison between UNSW grid-based algorithm and conventional algorithm, at PGGa region (excluding site “crfp”), for day 012, 1996.

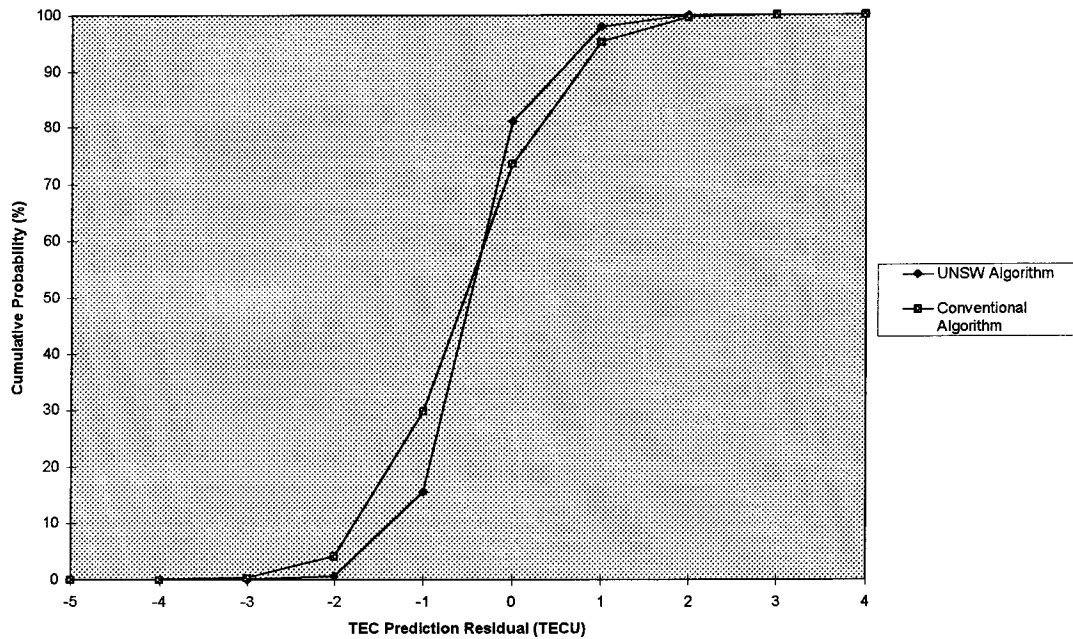


Figure 6.12. TEC prediction residual versus cumulative probability using UNSW grid-based algorithm and conventional algorithm, at PGGA region (excluding site “crfp”), for day 012, 1996.

Table 6.22. Statistical data comparison between UNSW grid-based algorithm and conventional algorithm, at site “crfp”, PGGA data, for day 012, 1996.

TPR (TECU)	UNSW Grid-Based Algorithm			Conventional Grid-Based Algorithm		
	Fre.	Pro. (%)	Cum. Pro. (%)	Fre.	Pro. (%)	Cum. Pro. (%)
-3.0	0	0.00	0.00	31	0.22	0.22
-2.0	45	0.32	0.32	691	5.01	5.23
-1.0	2777	20.14	20.46	3446	25.00	30.23
0.0	8602	62.39	82.86	5529	40.10	70.33
1.0	2139	15.52	98.38	3405	24.70	95.03
2.0	223	1.62	100.00	376	2.73	97.76
3.0	0	0.00	100.00	308	2.23	100.00

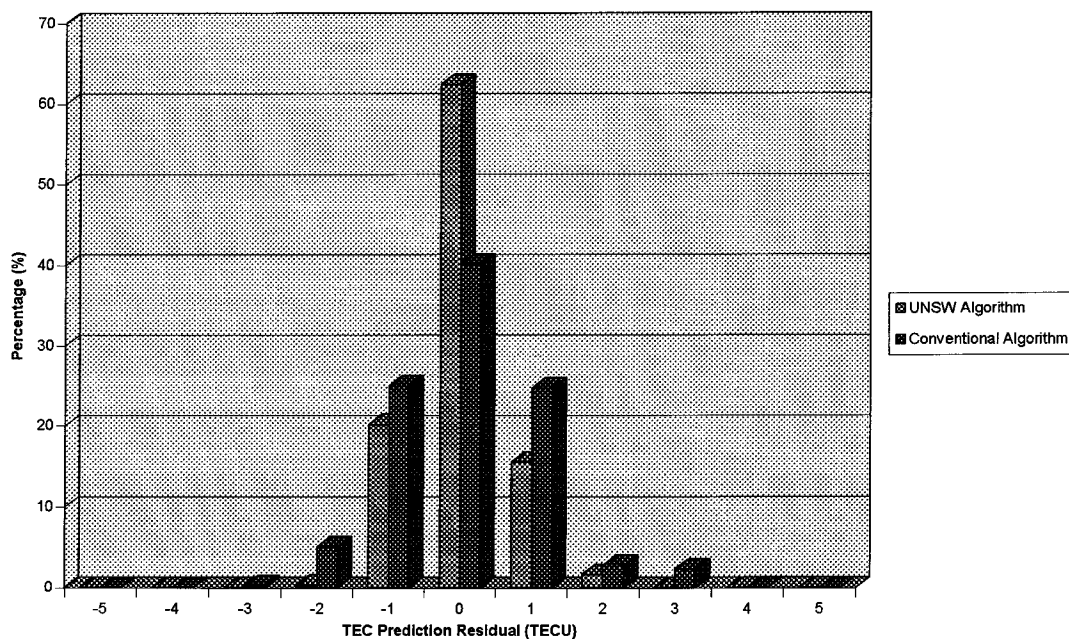


Figure 6.13. TEC prediction residual comparison between UNSW grid-based algorithm and conventional algorithm, at site “crfp”, PGGA data, for day 012, 1996.

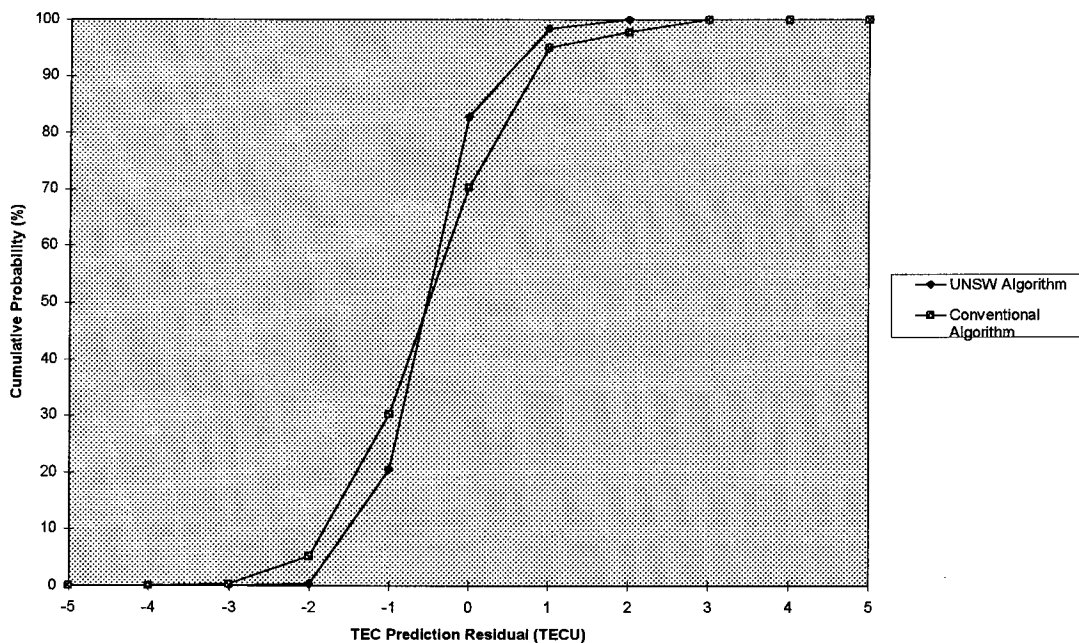


Figure 6.14. TEC prediction residual versus cumulative probability using UNSW grid-based algorithm and conventional algorithm, at site “crfp”, PGGA data, for day 012, 1996.

Table 6.23. Statistical data comparison between UNSW grid-based algorithm and conventional algorithm, at GSI region (excluding site “2110”), for day 118, 1996.

TPR (TECU)	UNSW Grid-Based Algorithm			Conventional Grid-Based Algorithm		
	Fre.	Pro. (%)	Cum. Pro. (%)	Fre.	Pro. (%)	Cum. Pro. (%)
-7.0	0	0.00	0.00	3	0.01	0.01
-6.0	29	0.06	0.06	101	0.20	0.21
-5.0	106	0.21	0.27	194	0.39	0.60
-4.0	390	0.78	1.05	499	0.99	1.59
-3.0	1034	2.06	3.11	1695	3.37	4.96
-2.0	3704	7.36	10.47	6172	12.27	17.23
-1.0	8617	17.14	27.61	12061	23.98	41.21
0.0	23785	47.30	74.91	13214	26.28	67.49
1.0	8444	16.79	91.70	8695	17.29	84.78
2.0	2873	5.71	97.41	5037	10.02	94.80
3.0	1002	1.99	99.40	1617	3.22	98.02
4.0	279	0.56	99.96	766	1.52	99.53
5.0	26	0.04	100.00	157	0.31	99.84
6.0	0	0.00	100.00	78	0.16	100.00
7.0	0	0.00	100.00	0	0.00	100.00

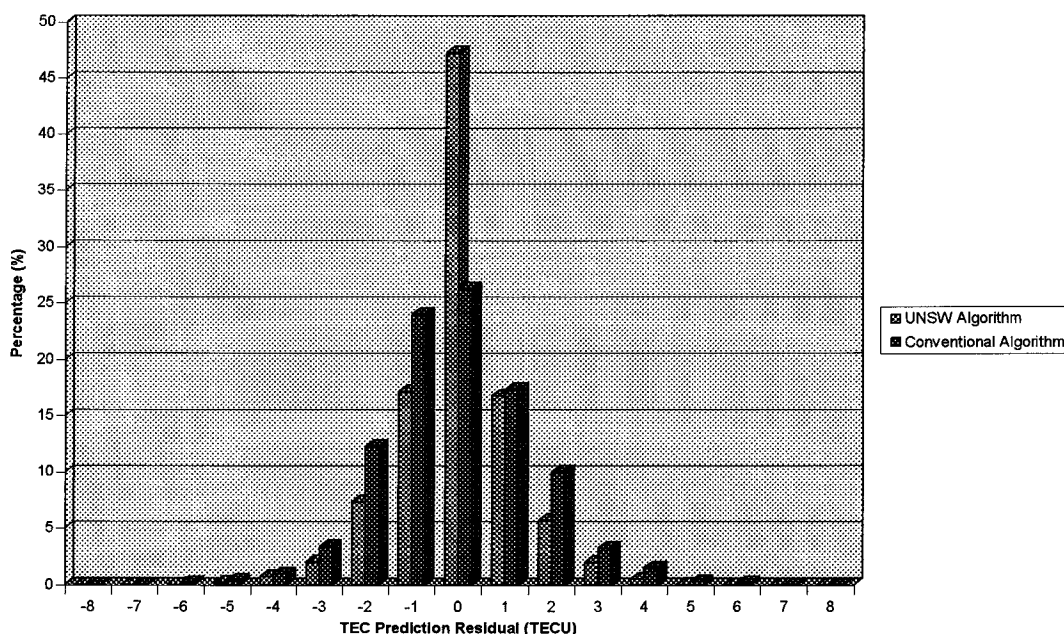


Figure 6.15. TEC prediction residual comparison between UNSW grid-based algorithm and conventional algorithm, at GSI region (excluding site “2110”), for day 118, 1996.

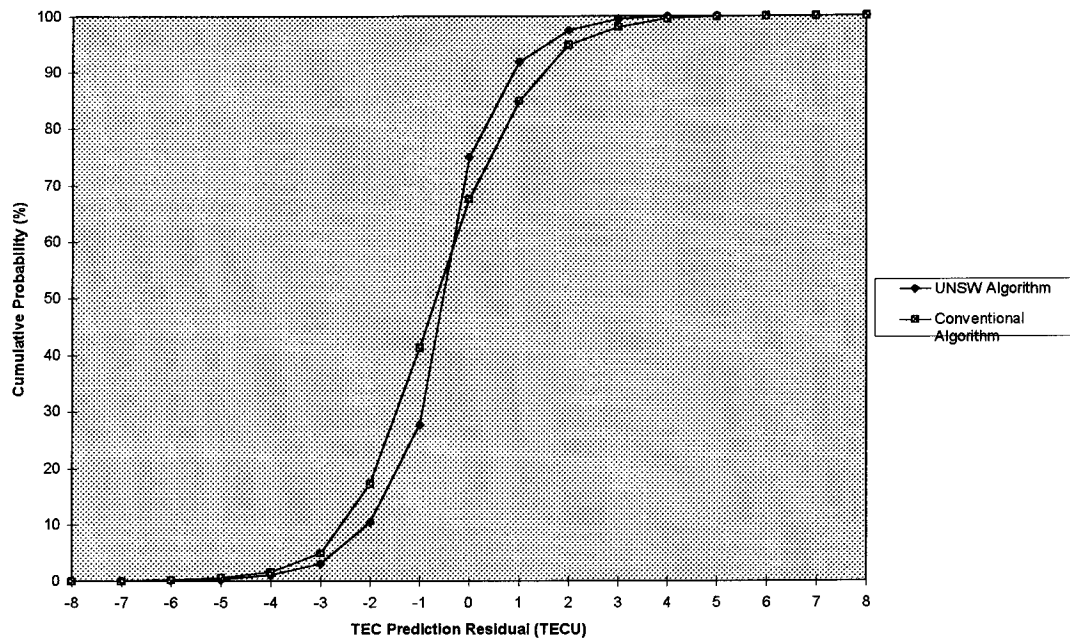


Figure 6.16. TEC prediction residual versus cumulative probability using UNSW grid-based algorithm and conventional algorithm, at GSI region (excluding site “2110”), for day 118, 1996.

Table 6.24. Statistical data comparison between UNSW grid-based algorithm and conventional algorithm, at site “2110”, GSI data, for day 195, 1995.

TPR (TECU)	UNSW Grid-Based Algorithm			Conventional Grid-Based Algorithm		
	Fre.	Pro. (%)	Cum. Pro. (%)	Fre.	Pro. (%)	Cum. Pro. (%)
-7.0	1	0.01	0.01	0	0.00	0.00
-6.0	91	0.92	0.93	36	0.36	0.36
-5.0	29	0.29	1.22	131	1.32	1.68
-4.0	84	0.84	2.06	121	1.22	2.90
-3.0	751	7.55	9.61	1179	11.85	14.75
-2.0	1456	14.64	24.25	1554	15.62	30.37
-1.0	2213	22.24	46.49	2134	21.45	51.82
0.0	2734	27.48	73.97	2125	21.36	73.18
1.0	1569	15.77	89.74	1239	12.45	85.63
2.0	744	7.48	97.22	861	8.65	94.28
3.0	203	2.04	99.26	525	5.28	99.56
4.0	72	0.73	99.99	43	0.44	100.00
5.0	0	0.00	99.99	0	0.00	100.00
6.0	1	0.01	100.00	0	0.00	100.00
7.0	0	0.00	100.00	0	0.00	100.00

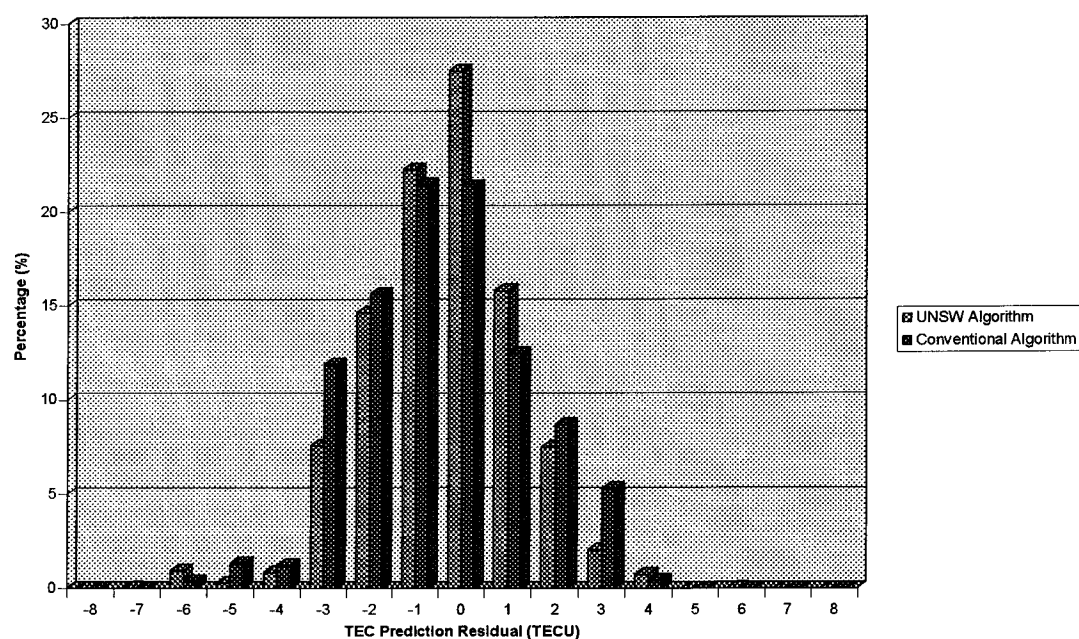


Figure 6.17. TEC prediction residual comparison between UNSW grid-based algorithm and conventional algorithm, at site “2110”, GSI data, for day 118, 1996.

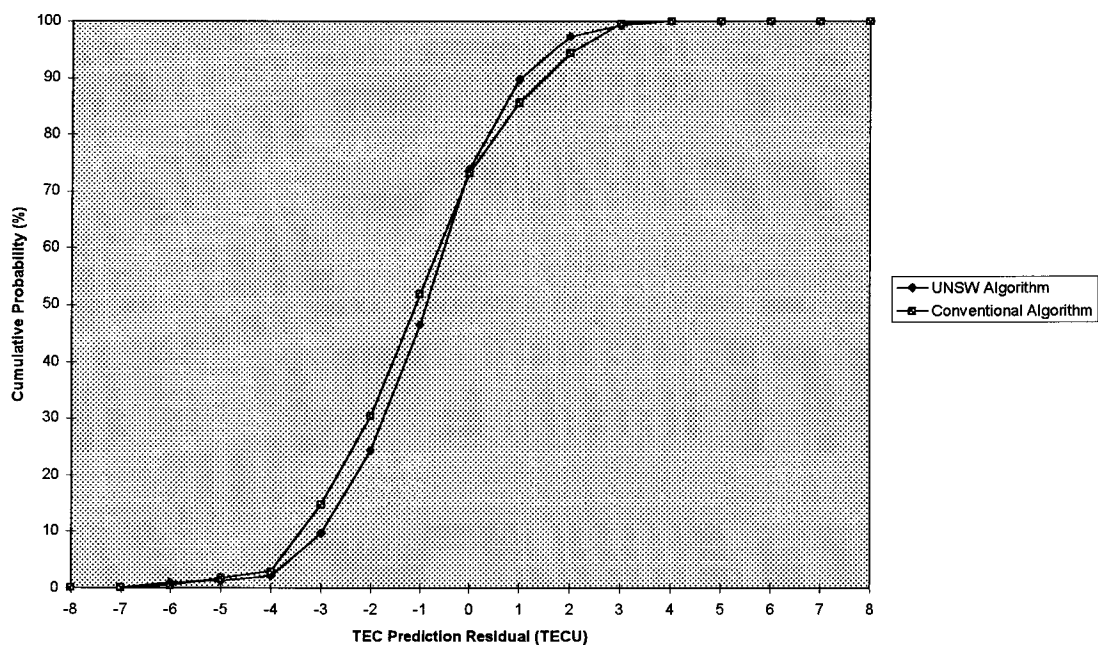


Figure 6.18. TEC prediction residual versus cumulative probability using UNSW grid-based algorithm and conventional algorithm, at site “2110”, GSI data, for day 118, 1996.

Table 6.25. Statistical data comparison between UNSW grid-based algorithm and conventional algorithm, at site “alic”, ARGN data, for day 195, 1995.

TPR (TECU)	UNSW Grid-Based Algorithm			Conventional Grid-Based Algorithm		
	Fre.	Pro. (%)	Cum. Pro. (%)	Fre.	Pro. (%)	Cum. Pro. (%)
-6.0	0	0.00	0.00	0	0.00	0.00
-5.0	0	0.00	0.00	0	0.00	0.00
-4.0	57	0.47	0.47	89	0.74	0.74
-3.0	111	0.92	1.39	353	2.91	3.65
-2.0	602	4.97	6.36	1080	8.91	12.56
-1.0	1590	13.12	19.48	2330	19.23	31.79
0.0	7750	63.97	83.45	3350	27.65	59.44
1.0	1374	11.34	94.79	2573	21.24	80.68
2.0	427	3.52	98.31	1385	11.43	92.11
3.0	143	1.18	99.49	595	4.91	97.02
4.0	35	0.29	99.78	240	1.98	99.00
5.0	3	0.03	99.81	116	0.96	99.96
6.0	23	0.19	100.00	4	0.03	100.00

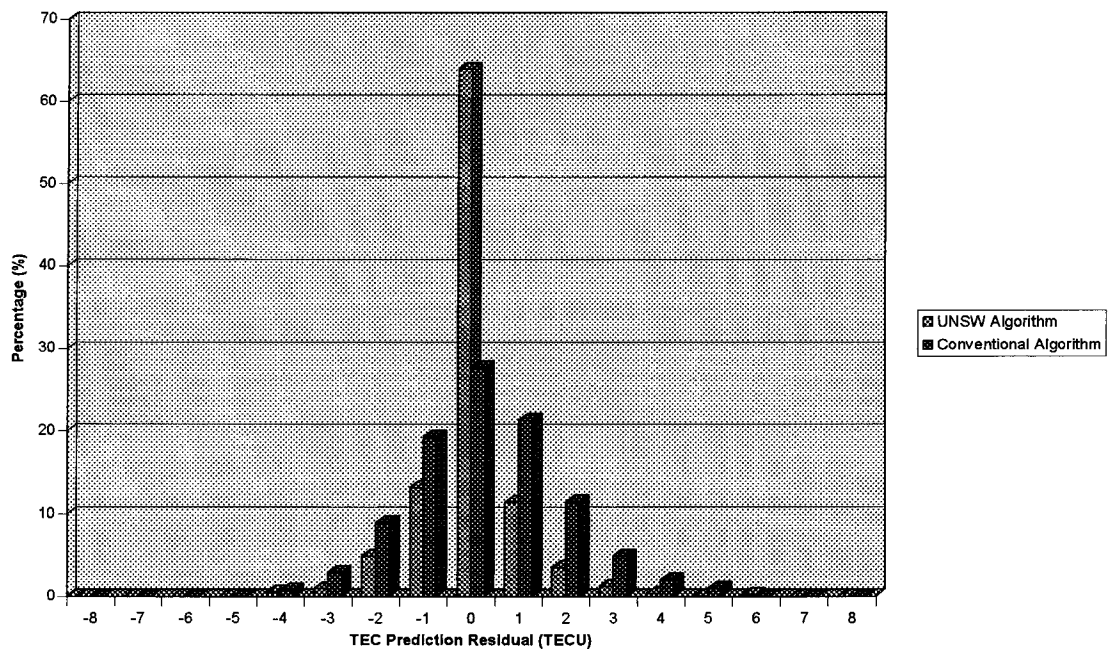


Figure 6.19. TEC prediction residual comparison between UNSW grid-based algorithm and conventional algorithm, at site “alic”, ARGN data, for day 195, 1995.

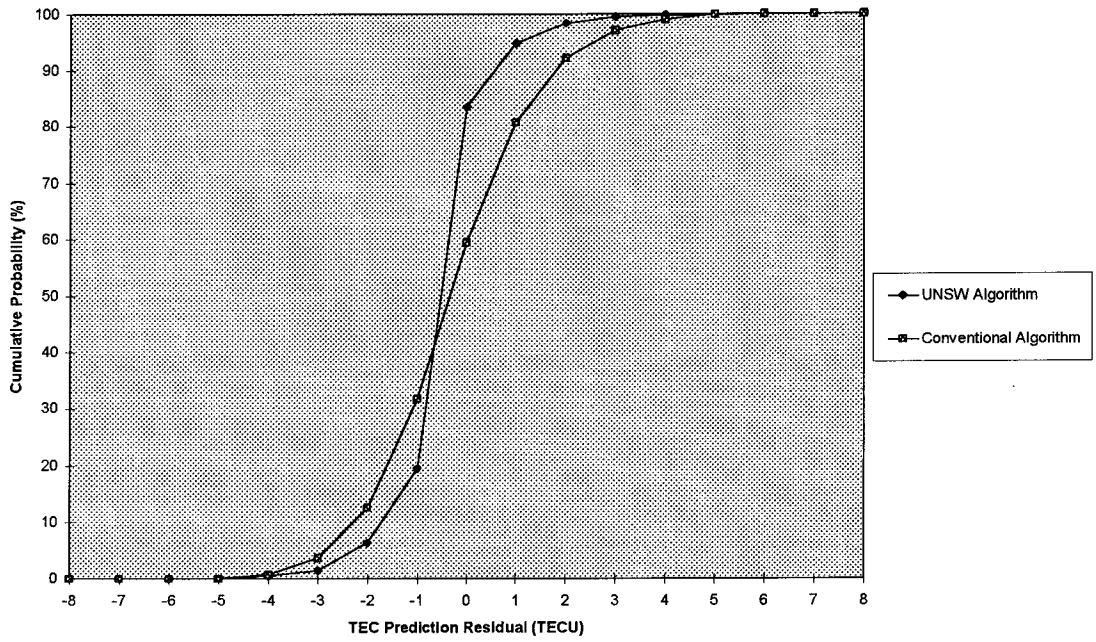


Figure 6.20. TEC prediction residual versus cumulative probability using UNSW grid-based algorithm and conventional algorithm, at site “alic”, ARGN data, for day 195, 1995.

6.5.4 Test Result Comparisons between UNSW Algorithm and Polynomial Algorithms

6.5.4.1 Polynomial Algorithms

As discussed in section 6.2, least-squares fit algorithms, such as a 15-term polynomial, is one of the possible real-time ionospheric estimation techniques which can be employed to model the regional ionosphere. From chapter 5, the vertical TEC, TEC_v , at the IPP is represented by the following polynomial:

$$\begin{aligned}
 TEC_v(\phi_{pp}, \lambda_{pp}) = & a_1 + a_2 \cdot \phi_{pp} + a_3 \cdot \lambda_{pp} + a_4 \cdot \phi_{pp}^2 + a_5 \cdot \lambda_{pp}^2 + a_6 \cdot \phi_{pp} \cdot \lambda_{pp} \\
 & + a_7 \cdot \phi_{pp}^3 + a_8 \cdot \lambda_{pp}^3 + a_9 \cdot \phi_{pp}^2 \cdot \lambda_{pp} + a_{10} \cdot \phi_{pp} \cdot \lambda_{pp}^2 + a_{11} \cdot \phi_{pp}^4 \\
 & + a_{12} \cdot \lambda_{pp}^4 + a_{13} \cdot \phi_{pp}^3 \cdot \lambda_{pp} + a_{14} \cdot \phi_{pp}^2 \cdot \lambda_{pp}^2 + a_{15} \cdot \phi_{pp} \cdot \lambda_{pp}^3
 \end{aligned} \quad (6.48)$$

where ϕ_{pp} is the geographic latitude of the IPP (cf. equation (6.1)), λ_{pp} is the geographic longitude of the IPP (cf. equation (6.3)), and a_0, \dots, a_{14} are the unknown polynomial

coefficients. Note that the coordinate system used in equation (6.48) is different from that used in equation (5.3).

In this section, three types of polynomials, namely the 6-term, 10-term, and 15-term are used to model the regional ionosphere. The number of unknown coefficients (α_i , $i=1, 2, 3, \dots, 15$) are 6, 10, and 15, for the 6-term, 10-term, and 15-term polynomials respectively.

6.5.4.2 Test Results and Discussion

The least-squares fit polynomial algorithm is similar to the grid-based algorithm, except that the polynomial coefficients are computed and sent to all users by the Wide-area Monitor Station. The user receiver computes the vertical TEC of each pierce point using equation (6.48).

In order to compare with the results from grid-based algorithms, the ARGN data set described in section 6.5.1.3 were processed and analysed. Program 8 (POSTEC) was used to compute the polynomial coefficients from the vertical TEC values of the reference IPPs using the least-squares adjustment method on an epoch-by-epoch basis. Program 10 was used to compute the predicted vertical TEC values and TEC prediction residuals of the IPPs at the user receiver using the estimated polynomial coefficients from Program 8 (cf. equation 6.48). Program 11 was used to sort the TEC prediction residuals.

The comparisons of standard deviations of TEC prediction residuals from the UNSW grid-based algorithm, the conventional grid-based algorithm, and the various (6-term, 10-term, and 15-term) polynomial algorithms at site “alic”, ARGN data, from day 182 to 195, 1995 are summarised in Table 6.26. Figure 6.21 shows the comparison of standard deviations of TEC prediction residuals using the 6-term, 10-term, and 15-term polynomial algorithms. From Table 6.26 and Figure 6.21, the performance of the 10-term polynomial algorithm is the best among these three polynomial algorithms. Therefore, only the results from the 10-term polynomial algorithm and the two grid-based algorithms are shown in the Figure 6.22. The results in Table 6.26 indicate the mean values of the standard deviations of TEC prediction residuals over the 14-day period as 0.89 ± 0.16 TECU, 1.39 ± 0.19 TECU, and

2.78±064 TECU for the UNSW grid-based algorithm, the conventional grid-based algorithm, and the 10-term polynomial algorithm respectively.

In order to further analyse the performance of the polynomial algorithms, the “TEC prediction residual comparison” and the “TEC prediction residual versus cumulative probability” for the various polynomial algorithms, at site “alic”, for day 195, 1995, are shown in Figures 6.23 and 6.24 respectively. The “TEC prediction residual comparison” and the “TEC prediction residual versus cumulative probability” for the UNSW grid-based algorithm, the conventional grid-based algorithm, and the 10-term polynomial algorithm, at site “alic”, for day 195, 1995, are shown in Figures 6.25 and 6.26 respectively. Table 6.27 summarises the statistical report of the TEC prediction residuals using the UNSW grid-based algorithm and the 10-term polynomial algorithm.

From Table 6.27 and Figure 6.26, it is found that the TEC prediction residuals of the 10-term polynomial algorithm is less than ±6.5 TECU at the 99% probability level. From section 6.5.3, the TEC prediction residuals of the UNSW grid-based algorithm and the conventional algorithm were less than ±4.5 TECU and ±5.5 TECU respectively, at the 99% probability level.

From Tables 6.26 to 6.27 and Figures 6.21 to 6.26 it can be concluded that: (1) the performance of the 10-term polynomial algorithm is the best among these three candidate (6-term, 10-term, and 15-term) polynomial algorithms, (2) the mean values of the standard deviations of TEC prediction residuals over the 14-day period are 0.89±0.16 TECU, 1.39±019 TECU, and 2.78±064 TECU for the UNSW grid-based algorithm, the conventional grid-based algorithm, and the 10-term polynomial algorithm respectively, (3) the TEC prediction residuals of the UNSW grid-based algorithm, the conventional algorithm and the 10-term polynomial algorithm are less than ±4.5 TECU, ±5.5 TECU, and ±6.5 TECU respectively at the 99% probability level, (4) the performance of the grid-based algorithm is better than that of the polynomial algorithm (eg. Lin et al., 1996a), and (5) the standard deviations of the TEC prediction residuals can be reduced significantly if the UNSW grid-based algorithm is used (eg. Lin & Rizos, 1997a).

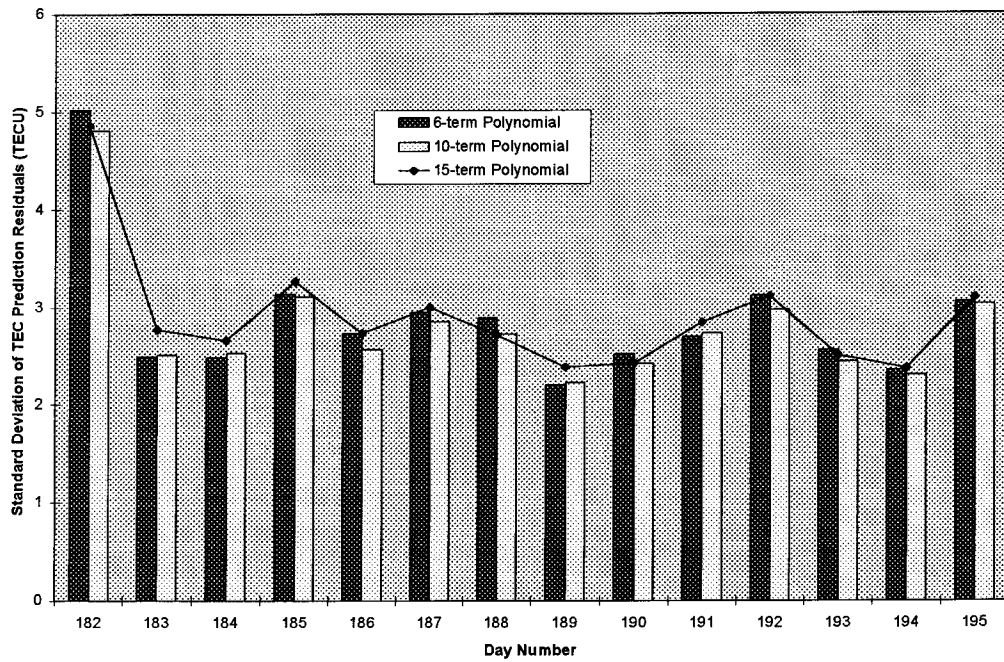


Figure 6.21. Comparison between 6-term, 10-term, and 15-term polynomial algorithms at site “alic”, ARGN data, from day 182 to 195, 1995.

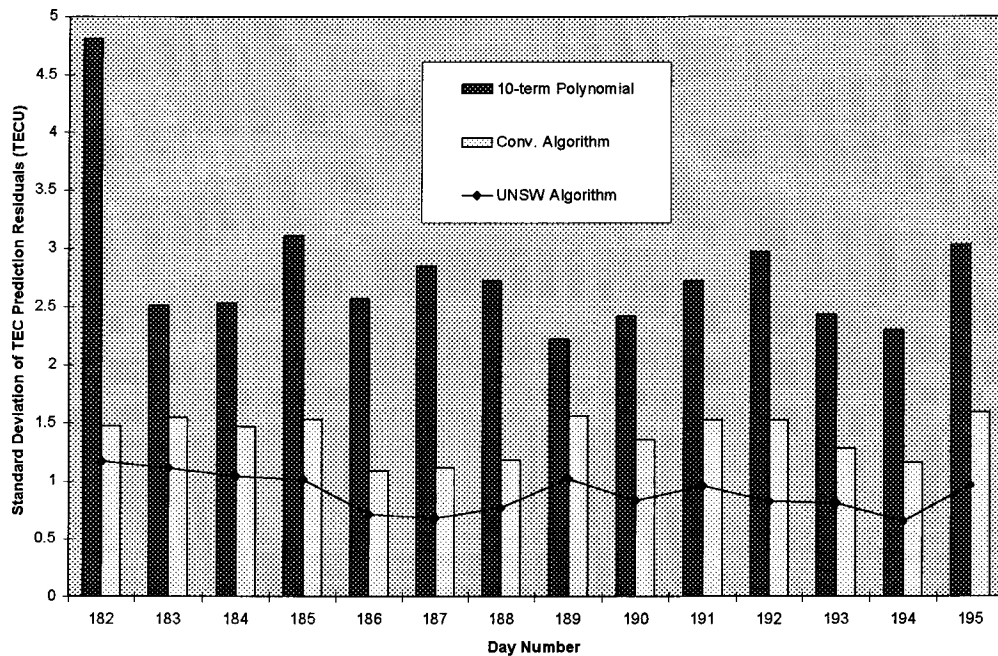


Figure 6.22. Comparison between UNSW grid-based algorithm, conventional grid-based algorithm, and 10-term polynomial algorithm at site “alic”, ARGN data, from day 182 to 195, 1995.

Table 6.26. Comparison of standard deviation of TEC prediction residuals between UNSW grid-based algorithm, conventional algorithm, and various polynomial algorithms at site “alic”, ARGN data, from day 182 to 195, 1995.

Day	UNSW (TECU)	Conv. (TECU)	6-term (TECU)	10-term (TECU)	15-term (TECU)
182	1.171	1.475	5.021	4.808	4.857
183	1.108	1.550	2.488	2.511	2.767
184	1.038	1.469	2.482	2.529	2.656
185	1.008	1.531	3.132	3.106	3.256
186	0.709	1.087	2.727	2.563	2.727
187	0.677	1.117	2.953	2.850	2.993
188	0.764	1.181	2.890	2.721	2.708
189	1.014	1.558	2.197	2.219	2.380
190	0.830	1.358	2.518	2.415	2.415
191	0.954	1.525	2.695	2.722	2.838
192	0.818	1.525	3.111	2.970	3.104
193	0.806	1.278	2.555	2.436	2.497
194	0.650	1.161	2.356	2.302	2.364
195	0.960	1.594	3.054	3.029	3.090

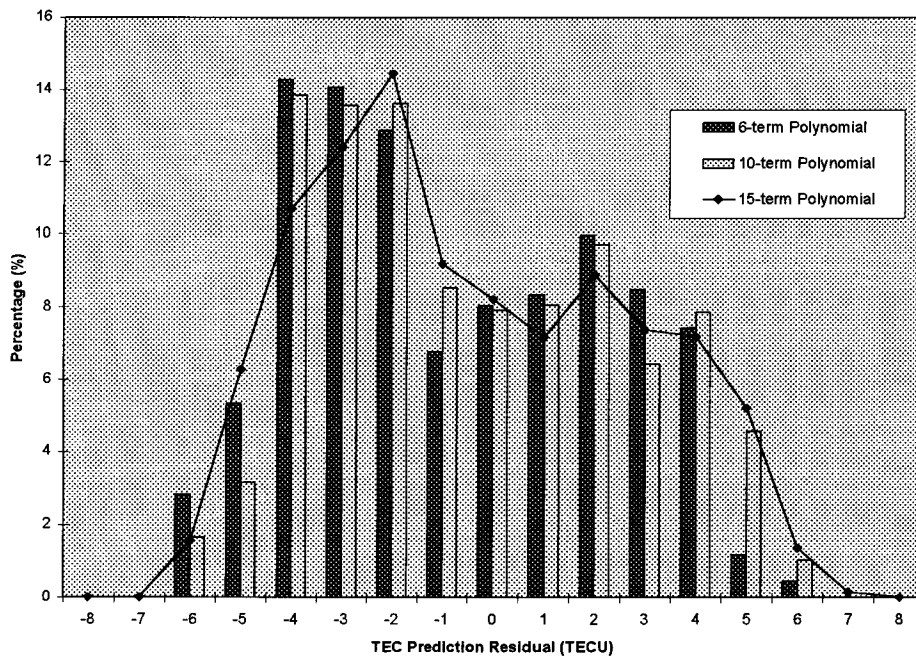


Figure 6.23. TEC prediction residual comparison between various polynomial algorithms, at site “alic”, ARGN data, for day 195, 1995.

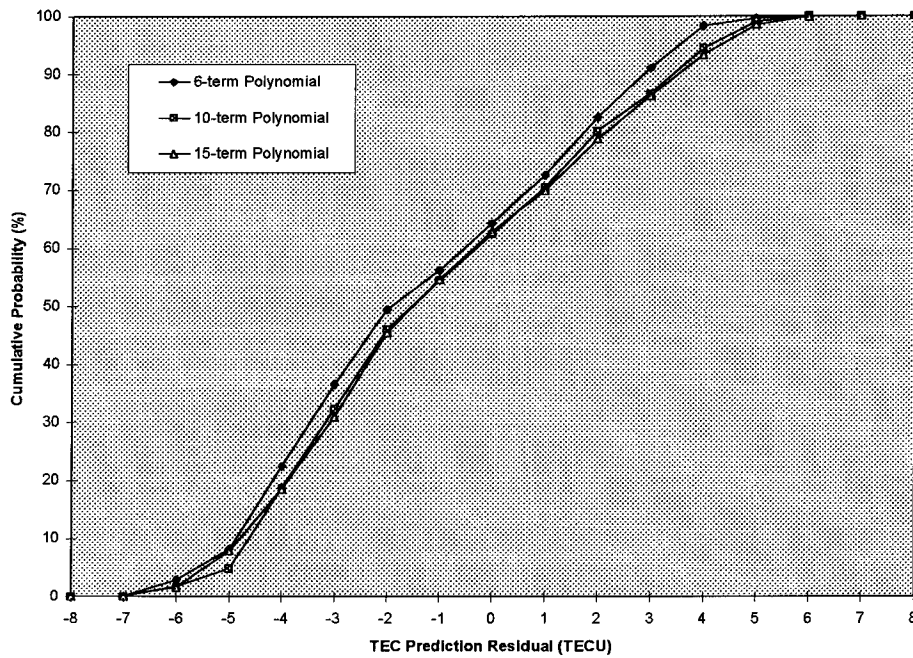


Figure 6.24. TEC prediction residual versus cumulative probability using various polynomial algorithms, at site “alic”, ARGN data, for day 195, 1995.

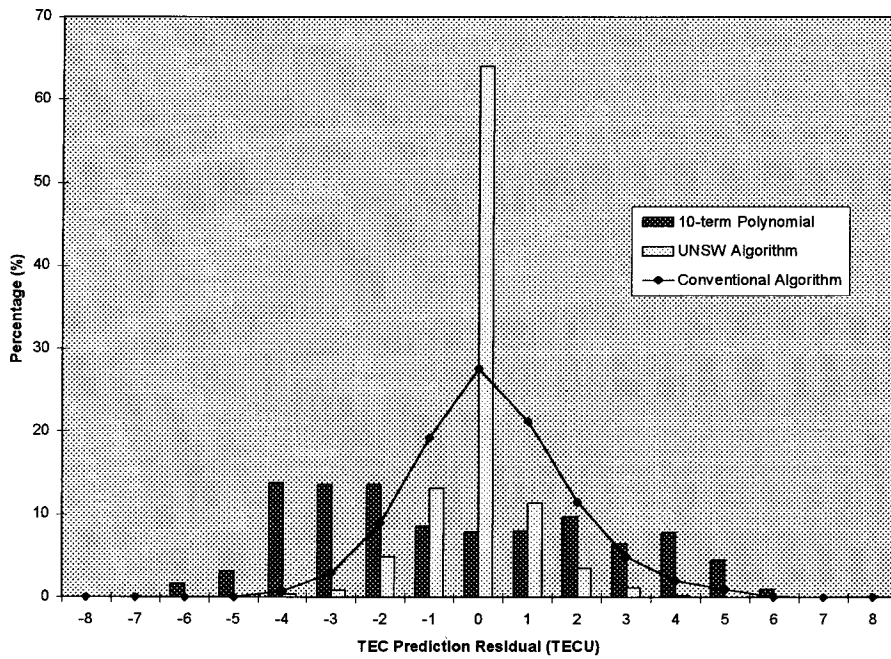


Figure 6.25. TEC prediction residual comparison between UNSW grid-based algorithm, conventional grid-based algorithm, and 10-term polynomial algorithm, at site “alic”, ARGN data, for day 195, 1995.

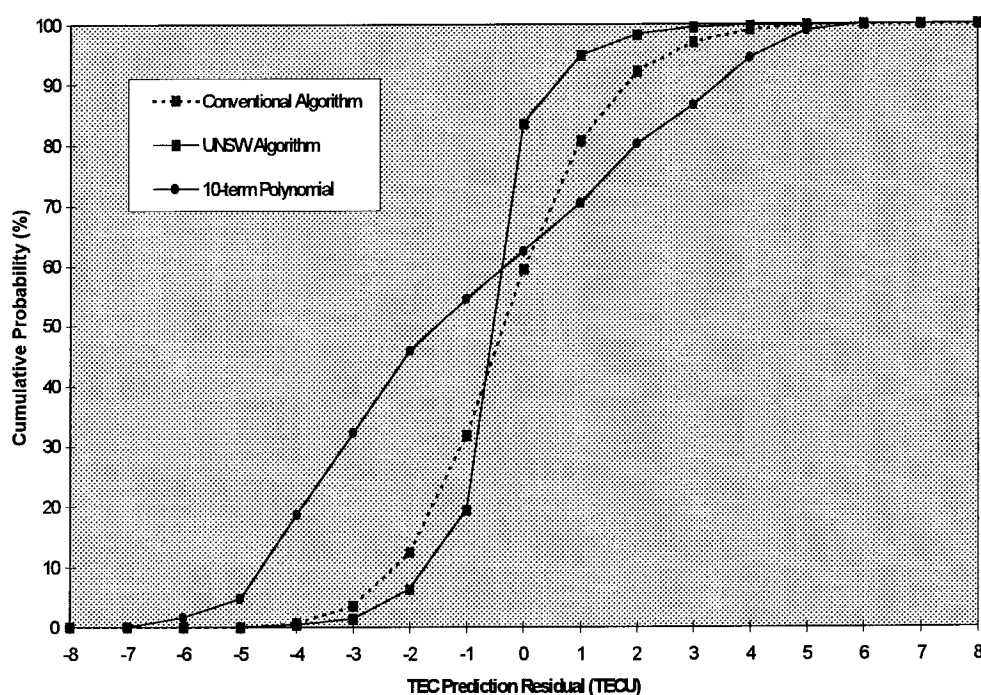


Figure 6.26. TEC prediction residual versus cumulative probability using UNSW grid-based algorithm, conventional grid-based algorithm, and 10-term polynomial algorithm, at site “alic”, ARGN data, for day 195, 1995.

Table 6.27. Statistical data comparison between UNSW grid-based algorithm and 10-term polynomial algorithm, at site “alic”, ARGN data, for day 195, 1995.

TPR (TECU)	UNSW Grid-Based Algorithm			10-term Polynomial Algorithm		
	Fre.	Pro. (%)	Cum. Pro. (%)	Fre.	Pro. (%)	Cum. Pro. (%)
-6.0	0	0.00	0.00	201	1.66	1.66
-5.0	0	0.00	0.00	383	3.16	4.82
-4.0	57	0.47	0.47	1677	13.85	18.67
-3.0	111	0.92	1.39	1644	13.57	32.24
-2.0	602	4.97	6.36	1649	13.62	45.86
-1.0	1590	13.12	19.48	1034	8.54	54.40
0.0	7750	63.97	83.45	959	7.92	62.32
1.0	1374	11.34	94.79	976	8.06	70.38
2.0	427	3.52	98.31	1178	9.73	80.11
3.0	143	1.18	99.49	778	6.42	86.53
4.0	35	0.29	99.78	953	7.87	94.40
5.0	3	0.03	99.81	552	4.56	98.96
6.0	23	0.19	100.00	126	1.04	100.00

6.6 Concluding Remarks

In order to improve the accuracy of the vertical TEC estimates of the grid points, a new grid-based algorithm is proposed. Although the UNSW grid-based algorithm is similar to the algorithm described in Conker et al. (1995), several modifications were made to the algorithm. The major modifications were: (1) an “*exponential function*”, instead of “inverse distance”, is adopted as the weighting function, and (2) the “*grid-based ionosphere model*” estimated from the previous day, instead of the Klobuchar model, is used to predict the ionospheric delay ratios between the grid point and reference points.

Due to these modifications the performance of the UNSW grid-based algorithm is much better than that of conventional grid-based algorithm, as well as 10-term polynomial algorithm. From the test results presented here it has been demonstrated that the standard deviations of the TEC prediction residuals can be reduced significantly, by approximately 29 to 31 percent in the case of PGGGA data, 10 to 20 percent in the case of the GSI data, and 36 percent in the case of the ARGN data.

El-Arini et al. (1995) used a 72 day set of data from four U.S.A. Air Force Phillips Laboratory GPS sites to evaluate the performance of grid-based algorithms and other real-time ionospheric algorithms that could be implemented at the WAAS ground ionospheric reference stations, as well as at an airborne receiver. From their test results it was concluded that all of the ionospheric algorithms used in their test (grid-based, 6-term polynomial, and spherical harmonics) demonstrated roughly equivalent performance. On the other hand, the performance of the UNSW grid-based algorithm appears to be significantly better than that of the conventional grid-based algorithm or the 10-term polynomial-based algorithm, based on the experimental results presented in this thesis. Hence, no further test was made to compare the performance of the UNSW grid-based algorithm to those based on spherical harmonics.

CHAPTER 7

SUMMARY, CONCLUSIONS, AND RECOMMENDATIONS

This chapter summarises the investigations, makes conclusions on the findings, and recommends topics for further studies.

7.1 Summary of the Research

The ionosphere is the earth's upper atmosphere which allows radio communication over the horizon. For shorter wavelength radio signals, such as Global Positioning System (GPS) signals, the ionosphere causes "group delay" or "phase advance" to those radio signals when they pass through the ionosphere.

GPS is an all-weather, space-based navigation system. The GPS signals are affected by the ionosphere. For the dual-frequency GPS receiver users, the ionospheric delay can be eliminated to the first order through a linear combination of L1 and L2 observables. For the single-frequency GPS receiver users, they may either ignore the ionospheric delay or apply the broadcast Klobuchar model to eliminate approximately 50% to 60% of the ionospheric delay.

GPS satellites represent *the latest generation of satellites of opportunity* for ionospheric scientists. In chapter 2, the ionospheric models used by the ionosphere community, and the GPS positioning and navigation community, were reviewed. Comments were made regarding: (1) issues relating to the ionospheric delay estimation using GPS measurements, such as the basic mathematical equations of the GPS observables, pseudo-range derived TEC, carrier phase derived TEC, etc., (2) potential limitations in making absolute TEC estimation using GPS, and (3) real-time ionospheric delay estimation versus post-processing ionospheric delay estimation.

This research was motivated by the following factors: (1) there is a growing community which utilises GPS for a variety of civilian applications, such as surveying and mapping, land, sea and air navigation, search and rescue operations, etc., (2) there are many permanent GPS networks comprising dual-frequency receivers around the world, (3) this present solar cycle maximum will come around the year 2000, and hence it is necessary to design a good algorithm to mitigate the ionospheric delay effects on GPS positioning and navigation applications, (4) real-time ionosphere modelling is an ideal method of providing ionospheric delay corrections to single-frequency users, and (5) there were some challenging problems needed to be solved in real-time ionospheric delay estimation.

Typically, GPS users are interested in algorithms that eliminate or reduce the ionospheric delays from observations used in positioning and navigation applications. Recently, with the advent of the concept of GPS error separation, such as for the Wide Area Differential GPS and the Wide Area Augmentation System, the concept of real-time ionospheric delay estimation using dual-frequency GPS observables has become feasible.

However, there are a number of challenging problems to be solved, some of which were identified in this thesis: (1) pseudo-range multipath effect the pseudo-range derived TEC, (2) carrier phase failures, such as the occurrence of cycle slip(s), effect the carrier phase derived TEC, (3) GPS satellite transmitter and receiver L1/L2 differential delays effect the absolute TEC estimates, and (4) the weighting function and ionosphere model used for real-time ionosphere modelling.

The concept and methodology for generating a “multipath template” for a static station using the previous days’ GPS dual-frequency observables was presented in chapter 3. The generated multipath template can be used in subsequent days to mitigate the pseudo-range effects on an epoch-by-epoch basis. The performance of multipath templates, both the single-day or multi-day variety, were tested and analysed. The test results of the application of the multipath template for real-time ionospheric delay estimation were presented in chapter 4.

The basis for real-time failure detection and repair, as it relates to ionospheric delay computations, by robust and conventional Kalman filter state estimates was introduced in

chapter 4. Here, “failure” refers to the occurrence of cycle slip(s) in carrier phase data. The failures are detected and repaired in real-time using a Kalman filter algorithm, mitigating the effects on the carrier phase derived TEC. The performance of this algorithm was tested using the “REALTEC” software package with a UNSW data set and a PGGA data set.

The definition of the GPS satellite transmitter and receiver L1/L2 differential delays, and their effect on the absolute TEC estimates are given in chapter 5. Methods of estimating the L1/L2 differential delays are reviewed. Recognising that there is no unique and perfect algorithm, an alternative L1/L2 differential delay estimation algorithm was proposed. This algorithm can estimate the sum of GPS satellite and receiver L1/L2 differential delays using either a single-site or a multi-site data set. The performance of the proposed algorithm was tested and comparison was made with the results of other organisations.

The conventional grid-based algorithm can be used for real-time ionosphere modelling. It was found that the accuracy of real-time ionosphere modelling is dependent on the weighting function and ionosphere model used. Consequently, a new UNSW grid-based algorithm was proposed. The basis and computational procedures for the conventional and UNSW grid-based algorithms were described in chapter 6. A computer package (“POSTEC”) was developed in the course of this thesis project. Data sets from different permanent GPS networks, from different time periods, were used to test the conventional and UNSW grid-based algorithms, as well as the various polynomial-based algorithms.

7.2 Conclusions of the Research

Based on the investigations carried out, and the results obtained from the data processing, the following conclusions can be drawn:

7.2.1 Multipath Template

In order to mitigate pseudo-range multipath, a “multi-day multipath template” algorithm has been implemented and tested. The following comments can be made:

- Both single-day and multi-day multipath templates are useful for mitigating the multipath effects on GPS pseudo-range measurements at a static site. However, the performance of the multi-day multipath template is superior to that of the single-day multipath template.
- The multipath effect on pseudo-range derived TEC can be mitigated effectively in real-time TEC estimation if the multipath template technique is implemented.
- In addition, this technique is suitable for mitigating pseudo-range multipath at reference stations for Local Area DGPS, Wide Area DGPS and Wide Area Augmentation System networks, GPS deformation monitoring networks, etc.

7.2.2 Real-Time Failure Detection and Repair

In order to improve the accuracy of real-time ionospheric delay estimation, a novel approach to the detection and repair of carrier phase failures was implemented. The proposed real-time failure detection and repair algorithm uses two procedures: (1) application of a statistical test on the state difference estimated from robust and conventional Kalman filters in order to detect and identify the carrier phase failure, and (2) application of a Kalman filter algorithm to repair the “identified carrier phase failure”. From the test results, it has been demonstrated that the carrier phase derived TEC “failure” caused by cycle slips can be detected and repaired promptly and correctly in real-time.

7.2.3 GPS Instrumental L1/L2 Differential Delay Estimation

One of the challenging problems in making absolute ionospheric measurements using dual-frequency observations of the GPS satellites is to estimate the satellite and receiver L1/L2 differential delays. An alternative GPS instrumental L1/L2 differential delay estimation algorithm, based on the single-site modelling technique, to estimate the sum of the satellite and receiver L1/L2 differential delay for each tracked GPS satellite, using 24-hour data sets, was developed.

Based on the experimental results, the following comments can be made:

- Features of this algorithm are: (1) a 24-hour data set at a site is divided into eight 3-hour sessions, (2) a fifteen-term polynomial is used to model the ionosphere for each session, and (3) it can be used to calibrate the dual-frequency GPS receivers for precise TEC measurements even when the receiver internal hardware calibration is not available.
- The experimental results indicate that the estimation precision of the SPR (Satellite-Plus-Receiver) differential delay is of the order of ± 1.24 TECU (± 0.43 ns).
- The SPR differential delay estimates with daily average removed, as obtained using the proposed algorithm, have been compared with those determined by other organisations. The standard deviation of “UNSW - DLR” is 0.33 ns. Note that both the UNSW and the DLR results refer to the same time period. The standard deviation of the differences between UNSW and other organisations (most of their results referring to a different time period) is at the 1 ns level.
- Based on these experimental results, and comparisons with the results of other organisations, it has been demonstrated that the UNSW algorithm is an effective alternative method for estimating the GPS satellite and receiver L1/L2 differential delays. It is especially useful for calibrating the dual-frequency GPS receivers by

obtaining precise absolute TEC measurements when the receiver internal hardware calibration value is not available.

- This technique can be used to calibrate dual-frequency GPS receivers so as to provide precise TEC measurements for the monitoring and modelling of the ionosphere.

7.2.4 UNSW Grid-Based Algorithm

One real-time regional ionosphere modelling method is the so-called “*grid-based algorithm*”, or “conventional grid-based algorithm”. Typically, a simple weighting function, such as “*inverse distance*”, is used, and the “*Klobuchar Model*” is used to predict the ionospheric delay ratios between the grid point and reference points. From the experimental results it was found that the accuracy of real-time ionosphere modelling depends on: (1) the weighting function, and (2) the ionosphere model. In order to improve the real-time regional ionosphere modelling performance, an alternative grid-based algorithm, called “UNSW grid-based algorithm”, was proposed. In this new algorithm, an “*exponential function*” is adopted as the weighting function and the “*grid-based ionosphere model*” estimated from the previous day is used to predict the ionospheric delay ratios between the grid point and reference points.

A suite of computer software called “POSTEC” was developed, and data from different GPS networks, such as the PGGGA, GSI, ARGN, were processed and analysed to investigate the performance of the UNSW grid-based algorithm.

Based on the experimental results, the following comments can be made:

- Comparing the results of the proposed grid-based algorithm and the conventional grid-based algorithm, the standard deviations of the “TEC prediction residuals” (differences between the vertical TEC values derived from GPS observables at a user site and that derived from regional ionosphere modelling) can be reduced significantly, by approximately 29 to 31 percent in the case of the PGGGA data, 10 to 20 percent in the case of the GSI data, and 36 percent in the case of the ARGN data.

- The TEC prediction residuals of the UNSW grid-based algorithm and the conventional algorithm are typically less than ± 2.5 TECU and ± 3.5 TECU respectively, at the 99% probability level in the case of the PGGA data. In the cases of the GSI data and ARGN data, the TEC prediction residuals of the UNSW grid-based algorithm and the conventional algorithm are less than ± 4.5 TECU and ± 5.5 TECU respectively, at the 99% probability level.

7.3 Recommendations

In this thesis several algorithms were developed to solve some of the challenging problems in real-time ionospheric delay estimation using GPS measurements. These algorithms were implemented within several computer software packages, “REALTEC”, “POSTEC”, etc. Data sets from different GPS networks were processed using these software packages to simulate the process of real-time ionospheric delay estimation. The conclusions based on the test results carried out were summarised in the previous section.

The recommendations for further research are summarised as follows:

- The multi-day multipath template algorithm should be implemented at permanent GPS stations in real-time mode. From the test results reported in chapter 3, the multi-day multipath template generated from the data of the previous 5 days can mitigate most of the pseudo-range multipath. However, before applying the multi-day multipath template, the optimal number of days combinations for the multi-day multipath template should be evaluated beforehand using the available data set.
- The real-time failure detection and repair algorithm by robust and conventional Kalman filters can be implemented at permanent GPS stations. However, the function of this algorithm is to detect and repair the carrier phase failures for real-time TEC estimation. It is possible to apply this algorithm in other ways, such as to “quantify” the level of GPS data quality, detect abrupt changes in position in deformation monitoring applications, etc.

- The UNSW grid-based algorithm can be applied for Wide Area DGPS systems, Wide Area Augmentation Systems, etc., to generate an accurate real-time ionosphere model. However, some issues, such as the data links between the reference stations and monitor station, the latency of the TEC generation, etc., need to be studied further.
- The Global Navigation Satellite System (GLONASS) is similar to GPS in that it is a space-based navigation system providing global, 24-hour a day, all-weather support for precise positioning, velocity and time determination, to appropriately equipped users (Besser, 1997). It consists of 24 satellites in 3 orbital planes at a 19,100 km altitude, corresponding to an 11 hr 15 minute period. However, knowledge about the characteristics and capabilities of GLONASS, as compared with those of GPS, is relatively scarce, because of the smaller number of receivers available, and the reduced quantity of literature published to date. Right now there are several combined GPS/GLONASS receivers available on the market (eg. *ibid*, 1997; Boesenberg, 1997). In principle, GLONASS could be used for ionosphere modelling, either as standalone system or in combination with GPS (Zarraoa et al., 1995). Hence, some tests should be carried out using GPS+GLONASS data to study the performance of these proposed algorithms.

REFERENCES

- Ajayi, G.O., Hedberg, A. & Hamberg, G. (1980): Accurate determination of ionospheric effects on satellite-based positioning systems in terms of residual range error. *Radio Science*, Vol. 15, No. 5, 1009-1016.
- Anderson, D.N., Forbes, J.M. & Codrescu, M. (1989): A fully analytic, low- and middle-latitude ionospheric model. *Journal of Geophysical Research*, Vol. 94, 1520-1524.
- Axelrad, P., Comp, C. & Macdorran, P. (1994): Use of signal-to-noise ratio for multipath error correction in GPS differential phase measurements: methodology and experimental results. Proceedings of ION GPS-94, Seventh International Technical Meeting of The Satellite Division of The Institute of Navigation, Salt Lake, Utah, 20-23 September, 655-666.
- Bassiri, S. & Hajj, G.A. (1993): Higher-order ionospheric effects on the Global Positioning System observables and means of modelling them. *Manuscripta Geodaetica*, Vol. 18, No. 6, 280-289.
- Bent, R.B., Llewellyn, S.K. & Schmid, P.E. (1972): Ionospheric refraction corrections in satellite tracking. *Space Research*, Vol. 12, 1186-1194.
- Besser, J. (1997): GPS/GLONASS Receivers: The key to a new world of possibilities. Satellite Navigation Technology 1997 and Beyond, Sydney, Australia, 8-10 April.
- Biel, H.A. (1990): The geomagnetic time and position of a terrestrial station. *Journal of Atmospheric and Terrestrial Physics*, Vol. 52, No. 9, 687-694.
- Bishop, G., Coco, D.S. & Coker, C. (1991): Variations in ionospheric range error with GPS look direction. Proceedings of ION GPS-91, Fourth International Technical Meeting of The Satellite Division of The Institute of Navigation, Albuquerque, New Mexico, 11-13 September, 1045-1054.
- Bishop, G.J., Coco, D.S., Coker, C., Fremouv, E.J., Secan, J.A., Greenspan, R.L. & Eyring, D.O. (1992): GPS application to global ionospheric monitoring: requirements for a ground-based system. Proceedings of ION GPS-92, Fifth International Technical Meeting of The Satellite Division of The Institute of Navigation, Albuquerque, New Mexico, 16-18 September, 339-353.
- Bishop, G.J., Coco, D.S., Kappler, P.H. & Holland, E.A. (1994a): Studies and performance of a new technique for mitigation of pseudo-range multipath effects in GPS ground stations. Proceedings of 1994 National Technical Meeting, The Institute of Navigation, Washington, D.C., January, 231-242.
- Bishop, G., Walsh, D., Daly P., Mazzella, A. & Holland, E. (1994b): Analysis of the temporal stability of GPS and GLONASS delay correction terms seen in various sets ionospheric delay data. Proceedings of ION GPS-94, Seventh International Technical Meeting of The Satellite Division of The Institute of Navigation, Salt Lake City, Utah, 20-23 September, 1653-1661.

- Blewitt, G. (1990): An automatic editing algorithm for GPS data. *Geophysical Research Letters*, Vol. 17, No. 3, March, 199-202.
- Boesenberg, C. (1997): GPS+GLONASS - the way forward with satellite navigation. *Satellite Navigation Technology 1997 and Beyond*, Sydney, Australia, 8-10 April.
- Brunner, F.K. & Gu, M. (1991): An improved model for the dual frequency ionospheric correction of GPS observations. *Manuscripta Geodaetica*, Vol. 16, 205-214.
- Burns, C.J., Turunen, E., Matveinen, H., Ranta, H. & Hargreaves, J.K. (1991): Chemical modelling of the quiet summer D and E regions using EISCAT electron density profiles. *Journal of Atmospheric and Terrestrial Physics*, Vol. 53, 115-134.
- Campbell, J., Maniatis, T., Muller, A. Vierbuchen, J. & Lohmar, F.J. (1986): On the generation of ionospheric refraction corrections for single frequency GPS-measurements. *Proceedings of the Fourth International Geodetic Symposium on Satellite Positioning*, Austin, Texas, 28 April - 2 May, 631-645.
- Chao, Y., Tsai, Y., Walte, T., Kee, C., Enge, P. & Parkinson, B. (1995): An algorithm for inter-frequency bias calibration and application to WAAS ionosphere modeling. *Proceedings of ION GPS-95, Eighth International Technical Meeting of The Satellite Division of The Institute of Navigation*, Palm Springs, California, 12-15 September, 639-646.
- Chao, Y., Pullen, S., Enge, P. & Parkinson, B. (1996): Study of WAAS ionospheric integrity. *Proceedings of ION GPS-96, Ninth International Technical Meeting of The Satellite Division of The Institute of Navigation*, Kansas City, Missouri, 17-20 September, 781-788.
- Clynch, J.R., Coco, D.S., Coker, C. & Bishop, G.J. (1989): A versatile GPS ionospheric monitor: high latitude measurements of TEC and scintillation. *Proceedings of ION GPS-89, Second International Technical Meeting of The Satellite Division of The Institute of Navigation*, Colorado Springs, Colorado, 27-29 September, 445-450.
- Coco, D.S., Coker, C. & Clynch, J.R. (1990): Mitigation of ionospheric effects for single frequency GPS users. *Proceedings of ION GPS-90, Third International Technical Meeting of The Satellite Division of The Institute of Navigation*, Colorado Springs, Colorado, 19-21 September, 169-173.
- Coco, D. (1991): GPS - Satellites of opportunity for ionospheric monitoring. *GPS World*, October, 2(10), 47-50.
- Coco, D.S., Coker, C., Dahlke, S.R. & Clynch, J.R. (1991): Variability of GPS satellite differential group delay biases. *IEEE Transaction on Aerospace and Electrical Systems*, Vol 27, No 6, 931-938.
- Coco, D.S., Coker, C. & Bishop, G.J. (1993): A real-time GPS ionospheric monitor system. *Proceedings of 1993 Ionospheric Effects Symposium*, J.H. Goodman, ed., Springfield VA, May, 1993, 219- 227.

- Cohen, C.E. & Parkinson, B.W. (1991): Mitigating multipath error in GPS based attitude determination. *Advances in the Astronautical Sciences, Guidance and Control*, Vol. 74, 53-68.
- Conker, R.S., El-Arini, M.B., Albertson, T.W., Klobuchar, J.A. & Doherty, P.H. (1995): Development of real-time algorithms to estimate the ionosphere error bounds for WAAS. Proceedings of ION GPS-95, Eighth International Technical Meeting of The Satellite Division of The Institute of Navigation, Palm Springs, California, 12-15 September, 1247-1258.
- Coster, A.J. & Gaposchkin, E.M. (1989): Use of GPS pseudo-range and phase data for measurement of ionospheric and tropospheric refraction. Proceedings of ION GPS-89, Second International Technical Meeting of The Satellite Division of The Institute of Navigation, Colorado Springs, Colorado, 27-29 September, 439-443.
- Coster, A.J., Gaposchkin, E.M. & Thornton, L.E. (1992): Real-time ionospheric monitoring system using GPS. *NAVIGATION: Journal of The Institute of Navigation*, Vol. 39, No. 2, Summer, 191-204.
- Daniell, R.E., Brown, L.D., Anderson, D.N., Fox, M.W., Doherty, P.H., Decker, D.T., Sojka, J.J. & Schunk, R.W. (1995): Parameterised ionospheric model: a global ionospheric parameterisation based on first principles models. *Radio Science*, Vol. 30, 1499-1510.
- Davies, K. (1969): *Ionospheric Radio Waves*. Blaisdell Publishing Company, A Division of Ginn and Company, Waltham, Massachusetts, Toronto, London, 460pp.
- DLR (1996): The ionospheric maps and GPS satellite and receiver biases. DLR Remote Sensing Ground Station Neustrelitz, <http://www.nz.dlr.de/gps-ion.html>, accessed in May, 1996.
- El-Arini, M.B., Conker, R.S., Albertson, T.W., Reagon, J.K., Klobuchar, J.A. & Doherty, P. H. (1995): Comparison of real-time ionospheric algorithms for a GPS Wide-Area Augmentation System (WAAS). *NAVIGATION: Journal of the Institute of Navigation*, Vol. 41, No. 4, 393-413.
- Engler, E., Sardon, E, Jakowski, N. & Klahn, D. (1995): Real-time monitoring of the ionosphere. Proceedings of 1995 IGS Workshop, Potsdam, Germany, 15-17 May, 67-76.
- Erickson, C. (1992): *Investigation of C/A code and carrier measurement and techniques for rapid static GPS surveys*. UCGE Reports No. 20044, The University of Calgary, Calgary, Canada, 180pp.
- Evans, A.G. (1986): Comparison of GPS pseudo-range and biased Doppler measurements to demonstrate signal multipath effects. Proceedings of the Fourth International Geodetic Symposium on Satellite Positioning, Austin, Texas, 28 April - 2 May, 573-587.

- Federal Aviation Administration (FAA) (1994): *Wide Area Augmentation System (WAAS) specification*. Attachment B, U.S. Department of Transportation. FAA-E-2892, 9 May.
- Feess, W.A. & Stephens, S.G. (1987): Evaluation of GPS ionospheric time-delay model. *IEEE Transaction on Aerospace and Electronic Systems*, Vol. AES-23, No. 3, May, 332-338.
- Feltens, J. (1995a): *GPS TDAF Ionosphere Monitoring Facility Mathematical Model Developments*. GTDAF-TN-08 (ESOC - internal document), 77pp.
- Feltens, J. (1995b): *GPS TDAF Ionosphere Monitoring Facility Examination of the Applicability of Gauss-Type Exponential Functions to Ionosphere Modeling*. GTDAF-TN-09 (ESOC - internal document), 63pp.
- Feltens, J., Dow, J.M., Martin-Mur, T.J., Martinez, C.G. & Bayoona-P'erez, M.A. (1996): Verification of ESOC ionosphere modeling and status of IGS intercomparison activity. Proceedings IGS 1996 Analysis Center Workshop, Silver Springs, Maryland, 19-21 March, 205-219.
- Gao, Y., Heroux, P. & Kouba, J. (1994): Estimation of GPS receiver and satellite L1/L2 signal delay biases using data from CACS. Proceedings of the International Symposium on Kinematic Systems in Geodesy, Geomatics and Navigation, Banff, Canada, 30 August - 2 September, 109-117.
- Gelb, A. (1974): *Applied Optimal Estimation*. The M.I.T. Press, Massachusetts Institute of Technology, Cambridge, Massachusetts, 374 pp.
- Georgiadou, Y. & Kleusberg, A. (1989): Multipath effects in static and kinematic GPS surveying. International Association of Geodesy Symposia, Global Positioning System: An Overview, Symposium No. 102, Edinburgh, Scotland, 7-8 August, 82-89.
- Håkegård, O.P. (1995): *A regional ionospheric model for real-time predictions of the Total Electron Content in Wide Area Differential Satellite Navigation Systems*. PhD thesis of Norwegian Institute of Technology, 131pp.
- Han, S.W. (1995): Ambiguity recovery for GPS long range kinematic positioning. Proceedings of ION GPS-95, Eighth International Technical Meeting of The Satellite Division of The Institute of Navigation, Palm Springs, California, 12-15 September, 349-360.
- Hargreaves, J.K. (1992): *The Solar-Terrestrial Environment*. An introduction to geospace - the science of the terrestrial upper atmosphere, ionosphere and magnetosphere. Cambridge University Press, 415pp.
- Hofmann-Wellenhof, B., Lichtenegger, H. & Collins, J. (1994): *Global Positioning System: Theory and Practice*. Third edition, Springer-Verlag Wien, New York, 355 pp.

- Huber, P.J. (1981): *Robust Statistics*. John Wiley & Sons, Inc. 308 pp.
- Jakowski, N., Sardon, E., Engler, E., Jungstand, A. & Klahn, D. (1995): About the use of GPS measurements for ionospheric studies. *International Association of Geodesy Symposia*, No. 115, Springer-Verlag, 248-252.
- Jakowski, N. (1996): TEC monitoring by using satellite positioning systems. In *Modern Ionospheric Science* (Kohl, J., et al. Eds), European Geophysical Society, Katlenburg-Lindau, Germany, 371-390.
- Jungstand, A., Engler, E., Sardon, E. & Klahn, D. (1995): Error separation concept in experimental TEC monitoring network. *Proceedings of 1995 ION National Technical Meeting*, Washington, D.C., 323-335.
- Junkins, J.L., Miller, G.W. & Jancaitis, J.R. (1973): A weighting function approach to modelling of irregular surfaces. *Journal of Geophysical Research*, Vol. 78, No. 11, April, 1794-1803.
- Kee, C. & Parkinson, B.W. (1994): Calibration of multipath errors on GPS pseudo-range measurements. *Proceedings of ION GPS-94, Seventh International Technical Meeting of The Satellite Division of The Institute of Navigation*, Salt Lake City, Utah, 20-23 September, 353-362.
- Klobuchar, J.A. (1987): Ionospheric time-delay algorithm for single-frequency GPS users. *IEEE Transactions on Aerospace and Electronic Systems*, Vol. AES-23, No. 3, 325-331
- Klobuchar, J.A. (1991): Ionospheric effects on GPS. *GPS World*, April, 2(4), 48-51.
- Klobuchar, J.A. (1996): Ionospheric effects on GPS. In *Global Positioning Systems: Theory and Applications* (Edited by Parkinson & Spilker), Vol. 1, American Institute of Aeronautics and Astronautics, Inc., 485-515.
- Klobuchar, J.A., Basu, S. & Doherty, P. (1993): Potential limitations in making absolute ionospheric measurements using dual frequency radio waves from GPS satellites. *Proceedings of Ionospheric Effects Symposium, IES-93*, May, 187-194.
- Knight, M. & Finn, A. (1996): The impact of ionospheric scintillations on GPS performance. *Proceedings of ION GPS-96, Ninth International Technical Meeting of The Satellite Division of The Institute of Navigation*, Kansas City, Missouri, 17-20 September, 555-564.
- Komjathy, A. & Langley, R. (1996a): An assessment of predicted and measured ionospheric total electron content using a regional GPS network. Presented at the ION National Technical Meeting, Santa Monica, California, 22-24 January.
- Komjathy, A. & Langley, R. (1996b): The effect of shell height on high precision ionospheric modelling using GPS. *Proceedings of IGS 1996 Analysis Centre Workshop in Silver Spring, Maryland, USA*, 19-21 March, 193-203.

- Komjathy, A. & Langley, R. (1996c): Improvement of a global ionospheric model to provide ionospheric range error corrections for single-frequency GPS users. Presented at the ION 52nd Annual meeting, Cambridge, MA., 19-21 June.
- Komjathy, A. (1997): *Global ionospheric total electron content mapping using the Global Positioning System*. PhD dissertation, Department of Geodesy and Geomatic Engineering Technical Report No. 188, University of New Brunswick, Fredericton, New Brunswick, Canada, 248pp.
- Lachapelle, G., Falkenberg, W. & Neufeldt, D. (1989): Marine DGPS using code and carrier in a multipath environment. Proceedings of ION GPS-89, Second International Technical Meeting of The Satellite Division of The Institute of Navigation, Colorado Springs, Colorado, 27-29 September, 343-347.
- Lachapelle, G. (1990): GPS observables and error sources for kinematic positioning. International Association of Geodesy Symposia, Kinematic Systems in Geodesy, Surveying, and Remote Sensing, Symposium No. 107, 17-26.
- Langley, R.B. (1992): The effect of the ionosphere and troposphere on satellite positioning systems. Proceedings of the symposium "Refraction of Transatmospheric Signals in Geodesy", Edited by De Munck, J.C. & Spoelstra, T.A.TH., The Hague, the Netherlands, 19-22 May, page 97.
- Langley, R.B. (1993): The GPS Observables, *GPS World*, April, 4(4), 52-59.
- Langley, R.B. (1996): "Propagation of the GPS Signals" in The Directions of GPS : The 1996 GPS Lecture Series, School of Geomatic Engineering, The University of New South Wales, Sydney, Australia, 30-31 July.
- Langley, R.B. & Komjathy, A. (1996): High precision ionospheric total electron content mapping using the NAVSTAR Global Positioning System. Paper presented at 1996 Western Pacific Geophysics Meeting, Brisbane, Australia, 23-27 July, 1996. (Paper No. G62A-3 in a Supplement to EOS, Transactions, American Geophysical Union Vol. 77, No. 22, 28 May, 1996, W18).
- Lanyi, G.E. & Roth, T. (1988): A comparison of mapped and measured total ionospheric electron content using Global Positioning System and beacon satellite observations. *Radio Science*, Vol. 23, No. 4, 483-492.
- Lin, L.S. (1995a): Aspects of the generation of GPS differential corrections. Proceedings of Satellite Navigation Technology 1995 and Beyond, Brisbane, Australia, 26-28 June, Paper 21, 1-11.
- Lin, L.S. (1995b): Mitigating multipath effects on GPS measurements. Paper presented at the Annual Research Seminars, School of Geomatic Engineering, The University of New South Wales, Sydney, Australia, 6-7 November (abstract *Geomatics Research Australasia*, No. 63, December, 1995, page 105).

- Lin, L.S. (1997): A novel approach to improving the accuracy of real-time ionospheric delay estimation using GPS. Paper presented at ION GPS-97, Tenth International Technical Meeting of The Satellite Division of The Institute of Navigation, Kansas City, Missouri, 16-19 September.
- Lin, L.S. & Rizos, C. (1996a): An algorithm to estimate GPS satellite and receiver L1/L2 differential delays and its application to regional ionosphere modelling. *Geomatics Research Australasia*, No. 65, December, 1-26.
- Lin, L.S. & Rizos, C. (1996b): Quality issues concerned with real-time estimation of ionospheric delay using GPS measurements. Paper presented at the Annual Research Seminars, School of Geomatic Engineering, The University of New South Wales, Sydney, Australia, 11-12 November (abstract *Geomatics Research Australasia*, No. 65 December, 1996, page 111).
- Lin, L.S. & Rizos, C. (1997a): On real-time regional ionosphere modelling using grid-based algorithms. Proceedings of Satellite Navigation Technology 1997 and Beyond, Sydney, Australia, 8-10 April, Session 10, Paper No. 5, 1-10.
- Lin, L.S. & Rizos, C. (1997b): Use of multipath template technique for mitigating GPS pseudo-range multipath: methodology and test results. Proceedings of the First Trans Surveyors Conference, Newcastle, Australia, 12-18 April, 22.1-22.9.
- Lin, L.S. & Rizos, C. (1997c): Study of real-time regional ionosphere modelling using GPS measurements. Paper presented at 1997 Joint Assemblies of IAMAS and IAPSO, Melbourne, Australia, 1-9 July, Paper No. CGM23a.
- Lin, L.S., Rizos, C. & Wang, Y.J. (1996a): Real-time estimation of ionospheric delays using GPS. Proceedings of 1996 International Conference on GPS, Taipei, Taiwan, R.O.C., 12-13 June, 117-127.
- Lin, L.S., Rizos, C. & Wang, Y.J. (1996b): Real-time estimation of ionospheric delays for single-frequency GPS users. Paper presented at 1996 Western Pacific Geophysics Meeting, Brisbane, Australia, 23-27 July, 1996. (Paper No. G62A-4, in a Supplement to EOS, Transactions, American Geophysical Union Vol. 77, No. 22, 28 May, 1996, W18).
- Mannucci, A.J., Wilson, B.D. & Edwards, C.D. (1993): A new method for monitoring the earth's ionospheric total electron content using the GPS global network. Proceedings of ION GPS-93, Sixth International Technical Meeting of The Satellite Division of The Institute of Navigation, Salt Lake City, Utah, 22-24 September, 1323-1332.
- Meehan, T.K. & Young, L.E. (1992): On-receiver signal processing for GPS multipath reduction. Proceedings of Sixth International Geodetic Symposium on Satellite Position, Columbus, Ohio, 17-20 March, 200-208.
- Mertikas, S.P. (1994): The description of accuracy using conventional and robust estimate of scale. *Marine Geodesy*, Vol. 42, 251-269.

- Mertikas, S.P. & Rizos, C. (1996a): Quality control of GPS measurements for real-time applications. Proceedings of the 8th FIG International Symposium on Deformation Measurements, 25-28 June, Hong Kong, 27-36.
- Mertikas, S.P. & Rizos, C. (1996b): Quality control issues for permanent GPS receiver applications. Paper presented at 1996 Western Pacific Geophysics Meeting, Brisbane, Australia, 23-27 July, 1996. (Paper No. G61A-9, in a Supplement to EOS, Transactions, American Geophysical Union Vol. 77, No. 22, May 28, 1996, W18).
- Mertikas, S.P. & Rizos, C. (1996c): Real-time failure detection in the carrier phase measurements of GPS by robust and conventional Kalman state estimates. Accepted for publication in *Marine Geodesy*.
- Mertikas, S.P. & Rizos, C. (1997): On-line detection of abrupt changes in the carrier phase measurement of GPS. *Journal of Geodesy*, Vol. 71, 469-482.
- PGGA (1996): PGGA - Southern California Permanent GPS Geodetic Array, <http://toba.ucsd.edu/docs/pgga.html>, <ftp://toba.ucsd.edu>, accessed in March, 1996.
- Qiu, W. (1993): *An analysis of some critical error sources in static GPS surveying*. UCGE Reports No. 20054, The University of Calgary, Calgary, Canada, 102pp.
- Rawer, R. & Bilitza, D. (1989): Electron density profile description in the international reference ionosphere. *Journal of Atmospheric and Terrestrial Physics*, Vol. 51, 781-790.
- Rishbeth, H., Kohl, H. & Barclay, L.W. (1996): A history of ionospheric physics and radio communications. In *Modern Ionospheric Science* (Kohl, J., et al. Eds), European Geophysical Society, Katlenburg-Lindau, Germany, 4-31.
- Rizos, C. (1997): *Principles and Practice of GPS Surveying*. Monograph 17, School of Geomatic Engineering, The University of New South Wales, Sydney, Australia, 560 pp.
- Rocken, C., Johnson, J., Braun, J., Meertens, C. & Perry, S. (1994): *UNAVCO facility GPS receiver tests*. Draft 7/2/94, 63 pp.
- Sardon, E., Rius, A. & Zarraoa, N. (1994): Estimation of the transmitter and receiver differential biases and the ionospheric total electron current from Global Positioning System observations. *Radio Science*, Vol. 29, No. 3, 577-586.
- Schunk, R.W. & Sojka, J.J. (1996): Ionospheric models. In *Modern Ionospheric Science* (Kohl, J., et al. Eds), European Geophysical Society, Katlenburg-Lindau, Germany, 181-215.
- Schupler, B.R. & Clark, T.A. (1991): How different antennas affect the GPS observable. *GPS World*, October, 2(10), 32-36.

- Schut, G.H. (1976): Review of interpolation methods for Digital Terrain Models. *The Canadian Surveyor*, Vol. 30, No. 5, 389-412.
- Seeber, G. (1993): *Satellite Geodesy*. Walter de Gruyter, Berlin. New York, 531 pp.
- Sovers, O.J. & Fanselow, J.L. (1987): *Observation model and parameter partials for the JPL VLBI parameter estimation software MASTERFIT-1987*. Jet Propulsion Lab. Publication 83-39, Revision 3, 60pp.
- Townsend, B. & Fenton, P.(1994): A practical approach to the reduction of pseudo-range multipath errors in a L1 GPS receiver. Proceedings of ION GPS-94, Seventh International Technical Meeting of The Satellite Division of The Institute of Navigation, Salt Lake City, Utah, 20-23 September, 143-148.
- Tranquilla, J.M. (1986): Multipath and imaging problems in GPS receiver antennas. Proceedings of the Fourth International Geodetic Symposium on Satellite Positioning, Austin, Texas, 28 April - 2 May, 557-571.
- Tranquilla, J.M., Colpitis, B.G. & Carr, J.P. (1989): Measurement of low-multipath antennas for TOPEX. Proceedings of the Fifth International Geodetic Symposium on Satellite Position, Las Cruces, New Mexico, 13-17 March, 356-361.
- Van Nee, R.D.J., Siereveld, J., Fenton, P.C. & Townsend, B.R. (1994): The multipath estimating delay lock loop: approaching theoretical accuracy limits. 1994 IEEE Position Location and Navigation Symposium, Las Vegas, Nevada, 11-15 April, 246-251.
- Wallace, D.L. (1959): Bounds on normal approximations to Student's and the chi-square distributions. *Annals of Mathematical Statistics*, Vol. 30, 1121-1130.
- Wang, Y.J. (1995): *Monitoring ionospheric TEC using GPS*. IPS Radio and Space Service internal report, Department of Administrative Services, Sydney, Australia, 33pp.
- Wang, Y.J. & Kubik, K.K. (1993): Robust Kalman filter and its geodetic applications. *Manuscripta Geodaetica* 18: 349 - 354.
- Wanninger, L. (1992): Monitoring total ionospheric electron content and ionospheric irregularities with GPS. In: Munck, J.C. de & Spolstra, T.A.Th. (Ed.) *Refraction of Transatmospheric Signals in Geodesy*, The Netherlands Geodetic Commission, Publications on Geodesy, No. 36, 141-146.
- Wanninger, L., Seeber, G & Campos, M.A. (1992): Limitations of GPS in Central and South America due to the ionosphere. International Conference "Cartography - Geodesy", Maracaibo, Venezuela, 24 November - 4 December.
- Wanninger, L. (1993a): Ionospheric monitoring using IGS Data. In: Beutler, G. & Brockmann, E. (Ed.), Proceedings of the 1993 IGS Workshop, Berne, 25-26 March, Astronomical Institute, University of Berne, Switzerland.

- Wanninger, L. (1993b): The influence of ionospheric disturbances on precise GPS measurements in Central Europe. *Zeitschrift für Vermessungswesen (zfv)*, Vol. 118, 25-36.
- Wanninger, L. (1993c): The occurrence of ionospheric disturbances above Japan and their effects on precise GPS positioning. Proceedings of the CRCM'93, Kobe, 6-11 December, 175-179.
- Wanninger, L. (1993d): Effects of the equatorial ionosphere on GPS. *GPS World*, July, 4(7), 48-54.
- Wanninger, L. (1994): *Der Einfluss der Ionosphäre auf die Positionierung mit GPS*. PhD thesis of University of Hannover, Germany, Nr. 201, 137pp.
- Wanninger, L., Sardon, E. & Warnant, R. (1994): Determination of the total electron content with GPS - difficulties and their solution. In: Kersley, L. (Ed.), Proceedings of International Beacon Satellite Symposium, Aberystwyth, UK, 13-16.
- Wells, D., et al. (1986): *Guide to GPS Positioning*. Canadian GPS Associates.
- Wild, U. (1994): *Ionosphere and geodetic satellite systems: permanent GPS tracking data for modelling and monitoring*. PhD thesis of ETH Zurich, Switzerland, 155pp.
- Wilson, B.D. & Mannucci, A.J. (1993): Instrumental biases in ionospheric measurements derived from GPS data. Proceedings of ION GPS-93, Sixth International Technical Meeting of The Satellite Division of The Institute of Navigation, Salt Lake City, Utah, 22-24 September, 1343-1351.
- Wilson, B. & Mannucci, A. (1994): Extracting ionospheric measurements from GPS in the presence of Anti-Spoofing. Proceedings of ION GPS-94, Seventh International Technical Meeting of The Satellite Division of The Institute of Navigation, Salt Lake City, Utah, 20-23 September, 1599-1608.
- Wilson, B.D., Mannucci, A.J. & Edwards, C.D. (1995): Subdaily northern hemisphere ionospheric maps using an extensive network of GPS receivers. *Radio Science*, Vol. 30, No. 3, 639-648.
- Zarraoa, N., Sardon, E., Klahn, D. & Jungstand, A. (1995): Evaluation of GLONASS performance in practical applications: comparison with GPS-based ionospheric TEC values. Proceedings of ION GPS-95, Eighth International Technical Meeting of The Satellite Division of The Institute of Navigation, Palm Springs, California, 12-15 September, 1031-1039.

VITA

Biodata

Full name: LAO-SHENG LIN
Date of birth: October 18, 1955
Nationality: Taiwan, Republic of China
Marital status: Married
Religion: Buddhism
Permanent address: 3F-1, No. 35, Section 2,
Tai-Yuan Road, Taichung
TAIWAN, R.O.C.

Universities attended and degrees obtained:

1973-1977: Bachelor of Surveying (Geodetic)
Department of Surveying and Mapping
Chung Cheng Institute of Technology
Tao-Yuan, Taiwan, R.O.C.

1980-1982: Master of Science
Institute of Photogrammetry
Department of Surveying Engineering
National Cheng Kung University
Tai-Nan, Taiwan, R.O.C.

1985-1986: Studied at
Department of Geodetic Science and Surveying
The Ohio State University
Columbus, Ohio, U.S.A.

1994-current: Ph.D candidate
 School of Geomatic Engineering
 The University of New South Wales
 Sydney, Australia

ACADEMIC CONTRIBUTIONS (1994 - 1997)

1. List of Publications

1. **Lin, L.S.** (1995): Aspects of the generation of GPS differential corrections. Proceedings of Satellite Navigation Technology 1995 and Beyond, Brisbane, Australia, 26-28 June, Paper 21, 1-11.
2. **Lin, L.S.**, Rizos, C. & Wang, Y.J. (1996): Real-time estimation of ionospheric delays using GPS. Proceedings of 1996 International Conference on GPS, Taipei, Taiwan, R.O.C., 12-13 June, 117-127.
3. **Lin, L.S.** & Rizos, C. (1996): An algorithm to estimate GPS satellite and receiver L1/L2 differential delays and its application to regional ionosphere modelling. Geomatics Research Australasia, No. 65, December 1996, 1-26.
4. **Lin, L.S.** & Rizos, C. (1997a): On real-time regional ionosphere modelling using grid-based algorithms. Proceedings of Satellite Navigation Technology 1997 and Beyond, Sydney, Australia, 8-10 April, Session 10, Paper No. 5, 1-10.
5. **Lin, L.S.** & Rizos, C. (1997b): Use of multipath template technique for mitigating GPS pseudo-range multipath: methodology and test results. Proceedings of the First Trans Surveyors Conference, Newcastle, Australia, 12-18 April, 22.1-22.9.
6. **Lin, L.S.** (1997): A novel approach to improving the accuracy of real-time ionospheric delay estimation using GPS. Proceedings of ION GPS-97, Tenth International Technical Meeting of The Satellite Division of The Institute of Navigation, Kansas City, Missouri, 19-21 September.

2. List of Presentations

1. **Lin, L.S.** (1995a): Aspects of the generation of GPS differential corrections. Paper presented at Satellite Navigation Technology 1995 and Beyond, Brisbane, Australia, 26-28 June, Paper 21.
2. **Lin, L.S.** (1995b): Mitigating multipath effects on GPS measurements. Paper presented at the Annual Research Seminars, School of Geomatic Engineering, The University of New South Wales, Sydney, Australia, 6-7 November (abstract *Geomatics Research Australasia*, No. 63, December, 1995, page 105).
3. **Lin, L.S., Rizos, C. & Wang, Y.J.** (1996a): Real-time estimation of ionospheric delays using GPS. Paper presented at 1996 International Conference on GPS, Taipei, Taiwan, R.O.C., 12-13 June.
4. **Lin, L.S., Rizos, C. & Wang, Y.J.** (1996b): Real-time estimation of ionospheric delays for single-frequency GPS users. Paper presented at 1996 Western Pacific Geophysics Meeting, at the Brisbane Convention and Exposition Center, Brisbane, Australia, 23-27 July, 1996. (Paper Number G62A-04, in a Supplement to EOS, Transactions, American Geophysical Union Vol. 77, No. 22, May 28, 1996, W18).
5. **Lin, L.S. & Rizos, C.** (1996): Quality issues concerned with real-time estimation of ionospheric delay using GPS measurements. Paper presented at the Annual Research Seminars, School of Geomatic Engineering, The University of New South Wales, Sydney, Australia, 11-12 November (abstract *Geomatics Research Australasia*, No. 65, December, 1996, page 111).
6. **Lin, L.S. & Rizos, C.** (1997a): On real-time regional ionosphere modelling using grid-based algorithms. Paper presented at the Satellite Navigation Technology 1997 and Beyond, Sydney, Australia, 8-10 April.
7. **Lin, L.S. & Rizos, C.** (1997b): Use of multipath template technique for mitigating GPS pseudo-range multipath: methodology and test results. Paper presented at the First Trans Surveyors Conference, Newcastle, Australia, 12-18 April.
8. **Lin, L.S. & Rizos, C.** (1997c): Study of real-time regional ionosphere modelling using GPS measurements. Paper presented at 1997 Joint Assemblies of IAMAS and IAPSO, 1-9 July, Paper No. CGM23a.
9. **Lin, L.S.** (1997): A novel approach to improving the accuracy of real-time ionospheric delay estimation using GPS. Paper presented at Conference of ION GPS-97, Tenth International Technical Meeting of The Satellite Division of The Institute of Navigation, Kansas City, Missouri, 16-19 September.

Publications from

THE SCHOOL OF GEOMATIC ENGINEERING

(Formerly School of Surveying)

THE UNIVERSITY OF NEW SOUTH WALES

All prices include postage by surface mail. Air mail rates on application. (Effective March 1998)

To order, write to Publications Officer, School of Geomatic Engineering
The University of New South Wales, Sydney 2052, AUSTRALIA

NOTE: ALL ORDERS MUST BE PREPAID

UNISURV REPORTS - S SERIES

S8 - S20	Price (including postage) :		\$10.00
S29 onwards	Price (including postage) :	Individuals	\$25.00
		Institutions	\$30.00
S8	A. Stolz, "Three-D Cartesian co-ordinates of part of the Australian geodetic network by the use of local astronomic vector systems", Unisurv Rep. S8, 182 pp, 1972.		
S10	A.J. Robinson, "Study of zero error & ground swing of the model MRA101 tellurometer", Unisurv Rep. S10, 200 pp, 1973.		
S12.	G.J.F. Holden, "An evaluation of orthophotography in an integrated mapping system", Unisurv Rep. S12, 232 pp, 1974.		
S14.	Edward G. Anderson, "The Effect of Topography on Solutions of Stokes` Problem", Unisurv Rep. S14, 252 pp, 1976.		
S16.	K. Bretreger, "Earth Tide Effects on Geodetic Observations", Unisurv S16, 173 pp, 1978.		
S17.	C. Rizos, "The role of the gravity field in sea surface topography studies", Unisurv S17, 299 pp, 1980.		
S18.	B.C. Forster, "Some measures of urban residential quality from LANDSAT multi-spectral data", Unisurv S18, 223 pp, 1981.		
S19.	Richard Coleman, "A Geodetic Basis for recovering Ocean Dynamic Information from Satellite Altimetry", Unisurv S19, 332 pp, 1981.		
S20.	Douglas R. Larden, "Monitoring the Earth's Rotation by Lunar Laser Ranging", Unisurv Report S20, 280 pp, 1982.		
S29	Gary S Chisholm, "Integration of GPS into hydrographic survey operations", Unisurv S29, 190 pp, 1987.		
S30.	Gary Alan Jeffress, "An investigation of Doppler satellite positioning multi-station software", Unisurv S30, 118 pp, 1987.		
S31.	Jahja Soetandi, "A model for a cadastral land information system for Indonesia", Unisurv S31, 168 pp, 1988.		
S33.	R. D. Holloway, "The integration of GPS heights into the Australian Height Datum", Unisurv S33, 151 pp., 1988.		
S34.	Robin C. Mullin, "Data update in a Land Information Network", Unisurv S34, 168 pp. 1988.		
S35.	Bertrand Merminod, "The use of Kalman filters in GPS Navigation", Unisurv S35, 203 pp., 1989.		
S36.	Andrew R. Marshall, "Network design and optimisation in close range Photogrammetry", Unisurv S36, 249 pp., 1989.		
S37.	Wattana Jaroondhampinij, "A model of Computerised parcel-based Land Information System for the Department of Lands, Thailand," Unisurv S37, 281 pp., 1989.		
S38.	C. Rizos (Ed.), D.B. Grant, A. Stolz, B. Merminod, C.C. Mazur "Contributions to GPS Studies", Unisurv S38, 204 pp., 1990.		

- S39. C. Bosloper, "Multipath and GPS short periodic components of the time variation of the differential dispersive delay", Unisurv S39, 214 pp., 1990.
- S40. John Michael Nolan, "Development of a Navigational System utilizing the Global Positioning System in a real time, differential mode", Unisurv S40, 163 pp., 1990.
- S41. Roderick T. Macleod, "The resolution of Mean Sea Level anomalies along the NSW coastline using the Global Positioning System", 278 pp., 1990.
- S42. Douglas A. Kinlyside, "Densification Surveys in New South Wales - coping with distortions", 209 pp., 1992.
- S43. A. H. W. Kearsley (ed.), Z. Ahmad, B. R. Harvey and A. Kasenda, "Contributions to Geoid Evaluations and GPS Heighting", 209 pp., 1993.
- S44. Paul Tregoning, "GPS Measurements in the Australian and Indonesian Regions (1989-1993)", 134 + xiii pp, 1996.
- S45. Wan-Xuan Fu, "A study of GPS and other navigation systems for high precision navigation and attitude determinations", 332pp, 1996.
- S46. Peter Morgan et al, "A zero order GPS network for the Australia region", 187 + xii pp, 1996.
- S47. Yongru Huang, "A digital photogrammetry system for industrial monitoring", 145 + xiv pp, 1997.
- S48. Kim Mobbs, "Tectonic interpretation of the Papua New Guinea Region from repeat satellite measurements", 256 + xc pp, 1997.
- S49. Shaowei Han, "Carrier phase-based long-range GPS kinematic positioning", 185 + xi pp, 1997.
- S50. Mustafa D Subari, "Low-cost GPS systems for intermediate surveying and mapping accuracy applications", 179 + xiii pp, 1997.
- S51. Lao-Sheng Lin, "Real-time estimation of ionospheric delay using GPS measurements", 199 + xix pp, 1997.
- S52. Merrin B Pearse, "A modern geodetic reference system for New Zealand", 324 + xviii pp, 1997.
- S53. David B Lemon, "The nature and management of positional relationships within a local government Geographic Information System", 273 + xvi pp, 1997.
- S54. Catherine Ticehurst, "Development of models for monitoring the urban environment using radar remote sensing", 282 + xix, 1998.

MONOGRAPHS

Prices include postage by surface mail

		Price
M1.	R.S. Mather, "The theory and geodetic use of some common projections", (2nd edition), 125 pp., 1978.	\$15.00
M2.	R.S. Mather, "The analysis of the earth's gravity field", 172 pp., 1971.	\$8.00
M3.	G.G. Bennett, "Tables for prediction of daylight stars", 24 pp., 1974.	\$5.00
M4.	G.G. Bennett, J.G. Freislich & M. Maughan, "Star prediction tables for the fixing of position", 200 pp., 1974.	\$8.00
M8.	A.H.W. Kearsley, "Geodetic Surveying", 96 pp, (revised) 1988.	\$12.00
M11.	W.F. Caspary, "Concepts of Network and Deformation Analysis", 183 pp., 1988.	\$25.00
M12.	F.K. Brunner, "Atmospheric Effects on Geodetic Space Measurements", 110 pp., 1988.	\$16.00
M13.	Bruce R. Harvey, "Practical Least Squares and Statistics for Surveyors", (2nd edition), 319 pp., 1994.	\$30.00
M14.	Ewan G. Masters & John R. Pollard (Ed.), "Land Information Management", 269 pp., 1991. (Proceedings LIM Conference, July 1991).	\$20.00
M15/1	Ewan G. Masters & John R. Pollard (Ed.), "Land Information Management - Geographic Information Systems - Advance Remote Sensing Vol 1" 295 pp., 1993 (Proceedings of LIM & GIS Conference, July 1993).	\$30.00
M15/2	Ewan G. Masters & John R. Pollard (Ed.), "Land Information Management - Geographic Information Systems - Advance Remote Sensing Vol 2" 376 pp., 1993 (Proceedings of Advanced Remote Sensing Conference, July 1993).	\$30.00
M16.	A. Stolz, "An Introduction to Geodesy", 112 pp., 1994.	\$20.00
M17	Chris Rizos, "Principles and Practice of GPS Surveying", 565 pp., 1997.	\$50.00